

**EXPERIMENTAL INVESTIGATION ON PRODUCTION  
AND OPTIMIZATION OF BIOGAS USING DIFFERENT  
FEEDSTOCKS AND ITS UTILIZATION IN AN IC ENGINE**

**Thesis Submitted  
in Fulfillment of the Requirements for the  
Degree of**

**DOCTOR OF PHILOSOPHY  
IN  
MECHANICAL ENGINEERING**

**by**

**S. LALHRIATPUIA  
Roll No.- 2K17/PhD/ME/07**

*Under the Supervision*

*Of*

**PROF. AMIT PAL  
(Department of Mechanical Engineering, DTU)**



**Department of Mechanical Engineering,  
Delhi Technological University  
(Formerly Delhi College of Engineering)  
Main Bawana Road, Shahabad Daultpur, Delhi- 110042, India  
January 2024**

## DECLARATION

---

I hereby declare that thesis entitled “**Experimental Investigation on Production and Optimization of Biogas using different Feedstocks and its Utilization in an IC Engine**” submitted by me in fulfillment of the requirement for the degree of Doctor of Philosophy to Delhi Technological University (Formerly Delhi College of Engineering) is a record of bona fide work carried out by me under the supervision of Dr. Amit Pal, Professor, Department of Mechanical Engineering, Delhi Technological University, Delhi.

I further declare that the work reported in this thesis has not been submitted, either in part or in full, for the award of any other degree or diploma in any other Institute or University.

**(S. LALHRIATPUIA)**

Roll No: 2K17/ Ph.D./ME/07

Department of Mechanical Engineering  
Delhi Technological University, Delhi (India)

## CERTIFICATE

---

This is to certify that the work embodied in the *thesis* entitled “**Experimental Investigation on Production and Optimization of Biogas using different Feedstocks and its Utilization in an IC Engine**” is a record of *bona fide research work* carried out by **Sh. S.Lalhriatpuia (2K17/Ph.D./ME/07)** in fulfillment of requirements for the award of the degree of **Doctor of Philosophy in Mechanical Engineering** with specialization in **Thermal Engineering**. He has worked under my guidance and supervision and has fulfilled the requirements that, to my knowledge, have reached the requisite standard for submitting the thesis.

The results in this thesis have not been submitted in part or whole at any other University or Institute for the award of any degree or diploma.

**(Dr. Amit Pal)**  
Professor  
Mechanical Engineering Department  
Delhi Technological University  
Delhi-110042 (India)  
(Supervisor)

## ACKNOWLEDGEMENT

---

I want to convey my profound appreciation to my supervisor, Dr. Amit Pal, for his essential mentorship from the beginning of this research endeavor. Dr. Amit Pal's dedication to his students is truly unparalleled. His constant encouragement and insightful advice have been the driving force behind my research journey. Beyond his academic brilliance, Dr. Pal's rare warmth and empathy makes him an incredible mentor. He truly cares about his students' success and well-being. I'm incredibly fortunate to have him as my research supervisor, and I cherish the memories and lessons learned under his guidance.

I would like to thank Prof. S.K. Garg, DRC Chairperson and Head of the Department of Mechanical Engineering, for his kind support in accomplishing this work. I also dedicate this work to all the faculty members and lab technicians of the Mechanical Engineering Department who tirelessly kept the doors of our research facilities open. My Ph.D. journey wouldn't have been possible without their unwavering support and dedication. Their willingness to grant me access to the lab, answer my endless questions, and troubleshoot countless technical hiccups was instrumental in my research progress.

I express my special thanks to my friends Mr. Neeraj Budhraj, research scholar, and Dr. Pradeep Kumar Meena, Delhi Technological University, Delhi, for helping me with difficult times and providing unflinching moral support.

To my extraordinary parents, Mr. SR Remsanga and Mrs. Rita Zonunmawii, words seem inadequate to express the ocean of gratitude that fills my heart. The path to this research work wasn't always smooth, but their guiding hands were always there to steady me.

My heart overflows with gratitude as I stand here; this thesis is a testament to the countless hands that helped shape it. While words cannot name them all, I acknowledge the immeasurable value they have added to the research process. And finally, to the divine force that I call God, my gratitude rises like a prayer.

**S. LALHRIATPUIA**

## ABSTRACT

---

To counter the concern of the future availability of fossil fuels due to ever-increasing energy demand and the emission generated due to their utilization, alternative renewable fuels such as biogas, biodiesel, and fuel additives in the form of nanoparticles emerge as viable alternative fuels. Biogas production was carried out to study the effects of feedstocks, temperature, and mixing duration, followed by optimization of process parameters on a lab scale for optimal Methane percentage and biogas production rate. A novel design for biogas digester agitation was prepared and fabricated for this study. Computational methods such as Response Surface Methodology (RSM) were used to establish a prediction model based on the Design of experiment (DOE) results.

The developed RSM model's F-value indicates Temperature was the most substantial influence in deciding the value of the ratio of methane ( $\text{CH}_4$ ) to Carbon dioxide ( $\text{CO}_2$ ). At the same time, Mixing Duration was the most considerable influence in determining the value of Cumulative Biogas Production (CBP). The highest Cumulative Biogas Production (CBP) and  $\text{CH}_4/\text{CO}_2$  were observed for Kitchen waste as feedstock for biogas production, followed by Vegetable waste and Fruit waste. At  $40^\circ\text{C}$  digester temperature, Anaerobic digestion of kitchen waste exhibits 9.67% and 18.63% higher CBP than Vegetable and Fruit waste, respectively. For Kitchen waste, an increase in CBP of 19.47% and 11.68% was observed for the digester temperature of  $50^\circ\text{C}$  and  $60^\circ\text{C}$ , compared to the digester at  $40^\circ\text{C}$ . As for the average  $\text{CH}_4/\text{CO}_2$ , a 62% and 45% increase was observed for the kitchen waste with a digester temperature of  $50^\circ\text{C}$  and  $60^\circ\text{C}$ , compared to kitchen waste with a digester at  $40^\circ\text{C}$ .

Regardless of the types of feedstocks, the highest CBP and  $\text{CH}_4/\text{CO}_2$  are observed for the digester with a mixing duration of 15 minutes, followed by the digester with 30 minutes and the digester with no mixing, respectively. For Kitchen waste at a digestion temperature of  $40^\circ\text{C}$ , an increase in CBP of 24% and 14% was observed for the digester at the mixing duration of 15 minutes and 30 minutes, compared to the digester with no mixing. The RSM model observed an optimum value of CBP and  $\text{CH}_4 / \text{CO}_2$  at the temperature of  $54.44^\circ\text{C}$ , a mixing duration of 14.51 min, and a feedstock mixture of 86% kitchen and 14% vegetable waste. The optimization findings confirm the positive effect of tumbling for both biogas production rate and methane production. The optimal biogas production process parameters are then used to replicate biogas production on a larger scale for biogas enrichment and its

utilization in the CI engine. Biogas Enrichment was conducted to increase the biogas methane (CH<sub>4</sub>) content to 89.3%.

Input parameters such as Engine load, Cobalt oxide nanoparticles doped rate (NDR), Linseed biodiesel blend rate (BBR), and Biogas flow rate (BFR) were studied for their effect on engine performance and emission outputs. Compared to the engine run on neat diesel, NO<sub>x</sub> and Smoke exhibit a decrease of 51% and 52%, respectively, for the engine run on BFR 1 kg/h. Compared to the engine run on the BBR 20 blend, HC, CO, and Smoke Opacity decreased by 17%, 14%, and 13%, respectively, for the engine run on the BBR20-NDR100 blend. RSM and ANN were used to study the interaction effects of input parameters and their optimization. The developed RSM model's F-value indicates engine load as the most significant input variable in deciding the value of output responses, followed by BFR, NDR, and BBR, respectively.

The statistical analysis using different evaluation metrics suggests the prediction made by the RSM model is more accurate and reliable than the ANN model. The optimization for the RSM model observed an optimal response at 67.45% engine load, 96.06 ppm NDR, 10.7 % BBR, and 0.85 kg/h BFR, while an optimal response for the ANN model was observed at 67.01% engine load, 98.39 ppm NDR, 8.41% BBR and 0.846 kg/h BFR. The optimization study findings concluded that an optimal combination of nanoparticles, biodiesel, and biogas could significantly improve CI engine performance and emission responses. Enriched biogas is utilized in a compression ignition (CI) engine, resulting in enhanced engine performance and decreased emissions, except for nitrogen oxides (NO<sub>x</sub>) when compared to engine run on raw biogas.

## CONTENTS

<b>DECLARATION</b> .....	<b>i</b>
<b>CERTIFICATE</b> .....	<b>ii</b>
<b>ACKNOWLEDGEMENT</b> .....	<b>iii</b>
<b>ABSTRACT</b> .....	<b>iv</b>
<b>LIST OF FIGURES</b> .....	<b>ix</b>
<b>LIST OF TABLES</b> .....	<b>xii</b>
<b>NOMENCLATURE</b> .....	<b>xiv</b>
<b>CHAPTER 1: INTRODUCTION</b> .....	<b>1</b>
1.1 Biomass .....	2
1.2 Environmental effects of MSW.....	5
1.3 Environmental effects of Untreated (Aerobic digestion) Cow dung.....	6
1.4 Biogas.....	7
1.5 Dual Fuel Concept .....	9
1.6 Anaerobic digestion.....	10
1.6.1 Hydrolysis .....	10
1.6.2 Acidogenesis .....	10
1.6.3 Acetogenesis.....	11
1.6.4 Methanogenesis.....	11
1.7 Factors Affecting Biogas Production .....	12
1.7.1 Temperature.....	12
1.7.2 Hydraulic Retention Time (HRT).....	13
1.7.3 pH.....	13
1.7.4 Organic Loading Rate .....	13
1.7.5 Substrate & Nutrients.....	14
1.7.6 Mixing.....	14
1.7.7 Volatile fatty acids.....	15
1.7.8 C/N ratio.....	15
1.8 Biodiesel.....	16
1.9 Nanoparticles .....	18
1.10 The Need for Regression Analysis and Optimization Techniques .....	19
1.11 Dissertation Layout .....	21
<b>CHAPTER 2: LITERATURE REVIEW</b> .....	<b>22</b>
2.1 Production of Biogas.....	22

2.2 Optimization of Biogas Process Parameters .....	25
2.3 Biogas in CI engine.....	29
2.4 Biodiesel & Nanoparticle blended fuels utilization in CI engine.....	32
2.5 Optimization of CI engine parameters .....	35
2.6 Research Gap .....	49
2.7 Objectives of the research .....	49
<b>CHAPTER 3: MATERIALS AND METHODS.....</b>	<b>50</b>
3.1 Research Methodology.....	50
3.2 Biogas Production and Optimization .....	52
3.2.1 Waste collection system .....	52
3.2.2 Characterization of Feedstock.....	53
3.2.3 Lab scale Digester .....	53
3.2.4 Heating Container .....	55
3.2.5 Temperature Control Panel.....	56
3.2.6 Large Scale Digester .....	57
3.2.7 Tumbling Setup .....	58
3.2.8 Biogas Enrichment Setup.....	58
3.2.9 Biogas Composition Analyzer.....	59
3.3 RSM Modelling for Biogas Production Process Parameters .....	60
3.3.1 RSM Modelling.....	62
3.4 Experimental testing setup .....	62
3.4.1 Measurement Instruments .....	64
3.4.2 Central chamber for fuel-air mixing.....	65
3.4.3 Biogas Distribution and Measuring Appliance .....	68
3.4.4 Methodology for Experimental Studies .....	69
3.5 Nanoparticles Characterization .....	70
3.6 Biodiesel Production and Properties .....	72
3.7 Nanoparticles Blends Preparation and Properties .....	73
3.8 RSM and ANN Modelling for Engine Performances and Emission Parameters .....	74
3.8.1 RSM Modelling.....	76
3.8.2 ANN Modelling.....	76
3.9 Optimization of the RSM model with the Desirability Approach.....	77
3.10 Optimization of ANN model with Genetic Algorithm (GA).....	78
3.11 Evaluation Metrics for ANN and RSM Model Predictions.....	79
3.12 Validation of optimized results from ANN and RSM Model.....	79
3.13 Uncertainty analysis.....	79
3.14 Summary .....	82



<b>CHAPTER 4 : BIOGAS PRODUCTION AND OPTIMIZATION.....</b>	<b>84</b>
4.1 Effect of process parameters on Biogas Production Rate & CH <sub>4</sub> /CO <sub>2</sub> .....	84
4.1.1 Effect of Feedstock on Biogas Production Rate & CH <sub>4</sub> /CO <sub>2</sub> .....	84
4.1.2 Effect of Temperature on Biogas Production Rate & CH <sub>4</sub> /CO <sub>2</sub> .....	86
4.1.3 Effect of Mixing Duration on Biogas Production Rate & CH <sub>4</sub> /CO <sub>2</sub> .....	90
4.2 Biogas Production Optimization.....	93
4.2.1 RSM Model Analysis.....	94
4.2.2 Interaction effects for CBP.....	95
4.2.3 Interaction effects for CH <sub>4</sub> /CO <sub>2</sub> .....	97
4.2.4 Evaluated metrics.....	99
4.2.5 Optimization of input parameters and Validation.....	100
4.3 Summary.....	101
<b>CHAPTER 5 : ENGINE PERFORMANCE AND EMISSION EVALUATION .....</b>	<b>103</b>
5.1 Effect of Biodiesel, Biogas, and Nanoparticles on CI Engine.....	103
5.1.1 Effect of Biogas Flow Rate (BFR) on Engine Performance and Emission.....	103
5.1.2 Effect of Biodiesel Blend Rate (BBR) on Engine Performance and Emission.....	110
5.1.3 Effect of Nanoparticles Doped Rate (NDR) on Engine Performance and Emission.....	115
5.2 Engine Performance and Emission Optimization.....	120
5.2.1 Design of Experiment Analysis.....	120
5.2.2 RSM Model Analysis.....	123
5.2.3 Interaction effects on BTE.....	123
5.2.4 Interaction Effects on BSEC.....	125
5.2.5 Interaction effects on NO <sub>x</sub> .....	127
5.2.6 Interaction effects on HC.....	129
5.2.7 Interaction Effects on CO.....	130
5.2.8 Interaction effects on SO.....	132
5.2.9 Interaction Effects on BGES.....	134
5.2.10 ANN Model Analysis.....	143
5.2.11 Comparison of the ANN Model and RSM Model.....	144
5.2.12 Optimization of Engine Performance and Emission Parameters.....	146
5.2.13 Validation of optimized results from ANN and RSM Model.....	148
5.3 Effect of Enriched Biogas on CI engine performance and emission.....	148
5.4 Summary.....	155
<b>CHAPTER 6 : CONCLUSIONS AND FUTURE SCOPE .....</b>	<b>157</b>
6.1 Conclusions.....	157
6.2 Key points for Future scope.....	159
<b>REFERENCES.....</b>	<b>160</b>

<b>LIST OF PUBLICATIONS .....</b>	<b>175</b>
<b>CURRICULUM VITAE .....</b>	<b>176</b>

## LIST OF FIGURES

<b>Fig. 1. 1</b> India Oil Consumption vs Production [3] .....	<b>1</b>
<b>Fig. 1. 2</b> Annual CO <sub>2</sub> emission of India from oil consumption[4].....	<b>2</b>
<b>Fig. 1. 3</b> Crop residue surplus for different states in India [5].....	<b>3</b>
<b>Fig. 1. 4</b> Livestock population for different states in India [6].....	<b>4</b>
<b>Fig. 1. 5</b> MSW for different states in India [8] .....	<b>4</b>
<b>Fig. 1. 6</b> Biogas Cycle .....	<b>8</b>
<b>Fig. 1. 7</b> Schematic diagram of dual fuel concept .....	<b>9</b>
<b>Fig. 1. 8</b> Stages of an Anaerobic Digestion system .....	<b>12</b>
<b>Fig. 1. 9</b> Factors Influencing Biogas Production .....	<b>16</b>
<b>Fig. 1. 10</b> Biodiesel cycle .....	<b>18</b>
<b>Fig. 1. 11</b> Effect of Nanoparticles on CI engine .....	<b>19</b>
<b>Fig. 3. 1</b> Research Methodology .....	<b>51</b>
<b>Fig. 3. 2</b> Distribution of color-coded dustbins on the university campus.....	<b>52</b>
<b>Fig. 3. 3</b> Layout of Biogas Lab scale digester .....	<b>54</b>
<b>Fig. 3. 4</b> Pictorial representation of Lab scale digester .....	<b>54</b>
<b>Fig. 3. 5</b> Biogas Digesters in a container of water.....	<b>55</b>
<b>Fig. 3. 6</b> Schematic Layout of the Biogas Production Setup.....	<b>56</b>
<b>Fig. 3. 7</b> Temperature Control Panel.....	<b>57</b>
<b>Fig. 3. 8</b> Large-scale Digester with tumbling setup.....	<b>57</b>
<b>Fig. 3. 9</b> Biogas Tumbling setup.....	<b>58</b>
<b>Fig. 3. 10</b> CO <sub>2</sub> Scrubber.....	<b>59</b>
<b>Fig. 3. 11</b> Portable Biogas Analyzer .....	<b>60</b>
<b>Fig. 3. 12</b> Schematic representation of test setup after modification .....	<b>63</b>
<b>Fig. 3. 13</b> Pictorial representation of test rig .....	<b>63</b>
<b>Fig. 3. 14</b> Pictorial representation of test rig after modification.....	<b>64</b>
<b>Fig. 3. 15</b> Schematic diagram of Fuel-air mixing chamber .....	<b>67</b>
<b>Fig. 3. 16</b> Illustration of the fuel-air mixing chamber .....	<b>67</b>
<b>Fig. 3. 17</b> Visual representation of Y-divider.....	<b>68</b>
<b>Fig. 3. 18</b> Biogas Flowmeter .....	<b>68</b>
<b>Fig. 3. 19</b> 2 m <sup>3</sup> biogas storage balloon .....	<b>69</b>
<b>Fig. 3. 20</b> SEM image of Co <sub>3</sub> O <sub>4</sub> at 20 μm.....	<b>70</b>
<b>Fig. 3. 21</b> EDX spectra of Co <sub>3</sub> O <sub>4</sub> .....	<b>71</b>
<b>Fig. 3. 22</b> Elemental mapping of (a)Co, (b) O, and (c) Co <sub>3</sub> O <sub>4</sub> .....	<b>71</b>
<b>Fig. 3. 23</b> Biodiesel production process .....	<b>72</b>
<b>Fig. 3. 24</b> GC-MS of Linseed Biodiesel .....	<b>72</b>
<b>Fig. 3. 25</b> Blending of Pilot fuel with nanoparticles via Ultrasonicator.....	<b>74</b>
<b>Fig. 3. 26</b> ANN Architecture (4-X1-X2-6).....	<b>77</b>

<b>Fig. 4. 1</b>	Biogas Production per day for varied feedstock .....	84
<b>Fig. 4. 2</b>	Cumulative Biogas Production for varied feedstock.....	85
<b>Fig. 4. 3</b>	CH <sub>4</sub> / CO <sub>2</sub> per day for varied feedstock .....	86
<b>Fig. 4. 4</b>	Biogas Production per day for varied feedstock and temperature .....	87
<b>Fig. 4. 5</b>	Cumulative Biogas Production for varied feedstock and temperature.....	88
<b>Fig. 4. 6</b>	CH <sub>4</sub> /CO <sub>2</sub> per day for varied feedstock and temperature .....	89
<b>Fig. 4. 7</b>	Biogas Production per day for varied feedstock and mixing duration.....	90
<b>Fig. 4. 8</b>	Cumulative Biogas Production for varied feedstock and mixing duration .....	92
<b>Fig. 4. 9</b>	CH <sub>4</sub> /CO <sub>2</sub> per day for varied feedstock and mixing duration.....	93
<b>Fig. 4. 10</b>	Interaction effects of input parameters on CBP .....	96
<b>Fig. 4. 11</b>	Interaction effects of input parameters on CH <sub>4</sub> /CO <sub>2</sub> .....	98
<b>Fig. 4. 12</b>	Error percentage for DOE runs for CBP .....	99
<b>Fig. 4. 13</b>	Error percentage for DOE runs for CH <sub>4</sub> /CO <sub>2</sub> .....	99
<b>Fig. 4. 14</b>	Desirability Plot.....	100
<b>Fig. 5. 1</b>	Effect of BFR on BTE.....	103
<b>Fig. 5. 2</b>	Effect of BFR on BSEC .....	104
<b>Fig. 5. 3</b>	Effect of BFR on NO <sub>x</sub> .....	105
<b>Fig. 5. 4</b>	Effect of BFR on HC.....	106
<b>Fig. 5. 5</b>	Effect of BFR on CO.....	107
<b>Fig. 5. 6</b>	Effect of BFR on Smoke Opacity.....	108
<b>Fig. 5. 7</b>	Effect of BFR on BGES .....	109
<b>Fig. 5. 8</b>	Effect of BBR on BTE .....	110
<b>Fig. 5. 9</b>	Effect of BBR on BSEC .....	111
<b>Fig. 5. 10</b>	Effect of BBR on NO <sub>x</sub> .....	112
<b>Fig. 5. 11</b>	Effect of BBR on HC.....	113
<b>Fig. 5. 12</b>	Effect of BBR on CO .....	114
<b>Fig. 5. 13</b>	Effect of BBR on Smoke Opacity .....	115
<b>Fig. 5. 14</b>	Effect of NDR on BTE .....	116
<b>Fig. 5. 15</b>	Effect of NDR on BSEC .....	117
<b>Fig. 5. 16</b>	Effect of NDR on NO <sub>x</sub> .....	117
<b>Fig. 5. 17</b>	Effect of NDR on HC .....	118
<b>Fig. 5. 18</b>	Effect of NDR on CO .....	119
<b>Fig. 5. 19</b>	Effect of NDR on Smoke Opacity.....	120
<b>Fig. 5. 20</b>	Interaction effects of (a) NDR and Load, (b) BBR and Load on BTE.....	124
<b>Fig. 5. 21</b>	Interaction effects of (a) BBR and Load, (b) BBR and NDR on BTE.....	124
<b>Fig. 5. 22</b>	Interaction effects of (a) BFR and NDR, (b) BBR and BFR on BTE .....	125
<b>Fig. 5. 23</b>	Interaction effects of (a) NDR and Load, (b) BBR and Load on BSEC .....	126
<b>Fig. 5. 24</b>	Interaction effects of (a) BBR and Load, (b) BBR and NDR on BSEC .....	126
<b>Fig. 5. 25</b>	Interaction effects of (a) BFR and NDR, (b) BBR and BFR on BSEC .....	127
<b>Fig. 5. 26</b>	Interaction effects of (a) NDR and Load, (b) BBR and Load on NO <sub>x</sub> .....	127
<b>Fig. 5. 27</b>	Interaction effects of (a) BBR and Load, (b) BBR and NDR on NO <sub>x</sub> .....	128

<b>Fig. 5. 28</b>	Interaction effects of (a) BBR and Load, (b) BBR and NDR on NO <sub>x</sub> .....	128
<b>Fig. 5. 29</b>	Interaction effects of (a) NDR and Load, (b) BBR and Load on HC.....	129
<b>Fig. 5. 30</b>	Interaction effects of (a) BBR and Load, (b) BBR and NDR on HC.....	130
<b>Fig. 5. 31</b>	Interaction effects of (a) BFR and NDR, (b) BBR and BFR on HC.....	130
<b>Fig. 5. 32</b>	Interaction effects of (a) NDR and Load, (b) BBR and Load on CO.....	131
<b>Fig. 5. 33</b>	Interaction effects of (a) BBR and Load, (b) BBR and NDR on CO.....	131
<b>Fig. 5. 34</b>	Interaction effects of (a) BFR and NDR, (b) BBR and BFR on CO.....	132
<b>Fig. 5. 35</b>	Interaction effects of (a) NDR and Load, (b) BBR and Load on SO.....	133
<b>Fig. 5. 36</b>	Interaction effects of (a) BBR and Load, (b) BBR and NDR on SO.....	133
<b>Fig. 5. 37</b>	Interaction effects of (a) BFR and NDR, (b) BBR and BFR on SO.....	134
<b>Fig. 5. 38</b>	Interaction effects of (a) NDR and Load, (b) BBR and Load on BGES.....	135
<b>Fig. 5. 39</b>	Interaction effects of (a) BBR and Load, (b) BBR and NDR on BGES.....	135
<b>Fig. 5. 40</b>	Interaction effects of (a) BFR and NDR, (b) BBR and BFR on BGES.....	135
<b>Fig. 5. 41</b>	R for the trained network in response to outputs (a) BTE, (b) BSEC.....	143
<b>Fig. 5. 42</b>	R for the trained network in response to outputs (a) NO <sub>x</sub> , (b) HC.....	143
<b>Fig. 5. 43</b>	R for the trained network in response to outputs (a)CO and (b) SO.....	144
<b>Fig. 5. 44</b>	R for the trained network in response to outputs BGES.....	144
<b>Fig. 5. 45</b>	Percentage in error for predicted engine performance and emission responses	145
<b>Fig. 5. 46</b>	Desirability Plot.....	147
<b>Fig. 5. 47</b>	Average spread vs Generation.....	147
<b>Fig. 5. 48</b>	Effect of enriched biogas on BTE.....	149
<b>Fig. 5. 49</b>	Effect of enriched biogas on BSEC.....	150
<b>Fig. 5. 50</b>	Effect of enriched biogas on NO <sub>x</sub> .....	151
<b>Fig. 5. 51</b>	Effect of enriched biogas on HC.....	152
<b>Fig. 5. 52</b>	Effect of enriched biogas on CO.....	152
<b>Fig. 5. 53</b>	Effect of enriched biogas on Smoke Opacity.....	153
<b>Fig. 5. 54</b>	Effect of enriched biogas on BGES.....	154

## LIST OF TABLES

<b>Table 1. 1</b>	CHG emission comparison of aerobic vs anaerobic digestion of cow dung.....	6
<b>Table 2. 1</b>	Literature Review on Biogas Production .....	38
<b>Table 2. 2</b>	Literature Review on Biogas Production Optimization .....	40
<b>Table 2. 3</b>	Literature Review on Biogas use in CI engine.....	42
<b>Table 2. 4</b>	Literature Review on Biodiesel, Nanoparticle blends use in CI engine.....	44
<b>Table 2. 5</b>	Literature Review on Optimization of CI engine performance and emission....	47
<b>Table 3. 1</b>	Physiochemical Properties of Feedstocks .....	53
<b>Table 3. 2</b>	Input Parameters and Levels .....	61
<b>Table 3. 3</b>	Design of Experiment for Biogas Production Optimization .....	61
<b>Table 3. 4</b>	Engine Specifications .....	65
<b>Table 3. 5</b>	Composition of Linseed Biodiesel .....	73
<b>Table 3. 6</b>	Fuel properties .....	73
<b>Table 3. 7</b>	Physiochemical properties of fuel blends.....	74
<b>Table 3. 8</b>	Input Parameters and Levels .....	75
<b>Table 3. 9</b>	Input Parameters and Levels .....	75
<b>Table 3. 10</b>	ANN architecture for engine outputs .....	77
<b>Table 3. 11</b>	Selection Parameters for GA Optimization .....	78
<b>Table 3. 12</b>	Uncertainty in Observed Parameter and List of Used Instruments with Uncertainties .....	82
<b>Table 4. 1</b>	Experimental Matrix of the Biogas Production.....	84
<b>Table 4. 2</b>	Experimental Matrix of the Biogas Production.....	87
<b>Table 4. 3</b>	Experimental Matrix of the Biogas Production.....	90
<b>Table 4. 4</b>	Design of Experiment for Biogas Production Optimization .....	94
<b>Table 4. 5</b>	ANOVA table for CBP .....	95
<b>Table 4. 6</b>	ANOVA table for CH <sub>4</sub> /CO <sub>2</sub> .....	97
<b>Table 4. 7</b>	Evaluation Metrics for RSM Model Predictions .....	100
<b>Table 4. 8</b>	Optimization Criteria for Biogas Production .....	100
<b>Table 4. 9</b>	RSM optimized parameter's validation test results and error percentage .....	101
<b>Table 5. 1</b>	Experimental Matrix of the Diesel-Biogas Run Dual Fuel Diesel Engine.....	103
<b>Table 5. 2</b>	Experimental Matrix of the Biodiesel Run Diesel Engine .....	110
<b>Table 5. 3</b>	Experimental Matrix of the Biodiesel-Nanoparticles Blend Run Diesel Engine .....	115
<b>Table 5. 4</b>	DOE with experimental responses .....	121
<b>Table 5. 5</b>	ANOVA for table BTE .....	136
<b>Table 5. 6</b>	ANOVA table for BSEC.....	137

<b>Table 5. 7</b> ANOVA table for NO <sub>x</sub> .....	138
<b>Table 5. 8</b> ANOVA table for HC .....	139
<b>Table 5. 9</b> ANOVA table for CO .....	140
<b>Table 5. 10</b> ANOVA table for SO .....	141
<b>Table 5. 11</b> ANOVA table for BGES .....	142
<b>Table 5. 12</b> R <sup>2</sup> , RMSE, and MAD evaluation metrics for RSM and ANN Model.....	146
<b>Table 5. 13</b> Optimization Criteria for Engine Performance and Emission.....	146
<b>Table 5. 14</b> Validation test result and Percentage of error for the ANN & RSM optimized parameter .....	148
<b>Table 5. 15</b> Experimental Matrix of the Diesel-Biogas Run Dual Fuel Diesel Engine.....	148

## NOMENCLATURE

<b>ACoD</b>	Anaerobic Co-digestion	<b>COD</b>	Chemical oxygen demand
<b>AD</b>	Anaerobic Digestion	<b>CP</b>	Cosubstrate Proportion
<b>AI</b>	Agitation intensity	<b>CR</b>	Compression ratio
<b>Al<sub>2</sub>O<sub>3</sub></b>	Alumina or Aluminium oxide	<b>CSTR</b>	Continuous Stirred Tank Reactors
<b>ALK</b>	Alkalinity	<b>CuNO<sub>3</sub></b>	Copper Nitrate
<b>ANN</b>	Artificial Neural Network	<b>CuO</b>	Copper Oxide
<b>ANOVA</b>	Analysis of Variance	<b>DAD</b>	Data acquisition device
<b>AT</b>	Agitation time	<b>df</b>	Degree of Freedom
<b>BBR</b>	Biodiesel Blend Rate	<b>DFM</b>	Dual Fuel mode
<b>BFR</b>	Biogas Flow Rate	<b>DOE</b>	Design of Experiment
<b>BGES</b>	Biogas Energy Share	<b>EGT</b>	Exhaust Gas Temperature
<b>BP</b>	Brake power (kW)	<b>FAME</b>	Fatty acid methyl ester
<b>BSEC</b>	Brake specific energy consumption	<b>FIP</b>	Fuel injection pressure
<b>BSFC</b>	Brake specific fuel consumption	<b>FW</b>	Fruit waste
<b>BTDC</b>	Before top dead center	<b>FW</b>	Fish waste
<b>BTE</b>	Brake Thermal Efficiency	<b>GA</b>	Genetic Algorithm
<b>CH<sub>4</sub></b>	Methane	<b>GHG</b>	Greenhouse gas
<b>CA</b>	Crank Angle	<b>GWP</b>	Global Warming Potential
<b>CBP</b>	Cumulative biogas production	<b>H<sub>2</sub>S</b>	Hydrogen sulphide
<b>CCD</b>	Central Composite Design	<b>HC</b>	Hydrocarbon
<b>CCFCD</b>	Central composite face-centered design	<b>HL</b>	Hidden Layer
<b>CD</b>	Combined Desirability	<b>HRT</b>	Hydraulic Retention Time
<b>CI</b>	Compression ignition	<b>IC</b>	Inoculum concentration
<b>CM</b>	Cow Manure	<b>IPCC</b>	Intergovernmental Panel on Climate Change
<b>CO</b>	Carbon monoxide	<b>IT</b>	Injection Timing
<b>CO<sub>2</sub></b>	Carbon dioxide	<b>KW</b>	Kitchen waste
<b>Co<sub>3</sub>O<sub>4</sub></b>	Cobalt oxide	<b>LCV</b>	Lower Calorific Value

<b>LHV</b>	Lower Heating value (MJ/kg)	<b>sfc</b>	Specific Fuel Consumption
<b>MAD</b>	Mean Absolute Deviation	<b>SLR</b>	Sludge loading rate
<b>MD</b>	Mixing Duration	<b>SO</b>	Smoke Opacity
<b>MSE</b>	Mean square error	<b>SS</b>	Sum of Squares
<b>MSW</b>	Municipal solid waste	<b>T</b>	Temperature
<b>N</b>	Speed	<b>TiO<sub>2</sub></b>	Titanium oxide
<b>NDR</b>	Nanoparticles doped rate	<b>TOC</b>	Total organic carbon
<b>NO<sub>x</sub></b>	Oxides of nitrogen(ppm)	<b>TS</b>	Total Solid
<b>OECD</b>	Organisation for Economic Co-operation and Development	<b>TSRB</b>	Tamarind seed and rice bran
<b>OLR</b>	Organic Loading Rate	<b>U</b>	Combined Uncertainty
<b>P</b>	Power	<b>V<sub>air</sub></b>	Volumetric Air Intake
<b>POME</b>	Palm oil mill effluent	<b>VFA</b>	Volatile Fatty acids
<b>PS</b>	Pistia stratiotes	<b>VS</b>	Volatile solid
<b>PW</b>	Potato Waste	<b>V<sub>s</sub></b>	Swept Volume
<b>R<sup>2</sup></b>	Correlation coefficient	<b>VW</b>	Vegetable waste
<b>RMSE</b>	Root Mean Square Error	<b>WH</b>	Water hyacinth
<b>rpm</b>	Revolution per Minute	<b>β</b>	(Diameter of Throat)/ (Diameter of Inlet Tube)
<b>RSM</b>	Response Surface Methodology	<b>θ<sub>1</sub></b>	Converging Angle of Venturi
<b>RT</b>	Reaction time	<b>θ<sub>2</sub></b>	Diverging Angle of Venturi
<b>S (%)</b>	Substitution of Diesel by Biogas	<b>θ<sub>n</sub></b>	Nozzle Angle with Horizontal
<b>SC</b>	Solid concentrations	<b>φ</b>	Equivalence Ratio
<b>SEM</b>	Scanning Electron Microscope	<b>η<sub>vol</sub></b> (%)	Vol. Efficiency



## CHAPTER 1: INTRODUCTION

Over the last few decades, fossil fuels have been the primary energy source for transportation and industry activities. However, due to the limited reserves and the environmental impact of extraction, the increasing demand for energy raises sustainability concerns. Also, automotive sectors primarily use fossil fuels as their power source, concluding that the significant emissions emitted are due to the combustion of these fossil fuels. Hence, there is a need to investigate alternative fuels to counter the issues on hand [1,2].

India is the third-largest oil consumer in the world while ranking 11<sup>th</sup> in oil production; the mismatch of demand vs supply is depicted in Fig. 1.1 [3]. Oil is a significant source of CO<sub>2</sub> emissions in the country. India has seen an exponential rise in CO<sub>2</sub> emissions over the years, as depicted in Fig. 1.2. In 2020, oil accounted for about 30% of India's CO<sub>2</sub> emissions. The use of oil for transportation is the largest source of CO<sub>2</sub> emissions from oil in India, followed by oil for electricity generation [4].

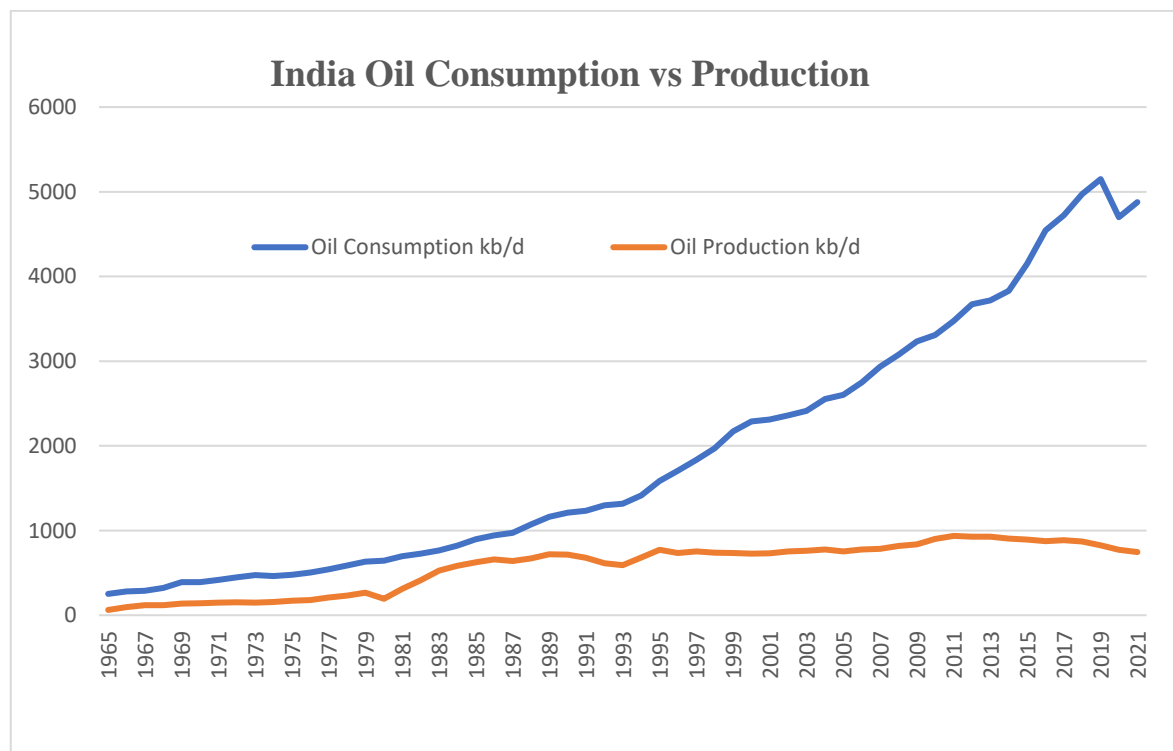


**Fig. 1. 1** India Oil Consumption vs Production [3]

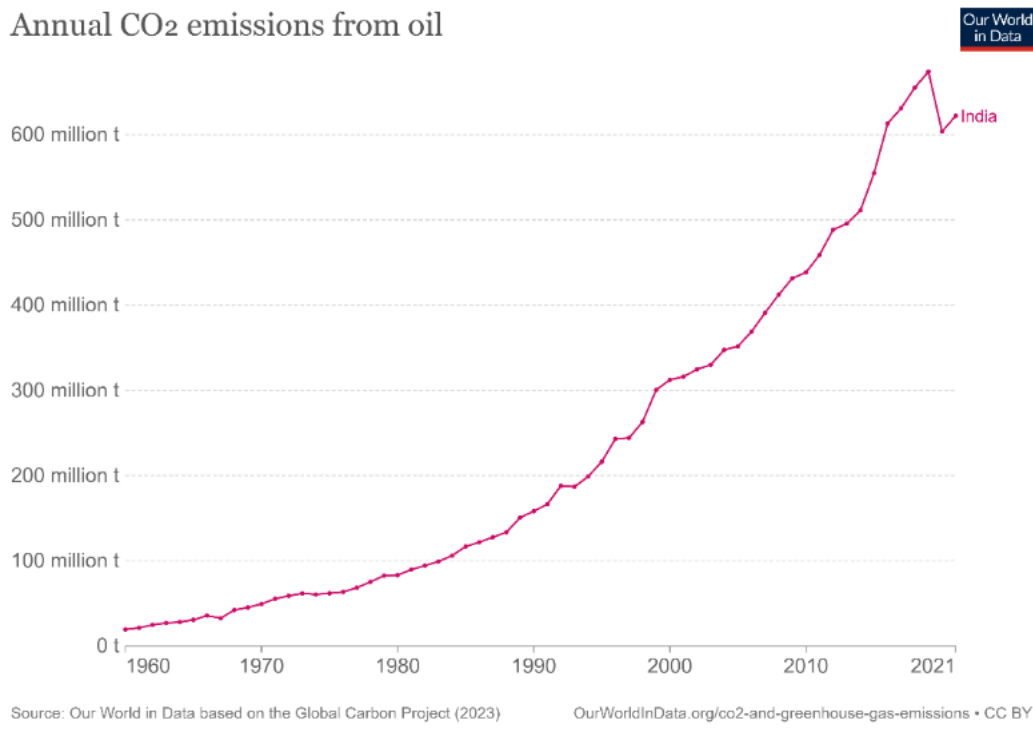


**Fig. 1. 2** Annual CO<sub>2</sub> emission of India from oil consumption [4]

### 1.1 Biomass

Biomass is a valuable resource spread across India's various states, as depicted in Fig.1.3 to 1.5. With the growing demand for energy and the need for sustainable solutions, it makes sense to explore the potential of biomass as an energy source. India could establish an efficient bioenergy production system by tapping into the vast reserves of agricultural and industrial residues, wood waste, food industry, municipal waste, animal waste, and industrial wastewater. This would help meet the country's energy needs and provide a cleaner and more sustainable alternative to traditional fossil fuels. Crop residue surplus is the amount of crop residue that remains after the crop has been harvested and used for various purposes such as cattle feed, domestic fuel, animal bedding material, etc. Fig.1.3 represents the top 10 states in India with the highest Crop residue surplus [5]. Nowadays, burning crop residues is a major environmental problem in India. When crop residues are burned, they spread harmful pollutants, such as particulate matter, nitrogen oxides, and sulfur dioxide, into the air. The government of India and various state governments are taking steps to reduce the burning of crop residues. These steps include promoting crop residue use for other purposes, such as biogas production, composting, and spraying chemicals to decompose them.

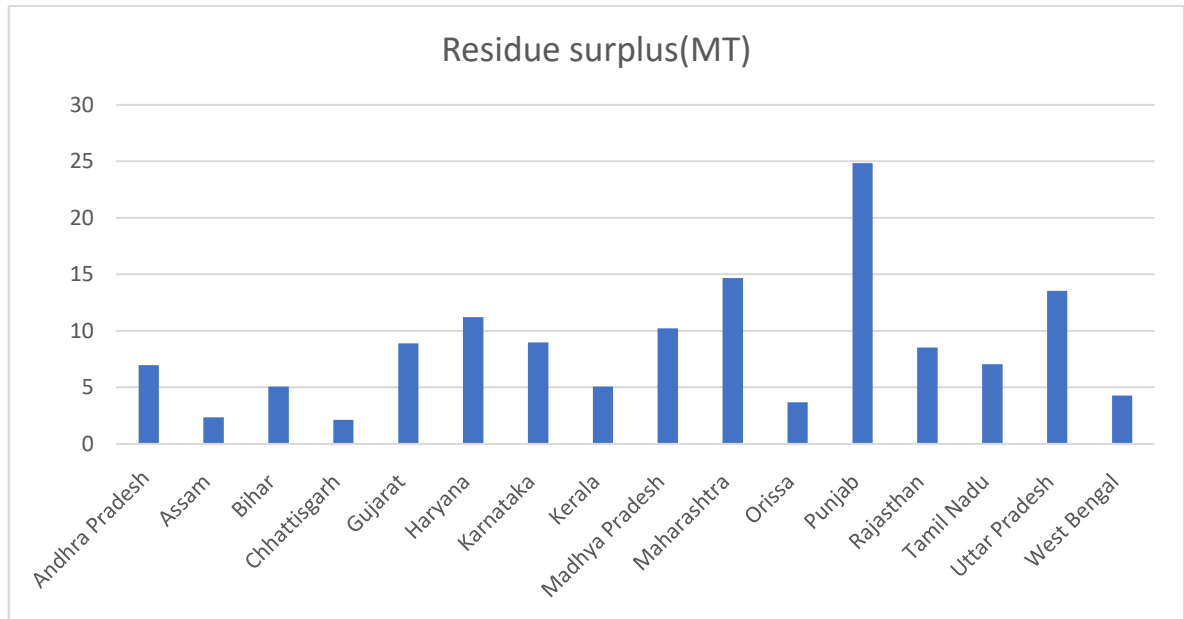


**Fig. 1. 3** Crop residue surplus for different states in India [5]

The livestock population in India is very high. As given in Fig.1.4, according to the 2019 livestock census, there were over 530 million livestock in India, including cattle, buffaloes, sheep, goats, pigs, and poultry. In India, there is a growing interest in biogas production from livestock manure [6]. Fig. 1.4 represents the top 10 states in India with the highest livestock population. The government of India has launched several initiatives to promote biogas production, such as the National Biogas Programme and the Pradhan Mantri Kaushal Vikas Yojana. These initiatives have helped to increase the number of biogas plants in India, and they have also helped to create jobs in the biogas sector.

Research on the manufacturing of biogas dates back to the early nineteenth century in India. Traditional forms of fuel for homes in rural areas included wood and cow dung cake. Agriculture is a vital source of livelihood in rural India, making biogas plants a practical option to deliver clean fuel and high-quality organic manure in the form of biogas slurry. Biogas plants enhanced women's health, reduced the need for firewood and cow dung cakes, and slowed forest loss [7]. Municipal solid waste (MSW) is a major environmental problem in India. Fig.1.5 represents the top 10 states in India with the highest MSW [8]. MSW management is a challenge for many Indian cities, as they lack the proper waste disposal resources. MSW is a good source of organic matter for biogas production, as it contains food scraps, yard waste, and other organic materials. Several biogas plants in India are using MSW to produce biogas. These plants are helping to reduce the amount of MSW that is sent to landfills, and they are also generating renewable energy.

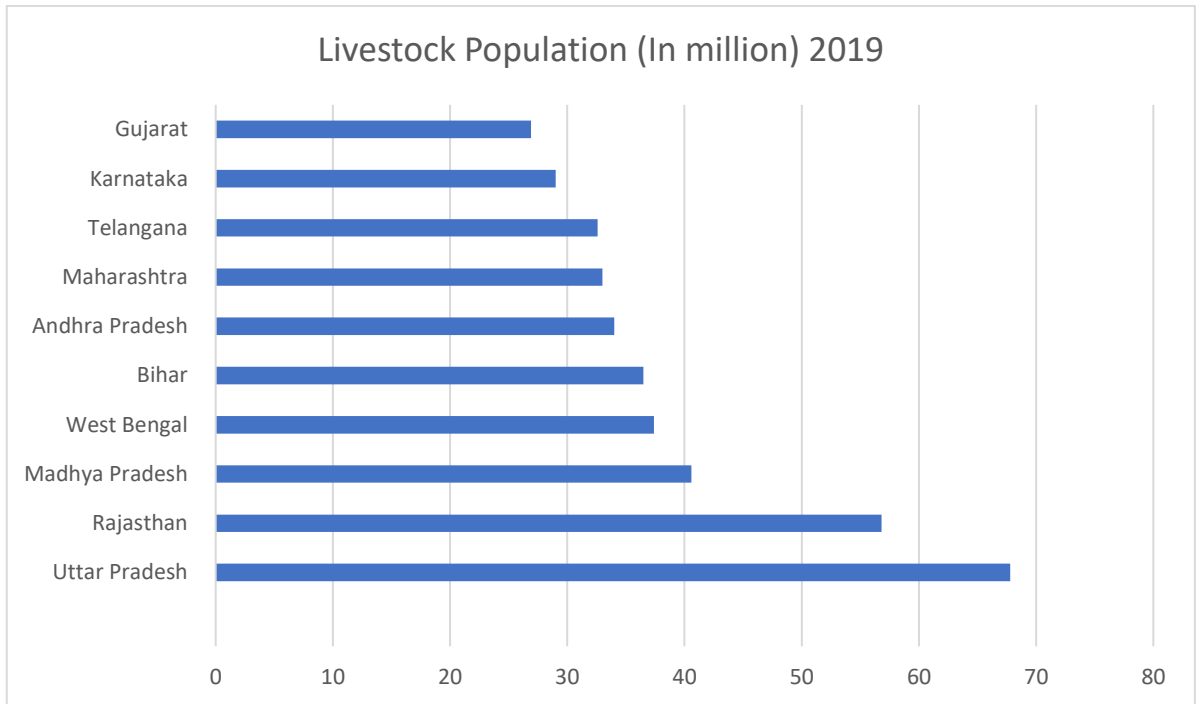


**Fig. 1. 4** Livestock population for different states in India [6]

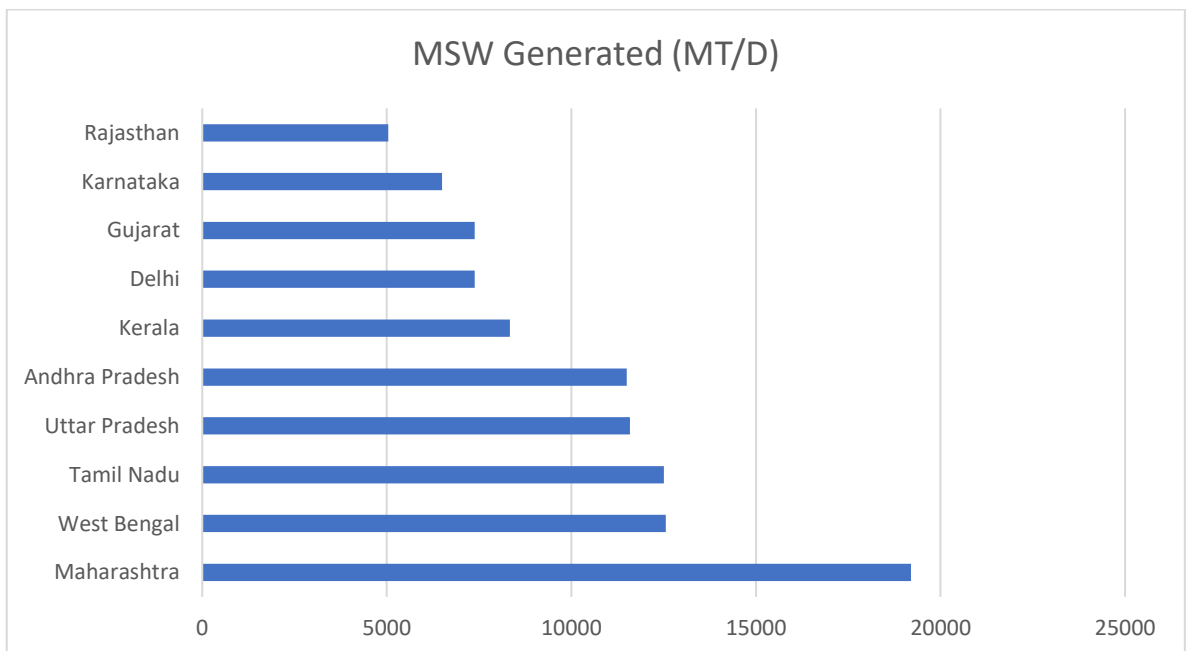


**Fig. 1. 5** MSW for different states in India [8]

Integrated solid waste management has been ranked according to importance by the Indian Ministry of Urban Development (2016). Their primary management strategy was to recycle and repurpose materials. Reusing products, such as shopping bags and jam jars, helps cut down on waste and helps the environment. Recycling came in third, after source reduction and reuse. Plastic, paper, metal, glass, and electronic waste are recyclable inorganic waste

products that may be recovered using this process. The second most popular approach was composting, which could be done in various ways. Waste-to-energy was the next best thing for dealing with garbage. There was also a waste-to-energy component to the project. The use of landfills, including the secure burial of inert residual waste in approved landfills, was the least preferred method of waste management [9].

## 1.2 Environmental effects of MSW

According to research by Cointreau (2006) for the World Bank, dumping municipal solid waste in developing nations poses serious environmental risks. Uncollected waste facilitates the abundance of vector-borne diseases and pathogen survival by providing ideal breeding sites for mosquitoes; clogged drains lead to stagnant waters encouraging mosquito growth; and methane and carbon dioxide emissions from land disposal facilities contribute to global warming [10].

Konnoth (1996) examined around 95 solid waste workers in Mumbai. The majority (80%) had some ocular issue, while 51% had some gastrointestinal issue, 73% had some respiratory issue, 40% had some skin illness or allergy, and 22% had some kind of orthopedic issue. Ninety percent had impaired vision, according to clinical testing. Burning, blurred vision, redness, itching, and moist eyes were the most common complaints from workers. Clinical evaluation indicated 27% had skin lesions, of which 30% were considered to be directly employment-related [11].

Lee et al. (2016) reported that the US created the most significant waste among Organisation for Economic Co-operation and Development (OECD) countries. The disposal of this waste contributes to greenhouse gas emissions, which can lead to various environmental and human health hazards, including air pollution, climate change, and respiratory illnesses. Since the United States has a lower recycling rate than other OECD countries, waste production is unlikely to decrease. Recycling has been proposed as a solution to address the issue of municipal solid waste and its impact on greenhouse gas emissions. Greenhouse gas (GHG) emissions might be reduced in addition to via recycling if the causal connection between MSW and GHGs could be severed. They pushed waste-to-energy options for enhanced MSW management [12].

Intergovernmental Panel on Climate Change (IPCC, 2006) reported that there is often a range or average time after disposal for trash to break down. About 50 years of methane emissions

from decomposition will be released when municipal solid waste is landfilled. With a global warming potential of 25 over 100 years, methane (CH<sub>4</sub>) is the second most significant contributor to climate change after carbon dioxide (CO<sub>2</sub>). The typical atmospheric lifetime of the climate pollutant CH<sub>4</sub> is 12 years [13]. According to the IPCC (2007), in 2004, the total CH<sub>4</sub> emissions accounted for 14.3% of global GHG emissions, whereas MSW processing accounted for 2.8% [14].

### 1.3 Environmental effects of Untreated (Aerobic digestion) Cow dung

The quantity of greenhouse gases (GHGs) emitted by aerobic and anaerobic digestion is contingent upon several aspects, such as the specific characteristics of the manure, the digestion methodology used, and how the resulting digestate is handled and controlled. Nevertheless, it is well-recognized that anaerobic digestion generally yields much less methane than aerobic digestion.

**Table 1. 1 CHG emission comparison of aerobic vs anaerobic digestion of cow dung**

<b>GHG emissions when aerobic (open) digestion of 1 ton of cow dung</b>	
Methane (CH <sub>4</sub> )	2.9 kg
Carbon dioxide (CO <sub>2</sub> )	73.55 kg
Total GHG emissions (CO <sub>2</sub> equivalent)	60.9 kg* + 73.55 = 134.55 CO <sub>2</sub>
<b>GHG emissions in anaerobic digestion of 1 ton of cow dung (after power generation)</b>	
CO <sub>2</sub> from biogas	16 kg
CO <sub>2</sub> produced by burning methane	44 kg
Total GHG emissions (CO <sub>2</sub> equivalent)	16+44 = 60 kg
*Methane is 21 times more polluting gas than CO <sub>2</sub> , thus 2.9 kg CH <sub>4</sub> = 60.9 kg CO <sub>2</sub> equivalent	

A calculation based on previous research [15–17] is stated in Table 1.1, which suggests that anaerobic digestion (after power generation) amounts to 55.4% less CO<sub>2</sub> equivalent than aerobic digestion for 1 ton of cow dung. Since CH<sub>4</sub> is 21 times more polluting than CO<sub>2</sub> when released directly into the atmosphere, combustion of methane is recommended. Additionally, the digestate, also known as digested manure, generated by anaerobic digestion exhibits enhanced stability and reduced odor compared to untreated manure. The rationale

for breaking complex organic molecules in manure into simpler and more stable ones is attributed to the anaerobic digestion process.

#### 1.4 Biogas

Systems for producing biogas, as opposed to biodiesel and bio-ethanol, are straightforward and may be operated on a wide range of scales in urban and rural settings. Global experience implies biogas technology is relatively simple to create and sustain. The technology is considered functional, adaptable, and acceptable in the locale. To replace traditional fuels like kerosene oil, cattle dung cake, agricultural leftovers, and firewood, biogas generated by anaerobic digesters is increasingly used in developing nations [18].

The current methods of disposing of manure slurry and food leftovers result in spontaneous methane emissions. According to research, agricultural emissions are responsible for around a third of the global greenhouse impact. Animal waste produces approximately 20-30 million tonnes of methane annually. A well-managed Anaerobic digestion (AD) plan might maximize methane output without releasing any gas to the environment, and these gases can be utilized as fuel using AD technology for the treatment of animal waste. By replacing fossil fuels with renewable energy, AD technology helps the environment in other ways, such as lowering carbon dioxide emissions. Its high Global Warming Potential (GWP) makes nitrous oxide emissions detrimental to climate change. A recent study indicates that AD of animal manure significantly lowers nitrous oxide emissions by preventing emissions from manure storage, use of inorganic nitrogen fertilizer, and fertilizer manufacture [19].

Most biogas produced at small plants in developing countries is used for domestic purposes, such as cooking, lighting, heating (including space heating, water heating, and grain drying), cooling, etc., as given in Fig.1.6. Biogas and natural gas, while both composed mainly of methane, exhibit distinct combustion characteristics. This necessitates minor adjustments to equipment designed for natural gas when operating with biogas [20].

Zheng et al. (2019) performed an experimental greenhouse pot research that examined how biogas slurry irrigation affected tomato growth, yield, quality, and soil environment. The authors studied an inorganic fertilizer control and three biogas slurry concentrations (20%, 15%, and 10%). The tomato plants' physiological, ecological, nutritional, and soil indicators were measured. Regarding tomato output, quality, soil structure, and nutrient delivery, 20%

biogas slurry performed best. Slurry treatment holds the potential to be a viable alternative or supplement to replace inorganic fertilizer with biogas slurry [21].

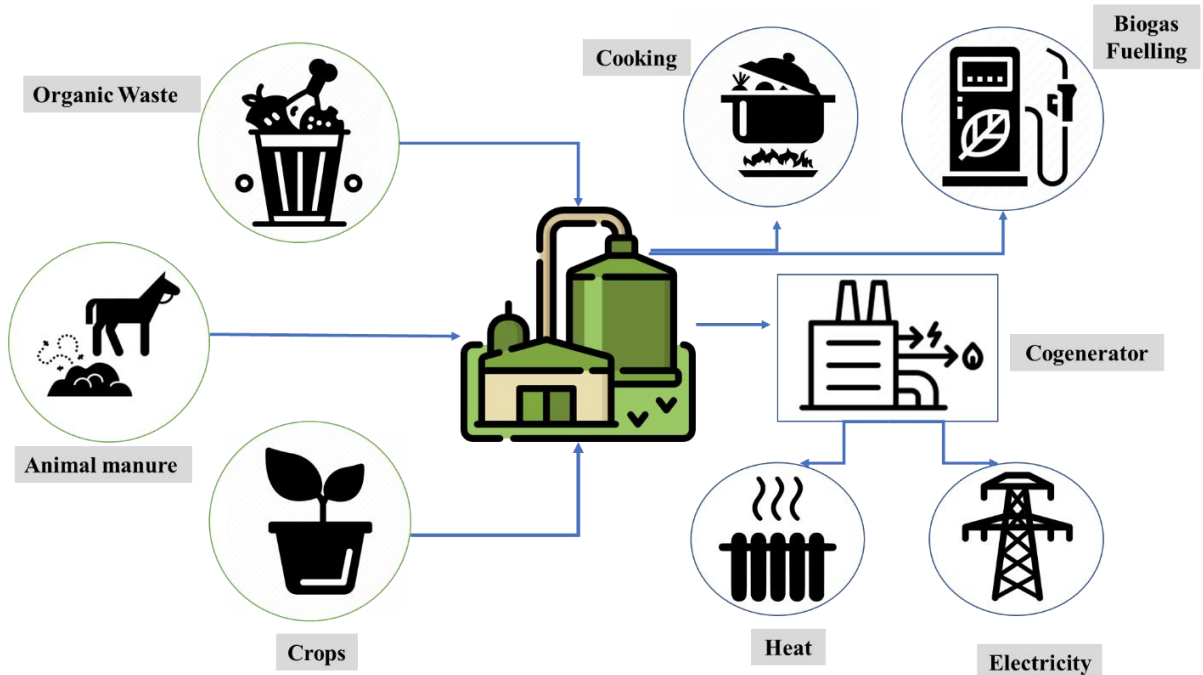


**Fig. 1. 6** Biogas Cycle

Biogas offers a vast range of utilization, as detailed below:

1. For both commercial and residential usage, biogas may be converted into usable heat or steam.
2. Biogas is an industrial energy source that may be utilized for a variety of purposes, including but not limited to heating, steam, power, cooling, etc.
3. Combined heat and power technology may be used to convert biogas into energy. Using this method, both electrical and thermal energy may be generated from the same fuel source.
4. Compressed enriched biogas may then be utilized as a transportation fuel in the form of biomethane.
5. Fuel cells employ an electrochemical process to transform chemical energy into electricity, and biogas may be used as a fuel for these cells.



### 1.5 Dual Fuel Concept

The dual fuel system is a CI engine upgrade, and its schematic diagram is given in Fig.1.7. Like a regular diesel engine, a carburetted mixture of air and high-octane index fuel is compressed in a dual-fuel diesel engine. Because of its high auto-ignition temperature, the compressed combination of air and vaporous fuel does not auto-ignite. As a result, it is released by a liquid fuel jet, which spontaneously ignites the charge towards the conclusion of compression. The gas-air combination near the injected spray ignites at various places, causing multiple flame fronts to form [22]. As a result, the combustion process begins smoothly and quickly. The quantity of liquid fuel required for adequate ignition is between 10% and 20% of the amount needed for operating only on liquid fuel [23]. Dual fuel combustion efficiently reduces toxic emissions from direct injection diesel engines, notably soot and  $\text{NO}_x$ . The disadvantage of this approach is that it uses a flammability differential between the fuels used. The downside is the need for liquid fuel for dual-fuel engine operation [24]. Thus, the dual fuel concept may be used to operate the readily available gaseous and liquid fuels fully.

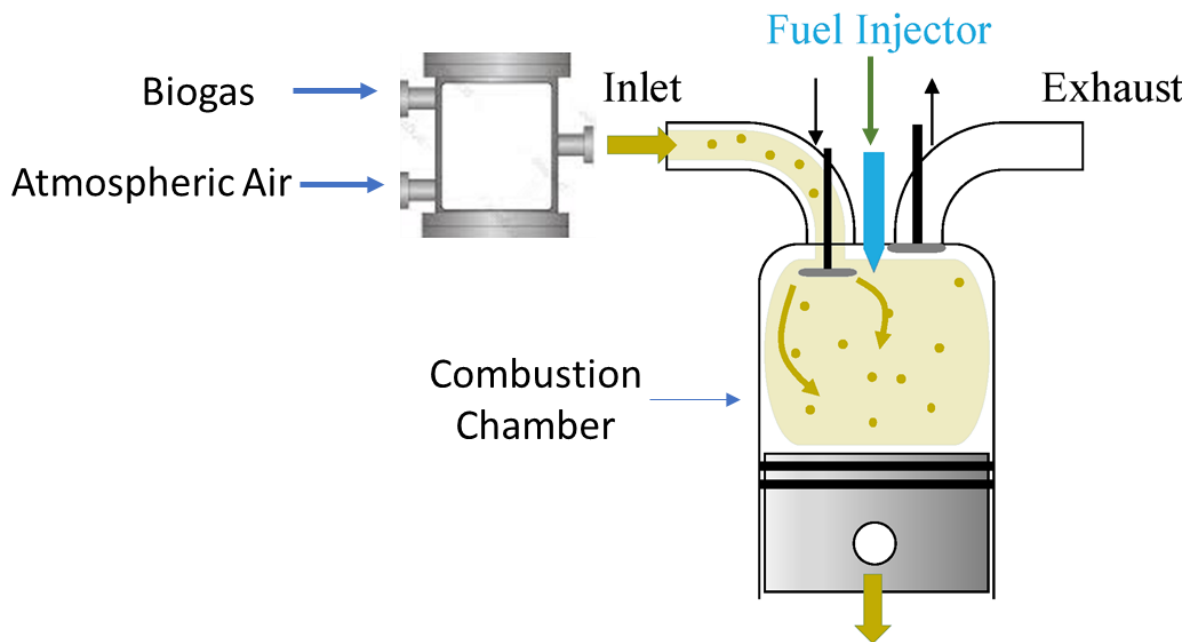


**Fig. 1. 7** Schematic diagram of dual fuel concept

## 1.6 Anaerobic digestion

This section elaborates on the metabolic steps involved in AD, as given in Fig.1.8, which include hydrolysis, acidogenesis, acetogenesis, and methanogenesis.

### 1.6.1 Hydrolysis

During the first phase of the anaerobic digestion process, the organic material undergoes hydrolysis. The hydrolysis step involves the breakdown of complex organic compounds, including carbohydrates, proteins, and lipids, into soluble organic molecules such as sugars, amino acids, and fatty acids. This process is facilitated by extracellular enzymes such as cellulase, amylase, protease, and lipase. The hydrolysis rate is influenced by several factors, including the size, shape, and surface area of organic material, the concentration of biomass, and the synthesis and adsorption of enzymes [25,26]. Post-hydrolysis, the substrate becomes accessible for cell transit, and fermentative bacteria break it down during acidogenesis. Improving the hydrolysis process is crucial to minimize the inefficient destruction of macromolecules, which may adversely affect digestion, biological activities, and biogas generation [27,28].

### 1.6.2 Acidogenesis

In the acidogenesis phase of anaerobic digestion, a wide range of fermentative microbes, both obligatory and facultative, decompose the monomers formed in the hydrolysis phase into weak acids, the majority of which are organic acids. Some examples of weak acids include lactic acid, alcohols, hydrogen and carbon dioxide (CO<sub>2</sub>), acetic acid, propionic acid, and butyric acid (VFAs) [29]. Half of the byproducts of the acidogenesis phase include acetic acid, 19% hydrogen carbonate, and 30% reduced products such as highly volatile fatty acids, alcohols, or lactate. The degradation pathway described herein offers a more significant energy yield for microorganisms, enabling direct utilisation of the resulting products by methanogenic microbes [30]. High organic acid generation during acidogenesis significantly impacts pH levels. The final product generated by acidogenic bacteria depends on the pH value and substrate concentration. Bischofsberger et al. (2003) state that neutral pH produces acetic acid, hydrogen, and carbon dioxide, whereas high substrate concentrations and pH  $\leq$  7 cause greater propionic and butyric acid production. If pH dips below 4.5, the process transforms into lactic acid generation. Preventing large concentrations of propionic and

lactic acid, which may hinder acetogenesis and methanogenesis, requires careful monitoring and management of the acidogenic process [31].

### 1.6.3 Acetogenesis

The process of third-stage anaerobic digestion encompasses the biochemical pathway known as acetogenesis. The acidogenesis process generates intermediates, namely short-chain acids, which are then used by bacteria participating in the acetogenesis reaction to make acetate, hydrogen, and carbon dioxide. During this particular stage, the coexistence of acetogenic and methanogenic bacteria occurs due to the ability of methane-producing microorganisms to remove hydrogen ( $H_2$ ), which would otherwise hinder the growth and activity of acetogenic bacteria [32].

Increased hydrogen production lowers pH, which inhibits acetogenic bacteria, which need a neutral or slightly alkaline environment to absorb energy. Hydrogen levels are controlled by hydrogenotrophic methanogenic bacteria, which produce methane from hydrogen and carbon dioxide. Low hydrogen generation from acetogenesis inhibits hydrogenotrophic methanogenesis because of substrate constraints. The low hydrogen consumption of methanogenesis further diminishes the possibility of acetogenesis in acidic environments. In the acetogenesis process, called acetogens, bacteria grow slowly, are anaerobic, and function best at a pH range of roughly 6 [33].

### 1.6.4 Methanogenesis

About 70% of the methane utilized in AD is produced at this step. Hence, it has a significant effect on the process overall. Acetoclastic methanogens use acetate to create methane, whereas carbon dioxide-reducing and hydrogen-oxidizing methanogens convert hydrogen and carbon dioxide to methane. Biogas, which is produced when methanogenic bacteria feed on these byproducts, is typically 50-75% methane ( $CH_4$ ), 50-25% carbon dioxide ( $CO_2$ ), and trace quantities of nitrogen, hydrogen ( $H_2$ ), and hydrogen sulfide ( $H_2S$ ). Methanogenesis indicates the level of biological activity and digestion in anaerobic systems. The more methane is generated, the more reliable and effective the system becomes [28].

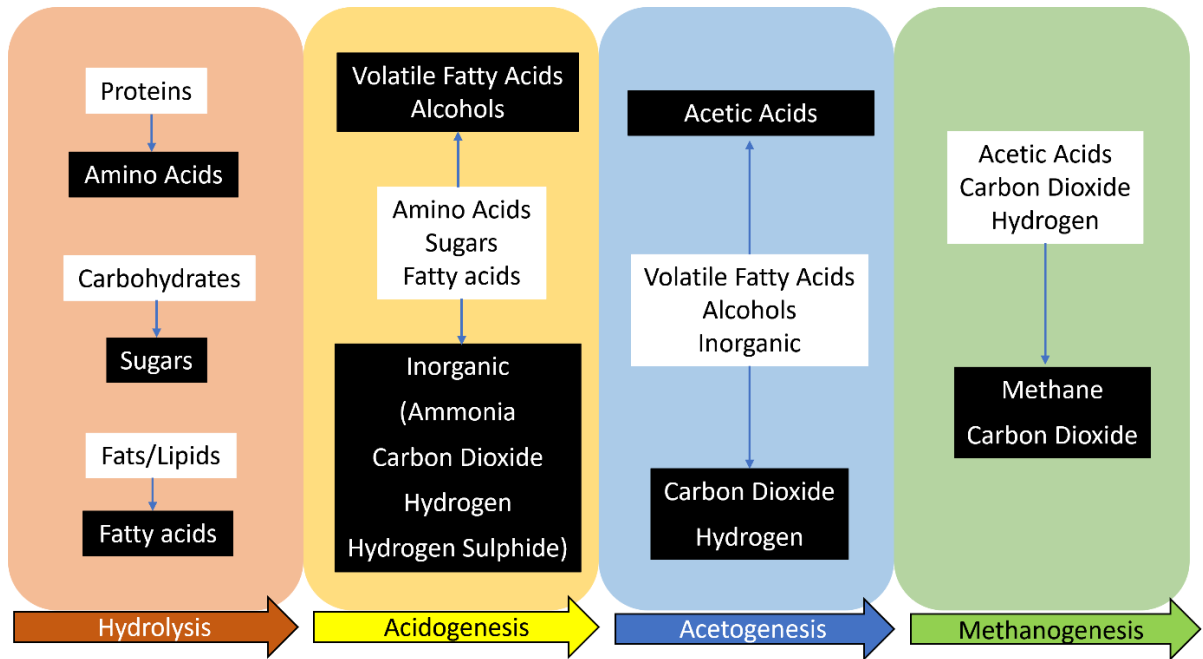


**Fig. 1. 8** Stages of an Anaerobic Digestion System

### 1.7 Factors Affecting Biogas Production

The digestion rate and the amount of biogas that may be produced from an anaerobic digester are both affected by the physical conditions inside the digester, as given in Fig.1.9. As a result, it's crucial to keep an eye on the following factors within permissible limits:

#### 1.7.1 Temperature

An anaerobic digestion system's efficiency (rate of substrate breakdown and gas generation rate) is drastically impacted by the temperatures at which its reactor operates since the anaerobes that produce Anaerobic digestion are temperature sensitive. Biogas may be produced at temperatures between 0 and 97 degrees Celsius, as stated by Dhaked et al. (2010). Anaerobic digestion relies on various microorganisms, each thrives in a specific temperature range [34]. Bacteria that thrive between 10 and 20 degrees Celsius are called psychrophilic. In contrast, those that thrive between 20 and 35 degrees Celsius are called mesophilic, and those that thrive between 45 and 60 degrees Celsius are called thermophilic [35]. Previous research has shown that in the mesophilic and thermophilic temperature ranges, anaerobic bacteria are the most active microorganisms [36]. The research shows that the system's effectiveness drops in a mountainous terrain at low temperatures. Insulation is used in the installation of most methane digesters to ensure that temperatures remain stable [37].

### 1.7.2 Hydraulic Retention Time (HRT)

The HRT measures how long the substrate is kept within the biogas digester before it is released. Retention time affects the reproduction rates of bacteria, which decompose organic matter and release the gas.

$$\text{HRT} = V_D/V_F \text{ days} \quad (1.1)$$

where  $V_D$  indicates the digester volume( $\text{m}^3$ ) and  $V_F$  indicate the feed rate( $\text{m}^3/\text{d}$ )

The optimal HRT for biogas generation varies with the substrate being utilised. Based on several previous research, the optimal duration of HRT was proposed to be between 16 and 60 days. HRT durations below 10–25 days may result in losing vital process bacteria and should be avoided [38]. Low biodegradation rates mean complex substrates like animal manure require longer retention (20-30 days). In comparison, high biodegradation materials like food waste may only need shorter retention times (15 days) to convert the biodegradable organic matter into biogas [39].

### 1.7.3 pH

The pH scale was established to help differentiate between acidic and basic substances. Anaerobic digestion relies heavily on pH since different microbes have optimal growth conditions at various pH levels. When dealing with anaerobic processes, the pH level is a crucial indication. It shows how well the system functions, particularly how well digestion is holding up. An abnormally low pH level, which may indicate system failure or poor buffering capacity, might hinder digestion. Acidic environments are unfavorable to methanogenic microorganisms due to their detrimental effects on bacterial development and methane generation. VFA concentration, bicarbonate concentration, system alkalinity, and the proportion of  $\text{CO}_2$  in digester gas affect the pH value. Maximum biogas output in AD may be achieved in a rather broad pH range of 6.5–7.5, as shown by Liu et al. (2008) [40]. Several research has used strategies like water recirculation and the inclusion of alkaline additives (NaOH, lime, biochar) to keep the pH of each reactor stable [41].

### 1.7.4 Organic Loading Rate

A crucial process control parameter in AD systems used to treat organic wastes is the Organic Loading Rate (OLR), which is the the quantity of volatile solids (VS) put into the digester per time and, therefore, indicates the amount of organics that the system must handle.

$$\text{OLR} = V_S/V_D \quad (1.2)$$

Where  $V_S$  is the Volatile solid fed, and  $V_D$  is the Volume of the digester

Low biogas generation occurs when the process is under-loaded with a low feeding rate. Under-loading is safer to avoid process failure but is uneconomical since it does not entirely use process capacity. Increasing organic load increases biogas generation but runs the danger of overloading. Overloading the reactor tends to cause VFA buildup. High VFA concentrations lower pH and increase methanogen toxicity, perhaps ending the AD process. Both under-load and excess cause process imbalance in anaerobic digesters [42,43].

### 1.7.5 Substrate & Nutrients

Anaerobic digestion may employ a wide variety of biomass feedstocks, including biowaste, agricultural waste, human waste, municipal sewage, and animal manure. The biogas's quality and yield depend on the feedstock utilised [44]. COD or VS are common ways of gauging the amount of anaerobic substrate introduced. Since a significant portion of the input may be anaerobically nonbiodegradable, it is crucial to differentiate between the accessible degradable fraction (substrate) and the overall intake [45].

Nutrients are essential for developing microorganisms, which is necessary for effective biodegradation. There are two basic types of nutrients: micronutrients and macronutrients. Low methane yields, acidification, and process instability in crop mono digestion are only some issues that have emerged from insufficient nutrient concentration in energy crops, necessitating low OLR and extended HRT [46]. The macronutrient ratio of 600:15:5:1 (C: N: P: S) is appropriate to create a viable process. Micronutrients, such as Fe, Ni, Co, Mo, and W, are essential for microbial development but may be lacking in the feedstock. Thus, they must be provided as a supplement to the process [47].

### 1.7.6 Mixing

An efficient mixing system is essential for anaerobic processes to succeed. The system ensures close contact between raw and digesting sludges, maintains a uniform temperature and solids mixture, prevents scum formation and settlement, and promotes gas release in the lower digester regions. Due to mixing, the toxicity of the substances in the reactor is therefore reduced since they are spread out more. Extra carbon dioxide ( $\text{CO}_2$ ) has a negative impact at partial pressures over 0.2 atm, and the reduction of this gas is aided by mixing. By

reducing the size of hydraulic dead zones and stopping the accumulation of large pockets of unfavorable conditions for digestion (low pH and high VFA). Mixing helps create a uniform environment and fully uses the digester's space [28]. Poor mixing may cause stratification in the digester, resulting in the withdrawal of partly digested sludge [48]. Approaches for digester mixing include mechanical mixers, recirculating biogas, and recirculating reactor content. Mixing systems are selected based on several criteria, including substrate density, mixing frequency, uniformity, mixing apparatus accessibility and expenses, maintenance and energy usage charges, and other considerations [39].

### **1.7.7 Volatile fatty acids**

Volatile fatty acids (VFA) are a byproduct of the hydrolysis and acidogenesis processes of anaerobic digestion. Syntrophic acetogens and methanogenic microbes use compounds in the list as substrates during the acetogenesis and methanogenesis stages of anaerobic digestion, respectively. It is common to see elevated VFA levels during digester start-up or after an organic overload. This often means that they are harmful or otherwise obstruct productive behavior. Some VFA are hazardous to anaerobic microorganisms on their own, even though it is widely accepted that VFA inhibition results from their buildup and the resulting decrease in pH [49]. It's generally accepted that an unbalanced biogas process leads to a rise in VFA concentration. Because of this, it is often used as a gauge in the anaerobic digester [50]. Megido et al. (2021) and Almomani (2020) argue that VFA concentrations over 2000 mg/L and 1900 mg/L, respectively, hinder the formation of methane and the anaerobic digestion process [51,52].

### **1.7.8 C/N ratio**

The C/N ratio is a metric that gauges the nutrient accessibility within the digester for microbial development. Microbes utilize Carbon as a energy source, whereas nitrogen is required to promote optimal microbial development. A high C/N ratio results in low nitrogen levels, which impacts protein production, which is essential for developing microbial communities. This will lead to a decrease in gas output [53]. On the other hand, a low C/N ratio leads to a rise in ammonia. The pH of the substance will rise as a result, and at a level over 8.5, it becomes hazardous to the subjects of methanogenic bacteria, which inhibits the anaerobic digestion process [54]. Materials having a high C/N ratio, such as organic solid

waste, may be combined with materials with a low C/N ratio, such as MSW or animal manure, to keep the C/N level of the digester material within acceptable ranges [52,54].

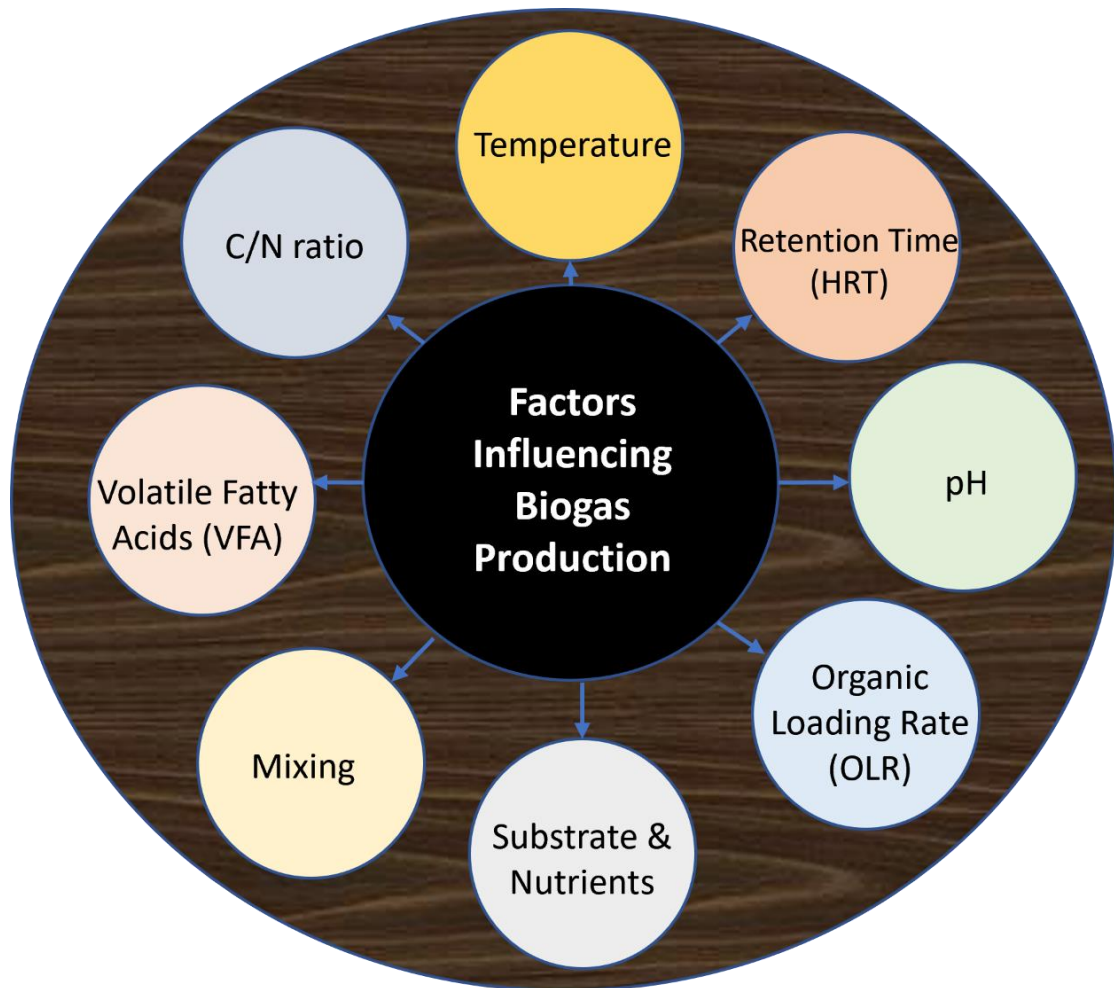


**Fig. 1. 9** Factors Influencing Biogas Production

### 1.8 Biodiesel

Methyl or ethyl esters of unsaturated fats in typical oils and fats that match the specifications for their use in CI engines are often converted into biodiesel. Biodiesel has evolved through four generations, each with its feedstock and technology. First-generation, made from edible crops, is familiar but faces land-use challenges. Second-generation uses waste materials, reducing conflict with food production. With its high-growth algae, the third generation holds immense potential but remains in its early stages. Finally, the fourth generation is still in its early stages of research and development but retains the potential to address some of the limitations of previous generations of biodiesel. The fourth generation employs genetically modified organisms and advanced conversion methods for even higher efficiency



but raises ethical and technological concerns. Each generation offers unique benefits and drawbacks, and the future likely lies in a mix of approaches as we strive for a sustainable future fuelled by biodiesel. As given in Fig.1.10, Vegetable oils or animal fats are often reacted with an alcohol such as methanol or ethanol in the presence of a catalyst to produce mono-alkyl esters, which are then refined into biodiesel. Glycerin is acquired as a by-product, extracted and may be utilised in personal care goods or a range of chemical applications [55]. Previous study states that oils derived from crops or animal fat are harmless and biodegradable. Because the feedstock used to produce biodiesel is so sensitive to weather and soil conditions, this alternative fuel source may not hold up well in the face of global warming and soil depletion. On the other hand, Biogas is a combustible fuel generated by the anaerobic decomposition of organic waste, such as manure, food scraps, and sewage sludge. The process often spans many weeks or months; however, the feedstock is easily accessible and continuously generated [56]. Even at ambient temperature, the high viscosity of straight mineral oils makes it challenging to produce a steady flow of fuel, and the presence of glycerin in vegetable oil leads to the accumulation of heavy carbon stores on the injector nozzle holes. The oil and fats must be processed into biodiesel for use in conventional Compression Ignition (CI) engines. Biodiesel contains minimal sulfur and aromatic ingredients and greater lubricity, Cetane number, flash point, biodegradability, and non-toxicity [57]. It has better lubricity than certain low-sulfur petro-diesels, which may reduce motor segment wear. Because it has a greater boiling point than diesel, biodiesel is also more user-friendly [58].

Biodiesel is a renewable, non-toxic, and environmentally friendly fuel that can replace petroleum diesel. It has many advantages over petroleum diesel, including:

- Reduces greenhouse gas emissions and air pollution
- Improves engine efficiency and performance
- Safer to handle and store
- Extends the life of diesel engines
- Provides a domestic and renewable source of energy
- Supports agriculture and rural economies

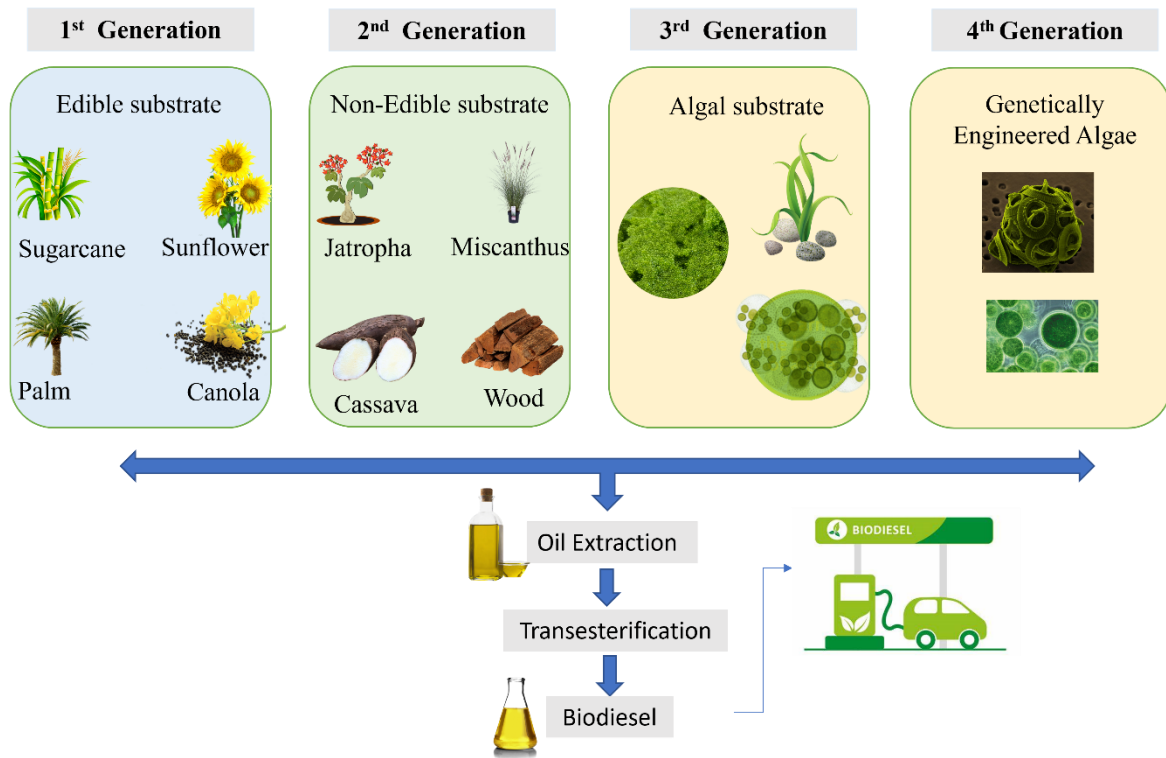


**Fig. 1. 10** Biodiesel cycle

### 1.9 Nanoparticles

There has been a rise in interest in using fuel additives to enhance the oxidation properties of biodiesel, which may help it overcome its drawbacks. The combination of diesel/biodiesel with fuel additives holds the potential to increase combustion performance and reduce GHG emissions effectively. A nanofluid is a colloidal combination of nanoparticles dispersed in a base liquid. Typically, researchers consider particles between 1 and 100 nm in size to be nanoparticles.

The literature on nano-additives in diesel-biodiesel summarised by Elahi et al. (2018) concluded that using a specific concentration of nanofluid additives improves the thermophysical properties, heat transfer rate, and fuel mixture stability of an engine while also raising its performance parameters and decreasing its emissions of harmful byproducts [59]. Additionally, it was noted that the presence of oxygen inside the structure of nanoparticles, along with water in the form of an emulsion, leads to micro-explosions resulting from fast evaporation. This process generates fuel droplets of tiny size, hence enhancing the combustion capabilities [60]. In general, nanofluid exhibits elevated surface energy due to its expansive surface area, which facilitates the tendency for agglomeration and the formation of particles on a micro-scale before deposition. The stability and

homogeneity of a nanofluid suspension are essential phenomena for both scientific and practical purposes. Stability is crucial in manufacturing nanofluids since it directly impacts their performance as heat carriers and thermophysical characteristics. Numerous techniques have been documented in the literature to enhance the stability of nanoparticles in a base fluid. These approaches include ultrasonication, surface modification, surfactant incorporation, and pH regulation [61,62].

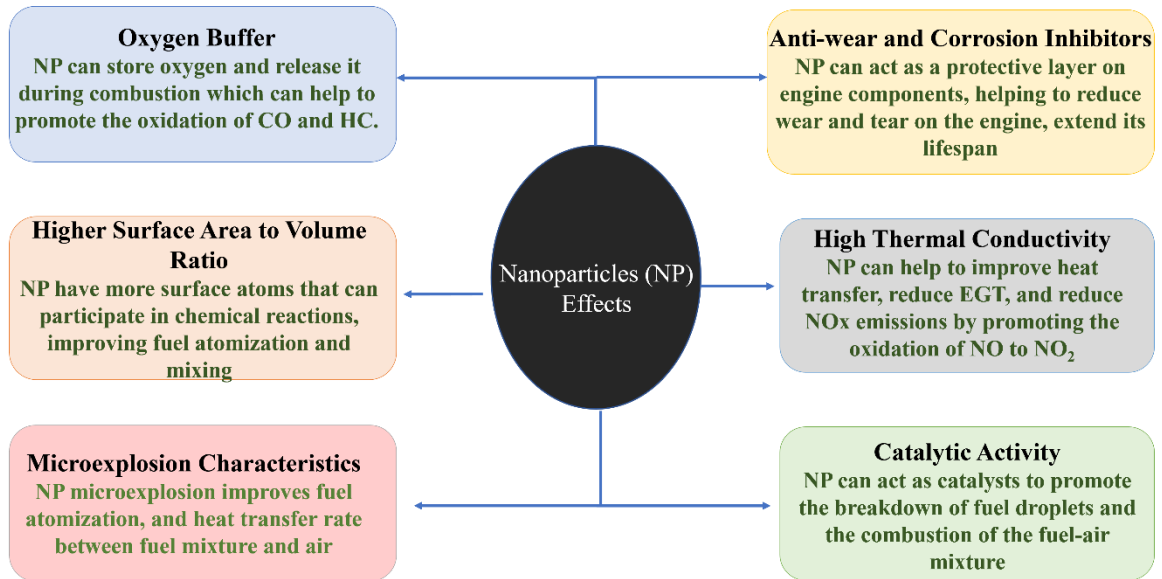


**Fig. 1. 11** Effect of Nanoparticles on CI Engine

Prior research has also highlighted the advantages of nanoparticles, including a faster rate of premixed combustion heat release, better thermal conductivity, and catalytic function, all of which work together to make CI engines more efficient, reduce pollutants, and lessen the prospect of Brake specific fuel consumption (BSFC) [63]. To date, there is a shortage of research examining the direct impact of nano-fuel on engine corrosion. However, prior investigations have demonstrated that nano-particles impede the accumulation of carbon and iron within the cylinder, thereby mitigating friction among the engine's diverse constituents. Consequently, this reduction in friction not only diminishes the occurrence of corrosion but also enhances overall engine performance [64]. A summary of the effect of Nanoparticles on the CI engine is given in Fig.1.11.

### 1.10 The Need for Regression Analysis and Optimization Techniques

Regression analysis is a statistical technique used to examine the association between a dependent variable and one or more independent variables. Regression tools such as

Response Surface Methodology (RSM) and Artificial Neural Networks (ANN) are powerful tools for identifying key variables affecting data insights. They help us understand the factors contributing to a particular outcome and evaluate their relative importance.

RSM is a statistical methodology used to optimise process parameters and predict response values. This approach yields enhanced repeatability of results and facilitates process improvement. This is achieved by enabling the analysis of the impacts of many factors and their interactions on multiple response variables. The methodology of Response Surface Methodology (RSM) is founded upon established regression concepts and variance analysis principles. These principles empower users to enhance, advance, and optimise the process or product being investigated [65]. ANNs are designed to mimic the structural organisation of the human brain. ANNs are composed of linked nodes referred to as artificial neurons. These neurons can transmit signals to other neurons via the connections established between them. ANNs can effectively represent intricate interactions between input and output variables, making them suitable for various tasks such as prediction, classification, and optimisation. ANNs can acquire knowledge from input data and enhance performance via iterative learning processes. ANNs can undergo training via several methods, including supervised learning, unsupervised learning, and reinforcement learning approaches [66].

The use of RSM proves to be advantageous in optimizing output parameters that include several independent variables and exhibit non-linear interactions among these variables. Genetic algorithms (GA) are a class of search heuristics that emulate the mechanism of natural selection to identify optimum solutions for optimisation issues. The GA starts by initialising a population of potential solutions, called chromosomes, which are encoded in a specific manner. The fitness of the chromosomes is then assessed, representing a quantitative evaluation of their ability to address the optimisation challenge at hand effectively. The fittest chromosomes are then chosen and used to develop novel solutions via the mechanisms of crossover and mutation. The procedure is iterated until a specified termination condition is satisfied, such as reaching a maximum number of generations or attaining a desired fitness value [65,66].

### 1.11 Dissertation Layout

The present work involves the production of biogas and biodiesel and the processing of its blends with nanoparticles to facilitate its utilization in the CI engine. This section provides a comprehensive overview of the work.

**Chapter 1** explores the underlying motivations for adopting alternative fuels, as well as the need for using regression analysis and optimisation techniques.

**Chapter 2** reviews biogas production and the optimization of its methane yield. This chapter also presents a literature review on the utilization of biogas, biodiesel, and diesel/biodiesel-nanoparticle blends in CI engines. Finally, it concludes with reviews on optimizing engine performance and emission parameters and identifying the research gap and objectives for the current work.

**Chapter 3** outlines the biogas-generating methodology used both on a lab scale and a larger scale. The chapter also discussed the biodiesel production process and the preparation of Nanoparticle blended fuels.

**Chapter 4** outlines the study of the intricate relationships between Temperature, Mixing Duration, and Feedstock, and their influence on the production rate and methane content of biogas.

**Chapter 5** outlines the analyses of the effects of Biogas, Biodiesel, and Nanoparticle blended fuels in CI engine. Additionally, the chapter offers the optimization of engine performance and emission parameters. The chapter also includes the analyses of the effects of enriched Biogas in the CI engine.

**Chapter 6** comprehensively summarizes the significant results derived from the conducted experiments. Additionally, this chapter presents suggestions for future research endeavors.

## CHAPTER 2: LITERATURE REVIEW

---

The Literature Review conducted in this study is classified into the following sections:

1. Production of Biogas
2. Optimization of Biogas Process Parameters
3. Biogas utilization in CI engine
4. Biodiesel and nanoparticle blended fuels utilization in CI engine
5. Optimization of Engine Performance and Emissions

### 2.1 Production of Biogas

Several researchers have undertaken studies on biogas production, as summarized in Table 2.1. **Achinas et al. (2018)** studied the biogas potential of animal slurries and investigated how the co-digestion of sheep manure and cow dung without inoculum affects the biogas production and methanogenic communities. Biogas output and quality were observed to be higher for cow dung. The co-digestion of cow dung and sheep manure improves biogas production compared to sheep manure alone but reduces it compared to cow dung alone. Methanobacteriales and Methanosarcinaceae are the dominant methanogens in cow dung and cow dung-based mixtures, while Methanomicrobiales are more abundant in sheep manure and sheep manure-based mixtures. Wet mono-digestion of Dutch cattle manure samples resulted in 64% CH<sub>4</sub> composition biogas (104 m<sup>3</sup> Mg<sup>-1</sup> VS) in 24 days at constant mesophilic conditions (36°C) with pH from 7.02 to 7.25. Meanwhile, the co-digestion sample with pH from 7.21 to 7.23 observed 61% CH<sub>4</sub> composition biogas (77 m<sup>3</sup> Mg<sup>-1</sup> VS) [67].

The **Cropgen project (2007)** demonstrated the feasibility of co-digesting cow manure with sugar beet tops, grass silage, and oat straw in terms of both biogas yield and quality. The study found that the highest proportion of total methane (CH<sub>4</sub>) potential, reaching 88%, was obtained by day 20 when digesting only manure. However, when co-digesting manure with sugar beet tops, grass silage, and oat straw, the CH<sub>4</sub> potential was reduced to 51%, 67%, and 68%, respectively. The study was carried out in laboratory CSTR under mesophilic conditions (35°C) for a period of 20 days. The best results were obtained with 30% VS of crops in the feedstock and an OLR of 2 kg VS m<sup>-3</sup> d<sup>-1</sup>. However, increasing proportions and loading rates have been shown to diminish the specific methane output and result in more undegraded matter remaining in the digestates [68].

**Li et al. (2009)** experimented with a 1 L laboratory-scale digester with 30 HRT for biogas production and process stability of co-digesting kitchen waste (KW) and cattle manure in laboratory-scale reactors. The study observed that co-digesting kitchen waste with cattle manure can significantly increase biogas production compared to digesting either substrate alone. This is because the two substrates have complementary compositions, with kitchen waste high in carbohydrates and cattle manure high in nitrogen. The co-digestion process also helps to break down the lignin and cellulose in cattle manure, which is typically difficult to digest. A 44% increase in methane was reported for co-digestion compared to biogas production from kitchen waste alone. The methane output was 32% higher in the KW with NaOH added than the raw KW. This was because the buffering capacity and alkalinity improved [69].

**Zhou et al. (2016)** studied the effect of pH on Biogas production rate and methane composition. The study was done with a 1 L laboratory-scale digester with the feedstock as pig manure (7.8 % TS). The neutral pH control method biogas yield was observed at 16.6 L compared to 6.9 L for 6 pH and 9.7 for 8 pH. The methane content increase of 58.35% and 41.35% was observed for pH 7 compared to pH 6 and 8, respectively. The biogas production rate was also more stable and consistent at pH 7. The neutral pH control method reduced the accumulation of volatile fatty acids (VFAs) and ammonia in the digester, which are known to inhibit methanogenesis and cause pH fluctuations. The authors found that the neutral pH control method increased the diversity and richness of methanogens, especially those belonging to the orders Methanobacteriales and Methanosarcinales [70].

**Valvilin et al. (2005)** studied anaerobic co-digestion of municipal household solid waste (MHSW) and digested manure (DM) in mesophilic conditions using different waste-to-biomass ratios and mixing intensities (strong, moderate, and light). The study used a 2D distributed model to show how the initial distribution of waste and methanogenic biomass and the diffusion and advection of VFA affect the anaerobic digestion process. They found that at moderate waste-to-biomass ratios, low mixing intensity allows the formation and expansion of methanogenic zones that can consume VFA and produce methane. However, high VFA concentration inhibits methanogenesis in all zones regardless of mixing intensity at high waste-to-biomass ratios. Additionally, the study asserts if methanogenesis serves as the limiting factor in the first phase, it is advisable to refrain from using intense mixing, as this may hinder the development and spread of methanogenic centers across the reactor's

whole. If hydrolysis becomes the process's limiting factor, increasing the mixing level may potentially improve both methane production and solids degradation [71].

**Kaparaju et al. (2008)** investigate how stirring in small and big reactors at 55 °C can affect the biogas production from cow dung. The authors used two stirring techniques—constant and periodic—in a big plant and three—constant, minimal, and periodic—in small CSTRs. In batch testing with various substrate-to-inoculum ratios, they also looked at the effects of stirring speed (strong, moderate, and light). The scientists found that, in small reactors, minimum stirring improved biogas output more than periodic or constant stirring. Periodic stirring increased biogas output in the large plant by an average of 7% compared to constant swirling. Furthermore, it was observed that especially at high substrate-to-inoculum ratios, Light and moderate stirring intensity observed 13% and 36% more CH<sub>4</sub> than strong stirring. Strong stirring, they reasoned, could disrupt syntrophic connections and impede methanogenesis by uniformizing biomass distribution [72].

**Ogiehor et al. (2014)** experimented with biogas production from poultry waste using 2-liter laboratory-scale digesters for a period of 14 days. The researchers combined poultry waste and water to create slurries with varying solid concentrations (SC-10% to 25%). The researchers used a water bath apparatus to regulate the temperature of the digesting process, namely at 30°C and 35°C, the initial pH of the slurries altered to values of 5 to 9 utilizing acid or base solutions. The study reported higher biogas yield was observed at 35°C than at 30°C for all solids concentrations and pH values due to a higher rate of biodegradation and activation of methanogens at 35°C. The study reports that the highest gas yield occurred at pH 7 for 15% and 20% solids concentration, pH 8 for 10% solids concentration, and pH 9 for 25% solids concentration, while pH 7 was the optimum range for anaerobic digestion. The study also reports increased gas production with increasing solids concentration from 10% to 25%, except for a drop at 25% for pH 5 and 6 [73].

**Pandey et al. (2012)** investigate the effects of temperatures (25°C, 37°C, 52.5°C) on the biogas yield from anaerobic digestion of dairy manure using 250 ml laboratory-scale batch reactors. The study reports that 52.5°C resulted in the highest biogas yield and methane content, followed by 37°C and 25°C digestion. The study also observed that the pH increased at 52.5°C and decreased at 37°C and 25°C, while the solids reduction was also more significant at higher temperatures. The CH<sub>4</sub> concentration in biogas at a temperature of



52.5°C was nearly 70%, whereas at 37°C, it was around 55%. However, the methane content at 25°C was not determined due to the limited production of biogas [74].

**Karim et al. (2005)** studied how different modes of mixing (biogas recirculation, impeller mixing, and slurry recirculation) affect the performance of a 3.73 L working volume laboratory-scale digester with cow manure, temperature set at 35 °C and HRT of 16.2 days. The mixed digesters were also more stable and resilient to sudden changes in the feed slurry than the unmixed digester. Digesters fed and mixed by slurry recirculation, impeller, and biogas recirculation produced approximately 29%, 22%, and 15% more biogas than unmixed digester, respectively. The authors attributed the effect of mixing to better substrate distribution, heat transfer, and gas removal in the mixed digesters. The authors measured the amount of solids deposited in the digesters after the completion of the study. They found that the unmixed digester had more deposits and a higher percentage of volatile solids than the mixed digester, suggesting that mixing helps to avoid stratification and accumulation of inert solids [75].

**Chang et al. (2006)** utilized a laboratory-scale experiment to study temperature fluctuation effects on anaerobic digestion of municipal organic solid waste (MOSW). The experiment simulates heating failure by decreasing temperature from 55 °C to 20 °C. The low-temperature durations are 1, 5, 12, and 24 h respectively. The study shows how biogas production was affected by different durations of low temperature (20 °C) after a sudden drop from 55 °C. The biogas production almost stopped during the low-temperature period and resumed after the temperature recovery. The biogas composition also changed, with more CO<sub>2</sub> and less CH<sub>4</sub> during the low-temperature period [76].

## 2.2 Optimization of Biogas Process Parameters

Several researchers have conducted studies on the optimisation of biogas production, as summarized in Table 2.2. **Elagroudy et al. (2020)** used ANN and GA to simulate and optimise Jordan's Russaifah biogas plant digester. A two-layer artificial neural network (ANN) model was developed to simulate a digester and forecast methane generation. The ANN model predicted methane production with a 0.87 correlation coefficient. Methane's optimum concentration was 77%, more than the plant's 70.1%. Methane production was optimised at 36 °C, 6.6% TS, 52.8% TVS, and 6.4 pH [77].

**Kana et al. (2012)** carried out a study to model and improve biogas generation from sawdust(SD), cow dung(CD), banana stem(BS), rice bran(RB), and paper waste(PW) using an artificial neural network-genetic algorithm (ANN-GA) technique. Twenty-five mini-pilot biogas fermentations trained and tested a structured artificial neural network (ANN) with a 5-2-1 configuration. SD, CD, BS, and RB concentrations varied from 5% to 30%, while PW varied from 15% to 60%. Optimised substrate profiles predict biogas performance of 10.144 L at 25% BS, 25% CD, 25% PW, 5% RB, and 20% SD. The optimized profile produced 10.28 L biogas on the third day of fermentation (eight days for the non-optimized system), 8.64% more than the non-optimized system. The process non-linearity was correctly predicted using ANN and GA [78].

**Jacob et al. (2016)** investigated the viability of co-digesting industrial potato waste (PW) with the aquatic weed *Pistia stratiotes* (PS) to reduce acidity. PS and PW co-digestion at a 1:1 weight ratio at an SC of 5 g/L (2.5 g PW + 2.5 g PS) increased CH<sub>4</sub> output by 76.45% compared to PW mono-digestion. Synergistic effects were seen. Central Composite Design (CCD)-based Response Surface Methodology (RSM) and an ANN-GA model were used to optimise process parameters. Substrate concentration (SC- 7 to 11 g TS/L), Inoculum concentration (IC- 60 to 90 % VS/VS), and Cosubstrate proportion (CP- 50 to 70 %TS, w/w) were the selected input parameters. RSM optimization suggested optimal input of SC-7 g TS/L, CP- 52.02% (w/w) and IC 67.27% (VS/VS), while ANN-GA suggested optimal input of SC-7 g TS/L, CP-69.08% (w/w) and IC- 78% (VS/VS). On validation, the ANN-GA model optimal input exhibits a 6% higher value than when operated at RSM optimal predicted input [79].

**Akbaş et al. (2015)** conducted a study that created a novel model to anticipate and optimise biogas output and quality. The model makes use of neural networks and particle swarm optimization. It was evaluated using data from a Hurma Wastewater Treatment Facility (HWTF) in Antalya, Turkey. Sludge loading rate (SLR, 232-576 m<sup>3</sup>/day), Sludge retention time (SRT, 15.6-38.7 day), pH(6.6-7.3), Temperature(T,34.38-37.35°C) was selected as the input parameter, while biogas yield as the output. pH (6.6-7.3), Temperature(T,34.38-37.35°C), Total solid (TS, 22046-31951 mg/l), Volatile solid(VS, 4-167 mg/l), and Alkalinity (ALK, 2310-3966 mg/l) was selected as the input parameter, while methane percentage as the output. The optimal condition for biogas yield was observed at SLR-403.79 m<sup>3</sup>/day, T-35, ph-6.85, and SRT-18.3 days. The optimal condition for methane percentage

was observed at T-35.4, pH-6.86, TS-31751 mg/lt, VFA-8.78 mg/lt, and ALK-2754 mg/lt. The findings demonstrated that the approach can boost biogas output and quality, possibly resulting in increased power output at the plant [80].

**Zaied et al. (2023)** observed that Biogas from anaerobic co-digestion (ACoD) of palm oil mill effluent (POME) and cow dung (CM) is gaining popularity due to its vast availability and simple energy conversion. Simulation of the ACoD process is complex due to substrate mixing. Modern ACoD prediction methods include ANNs. PSO optimizes ANN parameters. The study investigates using the ANN-PSO framework to simulate and predict biogas production from POME and CM ACoD. The suggested technique predicts biogas output from POME and CM's ACoD. The ANN-PSO system's MSE was observed at 0.0143, and the correlation coefficient is 0.9923, indicating high-level accuracy and reliable prediction capability. The optimum biogas yield of 2462.72 mL was observed by combining 50:50 POME and CM with 1% hydrogen peroxide and 10 mg/L ammonium bicarbonate [81].

**Gopal et al. (2020)** carried out a study to improve biogas production from flower waste using response surface methodology (RSM) and artificial neural network (ANN). Additionally, the effects of physical treatment and chemical treatment were studied. Temperature (T, 35 to 55°C), pH (6.6 to 7.8), Substrate Concentration (SC, 80 to 120 kg), and Agitation time (AT, 1 to 9 s) were the selected input parameters. The RSM model was used to identify the optimal conditions for biogas production, which were found to be 100 kg SC, 50°C T, 7.2 pH, and 5 s AT. The prediction of the ANN model ( $R^2 = 0.999$ ) was more accurate than that of the RSM model ( $R^2 = 0.995$ ). Physical pretreatment was shown to have a greater efficacy in reducing COD, VS, TS, and biogas yield. Chemical pretreatment improved biogas production by increasing the biomethane kinetics and cumulative yield [82].

**Otieno et al. (2023)** experimented to optimize the anaerobic digestion parameters for biogas production when pineapple wastes are co-digested with cow dung and abattoir wastes. The study employs RSM statistical methods to analyze and also serve as a prediction model for the effects of temperature (20-30°C), pH (6-7.2), and mixing ratio of pineapple to livestock waste (1:1 – 1:3) on the biogas yield and composition. The study employs Rehau home gas systems of 6 m<sup>3</sup> capacity as the digesters installed at the Jomo Kenyatta University of Agriculture and Technology, Kenya. The study observed that optimal conditions for biogas production are 30°C, pH 6.0, and a pineapple waste ratio of 62.5%. Digester, when run on the optimal conditions generated, biogas exhibits 65.4% methane, 25.3% carbon dioxide,

and traces of other gases. It was observed that Temperature was the most significant or sensitive input parameter for determining biogas yield and methane composition, followed by pH and pineapple ratio [83].

**Beevi et al. (2014)** carried out a study to optimize biogas production from the organic fraction of municipal solid waste (OFMSW) using anaerobic digestion. The study employs the statistical technique of RSM, which is used to analyze the effects of independent inputs such as initial pH (6-7), substrate concentration (SC, 83-115 g TS/L), and total organic carbon (TOC, 16.67-23.87 g/L), and the output parameter selected was biogas yield. The study reports the optimum conditions for maximizing the biogas yield at a substrate concentration of 99 g TS/L, an initial pH of 6.5, and a TOC of 20.32 g/L. The F-value from the RSM model suggests substrate concentration exhibited as the most significant or sensitive input parameter for determining biogas yield and methane composition, followed by pH and TOC [84].

**Ingabire et al. (2023)** carried out a study for biogas production from anaerobic co-digestion of fish waste (FW) and water hyacinth (WH). The study used conical flasks of 250 mL as batch digesters and maintained the temperature at 37 °C for biogas production. They varied the substrate ratio (SR- WH: FW, 8:92 to 92:8), inoculum concentration (IC, 1.6-8.4 g), and dilution (D, 81.6-98.4 mL) according to a CCD. The RSM optimization showed that the optimum values for maximum biogas with the highest methane yield of 68% were a substrate ratio of 25:75 g (WH: FW), inoculum concentration of 15 g/250 mL, and dilution of 95 mL. The F-value from the RSM model suggests substrate ratio as the most significant or sensitive input parameter for determining biogas yield and methane composition, followed by IC and Dilution [85].

**Sathish et al. (2014)** conducted an experimental and analytical study to optimize the conditions for biogas generation from a 1m<sup>3</sup> floating drum anaerobic digester of rice straw using RSM. The authors investigated the effects of temperature (T, 40-60°C), pH (6.8-7.6), substrate concentration (SC, 90-130 kg), and agitation time (AT, 2-10 s) on biogas production from rice straw. The F-value from the RSM model indicates substrate concentration as the most significant or sensitive input parameter for determining biogas yield, followed by Temperature, pH, and Agitation time. The authors found that the optimal conditions for maximum biogas production were temperature (50°C), pH (7.5), substrate concentration

(110.75 kg), and agitation time (5 sec). Under these conditions, the biogas yield was 0.72 m<sup>3</sup> with a high correlation coefficient (R<sup>2</sup>) of 0.99513 [86].

### 2.3 Biogas in CI engine

To substitute or supplement diesel use in CI engines, biogas has emerged as an appealing fuel among the gaseous fuels explored over the years due to its more straightforward production method and widespread accessibility of its feedstock. Utilizing dual fuel in diesel engines allows for the use of raw biogas. Dual fuelling ensures adaptability, allowing an engine to run alone or on diesel with biogas added. There is an apparent financial gain because biogas partly replaces diesel. Given the aim of lessening the dependence on diesel fuel, adding biogas as a dual fuel in CI engines could make a vital difference [87].

The following authors in Table 2.3 modified a single-cylinder, four-stroke, direct-injection diesel engine to operate under dual fuel (DF) mode by connecting a gas mixer to the inlet manifold.

**Mahla et al. (2018)** observed that the BSEC is higher and the BTE is lower under DF mode at all engine loads. At full load, the BTE of dual fuel mode with a biogas flow rate of 3.2 kg/h was 19.6% compared with 23.8% in the case of diesel fuel. Based on the performance and emission criteria, they also identify the optimum biogas flow rate as 2.2 kg/h. They find that the NO<sub>x</sub> and smoke emissions are significantly lower under DF mode, while the HC and CO emissions are higher. They attribute these results to the effects of biogas composition, combustion temperature, and oxygen availability on the combustion process. At full load, the NO<sub>x</sub> level at an optimum biogas flow rate of 2.2 kg/h was 8 g/kWh when compared with 20 g/kWh for neat diesel fuel, while SO was 39% DF mode compared with 65% for diesel fuel [88].

**Ambarita et al. (2017)** utilized raw biogas of CH<sub>4</sub> 60% and CO<sub>2</sub> 40% of volume, named BG60M, while enriched biogas consists of 70% CH<sub>4</sub> and 30% CO<sub>2</sub>, named BG70M. The flow rate of the biogas is varied from 2 to 6 L/min. The author also shows that higher methane concentration in biogas results in higher output power, maximum brake thermal efficiency, and biogas energy ratio (BGES), suggesting biogas in the CI engine can reduce diesel fuel consumption significantly by up to 87.5%. The author shows that the specific fuel consumption of the CI engine run in DF mode is higher than in pure diesel mode because of the lower heating value and higher CO<sub>2</sub> content of biogas. The specific fuel consumption

decreases with increasing methane concentration in biogas. The study also shows that using biogas in the CI engine reduces SO emissions because of the lower soot formation from biogas combustion [89].

**Aklouche et al. (2017)** utilized raw biogas in a CI engine and observed that increasing equivalence ratio( $\phi$ ) resulted in lower peak pressure, longer ignition delay, higher heat release peak, and shorter combustion duration. They attributed these trends to the changes in the volumetric efficiency, charge temperature, flame speed, and chemical reactions of the biogas-air mixture. BTE increased, and the energy-specific fuel consumption (ESFC) decreased with increasing  $\phi$ , indicating a better combustion process and lower fuel consumption. The study reported that the emissions of HC, CO, NO<sub>x</sub>, and soot decreased with increasing  $\phi$ , while the emissions of CO<sub>2</sub> increased. DF mode comparison with conventional mode shows a reduction of NO<sub>x</sub> emissions of about 42% when  $\phi = 0.7$  [90].

**Barik et al. (2014)** used *Pongamia pinnata* de-oiled cake (PPDC), a waste by-product of biodiesel production, as the feedstock for biogas production using a floating dome-type digester. They also used cow dung as a co-substrate and inoculum for anaerobic digestion. They observed that DF operation had lower BTE, higher BSFC and energy consumption, and lower volumetric efficiency than diesel operation. The CO emission in the DF operation is considerably higher than that of diesel under all test conditions. Compared with diesel, the CO and HC emissions are higher by 24% and 41% with biogas, respectively, at a 1.2 kg/h flow rate at full load. However, Smoke opacity (SO) and NO<sub>x</sub> decrements by 49% and 39%, respectively, were observed for the engine run on a BFR of 0.9 kg/h compared to the neat diesel run [91].

**Senthil and Vivekanandan (2016)** compared the performance of a CI engine running on diesel alone to that of a combination of diesel and biogas (20% to 80%) under varying loads and maintaining a constant speed. Diesel's greater calorific value gave it better BP, BTE, and EGT than biogas-diesel mixes. Given biogas's lower energy content, diesel had lower BSFC than biogas-diesel mixtures. Conclusion of Biogas partially replacing diesel fuel, saving 40-50% at varying engine loads was drawn, and recommended 20% biogas + 80% diesel above various combinations [92].

**Salve et al. (2016)** studied dual-fuel CI engine performance utilizing synthesized biogas and diesel. Higher compression ratio and lower BFR enhance dual fuel mode BTE, resulting in higher BSFC than diesel mode. The dual fuel mode has lower cylinder pressure than diesel at all compression ratios. The heat release rate is greater in diesel than dual fuel and rises with compression ratio and load. Dual fuel mode delays crank angle owing to biogas combustion. It demonstrates that dual fuel mode CO and CO<sub>2</sub> emissions are greater than diesel mode, while compression ratio and load lower them. Diesel mode emits more NO<sub>x</sub> than dual fuel mode, and compression ratio and load enhance NO<sub>x</sub> emissions [93].

**Murugan et al. (2016)** explored dual fuel operation, where the diesel injection time was adjusted in increments of 1.5 °CA from 23 °CA bTDC to 27.5 °CA bTDC. The investigation discovered that dual fuel operation with injection timing of 26 °CA bTDC performed best. Increasing pilot fuel injection duration to 3 °CA in dual fuel operation improved BTE by 4.7% at full load. The CO and HC emissions were 2% and 10% higher than diesel at full load. NO<sub>x</sub> emissions were 33% higher at 26 °CA bTDC injection time than at 23 °CA bTDC but 16% lower than diesel at full load in dual fuel operation. Using dual fuel with an injection time of 26 °CA bTDC decreased smoke emissions by 39% compared to diesel at full load [94].

**Debabrata et al. (2017)** examined the impact of IT on the pilot fuel's performance (Karanja biodiesel - KME) by adjusting it in 1.5 °CA increments from 21.5 to 27 °CA bTDC (21 BDFM to 27 BDFM). The shortest combustion duration for dual fuel mode combustion was observed at BDFM24.5. While load lowers BSFC, biogas replacement increases it. Dual-fuel mode BDFM24.5 has the lowest BSFC but is higher than KME by 23.9%. The BDFM24.5 showed a 6.6% increase in BTE at full load compared to the BDFM23.0. BDFM24.5 reduces CO, HC, and smoke emissions at maximum load by 17.1%, 18.2%, and 2.1% compared to BDFM23.0 and increases by 5.5% for NO<sub>x</sub> [95].

**Gnanamoorthi et al. (2018)** studied biogas production from tamarind seed and rice bran (TSRB) for 1 month and compared it with cow dung. While TSRB doesn't quite match the biogas production of cow manure, it's still on par. Because of the lack of oxygen and the low energy input, biogas lowers the BTE and raises the BSFC. In comparison to diesel runs, biogas-powered engine runs see a decrease in smoke by 7.1% and NO<sub>x</sub> by 23.27% due to lower peak temperatures. In contrast, biogas-included operations lead to an increase in CO, CO<sub>2</sub>, and unburned hydrocarbon emissions from partial combustion and charge dilution [96].

## 2.4 Biodiesel & Nanoparticle blended fuels utilization in CI engine

Other alternative fuels, such as biodiesel, may also be used in diesel engines without modification, according to research on engine combustion, performance, and emissions utilizing Sunflower-soybean biodiesel. Due to its physiochemical characteristics, biodiesel has been extensively studied for its use in diesel engines, making it an appealing choice as a diesel fuel alternative. Oils from different sources, such as cooking oils and edible and non-edible oils, can be processed to create biodiesel [97]. Several researchers have conducted experiments using biodiesel and biodiesel-nanoparticle blended fuels in compression ignition (CI) engines, as summarized in Table 2.4.

**Rai et al. (2021)** experimented with a CI engine for analyzing the use of Shorea robusta biodiesel blended with diesel in BBR of B10-B40 (10%,20%,30%,40%). They observed a decrease in BTE of 1.57%, 4.6%, 5.43%, and 7.39%, respectively, for each blended fuel of B10 to B40 because of biodiesel's lesser calorific value (CV) than diesel. Brake Specific Energy consumption (BSEC) and NOX increase were observed with the rise in blend percentage, while the effect observed for CO and HC was vice versa. Higher oxygen availability with an increase in biodiesel blend can be attributed to more NO<sub>x</sub> formation and the factor for lesser CO due to better combustion [98].

**Kalam et al. (2001)** evaluate the performance and emissions of a diesel engine using coconut oil blended(B10-B50) with conventional diesel fuel. It has been observed that B10 to B30 blends produce a similar heat release rate as traditional diesel, although the average calorific value of biodiesel blends is about 6% lower than conventional diesel. This is expected as a slight increase in the density of biodiesel blends could result in ignition delay, which allows more fuel to mix within combustible limits during the delay. Exhaust emissions are reduced with increasing biodiesel blend rate, except CO<sub>2</sub>. HC emission of B50 was 33.3% lower than that of neat diesel at 3000 rpm and 100% load [99].

**Gogoi et al. (2011)** used various combinations of diesel and Koroch seed oil methyl ester and assessed a CI engine's performance and combustion characteristics. Because of the KSOME mixes' higher fuel consumption and lower calorific content, it was observed that BTE and BSFC were lower and higher, respectively, than those of diesel. BTE drop of 0.77%, 1.29%, 1.54%, and 3.31% observed for B10, B20, B30, B40 compared to diesel. BSFC increase of 3.23%, 5.57%, 6.79%, and 15.49% observed for B10, B20, B30, B40



compared to diesel. Due to the blends' early premixed combustion, biodiesel blends displayed peak pressures comparable to or slightly higher than diesel's and an earlier pressure rise. It was also discovered that the blends up to B30 had greater net heat-release rates and cumulative heat-release than diesel, but blends up to B40 had lower values. This was because the blends up to B30 had a higher fuel flow rate and combusted earlier, whereas B40 had a reduced combustion duration and heat release [100].

**Palanisamy et al. (2020)** examined several amalgamations of nanoparticles such as Aluminium Oxide (A), Cerium Oxide (B), Cobalt Oxide (C), and Magnesium Oxide (D) using a CI engine. Fueling the engine with a mix of A0.75C0.25 (A 0.75 g + C 0.72 g) showed the highest improvement in BTE at CR 15 and 16; however, at CR 17, A0.5C0.5 exhibited higher BTE. The mix of A 0.75C0.25 is concluded to be the best overall. Compared to diesel and other combinations, A0.25C0.75 exhibits lower CO emission characteristics in CR 15 and 17, and A0.75C0.25 in CR 16. Diesel and different combinations emit more CO<sub>2</sub> and NO<sub>x</sub> than all A-C combinations, where A0.5C0.5 excels at CR 15 and 16, whereas A0.25C0.75 excels at CR 17. Nanoparticles enhance engine performance and reduce emissions owing to shortened ignition delay factors, resulting from nanoparticles' better ignition attribute [101].

**Sathiamurthi et al. (2019)** studied adding Alumina (Al<sub>2</sub>O<sub>3</sub>) nanoparticles with a size of 50nm in diesel at NDR of 0.5g/L and 1g/L for use in the diesel engine. The 0.5g and 1g fuel additive mix resulted in a 13% and 7% reduction in BSFC, 22% and 52% reduction in HC, and 52% and 57% reduction in CO<sub>2</sub> compared to diesel. The 0.5g and 1g fuel additive mix resulted in 14% and 9% improvement in BTE compared to diesel due to improved combustion characteristics. Compared to other fuel additive combinations, diesel produces less CO [102].

**Basha (2014)** investigated the impact of incorporating alumina nanoparticles at NDR of 25-100 ppm into diesel fuel and conducting engine tests. The research demonstrates that using nano-additive fuel in engines decreases a number of undesirable engine characteristics, including ignition delay, cylinder pressure, heat release rate, BSFC, and toxic emissions (NO<sub>x</sub>, HC, CO, and smoke). Additionally, the study demonstrates that the nano-additive enhances the engine's braking thermal efficiency. 100ppm blended fuels were concluded to be the best overall, considering performance and emission [103].

**Sahoo et al. (2019)** studied the use of Copper oxide (CuO) nanoparticles fed at the rate of 0.5%(wt./wt.) to diesel for CI engine. The study reports that CuO-induced fuel blends have a higher flash point, density, and calorific value than neat diesel, which indicates better fuel quality and stability. An increment and decline of 6.7% and 6% for BTE and Brake specific fuel consumption (BSFC), respectively, were reported for nanoparticle blended fuels as opposed to a neat diesel run due to enhanced fuel characteristics in the form of flash point and heating value. CO, CO<sub>2</sub>, NO<sub>x</sub>, and HC were observed to reduce by 17%, 13%, 19 %, and 40%, respectively, for nanoparticle blends in contrast to neat diesel run [104].

**Yasar et al. (2019)** compare the results of using regular diesel fuel with those of adding metallic nanoparticles such as titanium dioxide, copper nitrate, and cerium acetate hydrate at NDR of 25 ppm and 50 ppm. Nanoparticles enhanced gasoline's calorific value and cetane number but not viscosity or density. Except for CuNO<sub>3</sub>, which increased NO<sub>x</sub> release, other nanoparticles blended fuels reduced BSFC, CO, HC, and NO<sub>x</sub> emissions, engine vibration, and noise due to the higher heating value and surface area of metallic nanomaterial compounds. Fuel blends of cerium acetate hydrate decreased engine vibration and noise the most and reduced harmful emissions (excluding NO<sub>x</sub>). Compared to cerium acetate hydrate blends, copper nitrate fuel blends produced more NO<sub>x</sub> and were less effective in reducing vibration and noise [105].

**Fangsuwannarak et al. (2013)** use nano-titanium metalloid (TiO<sub>2</sub>) compound in a Diesel engine operating on commercial Diesel fuel (D) and B5 palm biodiesel. TiO<sub>2</sub>-based additives increased engine BP by 7.78% and 1.36% compared to pure Diesel and B5 fuels. Compared to pure Diesel, TiO<sub>2</sub> additives decreased BSFC by 13.22%. TiO<sub>2</sub> diesel fuel additives reduced NO<sub>x</sub>, CO, and CO<sub>2</sub> emissions due to metallic nanomaterial compounds' higher heating value and surface area [106].

**Suhel et al. (2021)** studied the use of Chicken fat biodiesel (B10, B20, B30) with the inclusion of ferrous ferric oxide (Fe<sub>3</sub>O<sub>4</sub>) nanoparticles (FO-50,100,150ppm) for its impact on CI engine outputs. At 4.13 bar BMEP, B30FO50 decreases CO emissions by 19.52%, B30FO100 by 56.66%, and B30FO150 by 34.28%. For B30FO50, B30FO100, and B30FO150 in the B30 mix, HC emissions are reduced by 6.81%, 22.72%, and 13.63%, respectively, when full BMEP is applied. For B10, nanoparticle blends B310FO50, B30FO100, and B10FO150 result in an BTE improvement of 1.05%, 2.13%, and 1.8%, respectively. B10FO100, B20FO100, and B30FO150 nano-additive blends show maximum

BSFC reductions of 8.10%, 10.64%, and 8.97% compared to non-additive blends. The optimum engine outputs were suggested for the B20-NDR 100 ppm blend [107].

**Kumaravel et al. (2019)** studied the use of Cerium oxide nanoparticle(50-100ppm) -infused biodiesel (B0-B20) generated from tyre oil in the CI engine. A drop in BTE of 0.6%, 1.5%, 2% and 2.5% for B5, B10, B15, and B20 were observed compared to pure diesel run due to the lower CV of biodiesel. An increment in BTE of 1.4% and 2% was observed for the B5 blend with 50 ppm and 100 ppm, respectively, due to the catalytic effect of nanoparticles, better atomization, and lower viscosity of nanoparticle fuel blends. The B5-100ppm fuel blends emit 1.4% more NO<sub>x</sub> than the B5 blend. A decline in SO emission of 6% was also reported for B5-100ppm blended fuel compared to neat diesel run due to enhanced ignition properties [108].

## 2.5 Optimization of CI engine parameters

Several researchers have conducted experiments on optimising the performance and emission of CI engines, as summarized in Table 2.5. **Mahla et al. (2020)** studied and analyzed the impacts of CR (16-18), engine load (20-100%), and BFR (1.2-3.2kg/h) on engine performance (BTE) and emission (SO, CO, HC, NO<sub>x</sub>) parameters were carried out in CI engine. BSEC when the biogas flow rate increased from 1.2 to 3.2 kg/h. A decline in SO by 40% and NO<sub>x</sub> by 45% was reported with an increment in BFR, while the effect observed for CO and HC was vice versa. The f-value from ANOVA for different outputs indicates that engine load is the most significant factor impacting the output among the input parameters, followed by BDR and CR. While lowering smoke, HC, and CO, increasing CR from 16 to 18 raises BTE by 16%. In all CR, diesel engines produced more NO<sub>x</sub> than dual-fuel runs. The optimum engine responses using RSM optimization were observed at 18 CR, 80% engine load, and 2.8 kg/h BFR [109].

**Ghanbari et al. (2021)** investigated the use of RSM in a CI engine about the amount of alumina nanoparticles NDR (40-160 ppm) and engine speed (800-1000rpm) as input factors and Brake power, Torque, BSFC, CO, HC, CO<sub>2</sub>, and NO<sub>x</sub> as its output parameter. The correlation coefficient ( $R^2$ ) was higher than 0.95 for all output models except NO<sub>x</sub> indicating high reliability and accuracy. The study observed an optimum value of output parameters for nanoparticles blend NDR at 160 ppm and 1000 rpm engine speed [110].

**Sekhar et al. (2018)** conducted a study to optimize biodiesel production from a sunflower-Pithecellobium dulce seed oil (SPD) through catalyzed transesterification. RSM was utilized to optimize the input variables of Reaction temperature (RTR, 55 to 65°C), Catalyst concentration (CC, 0.4 to 1.2 wt%), Reaction time (RT, 60 to 120 mins), and Molar ratio (MR, 1:3 to 1:9), resulting in a maximum biodiesel yield of 93.24% at MR-1:6, CC- 0.8 wt%, RTR- 60°C, RT- 90 mins. At 100% load, SPD-B20 shows a BSFC- 9.56% increase and, BTE- 2.08% drop compared to diesel. Raw Biodiesel and its blends utilization showed a decrease in HC emissions. Raw biodiesel utilization emits 33.82% less HC at full load than diesel fuel [111].

**Hosseini et al. (2020)** utilised waste cooking biodiesel (B5-B10) with the addition of Alumina nanoparticles (30-90 ppm) for an ANN study in the CI engine. The study observed an increment in BTE of 10.63% and a decrease in HC of 20.56% for the optimal fuel blend B10AL90. The ANN model could accurately predict engine responses (R values > 0.95). It has also been observed that the incorporation of nanoparticles reduces the amount of fuel used [112].

**Elkelawy et al. (2020)** conducted a study to optimize biodiesel production from a sunflower-soybean oil mixture through catalyzed transesterification. RSM was utilized to optimize the input variables of Agitation intensity (AI, 400 to 700 rpm), Catalyst concentration (CC, 0.3 to 1 wt%), Reaction duration (RD, 30 to 90 mins), and Methanol: oil (M:O, 150:1 to 250:1), resulting in a maximum biodiesel yield of 93.38% at M: O-203.5:1, CC- 0.57 wt%, AI-530 rpm, RD- 52 mins. RSM was also utilized to optimize the engine input variables of Brake power (BP, 0 to 7 kW) and Blend Rate (BR, 0 to 70%) for optimum engine performances, resulting in the optimal parameter of 2.05 kW BP and 70% BR. CI engine testing using biodiesel indicated that increasing the biodiesel blending rate resulted in lower CO, HC, and NO<sub>x</sub> emissions compared to diesel fuel, but higher CO<sub>2</sub> and SO emissions [113].

**Singh et al. (2020)** used RSM to optimise engine performance and emissions of a single-cylinder CI engine utilising a heterogeneous catalyst Calcium oxide (CaO) to produce Jatropha biodiesel. Load (0 to 12 kg), CR (14 to 18), and FIP (180 to 270) were the selected input parameters. An 81.6% yield was achieved using heterogeneous transesterification with a 5 wt% CC and a 12:1 methanol-to-oil. The f-value from ANOVA indicates that BTE and BP were most sensitive to load, followed by FIP and CR. Whereas HC and NO<sub>x</sub> were most susceptible to load, followed by CR and FIP. The RSM optimised engine parameters were

observed at 8.05 Kgf load, 18 CR, and 180 bar FIP. The B20-fueled engine performed similarly to diesel with HC emissions down 14.29% and NO<sub>x</sub> emissions up 1.98%. The projected and actual results for optimum engine combinations were satisfactory [114].

**Ardebili et al. (2020)** carried out an RSM study in a CI engine with input parameters of Fusel oil Fusel-derived biodiesel blend (B0-B20), engine speed (1800-2600 rpm), and Biochar nanoparticle (25-125 ppm). With a 20% increase in fusel oil concentration from 5%, improvements in NO<sub>x</sub> and HC of 20.51% and 14.6% were observed. By increasing the fusel oil concentration from 5% to 15%, an increment in CO of 33% was marked. A 9% fusel oil combination in diesel boosts engine BP by 5%. As the fusel oil ratio increases from 9% to 20%, the biodiesel blend run engine BP drops by 7.8%. The f-value from ANOVA for different outputs indicates that the biodiesel blend rate is the most significant parameter affecting the output among the input parameters. The optimized engine performance and emission outputs were monitored at B10 blend, 2300 rpm engine speed, and 100 ppm NDR [115].

Table 2. 1 Literature Review on Biogas Production

Authors	Parameters of Interest	Relevant Findings
<b>Achinas et al. (2018)</b>	Co-digestion of sheep manure and cow dung at constant mesophilic conditions (36°C)	Biogas output and CH <sub>4</sub> content were observed higher for cow dung (64% CH <sub>4</sub> biogas & 104 m <sup>3</sup> Mg <sup>-1</sup> VS), followed by co-digestion (61% CH <sub>4</sub> biogas & 77 m <sup>3</sup> Mg <sup>-1</sup> VS), and sheep manure (54% CH <sub>4</sub> biogas & 8 m <sup>3</sup> Mg <sup>-1</sup> VS)
<b>Cropgen project (2007)</b>	Co-digestion of cow manure(CM) with sugar beet tops(SB), grass silage(GS), and oat straw(OS) at 35°C	<ul style="list-style-type: none"> <li>▪ Highest proportion of total CH<sub>4</sub> potential was observed for mono-digested CM(88%), followed by Co-digestion of CM with SB (51%), GS (67%), and OS (68%)</li> <li>▪ Higher proportions of crops and OLR reduce CH<sub>4</sub> generation. The best result was observed at 30% VS of crops in the feedstock and 2 kg VS m<sup>-3</sup> d<sup>-1</sup> OLR.</li> </ul>
<b>Li et al. (2009)</b>	Co-digestion of kitchen waste(KW) with cattle manure at 35°C	<ul style="list-style-type: none"> <li>▪ A 44% CH<sub>4</sub> increase was reported for codigestion compared to biogas production from KW alone.</li> <li>▪ KW with NaOH added yielded 32% more methane than raw KW</li> </ul>
<b>Zhou et al. (2016)</b>	Effect of pH on pig manure AD at 38 ± 1 °C	<ul style="list-style-type: none"> <li>▪ At neutral pH, biogas output was 16.6 L, compared to 6.9 L at 6 pH and 9.7 at 8 pH.</li> <li>▪ Compared to pH 6 and pH 8, pH 7 had 58.35% and 41.35% more methane.</li> </ul>
<b>Valvilin et al. (2005)</b>	Effect of waste-to-biomass ratios and mixing intensities on Co-digestion of MHSW and DM at 37°C	<ul style="list-style-type: none"> <li>▪ At moderate waste-to-biomass ratios, low mixing intensity results in higher CH<sub>4</sub>.</li> <li>▪ Regardless of mixing intensity, high waste-to-biomass ratios results lower CH<sub>4</sub> generation.</li> </ul>

<b>Kaparaju et al. (2008)</b>	Effect of stirring duration (constant, minimal, and periodic) and intensity (light, moderate, strong) on biogas production from cow dung at 55°C	<ul style="list-style-type: none"> <li>▪ Optimum biogas output observed for Minimal stirring</li> <li>▪ Periodic stirring increased biogas output in the large plant by an average of 7% compared to constant swirling</li> <li>▪ At high substrate-to-inoculum ratios, Light and moderate stirring intensity observed 13% and 36% more CH<sub>4</sub> than strong stirring</li> </ul>
<b>Ogiehor et al. (2014)</b>	poultry waste and water to create slurries with varying levels of SC (10% to 25%) and pH (5 to 9) at 30°C and 35°C	<ul style="list-style-type: none"> <li>▪ Biogas yield was observed at 35°C than at 30°C for all SC and pH values</li> <li>▪ Highest gas yield occurred at pH 7 for 15% and 20% SC, at pH 8 for 10% SC, and pH 9 for 25% SC</li> <li>▪ Increase in gas production with increasing SC, except for a drop at 25% for pH 5 and 6</li> </ul>
<b>Pandey et al. (2012)</b>	Effects of temperatures (25°C, 37°C, 52.5°C) on the biogas yield from AD of dairy manure	<ul style="list-style-type: none"> <li>▪ 52.5°C resulted in the highest biogas yield and CH<sub>4</sub>, followed by 37°C and 25°C digestion</li> <li>▪ CH<sub>4</sub> concentration in biogas at a temperature of 52.5°C was nearly 70%, whereas at 37°C it was around 55%</li> </ul>
<b>Karim et al. (2005)</b>	Modes of mixing (biogas recirculation, impeller mixing, and slurry recirculation) for AD of cow manure at 35 °C	<ul style="list-style-type: none"> <li>▪ Slurry recirculation, impeller, and biogas recirculation produced approximately 29%, 22%, and 15% more biogas than unmixed digester.</li> <li>▪ The unmixed digester, compared to the mixed, had more solid deposits and a higher percentage of volatile solids</li> </ul>
<b>Chang et al. (2006)</b>	Effects of temperature fluctuation (55 °C to 20 °C) on AD of MOSW	<ul style="list-style-type: none"> <li>▪ Biogas production almost stopped during the low-temperature period and resumed after the temperature recovery</li> <li>▪ Biogas composition also changed, with more CO<sub>2</sub> and less CH<sub>4</sub> during the low-temperature period</li> </ul>

**Table 2. 2** Literature Review on Biogas Production Optimization

<b>Authors</b>	<b>Parameters of Interest</b>	<b>Relevant Findings</b>
<b>Elagroudy et al. (2020)</b>	ANN and GA to simulate and optimise Jordan's Russaifah biogas plant digester	<ul style="list-style-type: none"> <li>▪ The ANN model predicted methane production with a 0.87 correlation coefficient</li> <li>▪ CH<sub>4</sub> optimum concentration was 77%, more than the plant's 70.1%, and was optimized at 36 °C, 6.6% TS, 52.8% TVS, and 6.4 pH</li> </ul>
<b>Kana et al. (2012)</b>	SD, CD, BS, and RB concentrations were varied from 5% to 30%, while PW varied from 15% to 60%. Optimize for biogas generation using ANN-GA	<ul style="list-style-type: none"> <li>▪ Predicted biogas production of 10.144 L at 25% BS, 25% CD, 25% PW, 5% RB and 20% SD</li> <li>▪ The optimized profile produced 10.28 L (8.64% more than the non-optimized system), and biogas production started on the third day of fermentation (eight for the non-optimized system)</li> </ul>
<b>Jacob et al. (2016)</b>	PS and PW co-digestion and optimization using RSM and ANN for SC- 7 to 11 g TS/L, IC- 60 to 90 % VS/VS, and CP- 50 to 70 %TS, w/w	<ul style="list-style-type: none"> <li>▪ RSM optimization at SC-7 g TS/L, CP- 52.02% (w/w) and IC 67.27% (VS/VS)</li> <li>▪ ANN-GA suggested optimal input of SC-7 g TS/L, CP-69.08% (w/w), and IC- 78% (VS/VS)</li> <li>▪ On validation, the ANN-GA optimal input exhibits 6% higher than the RSM optimal input</li> </ul>
<b>Akbaş et al. (2015)</b>	ANN-GA Optimization of biogas yield at SLR, SRT, pH, T, and CH <sub>4</sub> at pH, T, TS, VS, ALK,	<ul style="list-style-type: none"> <li>▪ Biogas yield optimized at SLR-403.79 m<sup>3</sup>/day, T-35, ph-6.85, and SRT-18.3 days</li> <li>▪ CH<sub>4</sub> percentage was optimized at T-35.4, ph-6.86, TS-31751 mg/lt, VFA-8.78 mg/lt, and ALK-2754 mg/lt</li> </ul>
<b>Zaied et al. (2023)</b>	ANN-PSO framework to simulate and predict biogas production from POME and CM ACoD	<ul style="list-style-type: none"> <li>▪ ANN-PSO system's MSE is 0.0143, and the correlation coefficient is 0.9923</li> </ul>



		<ul style="list-style-type: none"> <li>▪ Optimum biogas yield of 2462.72 mL observed by combining 50:50 POME and CM with 1% hydrogen peroxide and 10 mg/L ammonium bicarbonate</li> </ul>
<b>Gopal et al. (2020)</b>	Optimize biogas production from flower waste using RSM and ANN. Parameters considered- T, SC, AT, pH	<ul style="list-style-type: none"> <li>▪ RSM optimized at 100 kg SC, 50°C T, 7.2 pH, and 5s AT</li> <li>▪ The ANN model (<math>R^2 = 0.999</math>) prediction was found to be more accurate than the RSM model (<math>R^2 = 0.995</math>)</li> </ul>
<b>Otieno et al. (2023)</b>	RSM optimization for the effects of temperature, pH, and mixing ratio of pineapple to livestock waste on the biogas yield and composition	<ul style="list-style-type: none"> <li>▪ Optimal conditions obtained at 30°C, pH 6.0, and pineapple waste ratio of 62.5%</li> <li>▪ Digester, when run on the optimal conditions generated, biogas exhibits 65.4% methane, 25.3% carbon dioxide</li> <li>▪ Temperature exhibited as the most significant input parameter for determining biogas yield and quality</li> </ul>
<b>Beevi et al. (2014)</b>	RSM optimization for the effects of pH, SC, and TOC on biogas yield and quality from OFMSW AD	<ul style="list-style-type: none"> <li>▪ Optimal conditions obtained at a SC of 99 g TS/L, an initial pH of 6.5, and a TOC of 20.32 g/L</li> <li>▪ SC exhibited as the most significant parameter for determining output, followed by pH and TOC</li> </ul>
<b>Ingabire et al. (2023)</b>	RSM optimization for the effects of SR, IC, D on AD Codigestion of Fish water and water hyacinth	<ul style="list-style-type: none"> <li>▪ optimum values for biogas yield with the highest CH<sub>4</sub> yield of 68% were an SR of 25:75 g, IC of 15 g/250 mL, and D of 95 mL</li> <li>▪ SR exhibited as the most significant parameter on output, followed by IC and Dilution</li> </ul>
<b>Sathish et al. (2014)</b>	RSM optimization for the effects of T, pH, SC, and AT on AD of rice straw	<ul style="list-style-type: none"> <li>▪ Optimal conditions obtained at T 50°C, pH 7.5, SC 110.75 kg, and AT 5 sec</li> <li>▪ Under optimal conditions, the biogas yield was 0.72 m<sup>3</sup> with a high correlation coefficient (<math>R^2</math>) of 0.9951</li> </ul>

Table 2.3 Literature Review on Biogas use in CI engine

Authors	Parameters of Interest	Relevant Findings
<b>Mahla et al. (2018)</b>	Effect of BFR(1.2 kg.h to 3.2kg.h)	<ul style="list-style-type: none"> <li>▪ At full load, the BTE of dual fuel mode with a BFR of 3.2 kg/h was 19.6%, while the BTE of 23.8% for neat diesel</li> <li>▪ Optimum biogas flow rate as 2.2 kg/h based on the performance and emission criteria</li> <li>▪ At full load, the NO<sub>x</sub> and SO emission at an optimum BFR of 2.2 kg/h was 8 g/kWh and 39%, while 20 g/kWh and 65% for neat diesel run</li> </ul>
<b>Ambarita et al. (2017)</b>	Biogas consisting of CH <sub>4</sub> 60% and CO <sub>2</sub> 40% of volume, while enriched biogas consists of 70% CH <sub>4</sub> and 30% CO <sub>2</sub>	<ul style="list-style-type: none"> <li>▪ Higher CH<sub>4</sub> in biogas results in higher BP, maximum BTE, and BGES</li> <li>▪ BSFC decreases with increasing CH<sub>4</sub> in biogas</li> <li>▪ Biogas in the CI engine can reduce diesel fuel consumption significantly, up to 87.5%.</li> </ul>
<b>Aklouche et al. (2017)</b>	Effect of equivalence ratio ( $\phi$ ) on engine performance and emission	<ul style="list-style-type: none"> <li>▪ Increasing <math>\phi</math> resulted in better combustion characteristics</li> <li>▪ BTE increased, and ESFC decreased with increased <math>\phi</math></li> <li>▪ HC, CO, NO<sub>x</sub>, and soot decreased with increasing <math>\phi</math></li> </ul>
<b>Barik et al. (2014)</b>	DF fuel- Biogas produced from co-digested PPDC and cow dung	<ul style="list-style-type: none"> <li>▪ CO and HC higher by 24% and 41% for DF run of BFR-1.2 kg/h at full load, compared with diesel</li> <li>▪ Decrements in SO and NO<sub>x</sub> by 49% and 39% for BFR-0.9 kg/h compared to the neat diesel run</li> </ul>
<b>Senthil and Vivekanandan (2016)</b>	BFR varied from 20% to 80%, the rest being diesel	<ul style="list-style-type: none"> <li>▪ Diesel had lower BSFC than biogas-diesel engine run</li> <li>▪ Biogas partially replacing diesel fuel, saving 40-50% at varying engine loads</li> </ul>

		<ul style="list-style-type: none"> <li>▪ 20% biogas + 80% diesel above various combinations for optimum engine performance and emission</li> </ul>
<b>Salve et al. (2016)</b>	Synthesized biogas BFR varied from 20% to 80%, the rest being diesel	<ul style="list-style-type: none"> <li>▪ high CR and low BFR of DF mode result in higher BTE and lower BSFC than diesel mode.</li> <li>▪ Dual fuel mode CO and CO<sub>2</sub> emissions exhibits greater than diesel</li> <li>▪ Diesel mode emits more NO<sub>x</sub> than dual fuel mode</li> </ul>
<b>Murugan et al. (2016)</b>	Injection time adjusted in increments of 1.5 °CA from 23 °CA bTDC to 27.5 °CA bTDC	<ul style="list-style-type: none"> <li>▪ 26 °CA performed best in DF mode, where BTE improved by 4.7% at full load compared to 23 °CA</li> <li>▪ At 26 °CA, DF mode CO and HC were 2% and 10% higher than diesel.</li> <li>▪ NO<sub>x</sub> was 33% higher at 26 °CA bTDC than at 23 °CA bTDC; however 16% lower than diesel in DF mode</li> </ul>
<b>Debabrata et al. (2017)</b>	Impact of IT from 21.5 to 27 °CA bTDC (21 BDFM to 27 BDFM) on KME and biogas DF run	<ul style="list-style-type: none"> <li>▪ Among DF run on different IT, BDFM24.5 has the lowest BSFC but is higher than KME by 23.9%</li> <li>▪ BDFM24.5 showed a 6.6% increase in BTE compared to the BDFM23.0</li> <li>▪ BDFM24.5 reduces CO, HC, and SO by 17.1%, 18.2%, and 2.1% compared to BDFM23.0</li> </ul>
<b>Gnanamoorthi et al. (2018)</b>	Biogas production from TSRB and utilization as DF	<ul style="list-style-type: none"> <li>▪ Though there is less biogas production than cow dung, TSRB as feedstock is comparable.</li> <li>▪ Biogas inclusion lowers the BTE and raises BSFC</li> <li>▪ Decrease in smoke by 7.1% and NO<sub>x</sub> by 23.27% for DF mode, compared to diesel run</li> </ul>

**Table 2. 4** Literature Review on Biodiesel, Nanoparticle blends use in CI engine

<b>Authors</b>	<b>Parameters of Interest</b>	<b>Relevant Findings</b>
<b>Rai et al. (2021)</b>	Shorea robusta biodiesel blended with diesel in BBR of B10-B40	<ul style="list-style-type: none"> <li>▪ Decrease in BTE of 1.57%, 4.6%, 5.43%, and 7.39% for B10 to B40, in comparison to diesel</li> <li>▪ An increase in BSEC and NO<sub>x</sub> was observed with the rise in BBR, while the effect for CO and HC was vice-versa</li> </ul>
<b>Kalam et al. (2003)</b>	Coconut oil blended Biodiesel (B10-B50)	<ul style="list-style-type: none"> <li>▪ The average calorific value of biodiesel blends is about 6% lower than conventional diesel</li> <li>▪ B10 to B30 blends produce a similar heat release rate as conventional diesel</li> <li>▪ For full engine loading, HC of B50 was 33.3% lower than that of diesel at 3000 rpm</li> </ul>
<b>Gogoi et al. (2011)</b>	Koroch seed oil methyl ester blends (B10 to B40)	<ul style="list-style-type: none"> <li>▪ BTE drop of 0.77%, 1.29%, 1.54%, and 3.31% observed for B10, B20, B30, B40 compared to diesel</li> <li>▪ BSFC increase of 3.23%, 5.57%, 6.79%, and 15.49% observed for B10, B20, B30, B40 compared to diesel</li> <li>▪ Blends up to B30 had greater net heat-release rates and cumulative heat-release than diesel</li> </ul>
<b>Palanisamy et al. (2020)</b>	Nanoparticles such as Aluminium Oxide (A), Cerium Oxide (B), Cobalt Oxide (C), and Magnesium Oxide (D)	<ul style="list-style-type: none"> <li>▪ Blends of A0.75C0.25 improved BTE most at CR 15 and 16, although A0.5C0.5 performed better at CR 17</li> <li>▪ A0.75C0.25 blends concluded as the overall best</li> </ul>

		<ul style="list-style-type: none"> <li>▪ Diesel and other combinations emit more CO<sub>2</sub> and NO<sub>x</sub> than all A-C combinations</li> </ul>
<b>Sathiamurthi et al. (2019)</b>	Alumina nanoparticles with a size of 50nm at NDR of 0.5g/L and 1g/L	<ul style="list-style-type: none"> <li>▪ 0.5g/L and 1g/L NDR fuel blends resulted in 13% and 7% reduction in BSFC, 22% and 52% reduction in HC, 52% and 57% reduction in CO<sub>2</sub> compared to diesel</li> <li>▪ 0.5g and 1g fuel additive blend resulted in 14% and 9% improvement in BTE compared to diesel</li> </ul>
<b>Basha (2014)</b>	Alumina nanoparticles at NDR of 25-100 ppm	<ul style="list-style-type: none"> <li>▪ Nano-additive fuel in engines ignition delay, cylinder pressure, heat release rate, BSFC, and emissions (NO<sub>x</sub>, HC, CO, and smoke)</li> <li>▪ BTE improved for the nanoparticle blends</li> <li>▪ 100ppm blended fuels were concluded to be the best overall, considering performance and emission</li> </ul>
<b>Sahoo et al. (2019)</b>	Copper oxide (CuO) nanoparticles fed at the rate of 0.5%(wt./wt.)	<ul style="list-style-type: none"> <li>▪ Nanoparticle blended fuels observed higher flash point, density, and calorific value than neat diesel</li> <li>▪ Increment and decline of 6.7% and 6% for BTE and BSFC were reported for nanoparticle blended fuels as opposed to a neat diesel run</li> <li>▪ CO, CO<sub>2</sub>, NO<sub>x</sub>, and HC were observed to reduce by 17%, 13%, 19%, and 40% for nanoparticle blends in contrast to neat diesel run</li> </ul>
<b>Yasar et al. (2019)</b>	Titanium dioxide, copper nitrate, and cerium acetate hydrate. Nanoparticles at NDR of 25ppm and 50 ppm	<ul style="list-style-type: none"> <li>▪ Nanoparticles blend enhanced calorific value and cetane number but not viscosity or density</li> </ul>

		<ul style="list-style-type: none"> <li>▪ Except <math>\text{CuNO}_3</math>, which increased <math>\text{NO}_x</math> release, other nanoparticles blended fuels reduced BSFC emissions of CO, HC, and <math>\text{NO}_x</math></li> <li>▪ Compared to cerium acetate hydrate blends, copper nitrate mixes produced more <math>\text{NO}_x</math> and were less effective in reducing vibration and noise</li> </ul>
<b>Fangsuwannarak et al. (2013)</b>	TiO <sub>2</sub> nanoparticles blended with diesel and B5 palm biodiesel	<ul style="list-style-type: none"> <li>▪ TiO<sub>2</sub>-based additives increased engine BP by 7.78% and 1.36% compared to pure Diesel and B5 fuels</li> <li>▪ TiO<sub>2</sub> blends decreased BSFC by 13.22% compared to diesel</li> <li>▪ TiO<sub>2</sub> blends reduced <math>\text{NO}_x</math>, CO, and CO<sub>2</sub></li> </ul>
<b>Suhel et al. (2021)</b>	Chicken fat biodiesel (B10, B20, B30) with the inclusion of ferrous ferric oxide ( $\text{Fe}_3\text{O}_4$ ) nanoparticle (FO-50,100,150ppm)	<ul style="list-style-type: none"> <li>▪ At 4.13 bar BMEP, B30FO50 decreases CO emissions by 19.52%, B30FO100 by 56.66%, and B30FO150 by 34.28%</li> <li>▪ For B30FO50, B30FO100, and B30FO150 in the B30 mix, HC emissions are reduced by 6.81%, 22.72%, and 13.63%, at highest BMEP</li> <li>▪ For B10, nano blends B310FO50, B30FO100, and B10FO150 result in an BTE improvement of 1.05%, 2.13%, and 1.8%, respectively</li> </ul>
<b>Kumaravel et al. (2019)</b>	Cerium oxide nanoparticle(50-100ppm) with tyre oil biodiesel (B0-B20)	<ul style="list-style-type: none"> <li>▪ Drop in BTE of 0.6%, 1.5%. 2% and 2.5% for B5, B10, B15, and B20 compared to pure diesel run</li> <li>▪ For B5, an increment in BTE of 1.4% and 2% for the B5 blend with 50 ppm and 100 ppm</li> <li>▪ B5-100ppm fuel blends emit 1.4% more <math>\text{NO}_x</math> than the B5 blend</li> </ul>

**Table 2. 5** Literature Review on Optimization of CI engine performance and emission

<b>Authors</b>	<b>Parameters of Interest</b>	<b>Relevant Findings</b>
<b>Mahla et al. (2020)</b>	CR (16-18), engine load (20-100%), and BFR (1.2-3.2kg/h)	<ul style="list-style-type: none"> <li>▪ A decline in SO by 40% and NO<sub>x</sub> by 45% was reported with an increment in BFR, while the effect observed for CO and HC was vice versa</li> <li>▪ Optimum engine responses using RSM optimization were observed at 18 CR, 80% engine load, and 2.8 kg/h BFR</li> <li>▪ F-value from ANOVA analysis indicates that among the input parameters, engine load is the most significant factor in impacting the output, followed by BFR and CR</li> </ul>
<b>Ghanbari et al. (2021)</b>	Alumina nanoparticles NDR (40-160 ppm) and engine speed (800-1000rpm)	<ul style="list-style-type: none"> <li>▪ R<sup>2</sup> was observed to be higher than 0.95 for all output models except NO<sub>x</sub>, indicating high reliability and accuracy.</li> <li>▪ Optimum value of output parameters for nanoparticles blend NDR at 160 ppm and 1000 rpm engine speed</li> </ul>
<b>Sekhar et al. (2018)</b>	Biodiesel yield optimization by RT, CC, RTR, and MR	<ul style="list-style-type: none"> <li>▪ Maximum biodiesel yield of 93.24% at MR-1:6, CC- 0.8 wt%, RTR- 60°C, RT- 90 mins</li> <li>▪ At 100% load, SPD-B20 observed a BSFC- 9.56% gain, BTE- 2.08% drop compared to diesel</li> <li>▪ At full load, pure PDSOME emits 33.82% less HC than diesel fuel</li> </ul>
<b>Elkelawy et al. (2020)</b>	Biodiesel yield optimization by M:O, CC, AI, RD	<ul style="list-style-type: none"> <li>▪ Maximum biodiesel yield of 93.38% at M:O-203.5:1, CC- 0.57 wt%, AI- 530 rpm, RD- 52 mins</li> </ul>

	Engine performance optimization by BP and BR	<ul style="list-style-type: none"> <li>▪ Increased BBR resulted in lower CO, HC, and NO<sub>x</sub> emissions compared to diesel fuel, although higher CO<sub>2</sub> and SO emissions</li> <li>▪ RSM engine performance at optimal value of 2.05 kW BP and 70% BR</li> </ul>
<b>Singh et al. (2020)</b>	Load (0 to 12 kg), CR (14 to 18), and FIP(180 to 270)	<ul style="list-style-type: none"> <li>▪ The B20-fueled engine performed similarly to diesel with HC emissions down 14.29% and NO<sub>x</sub> emissions up 1.98%.</li> <li>▪ F-value indicates BTE and BP are most sensitive to change in load, followed by FIP and CR. Whereas HC and NO<sub>x</sub> are most susceptible to changes in load, followed by CR and FIP</li> <li>▪ RSM optimised engine parameters were 8.05 Kgf load, 18 CR, and 180 bar FIP.</li> </ul>
<b>Hosseini et al. (2020)</b>	ANN Optimization Waste cooking biodiesel (B5-B10) + Alumina nanoparticles (30-90 ppm)	<ul style="list-style-type: none"> <li>▪ Increment in BTE of 10.63% and a decrease in HC and CO of 20.56% and 2.94% for the optimal fuel blend B10AL90</li> <li>▪ ANN model could predict engine responses with high accuracy (R values &gt; 0.95)</li> </ul>
<b>Ardebili et al. (2020)</b>	RSM optimization Engine speed (1800-2600 rpm), Fusel oil Biodiesel blend (BBR: 0-20%), and Biochar nanoparticle (NDR: 25-125 ppm)	<ul style="list-style-type: none"> <li>▪ At B20, NO<sub>x</sub> and HC improved 20.51% and 14.6% versus B5</li> <li>▪ At B15, CO increment of 33% versus B5</li> <li>▪ F-value indicates engine output is most sensitive to change in BBR</li> <li>▪ RSM optimized engine output observed at B10 blend, 2300 rpm engine speed, and 100 ppm NDR</li> </ul>



## 2.6 Research Gap

After an Exhaustive Literature review as discussed above, the following gaps in the literature are identified:

1. Very few studies have been conducted on utilizing segregated waste as feedstock for biogas production.
2. Co-digestion remains largely unstudied. The industrial application of co-digestion requires further work on selecting feedstocks and suitable mixing ratios.
3. The tumble motion for mixing the feed in the digester has not yet been studied.
4. The investigation of enhancing Biogas production and methane generation rate has not been extensively explored.
5. Limited studies have been conducted on the effects of combining nanoparticles blended fuel with biogas.
6. No research has been done on optimizing nanoparticles, biodiesel, and biogas' addition rate in a CI engine.
7. The exploration of utilizing enriched Biogas in the CI engine has been limited.

## 2.7 Objectives of the research

The present study aims to:

1. Characterization of different feedstock for identification of maximum yield of biogas.
2. Production Optimization of biogas from different feedstocks.
3. Preparation and Characterization of Biodiesel-Nanoparticle blended fuels.
4. Experimental investigation on utilization of raw biogas, Biodiesel-Nanoparticle blended fuels in a diesel engine under dual fuel mode.
5. To conduct an experimental study to investigate the use of enriched biogas as a fuel in a diesel engine operating in dual fuel mode.

## CHAPTER 3: MATERIALS AND METHODS

---

### 3.1 Research Methodology

To accomplish the research objectives, a systematically planned path is followed as mentioned below:

1. *Identify and characterize feedstock:* The feedstock is identified and characterized. This includes determining the feedstock's composition and testing feedstocks' physicochemical properties.
2. *Design and Fabricate the digester, control unit, and tumbling unit:* The digester, control unit, and tumbling unit are designed and fabricated. The digester is where the biogas will be produced, the control unit will monitor and control the process, and the tumbling unit will be used to mix the feedstock.
3. *Produce biogas from feedstock at different process parameters:* Biogas is produced at different process parameters. This helps to determine the optimal process parameters for producing biogas from the specific feedstock.
4. *Optimize biogas production process parameters:* The biogas production process parameters are optimized. This involves changing the feedstock, the digester, the control unit, or the tumbling unit.
5. *Produce biogas at a large scale with optimized parameters and enrichment of biogas:* Biogas is produced at a large scale with optimized parameters and enrichment of biogas. This involves building a larger digester. The biogas is enriched by removing carbon dioxide and hydrogen sulfide (H<sub>2</sub>S) to increase its energy content.
6. *Production of biodiesel from raw linseed oil and properties testing:* Biodiesel is produced from raw linseed oil, and its properties are tested. The properties of the biodiesel are tested to ensure that it meets the required standards.
7. *Characterization of nanoparticles:* Nanoparticles are characterized by their size, shape, and surface properties.
8. *Preparation of fuel blends of diesel/biodiesel and nanoparticles, and properties testing of the blends:* Fuel blends are prepared by mixing diesel, biodiesel, and

nanoparticles. The properties of the fuel blends, such as their viscosity and cetane number, are tested to ensure that they meet the required standards.

9. *Performance and emission evaluation of dual fuelling of fuel blends with biogas:* The performance and emissions of dual fuelling of fuel blends with biogas are evaluated. Dual fuelling is a technology that allows vehicles to run on a mixture of fuel and biogas.
10. *Optimization of engine parameters and addition of nanoparticles in biodiesel:* The engine parameters and the addition of biogas, nanoparticles, and biodiesel are optimized to improve the performance and emissions of dual fuelling.
11. *Result and discussions:* The results of the experiments are discussed in detail. This includes a discussion of the findings, the limitations of the study, and the implications of the findings.

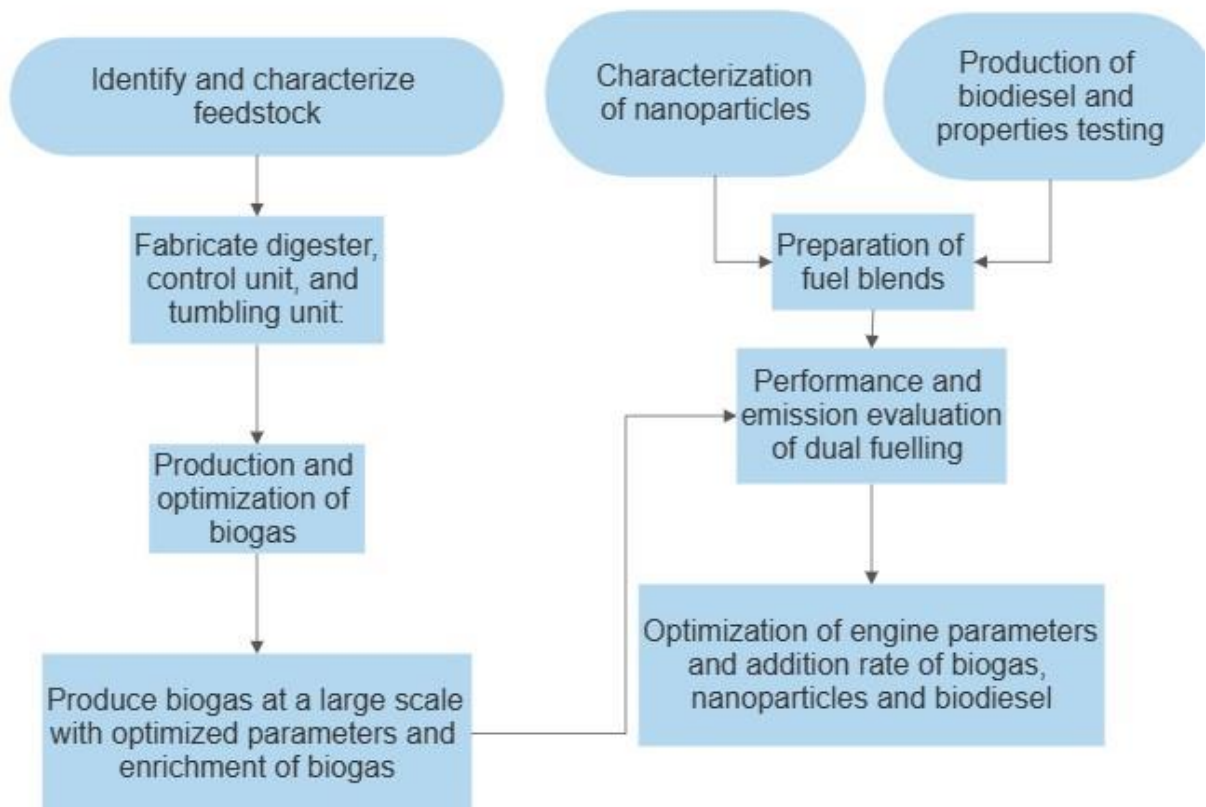


**Fig. 3. 1** Research Methodology

### 3.2 Biogas Production and Optimization

This section covers the essential components for biogas production, from waste collection and feedstock characterization to digestion systems, both lab-scale and large-scale. Then, it delves further into the biogas enrichment setup. This section further explores the process of transforming raw biogas into enriched biogas.

#### 3.2.1 Waste collection system

The research methodology for this project adopts a rigorous, multi-stepped approach to biogas potential analysis of Delhi Technological University Campus organic waste. An initiative was made to make DTU a zero-organic waste campus. The university campus underwent a comprehensive waste management makeover to kickstart its zero organic waste journey. The initiative began with strategically deploying 750 color-coded dustbins across the residential apartments and canteens. These 13-kg capacity bins were readily accessible, with blue color bins designated for dry waste and green color bins for wet organic waste, making it easy for users to segregate their discards right at the source. Following initial semi-segregation on campus, the study delves deeper by further partitioning the waste into three distinct categories: vegetable waste (VW), fruit waste (FW), and kitchen waste (KW). This meticulous segregation step serves as the cornerstone of the research, enabling a precise and targeted assessment of each waste stream's biogas production potential. By isolating and analyzing each category individually, the research gains valuable insights into the specific properties and biogas conversion efficiencies of different organic waste types.



(a) Distribution of Dustbin



(b) Color Coded Dustbin

**Fig. 3. 2** Distribution of color-coded dustbins on the university campus

### 3.2.2 Characterization of Feedstock

Kitchen waste, Vegetable waste, and Fruit waste were selected as feedstock for biogas production. Each waste was then mixed with cow dung in a ratio of 1:1. The physicochemical properties are given in Table 3.1. Here, kitchen waste indicates the leftover cooked foods. Vegetable waste covers the unused and discarded portions of vegetables. Fruit waste covers discarded or non-consumed items such as Peels, Cores, seeds, and pulp.

**Table 3. 1** Physiochemical Properties of Feedstocks

Parameters	Fruit waste (FW)	Kitchen waste (KW)	Vegetable waste (VW)
pH	5.6	6.4	5
Total Solids (%)	22	33	29
Volatile Solids (%)	19.5	22	27
Total Organic Carbon (%)	11.4	9.8	9.3
Chemical Oxygen Demand (mg/L)	76	82	105
Carbon-to-Nitrogen Ratio (C/N)	19.7	19.5	22

### 3.2.3 Lab scale Digester

As given in Fig.3.3, biogas digesters of 10-liter capacity are placed in a container filled with water. The dimensions of the digester are as follows: radius = 12.7 cm and height = 19.7 cm. The digester has an inlet feed pipe going inside, the opening of which is controlled by the inlet feed valve attached to the top of the container. An outlet feed valve is attached to the side wall of the digester. The digester is constructed with mild steel sheets covered with a specialised paint designed to improve heat retention. This paint is specifically formulated to capture solar heat, promoting the fermentation and conversion of organic waste inside the digester into biogas. The paint also has corrosion resistance properties, prolonging the digester's lifespan. The Biogas outlet valve and thermocouple holder are also attached to the top of the container. A standard and widely used temperature sensor in industrial applications is the thermocouple. Two wires, one made of one metal and the other of another, are joined at one end of the arrangement. Any variation in temperature at the point where the two wires meet causes a voltage to be generated, which is directly proportional to the temporal difference. It is possible to detect the voltage and utilise it to determine the temperature of

the surrounding environment. Biogas is collected from the outlet valve and stored in a collapsible 10-liter bag.

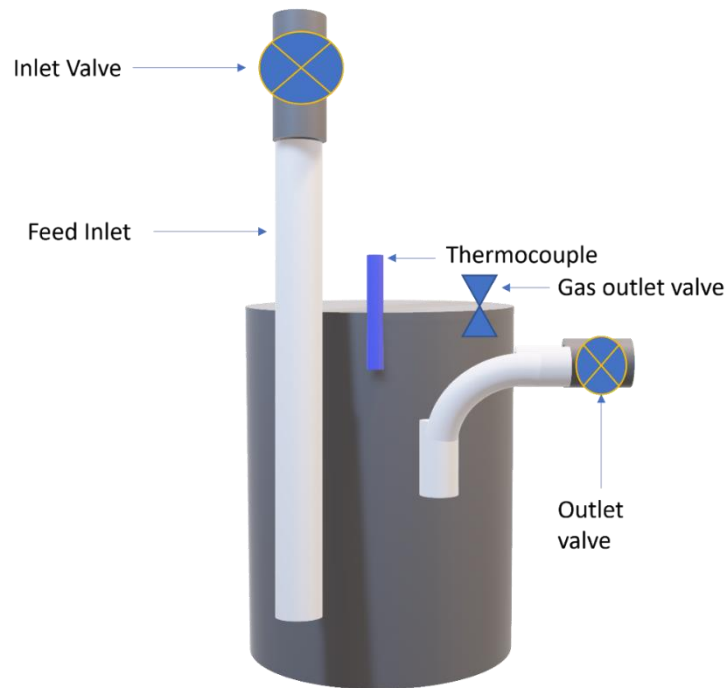


**Fig. 3. 3** Layout of Biogas Lab scale digester

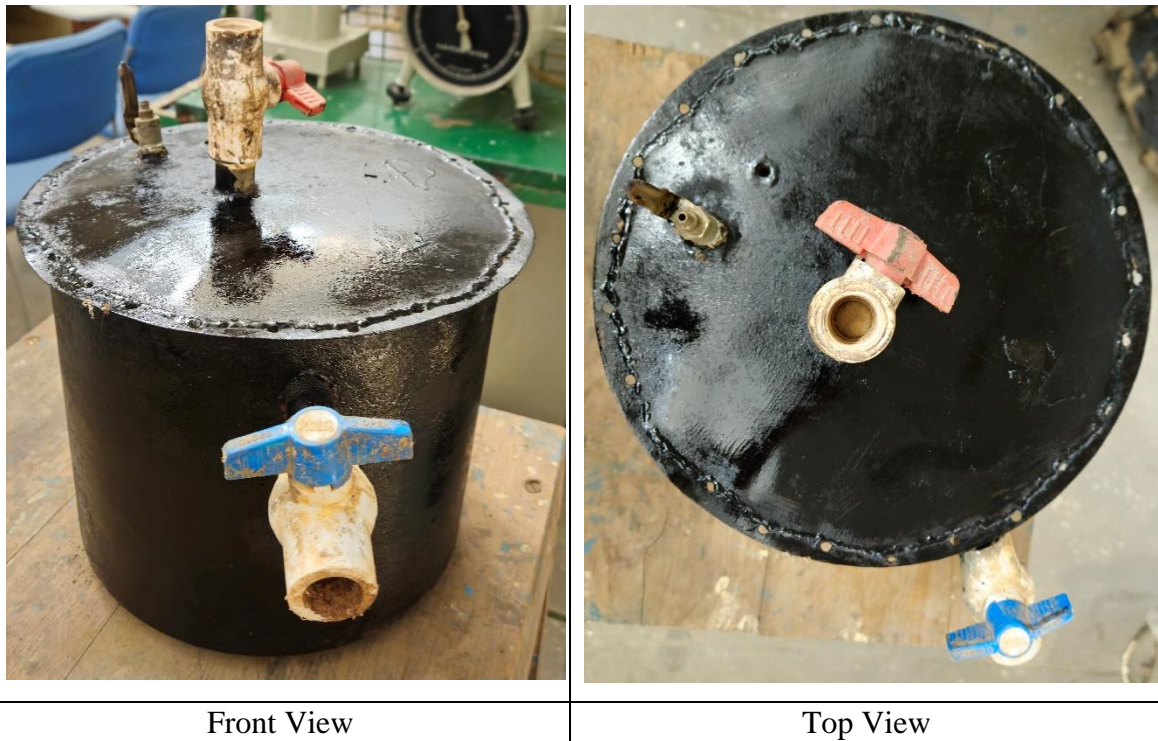


**Fig. 3. 4** Pictorial representation of Lab scale digester

### 3.2.4 Heating Container

In this configuration, three containers are used. Each container measures 1220 mm in length and 762 mm in width, as given in Fig.3.5. The biogas digesters are assembled within these three containers, with each container having the capacity to house three biogas digesters, resulting in a total of nine digesters, as given in the schematic layout of the biogas production setup in Fig.3.6.



**Fig. 3. 5** Biogas Digesters in a container of water

The containers are constructed to accommodate the digesters while guaranteeing that heat transmission is carried out effectively. The heat supplied to the biogas digesters is transported via the medium of water. Water is poured into the containers, and the heating element maintains the desired temperature. The containers are constructed in such a way as to guarantee an effective passage of heat to the biogas digesters, which is an essential condition for the anaerobic digestion process. One of the most typical practices in the generation of biogas is the use of water as a channel for the transmission of heat. The water is heated using the heating element, which transfers heat to the biogas digesters. This makes the fermentation process and the transformation of organic waste into biogas more efficient.

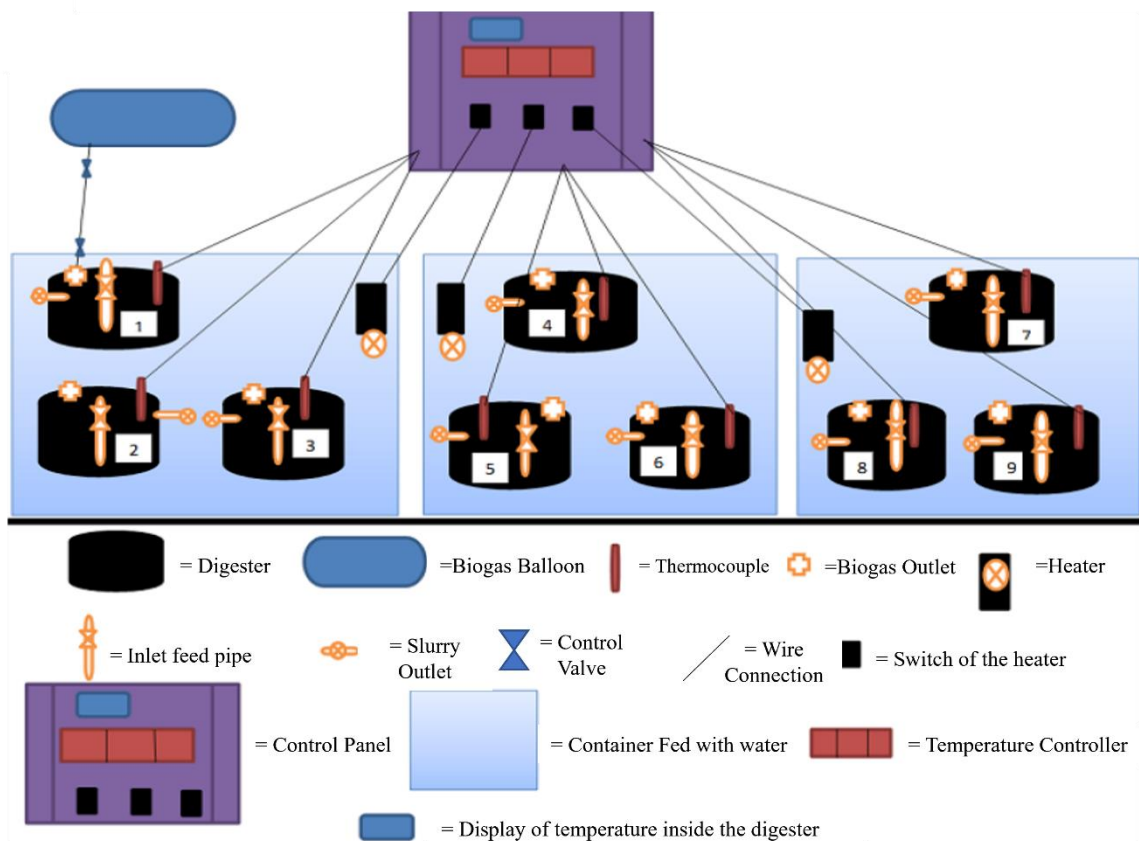


**Fig. 3. 6** Schematic Layout of the Biogas Production Setup

### 3.2.5 Temperature Control Panel

An immersion rod is used to heat the water in the container to the desired temperature, controlled by a temperature controller, as shown in Fig.3.7. The controller senses the water temperature through a thermocouple placed directly in the container and activates or deactivates the heater to maintain the desired temperature. Precise temperature control is a vital advantage of the temperature control system. It allows independent temperature management for each heating container, catering to the desired temperature requirements. The temperature controller can dynamically adjust the heating container's temperature to compensate for environmental changes, ensuring a stable temperature throughout the process.





**Fig. 3. 7** Temperature Control Panel

### 3.2.6 Large Scale Digester

The optimized parameters are then replicated on a larger scale, as given in Fig.3.8. A 230-liter oil barrel was chosen for the digester. The heating coil wrapped around the container was used to heat the digester at the desired temperature, as controlled by the thermocouple meter attached to the front panel. The front panel also constitutes an attachment for the gas outlet.

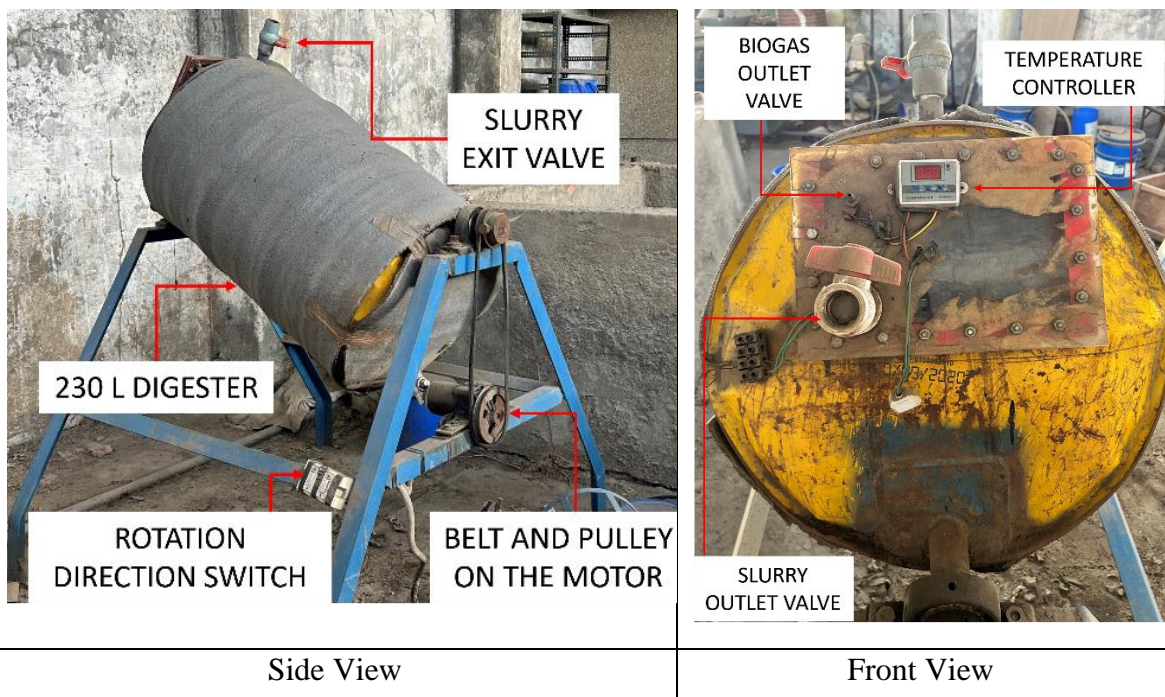


**Fig. 3. 8** Large-scale Digester with tumbling setup

### 3.2.7 Tumbling Setup

As given in Fig. 3.9, The tumbling setup consists of a digester holder, and the rotation arrangement was done through a belt and pulley on the motor. A provision was also made to control the direction of rotation, i.e., clockwise and anticlockwise. The motor can drive the digester holder at a speed of 12 rpm. A slow rpm motor was chosen to negate vigorous mixing, which holds the possibility of killing the methane-producing bacteria in the digester. While the small digester tumbling setup and large digester tumbling setup share a common motor, the belt and pulley are different for both.



**Fig. 3. 9** Biogas Tumbling setup

### 3.2.8 Biogas Enrichment Setup

To enrich the raw biogas, the gas is made to pass through the CO<sub>2</sub> scrubber, as shown in Fig.3.10. The scrubber has a water inlet pipe at the top, where the waste is dispersed in the



out of biogas management, having the benefits of instantly revealing its composition and quality from various sources like farms, landfills, and wastewater plants. Accurately measures methane content, the main primary content in biogas, with +/- 0.5% accuracy for the 0-100% range. It provides instant insights into methane content, letting the user fine-tune production. The analyzer measures other vital parameters like CO<sub>2</sub>, H<sub>2</sub>S, and O<sub>2</sub> for process control, emission monitoring, and compliance. The analyzer can store up to 500 readings and transfer data easily for analysis and reports.



(a) Raw Biogas

(b) Enriched Biogas

**Fig. 3. 11** Portable Biogas Analyzer

### 3.3 RSM Modelling for Biogas Production Process Parameters

The design of the Experiment (DOE) was prepared by applying the Central composite face-centered design (CCFCD) to the selected input variables and output parameters in Design Expert Software. Since each face in the design domain has axial points, the alpha is 1 for the model. The Central composite design (CCD) with alpha equal to 1 is termed CCFCD. The number of runs in the CCFCD for three inputs and five replicates translates to 20. The independent input variables selected and their coded levels are mentioned in Table 3.2. The levels for each input variable were determined based on prior studies.

**Table 3. 2** Input Parameters and Levels

Input Parameters	Units	Symbol	Levels		
			- 1	0	1
Temperature	°C	Temp	40	50	60
Mixing Duration	Min	MD	0	15	30
Feedstock			Kitchen Waste (KW)	Vegetable Waste (VW)	Fruit Waste (FW)

**Table 3. 3** Design of Experiment for Biogas Production Optimization

	Input 1	Input 2	Input 3	Response 1	Response 2
Run	Temp	Mixing Duration	Type of waste	CBP	CH <sub>4</sub> / CO <sub>2</sub>
Unit	°C	min		L	
1	50	15	KW	-	-
2	60	0	KW	-	-
3	50	15	VW	-	-
4	60	30	KW	-	-
5	40	0	KW	-	-
6	60	30	FW	-	-
7	50	15	VW	-	-
8	50	15	VW	-	-
9	50	15	FW	-	-
10	50	30	VW	-	-
11	50	0	VW	-	-
12	60	15	VW	-	-
13	40	30	FW	-	-
14	60	0	FW	-	-
15	40	0	FW	-	-
16	50	15	VW	-	-
17	40	30	KW	-	-
18	40	15	VW	-	-
19	50	15	VW	-	-
20	50	15	VW	-	-

### 3.3.1 RSM Modelling

RSM was evaluated using Design Expert Software by fitting a second-order polynomial equation (Eqn. 3.1) to the DOE experimental data to establish a correlation between independent inputs and dependent outputs.

$$Y = \beta_0 + \beta_1 x_1 + \beta_2 x_2 + \beta_3 x_3 + \beta_{12} x_1 x_2 + \beta_{13} x_1 x_3 + \beta_{23} x_2 x_3 + \beta_{11} x_1^2 + \beta_{22} x_2^2 + \beta_{33} x_3^2 \quad (3.1)$$

Y is the dependent output on the independent input factor of  $x_1$ ,  $x_2$ , and  $x_3$ .  $\beta_0$  represents the intercept coefficient of the polynomial Equation (Eqn. 3.1).  $\beta_1$ ,  $\beta_2$ , and  $\beta_3$  represent the linear coefficients for Temperature, Mixing Duration, and feedstock, respectively, while  $\beta_{12}$ ,  $\beta_{13}$ , and  $\beta_{23}$  are the interactive coefficients, and  $\beta_{11}$ ,  $\beta_{22}$ ,  $\beta_{33}$  are the quadratic coefficients. Analysis of variance (ANOVA) was used to determine model reliability and the contribution significance of each input variable in determining output responses. The interaction impact of input factors on output was studied using a 3D response surface plot, where two input interactions on output are studied at once, while the third input variable is kept constant. The RSM model prediction reliability is studied using the evaluation metrics defined in section 3.10. The Optimization of the RSM model is carried out by the desirability function as given in Section 3.8.

### 3.4 Experimental testing setup

The experiment utilised a 3.5 kW rated power, single-cylinder, four-stroke, constant-speed CI engine. An eddy current type dynamometer was employed to apply engine load. The engine load for this study ranges from 2.4 kg (20%) to 12 kg (100%). Rotameters were utilized to measure the flow of the cooling water. Airflow and fuel flow are measured using a manometer and a fuel flow meter, respectively. Temperature sensors (PT100) are installed at various engine cylinder locations to gather data continuously. These sensors are coupled with an NI unit, which records signals and transmits them to the computer using Engine Soft software. A gas-air mixing device is incorporated into the setup to enable dual fuel operation. The gas-air mixing system was built using the data from engine specifications, given in Table 3.4. Fig. 3.12 and 3.14 provide a schematic layout and pictorial representation, respectively, of the test setup after modification. Fig. 3.13, on the other hand, presents the visual representation of the test rig before modification.

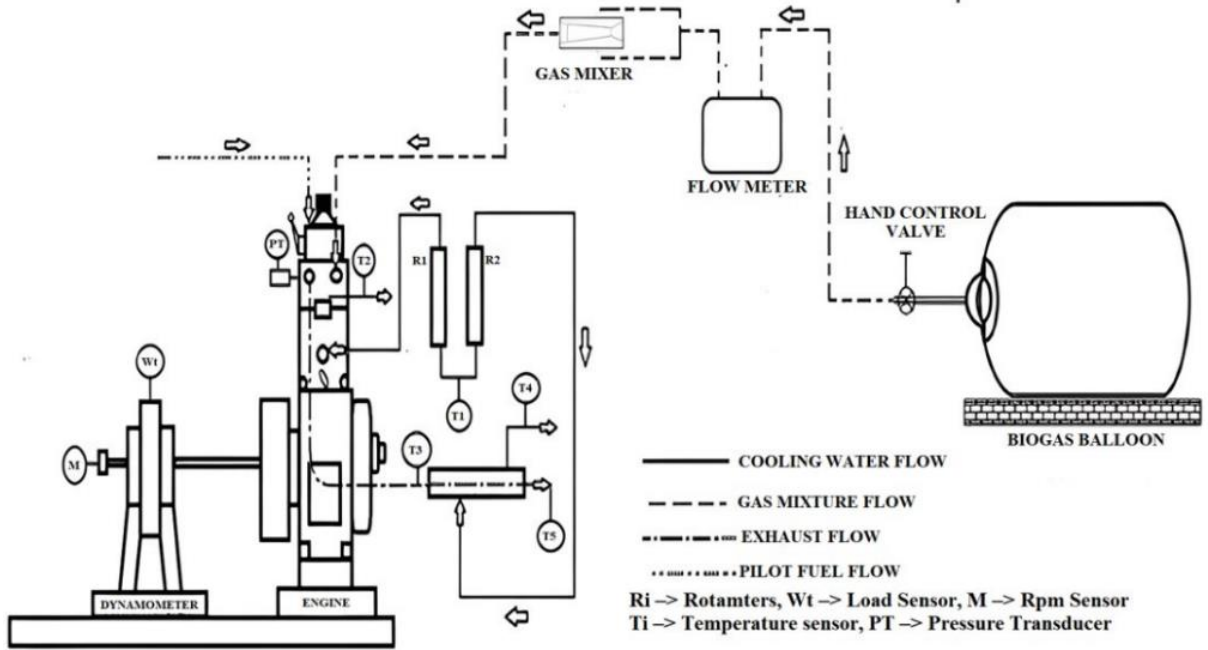


Fig. 3. 12 Schematic representation of test setup after modification

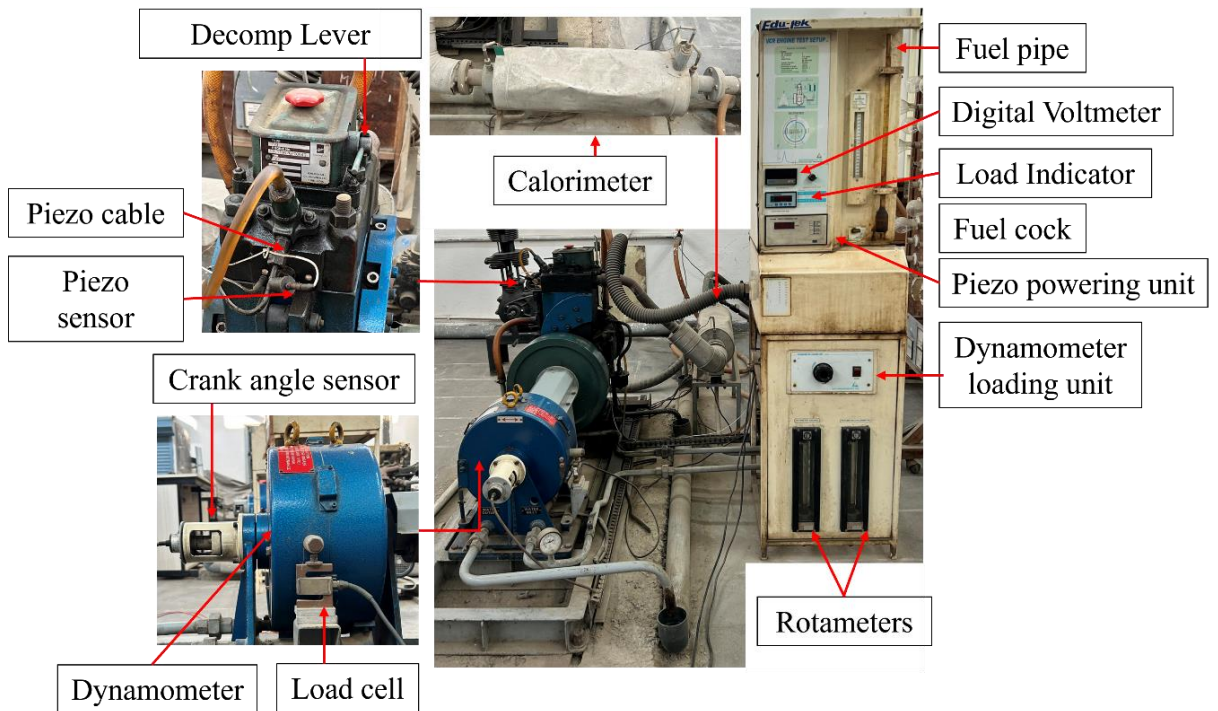


Fig. 3. 13 Pictorial representation of test rig



**Fig. 3. 14** Pictorial representation of test rig after modification

### 3.4.1 Measurement Instruments

The CI engine setup has several indicators, transmitters, and sensors. These are connected to the data acquisition device (DAD) so that nearly all direct and indirect performance metrics can be measured automatically.

#### Monitoring the Flow of Air and Fuel

It is possible to measure the flow of both air and fuel automatically or manually. The manometer is used to manually measure airflow by measuring the variation in water column height. The air enters the engine panel box through the orifice meter, which is attached to it. Air then exits towards the engine manifold. To manually measure fuel, pour fuel into the measuring tube and wait a predetermined amount of time.

#### Temperature Monitoring

At the intake and output positions of the engine, four PT100 temperature sensors measure the temperatures of the water flowing through the calorimeter and the cooling water for the engine. Exhaust gas temperatures are measured at the inlet and outlet of the calorimeter using



two K-type thermocouples. The response time of these thermocouples is more than 0.08 seconds, which applies to an engine running at a constant speed of about 1500 revolutions per minute. So that the exhaust gas flow becomes nearly steady at a particular load after a certain amount of time (approximately five minutes).

### Assessment of Performance

Manual data collection from the various indicators is used to measure the performance characteristics after the engine is configured to run at a certain load level. This is executed following the establishment of a specific load level for the engine.

#### 3.4.2 Central chamber for fuel-air mixing

The actual modification needed to convert a diesel engine to dual fuel mode is to connect a central chamber for fuel-air mixing to the intake manifold. The fuel-air mixing chamber is essential in dual-fuel mode for optimal engine performance in all situations. It provides a burnable mixture of fuel gas and air in the precise quantity and quality needed. Gas flow may be varied according to performance requirements. Moreover, it enables providing a suitable amount of air at maximum load and speed. With the ultimate objective of ensuring combustion even for the pilot fuel, the maximum air-to-fuel proportion should not be less than 1.5. The engine specification in Table 3.4 is considered primary consideration for designing the fuel-air mixing chamber.

**Table 3. 4** Engine Specifications

<b>Bore Diameter</b>	$D_B$	87.5 mm
<b>Stroke Length</b>	L	110 mm
<b>Speed</b>	N	1500 rpm
<b>Power</b>	P	3.5 kW
<b>Specific Fuel Consumption</b>	sfc	0.678m <sup>3</sup> /kWh
<b>Volumetric Efficiency</b>	$\eta_{vol}$	90%
<b>Substitution Percent of diesel by biogas</b>	S	80%
<b>Diameter of Inlet Manifold</b>	$d_i$	40 mm (measured)
<b>Type of Engine</b>	4-Stroke	
<b>No. of cylinders</b>	k	1

The fuel-air mixing chamber, sometimes called a "venturi gas mixer," was designed using the venturimeter concept. The gas mixer consists of three parts: passages for the gas inlet, air inlet, and a mixture of the two outlets. There is an expansion segment and a smooth contraction part. The minimal irreversible pressure loss results from the smooth contraction and expansion. The fluid's velocity and, for a short time, its static pressure are both reduced by the converging section. Because of the highest velocity, the lowest pressure will be achieved in the neck region. A pressure gradient changes from the intake to the throat. The pressure differential is proportional to this flow rate. The methodology proposed by von Mitzlaff (1988) led to the determination that the biogas inlet nozzle should have a diameter of 9 mm (as given in Eqn. 3.9) [23]. Four primary factors are used in the design process: the converging angle ( $\theta_1=20^\circ$ ), the diverging angle ( $\theta_2=5^\circ$ ), the nozzle angle ( $\theta_n=35^\circ$ ), and the ratio between the throat and intake manifold diameters ( $\beta=0.46$ ). Following Stewart et al. (2007), with a diverging angle of  $5^\circ$ , the optimal length for the diverging section equals ten times the inlet manifold diameter, making it 250 mm for a 40 mm manifold [116].

### Calculations for the diameter of the nozzle:

#### Step- 1

Swept Volume,

$$V_s = \left(\frac{\pi}{4} \times D_B^2 \times L\right) = 0.661 \times 10^{-3} m^3 \quad (3.2)$$

Volumetric Air Intake,

$$V_{air} = \left[\frac{(\eta_{vol} \times V_s \times N)}{(2 \times 60)}\right] = 0.00744 \text{ m}^3/s \quad (3.3)$$

#### Step- 2

Cross Sectional Area of Intake,

$$A_i = \left(\frac{\pi}{4} \times d_i^2\right) = 1.256 \times 10^{-3} m^2 \quad (3.4)$$

#### Step- 3

Intake Velocity,

$$C_i = (V_{air}/A_i) = 5.92 \text{ m/s} \quad (3.5)$$

#### Step- 4

Volume flow of fuel at rated power,

$$f_c = sfc \times P = 1.15 \times 10^{-3} m^3/s \quad (3.6)$$

#### Step- 5

Volume flow of biogas,

$$f_{c1} = s \times f_c = 0.924 \times 10^{-3} \text{ m}^3/\text{s} \quad (3.7)$$

### Step- 6

Area of nozzle,

$$A_2 = (f_{c1}/C_2) = 0.046 \times 10^{-3} \text{ m}^2 \quad (3.8)$$

Diameter of nozzle,

$$d_2 = \left(4 \times A_2/\pi\right)^{0.5} = 7.65 \text{ mm} \quad (d_2)_{\text{safe}} = 110\% \text{ of } d_2 = 8.41 \text{ mm} \approx 9 \quad (3.9)$$

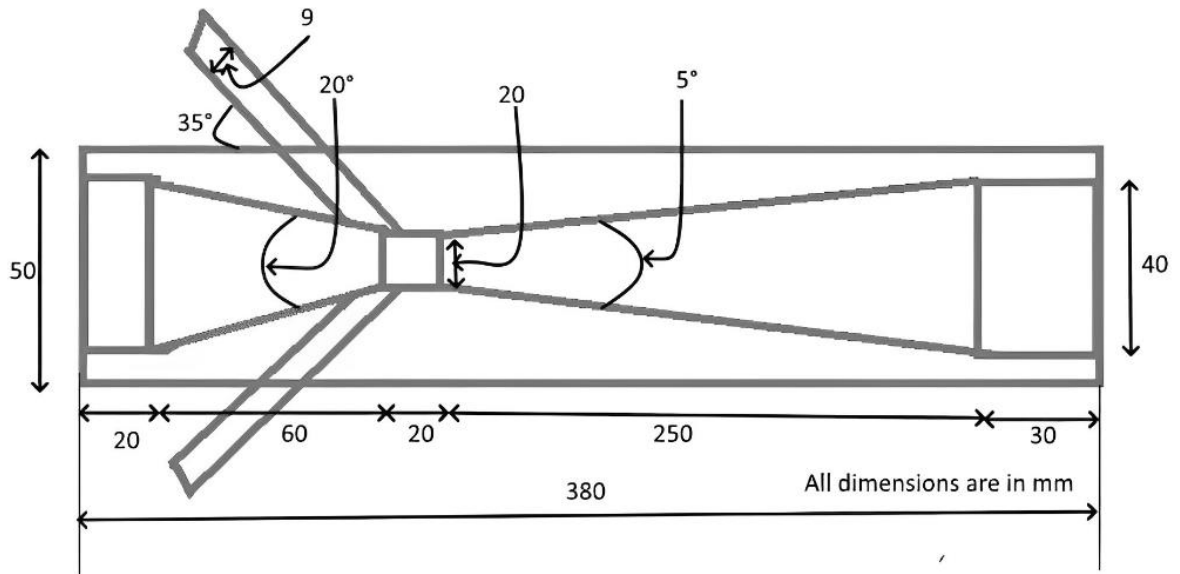


**Fig. 3. 15** Schematic diagram of Fuel-air mixing chamber



**Fig. 3. 16** Illustration of the fuel-air mixing chamber

A fuel-air mixing chamber is to be set up between the lines of the intake manifold. Following this, a single "Y-Divider" will link the two biogas nozzles. With this divider, the biogas will be divided into equal portions.



**Fig. 3. 17** Visual representation of Y-divider

### 3.4.3 Biogas Distribution and Measuring Appliance

Biogas was used to run the modified diesel engine in dual fuel mode and was supplied to the engine from a flexible biogas storage balloon, through a flow meter to measure the amount of gas consumed by the engine. The BFR was measured using a biogas flow meter (Siya SI 2.5), and the change in gas flow rate was facilitated by modulating the ball valves. The system consisted of a flexible (collapsible) gas bag of 2m<sup>3</sup> capacity, flexible clear tubes, a flow meter, a Y-divider, and a flow switch. The flow switch (shut-off valve) was used to regulate the gas flow by turning it to the desired positions and for closing the gas supply when not in use.



**Fig. 3. 18** Biogas Flowmeter



**Fig. 3. 19** 2 m<sup>3</sup> biogas storage balloon

#### **3.4.4 Methodology for Experimental Studies**

In dual fuel mode, the engine's performance was dictated by the combination of diesel and biogas, or by diesel alone. The CI engine is operated at an injection timing of 23°BTDC and a CR of 18. The engine is warmed up to achieve effective fuel combustion while the load is off. Engine loads of 20%, 40%, 60%, 80%, and 100% were used in the experiment. Engine rpm decreases as load increases. Cylinder, exhaust gas, and cooling water outlet temperatures were observed to increase due to the increased heat release required to maintain BP when fuel is added. To get the engine to a steady state, it was let run for a few minutes under any load condition. Afterward, the indicator retained the temperature, speed, and load readings. Diesel fuel consumption was determined by measuring fuel consumption in 30 seconds. Before every experiment, the fuel tank was filled and the outlet valve was closed. To begin the experiment, fuel was added to the burette by opening the outlet valve of the fuel tank. Fuel was measured in milliliters per minute as the engine ran on fuel measured from the metering burette, with the fuel tank outlet valve closed. The air flow rate was calculated with the measured difference in the water column height of the manometer. Simultaneously, temperature at various locations, fuel consumption rate, air flow rate, engine speed, cylinder pressure variation were recorded via DAD. The biogas supply valve is slowly released when the desired flow rate is reached. The engine's biogas flow meter reading was then registered after a few minutes of operation. Every test included 30 seconds of recording

the first and last meter readings. By subtracting the starting gas reading from the ending gas reading, the resulting value was noted.

NO<sub>x</sub>, HC, and CO emissions were assessed using a gas analyzer (Make: AVL DiGas 480), and smoke opacity was measured using a smoke meter (Make: AVL 437C).

### 3.5 Nanoparticles Characterization

Cobalt oxide (Co<sub>3</sub>O<sub>4</sub>) was procured from Sigma Aldrich company. The morphological structure of nanoparticles is determined using a Zeiss scanning electron microscope (SEM) EVO 50. The SEM image shows non-uniform, larger agglomerated clusters with primarily round and oval shapes. The magnetic induction between particles causes agglomeration [117]. The images from Fig.3.20 confirmed the nanoparticles have an average size of less than 100 nm.

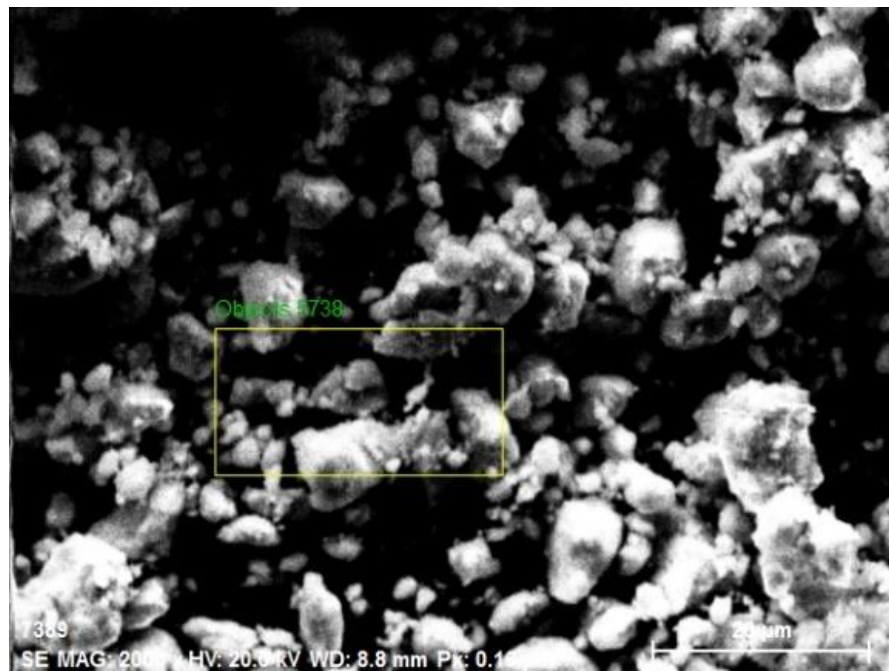


**Fig. 3. 20** SEM image of Co<sub>3</sub>O<sub>4</sub> at 20 μm

Utilizing the RONTEC EDX system model Quantax 200, the elemental composition of Co<sub>3</sub>O<sub>4</sub> nanoparticles is identified. The presence of Co and O has been established in Fig.3.21, and the absence of foreign element peaks indicates the nanoparticles utilized are of the highest purity. The Co<sub>3</sub>O<sub>4</sub> theoretical ratio of 3:4 is also confirmed by the close proximity in observing atomic% of Co and O at 37.29% and 62.71, respectively. Co and O are evenly distributed across the lattice, according to the elemental mapping pictures in Fig. 3.22.

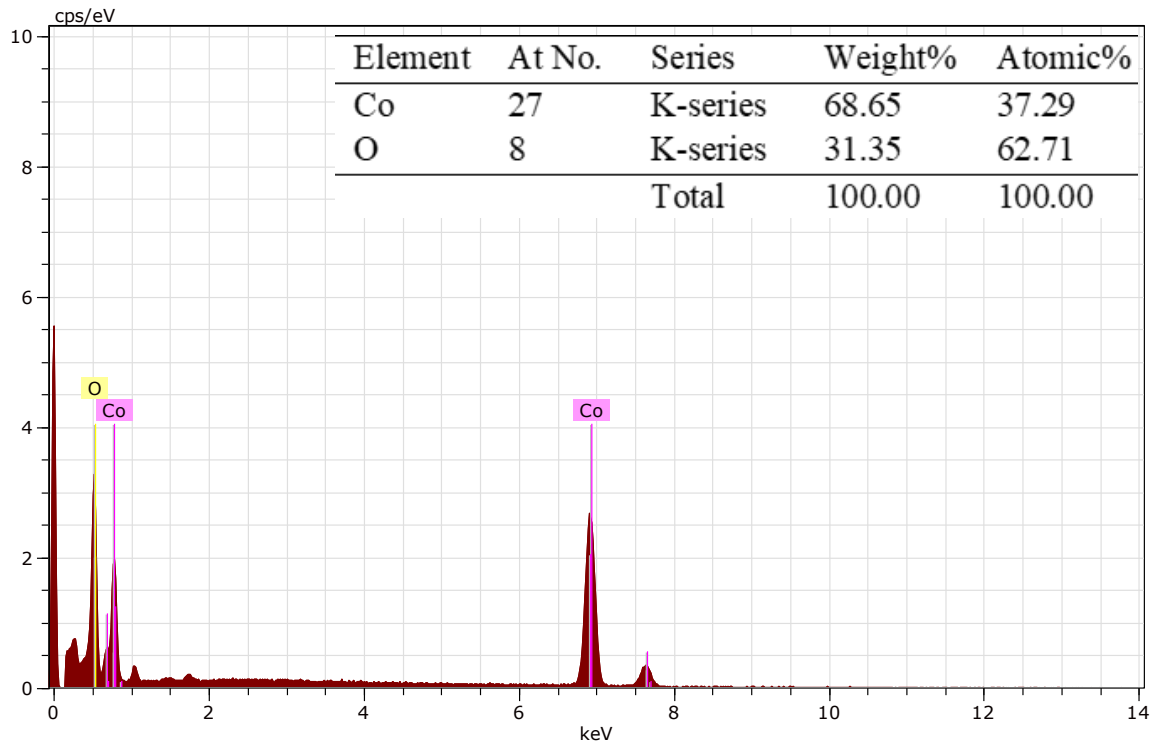


Fig. 3. 21 EDX spectra of  $\text{Co}_3\text{O}_4$

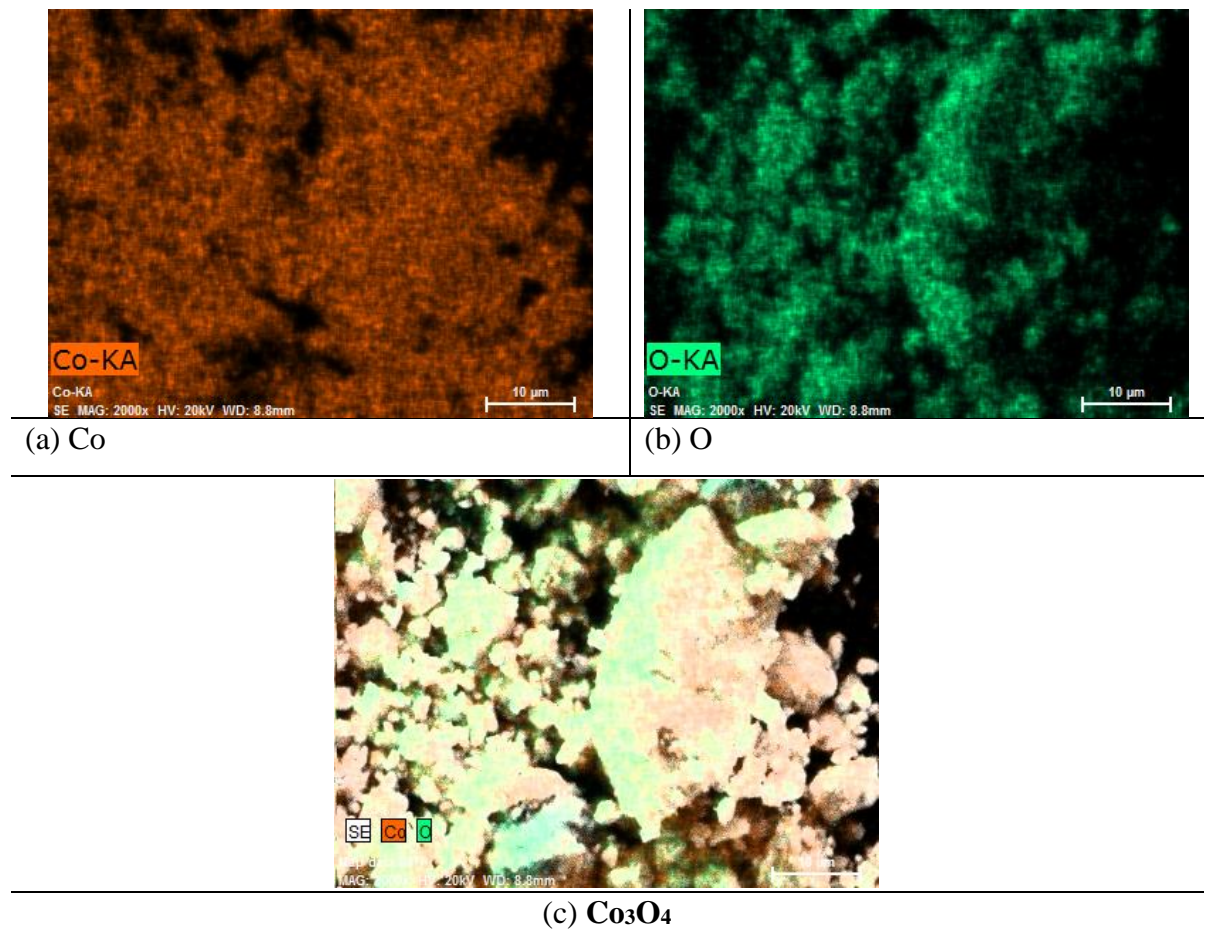
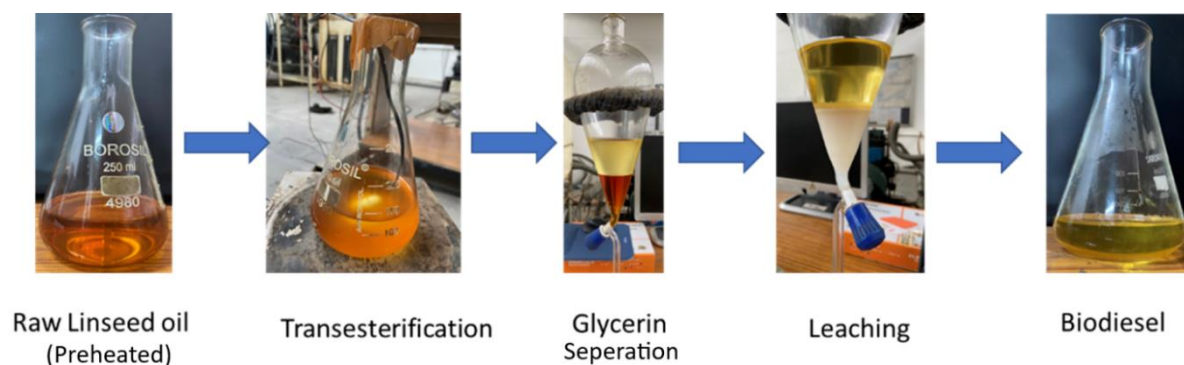


Fig. 3. 22 Elemental mapping of (a)Co, (b) O, and (c)  $\text{Co}_3\text{O}_4$

### 3.6 Biodiesel Production and Properties

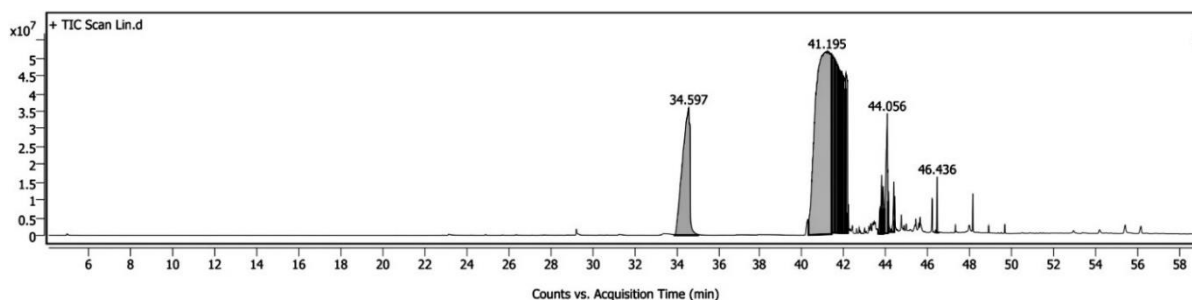
This study converts raw linseed oil to biodiesel by the transesterification method. Raw linseed oil was heated for moisture removal at 105-110°C for 10 minutes.



**Fig. 3. 23** Biodiesel production process

20% v/v of Methanol and 1% KOH w/w were mixed homogeneously, and this mixture was added to the linseed oil after the oil cooled down to 45°C. The mixture is then stirred and heated to 50-55°C for the transesterification process using a magnetic stirrer for 90-100 minutes. The mixture is then fed to a conical separator and let to rest for 12 hours. The lower layer forming glycerol is removed thereafter. Water washing is then done with the linseed oil to remove the catalyst and impurities. The oil is heated to 110°C for 2–5 minutes to eliminate the moisture content. The final biodiesel obtained is then stored in a container for testing and blending purposes.

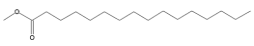
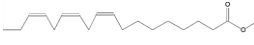
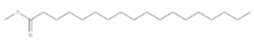
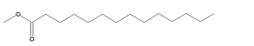
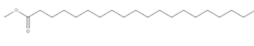
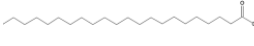
Agilent 8890 Gas chromatography-mass spectrometry (GC-MS) was used to validate the biodiesel synthesis and determine the chemical composition. The analysis observed 18 fatty acid methyl ester (FAME) peaks, as given in Fig.3.24. The peaks were observed at unique acquisition time, as mentioned in Table 3.5. The fatty acid observed for the biodiesel prepared in this study adheres to the commonly observed fatty acid for most biodiesel tested [118].



**Fig. 3. 24** GC-MS of Linseed Biodiesel



**Table 3. 5** Composition of Linseed Biodiesel

Sl. No.	Fatty acid	Peak area %	Acquisition time(min)	Fatty acids	Chemical Formula	Chemical structure
1.	Palmitic acid, methyl ester	14.87	34.597	Saturated	C <sub>17</sub> H <sub>34</sub> O <sub>2</sub>	
2.	Linoleic acid, methyl ester	77.03	41.195, 41.412, 41.549, 41.584, 41.698, 41.767, 41.881, 41.904, 41.961, 44.056, 44.113	Un-saturated	C <sub>19</sub> H <sub>34</sub> O <sub>2</sub>	
3.	Stearic acid, methyl ester	4.66	42.076	Saturated	C <sub>18</sub> H <sub>38</sub> O <sub>2</sub>	
4.	Myristic acid, methyl ester	2.19	43.707, 43.787, 43.855	Saturated	C <sub>15</sub> H <sub>26</sub> O <sub>2</sub>	
5.	Eicosanoic acid, methyl ester	0.73	44.37	Saturated	C <sub>21</sub> H <sub>42</sub> O <sub>2</sub>	
6.	Behenic acid methyl ester	0.50	46.43	Saturated	C <sub>23</sub> H <sub>46</sub> O <sub>2</sub>	

Biodiesel is blended with diesel in a proportion of 10:90 and 20:80 for BBR 10 and BBR 20 blends, respectively. The measured physiochemical properties tested using multiple ASTM testing procedures of the diesel (D 100), raw linseed oil (LO), and pure biodiesel (BBR100) are given in Table 3.6.

**Table 3. 6** Fuel properties

Properties	Unit	Testing methods	D 100	LO	BBR 10	BBR 20	BBR 100
Kinematic Viscosity (40 °C)	cSt	D-445	2.98	30.6	3.15	3.36	4.21
Density (40 °C)	kg/m <sup>3</sup>	D-1298	841	920	828.3	834.2	881
Calorific Values	MJ/kg	D-240	43.9	38.4	43.5	43.03	40.5
Flash Point	°C	D-93	60	244	90	107	169
Pour Point	°C	D-97	-14	-16	-14	-15	-18
Cetane Number	-	D-4737	51	38	50	49	42

### 3.7 Nanoparticles Blends Preparation and Properties

Nanoparticles and diesel/biodiesel were blended for one hour in an ultrasonication bath at 50 ppm (NDR 50) and 100 ppm (NDR 100) concentrations. The blend undergoes another round of mixing using an ultrasonicator probe at 50 Hz for 30 minutes.



**Fig. 3. 25** Blending of Pilot fuel with nanoparticles via Ultrasonicator

To minimize agglomeration caused by surface tension, 1% by weight of Triton X-100 surfactant was used. After 24 hours of observation, there was no agglomeration or particle settling. The properties of the diesel-nanoparticle blends and biodiesel-nanoparticles blends were then tested using multiple ASTM testing procedures (TP), as shown in Table 3.7.

**Table 3. 7** Physiochemical properties of fuel blends

Properties	Unit	TP	D100 - NDR 50	D100 - NDR 100	BBR 10 - NDR 50	BBR 10- NDR 100	BBR 20 - NDR 50	BBR 20 - NDR 100
Kinematic Viscosity (40 °C)	cSt	D-445	3.07	3.16	3.25	3.35	3.46	3.56
Density (40 °C)	kg/m <sup>3</sup>	D-1298	843	845	830	832	836	838
Calorific Values	MJ/kg	D-240	44.1	44.3	43.63	43.83	43.16	43.27
Flash Point	°C	D-93	61	62	91	93	109	110
Pour Point	°C	D-97	-14	-15	-14	-15	-16	-16
Cetane Number	-	D-4737	51.9	52.6	50.8	51.5	49.7	50.4

### 3.8 RSM and ANN Modelling for Engine Performances and Emission Parameters

Design Expert Software was utilized to create the DOE as given in Table 3.9 by applying the Central Composite Face-Centered Design (CCFCD) to the chosen input variables and output parameters. Since there are axial points on every face in the design domain, the model's alpha value is 1. CCFCD is the term for the Central Composite Design (CCD) with alpha equal to 1. For 16 factorial points, 8 axial points, and 6 replicates, the total number of runs for CCFCD design translates to 30. The independent input variables selected and their coded levels are mentioned in Table 3.8. The levels for each input variable were determined based on prior studies.

**Table 3. 8** Input Parameters and Levels

Input Parameters	Units	Symbol	Levels		
			-1	0	1
Engine load	%	Load	20	60	100
Nanoparticles doped rate	ppm	NDR	0	50	100
Biodiesel blend rate	%	BBR	0	10	20
Biogas Flow rate	kg/h	BFR	0.5	0.75	1

**Table 3. 9** Input Parameters and Levels

Run	A:load %	B:NDR ppm	C: BBR %	C:BFR kg/h	BTE %	BSEC MJ/kWh	NO <sub>x</sub> ppm	HC ppm	CO %	SO %	BGES %
1	60	50	10	0.75	-	-	-	-	-	-	-
2	20	0	0	0.5	-	-	-	-	-	-	-
3	20	0	20	0.5	-	-	-	-	-	-	-
4	60	50	10	0.5	-	-	-	-	-	-	-
5	20	100	20	0.5	-	-	-	-	-	-	-
6	60	50	10	0.75	-	-	-	-	-	-	-
7	100	0	20	1	-	-	-	-	-	-	-
8	100	100	20	0.5	-	-	-	-	-	-	-
9	60	100	10	0.75	-	-	-	-	-	-	-
10	100	0	20	0.5	-	-	-	-	-	-	-
11	60	0	10	0.75	-	-	-	-	-	-	-
12	20	100	0	1	-	-	-	-	-	-	-
13	60	50	10	1	-	-	-	-	-	-	-
14	100	100	0	0.5	-	-	-	-	-	-	-
15	20	0	0	1	-	-	-	-	-	-	-
16	100	50	10	0.75	-	-	-	-	-	-	-
17	60	50	10	0.75	-	-	-	-	-	-	-
18	20	100	20	1	-	-	-	-	-	-	-
19	60	50	20	0.75	-	-	-	-	-	-	-
20	60	50	10	0.75	-	-	-	-	-	-	-
21	20	0	20	1	-	-	-	-	-	-	-
22	100	0	0	1	-	-	-	-	-	-	-
23	100	100	0	1	-	-	-	-	-	-	-
24	100	100	20	1	-	-	-	-	-	-	-
25	60	50	10	0.75	-	-	-	-	-	-	-
26	60	50	0	0.75	-	-	-	-	-	-	-
27	100	0	0	0.5	-	-	-	-	-	-	-
28	60	50	10	0.75	-	-	-	-	-	-	-
29	20	50	10	0.75	-	-	-	-	-	-	-
30	20	100	0	0.5	-	-	-	-	-	-	-

### 3.8.1 RSM Modelling

RSM was executed by fitting a second-order polynomial equation (Eqn. 3.10) to the DOE experimental data to establish a correlation between independent inputs and dependent outputs.

$$Y = b_0 + \sum_{i=1}^4 b_i x_i + \sum_{i=1}^4 b_{ii} x_i^2 + \sum_{i < j}^4 b_{ij} x_i x_j \quad (3.10)$$

Y is the dependent output on the independent input factor of  $x_i$ .  $b_0$  represents the intercept coefficient of the polynomial equation.  $b_i$  represents the linear coefficients for Load, NDR, BBR, and BFR, while  $b_{ii}$  is the interactive coefficients, and  $b_{ij}$  is the quadratic coefficients. The model fitting was achieved through Design Expert software. Analysis of variance (ANOVA) was used to establish model reliability and the contribution significance of each input variable in determining output responses. The interaction impact of input factors on output was studied using a 3D response surface plot. Two input interactions on output are studied at once, while the other input variable is kept constant.

### 3.8.2 ANN Modelling

ANN is an analytical tool for establishing the data's predictability regression and validating the correlation between input and output variables. In this ANN study, the backpropagation algorithm is utilized for the multilayer perceptron (MLP) neural network architecture, using Matlab R2020a for coding and execution purposes. This MLP architecture as shown in Fig. 4 holds the forms of A-X1-X2-Z, where the number of neurons in the input layer, first hidden layer (HL1), second hidden layer (HL2), and output layer is indicated by A, X1, X2, and Z respectively. The number of hidden layers is set to 2. Optimal neuron combinations for hidden layers can be obtained using the Trial and error method. A network is created for each output to train DOE results. The network is trained with different neuron combinations with each hidden layer neuron ranging from 1-10. The neuron combinations exhibiting the least RMSE are then selected as in Table 4. The optimal neuron combination obtained is then used to create a new network corresponding to each output. Levenberg Marquardt(trainlm) was employed as the training function, and Mean square error (MSE) was employed as the performance function. Log-sigmoid and Tan-sigmoid transfer functions were employed for the hidden layer and output layer, respectively. The DOE consists of 30 runs, of which 21 runs (70% of DOE) were used to train the network, four runs (15% of

DOE) were used for testing, and four runs (the remaining 15% of DOE) were used for validation.

**Table 3. 10** ANN architecture for engine outputs

BTE	BSEC	NO <sub>x</sub>	HC	CO	SO
4-6-5-6	4-9-3-6	4-9-3-6	4-10-8-6	4-6-6-6	4-4-2-6

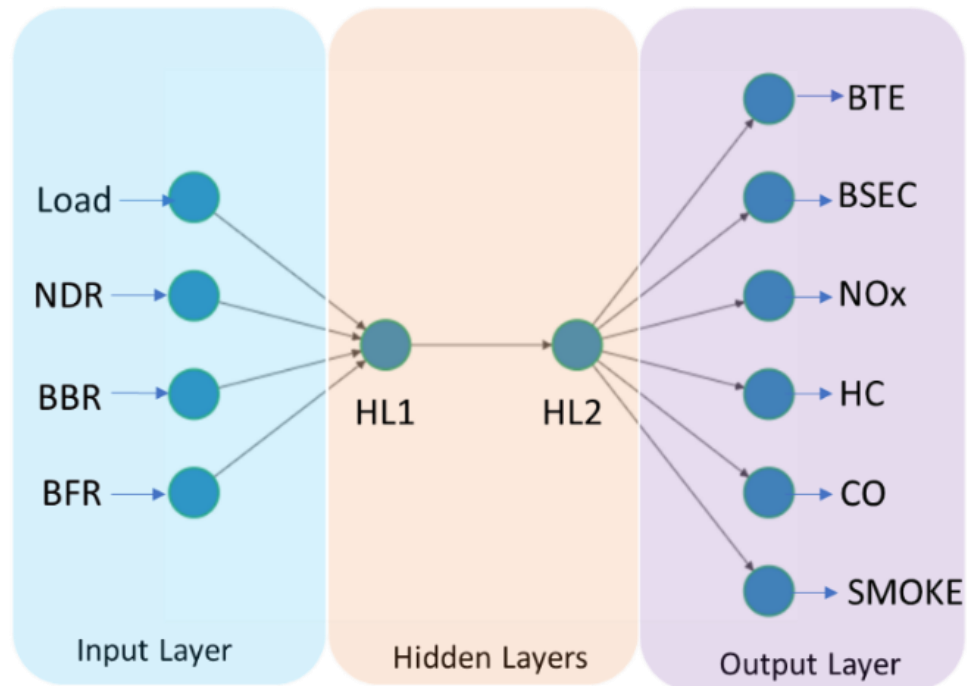


**Fig. 3. 26** ANN Architecture (4-X1-X2-6)

### 3.9 Optimization of the RSM model with the Desirability Approach

A definite optimal solution without compromise is unattainable for more than one output parameter. RSM with a desirability function is utilized to obtain the optimal solution for the multi-objective response. In the Desirability approach, the solution with the highest combined desirability factor is considered the optimal solution. The individual desirability( $d_n$ ) for the output parameter with the goal to maximize is determined with Equation 3.11, and for the output parameter with the goal to minimize is determined with Equation 3.12. The combined desirability (CD) is determined as provided in Equation 3.13.

$$d_n = \begin{cases} 0 & n < L_n \\ \frac{n-L_n}{G_n-L_n} \times r_n & L_n < n < G_n \\ 1 & n > G_n \end{cases} \quad (3.11)$$

$$d_n = \begin{cases} 0 & n > H_n \\ \frac{H_n - i}{H_n - G_n} \times r_n & G_n < n < H_n \\ 1 & n < G_n \end{cases} \quad (3.12)$$

$$CD = [\Pi(d_n w_n)]^{\frac{1}{W}} \quad (3.13)$$

Where  $n$ ,  $G_n$ ,  $L_n$ ,  $H_n$ ,  $r_n$  represent predicted, goal value, lower suitable values, higher suitable value, desirability function weight for  $n^{\text{th}}$  outputs respectively,  $w_n = n^{\text{th}}$  output importance,  $W = \sum w_n$ . The desirability factor varies from 0 to 1, with 1 being the most desired ideal option and 0 being the least desired. Each output parameter's goal has been specified.

For the Biogas Production Process Parameters Optimization, both CBP and  $\text{CH}_4/\text{CO}_2$  are given the goal to maximize. Both of the output parameter goals and weight were assigned equal importance.

For the Engine Performance Optimization, while the other five outputs goals are set to minimize, the BTE and BGES goal is set to maximize. Each of the output parameter goals and weight was assigned equal importance.

### 3.10 Optimization of ANN model with Genetic Algorithm (GA)

GA is an evolutionary algorithm that is an exploration and investigation method akin to the principle of natural selection. The trained network created corresponding to each output response in the ANN model is used to define a fitness function in GA. A fitness function is an objective function where the goals of either maximizing or minimizing the responses are fed. The input parameters' upper and lower bounds are then provided to the GA program, including the selection parameters listed in Table 3.11. Initial Population, Fitness function, Selection, Crossover, and Mutation are the five phases that are utilized for GA optimization. GA is accountable for grading and selecting the solution from the ANN-based objective function [119].

**Table 3. 11** Selection Parameters for GA Optimization

Population	Initial	Mutation	Crossover	Selection
Type	Population	Rate	Fraction	Function
Double Vector	50	0.01	0.8	Tournament

### 3.11 Evaluation Metrics for ANN and RSM Model Predictions

For each DOE run for both Biogas Production Optimization (Table 3.3) and Engine Performance Optimization (Table 3.9), a percentage of error is calculated for both the RSM and ANN predicted data and observed data using Equation 3.14. Coefficient of determination ( $R^2$ ), Root Mean Square error (RMSE), and Mean Absolute deviation (MAD) are the evaluation metrics chosen to compare the predictive effectiveness of the ANN and RSM models, calculated using Equation. 3.15, 3.16, and 3.17, respectively.

$$\text{Percentage of error} = \frac{|\text{Observed result} - \text{Predicted result}|}{\text{Observed result}} \quad (3.14)$$

$$R^2 = 1 - \left( \frac{\sum_{t=1}^n (A_t - F_t)^2}{\sum_{t=1}^n (F_t)^2} \right) \quad (3.15)$$

$$\text{RMSE} = \sqrt{\frac{\sum_{t=1}^n (A_t - F_t)^2}{n}} \quad (3.16)$$

$$\text{MAD} = \frac{\sum_{t=1}^n |A_t - F_t|}{n} \quad (3.17)$$

Where  $A_t$  is the actual observed data,  $F_t$  is the predicted data, and  $n$  denotes overall number of runs in DOE.

### 3.12 Validation of optimized results from ANN and RSM Model

Validation is necessary to assess the correctness of the outcome attained from optimization. A test is performed to validate the optimised input parameters obtained from the RSM model of Biogas Production Optimisation. Similarly, an experimental test is conducted for the optimized input parameters from the Engine Performance Optimization's RSM and ANN model. The percentage of error for experimental results in comparison to the RSM and ANN models predicted optimized response parameters is calculated as per Equation 3.18.

$$\text{Percentage of error} = \frac{|\text{Observed result} - \text{Predicted result}|}{\text{Observed result}} \quad (3.18)$$

### 3.13 Uncertainty analysis

When checking the integrity of experimental results, uncertainty analysis is required. It entails contemplating the two most common kinds of uncertainty: Type A, which deals with random errors, and Type B, which deals with systematic errors. The emphasis here is on type B uncertainty because the data is normally distributed. Utilizing Equation 3.19, which posits:

$$\text{Standard Uncertainty} = (\text{Accuracy of the instrument}) / \sqrt{3} \quad (3.19)$$

In this case, the standard uncertainty is calculated by dividing the instrument's accuracy by the square root of 3.

Equation 3.20 is used to find the uncertainty in the observed value of a function Y when Y is dependent on numerous input parameters or independent variables:

$$U(Y) = \sqrt{\left(\frac{\partial Y}{\partial x_1} \cdot u(x_1)\right)^2 + \left(\frac{\partial Y}{\partial x_2} \cdot u(x_1)\right)^2 \dots \dots \dots \left(\frac{\partial Y}{\partial x_n} \cdot u(x_n)\right)^2} \quad (3.20)$$

The symbol U(Y) denotes the level of uncertainty related to the measured function Y in this equation. The variables u(x<sub>1</sub>) to u(x<sub>n</sub>) denote the uncertainty associated with the independent variables (x<sub>1</sub> to x<sub>n</sub>) that impact the function Y. The partial derivatives (∂Y/∂x<sub>1</sub>, ∂Y/∂x<sub>2</sub>, ..., ∂Y/∂x<sub>n</sub>) measure the impact of variations in each independent variable on the function Y. These derivatives are then multiplied by their corresponding uncertainties and squared. The findings are then aggregated and subjected to a square root operation to get the total uncertainty in the measured value of Y.

### Estimates based on examples

To do a CO<sub>2</sub> emission uncertainty analysis using the given instrument specifications and several measurements, the following steps are followed:

#### Step 1: Obtain Multiple Measurements

The acquired results from the repeated measurements are as follows: 23%, 22.5%, 22%, 23%, 22.6.

#### Step 2: Determine the Mean

Determine the mean of these measurements:

$$\text{Mean } (\bar{x}) = (23 + 22.5 + 22 + 23 + 22.6) / 5 = 113.1 / 5 = 22.62\% \quad (3.21)$$

#### Step 3: Determine Type A Uncertainty's Variance and Standard Deviation

To estimate the dispersion of the data around the mean, compute the standard deviation and variance respectively:

$$\text{Variance } (s^2) = \Sigma(x_i - \bar{x})^2 / (n - 1) \quad (3.22)$$

$$\text{Variance} = [(0.38)^2 + (0.12)^2 + (0.62)^2 + (0.38)^2 + (0.02)^2] / 4 \approx 0.172\%$$



$$\text{Standard Deviation } (\sigma) \approx \sqrt{\text{Variance}} \approx \sqrt{(0.172\%)} \approx 0.4147\% \quad (3.23)$$

**Step 4: Determine the Standard Error of the Mean (SEM)**

The following is the formula for calculating the SEM:

$$\text{SEM} = \sigma / \sqrt{n} \approx 0.4156\% / \sqrt{5} \approx 0.1855\% \quad (3.24)$$

**Step 5: Estimate the Instrument's Type B Standard Uncertainty**

Considering the parameters of the device:

$$\text{Accuracy} = \pm 0.1\% \text{ (Type B uncertainty)} \quad (3.25)$$

$$\text{Standard Uncertainty of the Instrument} = (\text{Accuracy of instrument}) / \sqrt{3} \approx 0.1\% / \sqrt{3} \approx 0.0577\%$$

**Step 6: Integration of Types A and B Uncertainties**

Integrate the root-sum-of-squares-derived standard uncertainties (Type B) and standard errors of the means (Type A):

$$\text{Combined Uncertainty (U)} = \sqrt{(\text{SEM}^2 + (\text{Standard Uncertainty of the Instrument})^2)} \quad (3.26)$$

$$U \approx \sqrt{((0.1855\%)^2 + (0.0577\%)^2)} \approx 0.1942\%$$

When the Type A and Type B uncertainties are added together, the range that the actual CO<sub>2</sub> concentration is expected to lie within is about  $\pm 0.1942\%$ . The uncertainty in the instrument's precision and the random fluctuation in measurements are taken into account by this number. Other parameter uncertainty will also be computed similarly.

**Table 3. 12** Uncertainty in Observed Parameter and List of Used Instruments with Uncertainties

<b>Instruments</b>	<b>Observed Parameter</b>	<b>Accuracy</b>	<b>Range</b>	<b>Standard Uncertainty of the Instrument</b>	<b>Uncertainty calculated in observed parameter</b>
AVL Exhaust Gas Analyzer	Gas Concentrations (CO)	$\pm 0.02\%$	0-10 %	$\pm 0.011\%$	$\pm 0.015\%$
	Gas Concentrations (CO <sub>2</sub> )	$\pm 0.1\%$	0-25 %	$\pm 0.05\%$	$\pm 0.19\%$
	Gas Concentrations (HC)	$\pm 20$ ppm	0-10000 ppm	$\pm 11$ ppm	$\pm 12.5$ ppm
	Gas Concentrations (NO <sub>x</sub> )	$\pm 10$ ppm	0-5000 ppm	$\pm 05$ ppm	$\pm 12.5$ ppm
	Brake power (BP)				$\pm 0.5 \%$
	Brake specific energy consumption (BSEC)				$\pm 1.6$
	Brake Thermal efficiency (BTE)				$\pm 2.1\%$

### 3.14 Summary

This chapter delves into the materials and methods employed in the research. It encompasses various aspects, including:

1. The research methodology employed in the study is described.
2. Details of the biogas production process, from waste collection and feedstock characterization to the setup and operation of digesters and enrichment systems.
3. RSM modeling is used to establish predictive models for the biogas production parameters, based on regression analysis. The optimization of RSM models, evaluation metrics for their predictions, and the validation of optimized results are presented.
4. The experimental testing setup, including the measurement instruments and central chamber for fuel-air mixing are described.
5. Nanoparticle characterization, biodiesel production, and the preparation and property testing of nanoparticle blends are discussed.

6. RSM and ANN modeling are employed to establish predictive models for engine performance and emission parameters, based on regression analysis. We further describe the optimization of RSM and ANN models using the Desirability Approach and Genetic Algorithm, respectively. Evaluation metrics for their predictions and the validation of optimized results are presented.
7. Uncertainty Analysis are tabulated for Instruments used and observed parameters.

## CHAPTER 4 : BIOGAS PRODUCTION AND OPTIMIZATION

### 4.1 Effect of process parameters on Biogas Production Rate & CH<sub>4</sub>/CO<sub>2</sub>

The effect of process parameters such as Temperature, Mixing Duration, and different feedstock were studied for their effect on the Biogas Production rate and CH<sub>4</sub>/CO<sub>2</sub>

#### 4.1.1 Effect of Feedstock on Biogas Production Rate & CH<sub>4</sub>/CO<sub>2</sub>

Kitchen Waste, Vegetable Waste, and Fruit Waste were considered to study the effect of feedstock on biogas production. The production was made at the condition of digester temperature being 40°C and no mixing or agitation of digester.

**Table 4. 1** Experimental Matrix of the Biogas Production

Feedstock	Temperature	Mixing Duration
Kitchen Waste	40°C	Nil
Vegetable Waste		
Fruit Waste		

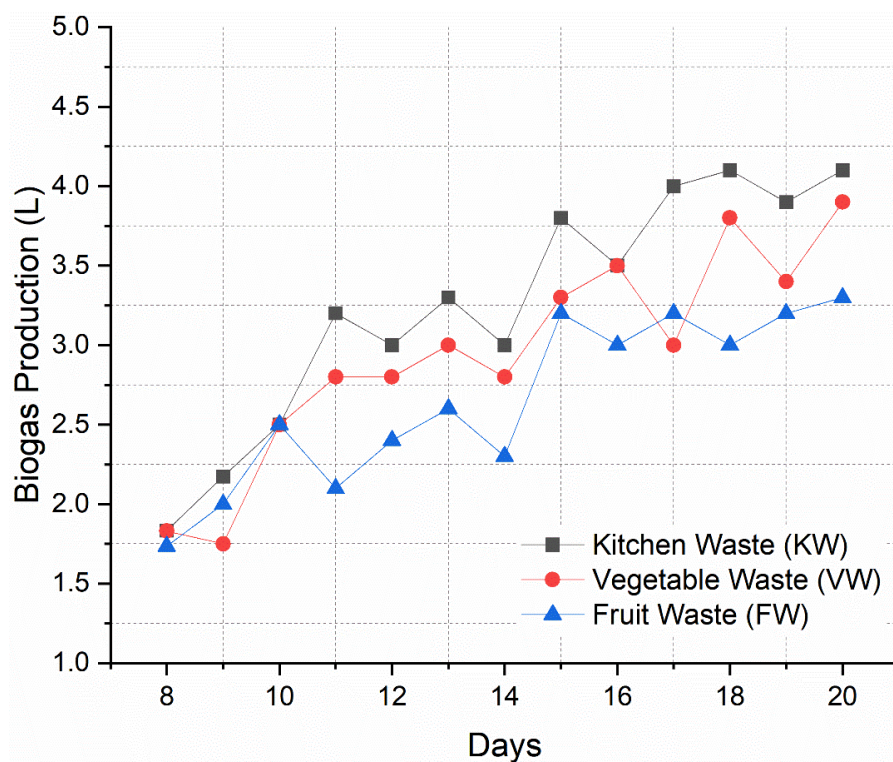


**Fig. 4. 1** Biogas Production per day for varied feedstock

As given in Fig. 4.1, A daily biogas production of above 3L per day was observed on the 11<sup>th</sup> day for the digester with kitchen waste as the feedstock, the 13<sup>th</sup> day for the digester with vegetable waste as the feedstock, the 15<sup>th</sup> day for the digester with fruit waste as the feedstock.

It was also noted that the digested substrates tended to clog the outlet pipes and slow down the sludge removal process when dealing with fruit and vegetable waste. There was undigested fruit and vegetable substrate in the sludge. The fruit and vegetable substrates were not fully digested during the procedure. Maximising biogas production requires proper pre-treatment of vegetable and fruit waste before it is utilised as feedstock for digestion facilities.

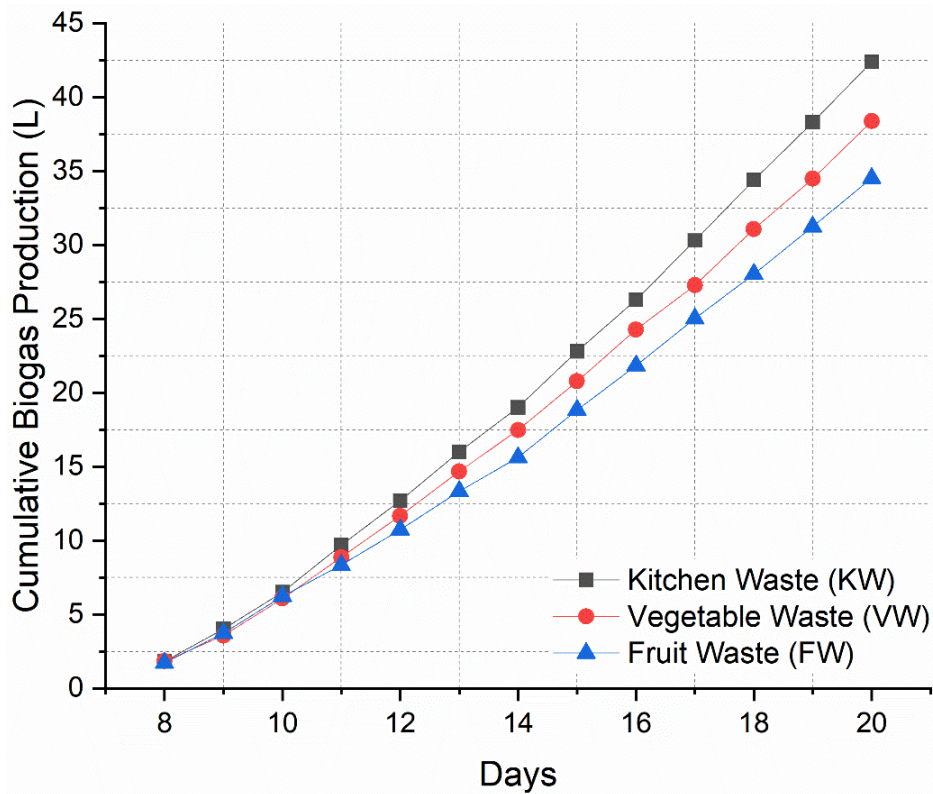


**Fig. 4. 2** Cumulative Biogas Production for varied feedstock

As given in Fig. 4.2, The highest Cumulative Biogas Production (CBP) was observed at 42.4 L for the digester with feedstock of Kitchen waste, followed by 38.3 L for the digester with vegetable waste and 34.5 L for the digester with Fruit waste. The higher CBP of kitchen waste than Raw vegetable waste is because kitchen waste is more easily digestible by the methanogenic bacteria that produce biogas. The presence of accessible nutrients could be another reason for increased biogas production for Kitchen waste, in comparison to vegetable waste and fruit waste. Previous research for biogas production using multiple feedstocks similarly observed the highest CBP for Kitchen waste, followed by Vegetable waste and Fruit Waste, respectively [120]. A study observed 13.2% higher CBP for biogas production with kitchen waste, in comparison to biogas production on co-digestion of fruit and vegetable waste [121]. A similar study observed 26.67% higher CBP for biogas

production on Cafeteria Kitchen waste, in comparison to biogas production on vegetable waste [122].

The highest  $\text{CH}_4 / \text{CO}_2$  was observed for the digester with feedstock of Kitchen waste, followed by the digester with vegetable waste and Fruit waste, as given in Fig. 4.3. The peak  $\text{CH}_4 / \text{CO}_2$  was observed at 1.16 for Kitchen waste at 18<sup>th</sup> day, followed by 0.94 for Vegetable waste at 19<sup>th</sup> day, and 0.81 for fruit waste at 19<sup>th</sup> day. As for the average  $\text{CH}_4 / \text{CO}_2$  for the recorded 13 days, the highest was observed for Kitchen waste with 1.07, followed by 0.87 for Vegetable waste and 0.73 for Fruit waste. The higher methane content of kitchen waste than the other two feedstock is because kitchen waste contains more easily digestible carbohydrates, which are converted into methane by the methanogenic bacteria.

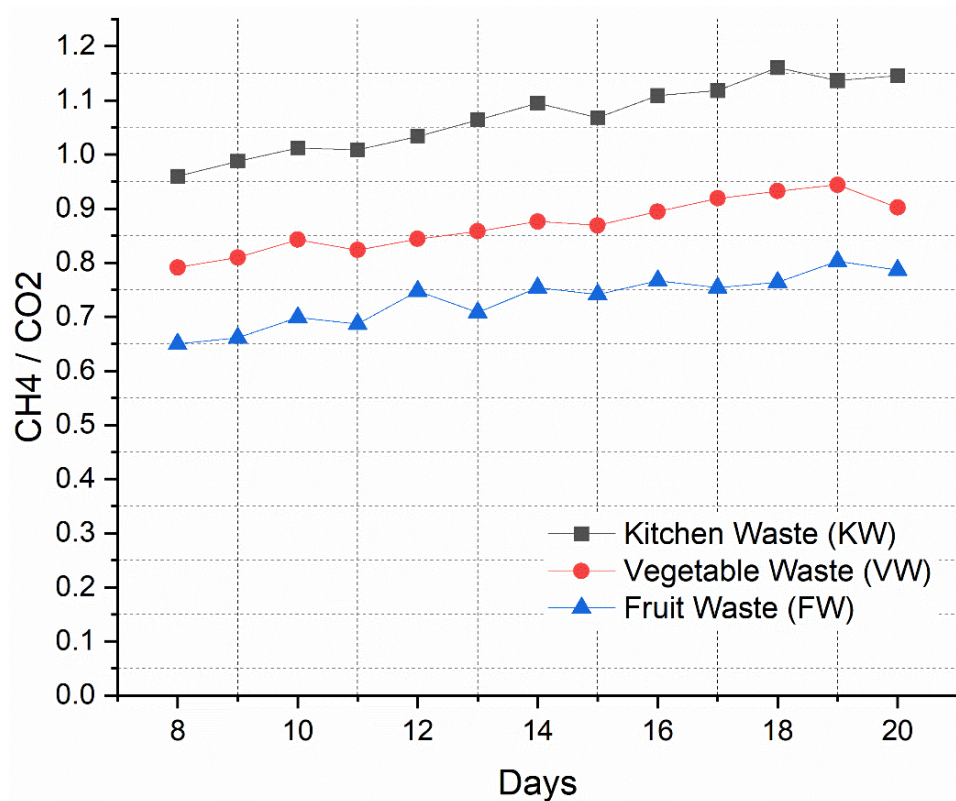


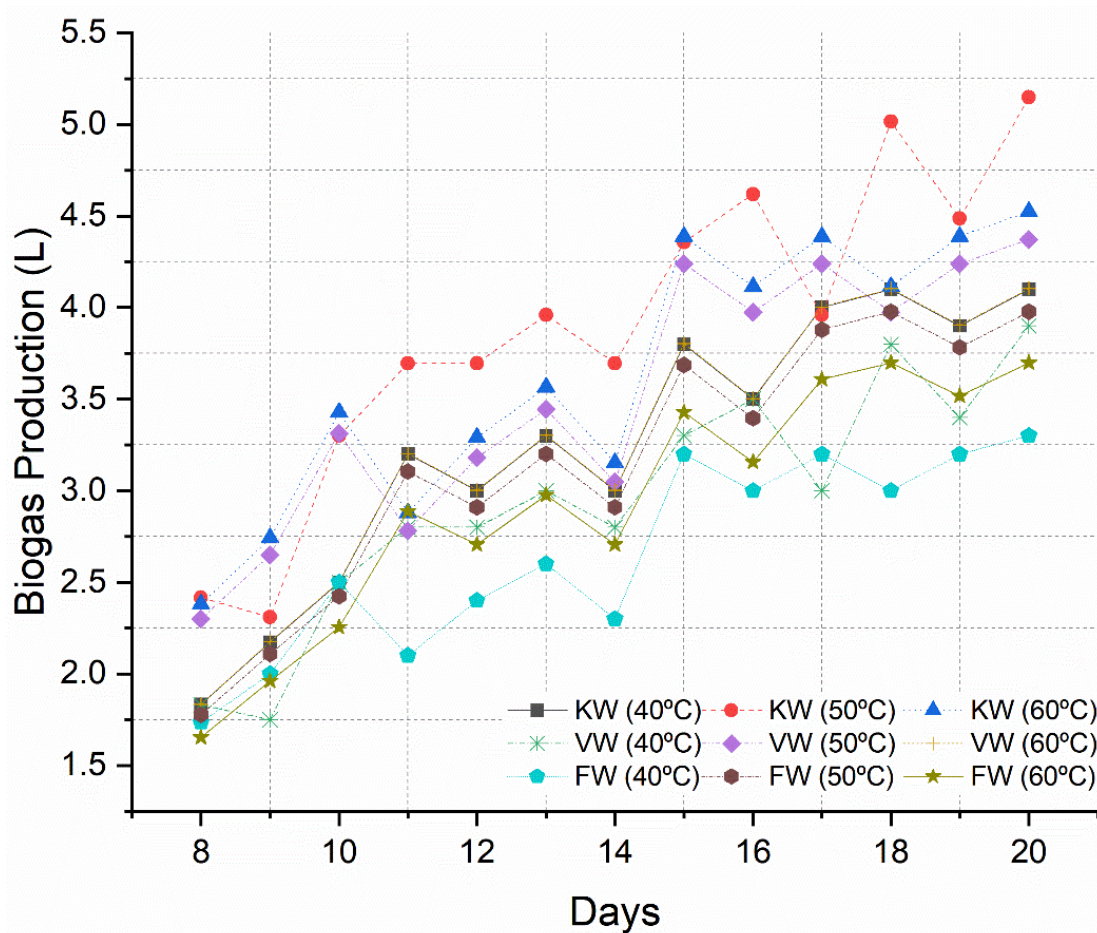
Fig. 4. 3  $\text{CH}_4 / \text{CO}_2$  per day for varied feedstock

#### 4.1.2 Effect of Temperature on Biogas Production Rate & $\text{CH}_4 / \text{CO}_2$

Kitchen Waste, Vegetable Waste, and Fruit Waste were considered to study the effect of temperature on biogas production. The production was made at the condition of digester temperature being 40°C, 50°C, 60°C, and no mixing or agitation of digester.

**Table 4. 2** Experimental Matrix of the Biogas Production

Feedstock	Temperature	Mixing Duration
Kitchen Waste	30°C, 40°C, 50°C	Nil
Vegetable Waste		
Fruit Waste		

**Fig. 4. 4** Biogas Production per day for varied feedstock and temperature

Feedstock (substrate nutrients) and temperature are among the most important variables influencing the stability and efficiency of anaerobic digestion. As given in Fig. 4.4, for each feedstock, biogas production per day was observed highest for the digester at 50°C, followed by 60°C and 40°C. The three highest biogas production peaks were observed at 5.15 L for the digester with kitchen waste at 50°C, followed by 4.52 L for the digester with kitchen waste at 60°C and 4.37 L for the digester with Vegetable waste at 50°C. Microbial activity is temperature dependent, peaking around 50°C and then declining. Anaerobic organic material breakdown and microbial growth and survival are both significantly impacted by temperature.

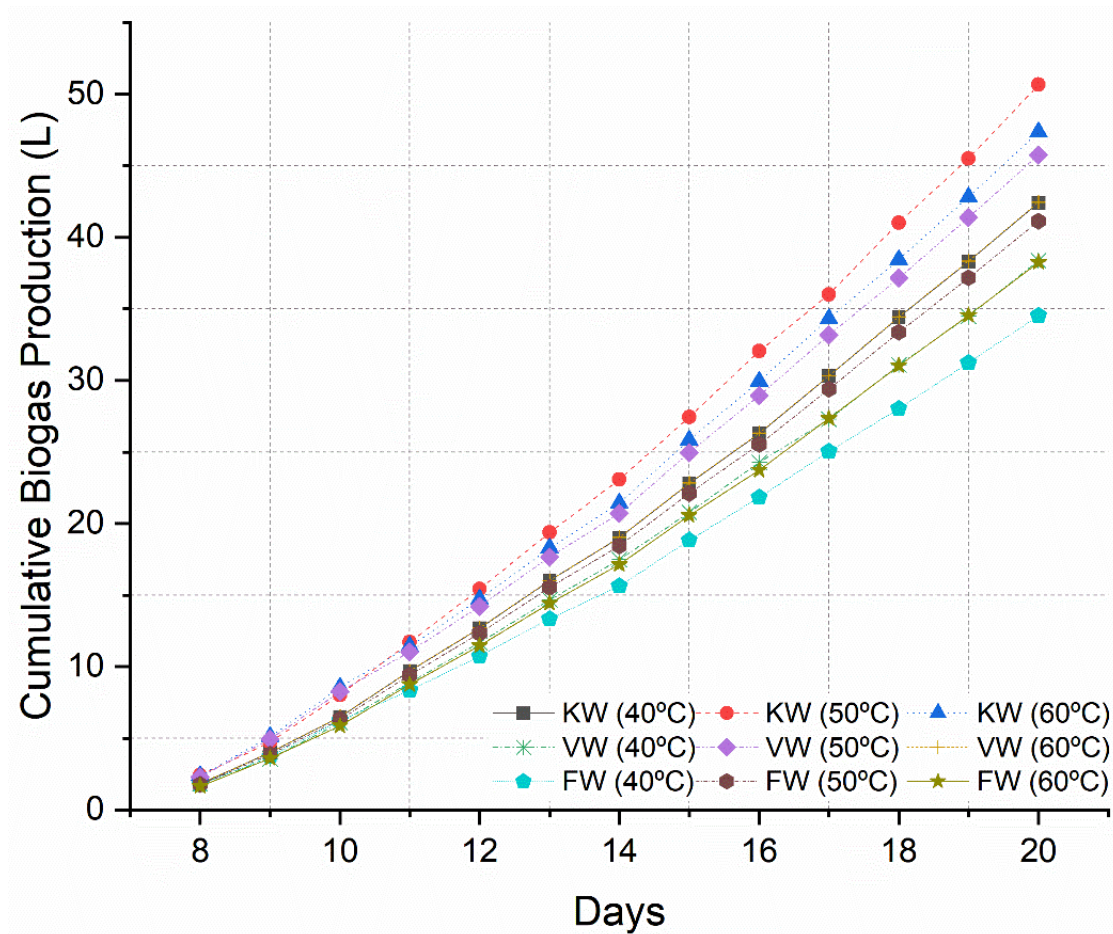


**Fig. 4.5** Cumulative Biogas Production for varied feedstock and temperature

Regardless of the types of feedstocks, the cumulative biogas production was observed highest for the digester at 50°C, followed by 60°C and 40°C, as given in Fig. 4.5. The rate of chemical reactions increases with temperature, which means that the microbes that produce biogas can work faster at higher temperatures. Additionally, water viscosity decreases with temperature, which helps distribute nutrients and oxygen more evenly throughout the digester. Elevated temperatures of 60°C result in the mortality of the microorganisms responsible for biogas production, leading to a decrease in methanogenic activity for biogas production, and hence lower CBP in comparison to 50°C. For Kitchen waste, an increase in CBP of 19.47% and 11.68% was observed for the digester at 50°C and 60°C, in contrast to the digester at 40°C. A previous study with food waste as its feedstock, observed CBP highest for anaerobic digestion at 50°C, followed by 60°C, 40°C and 30°C respectively. Higher CBP of 16.98% and 9.81% was observed for 50°C and 60°C, in comparison to 40°C for the period of 20 days [123]. Another study that studied the effects of temperature (30 to



60°C) on Anaerobic digestion of food waste, observed similar effects of highest CBP for 50°C, followed by 60°C, 40°C, and 30°C respectively. Increased CBP of 13.87% and 9.53% was observed for 50°C and 60°C, in comparison to 40°C, for the period of 20 days [124].

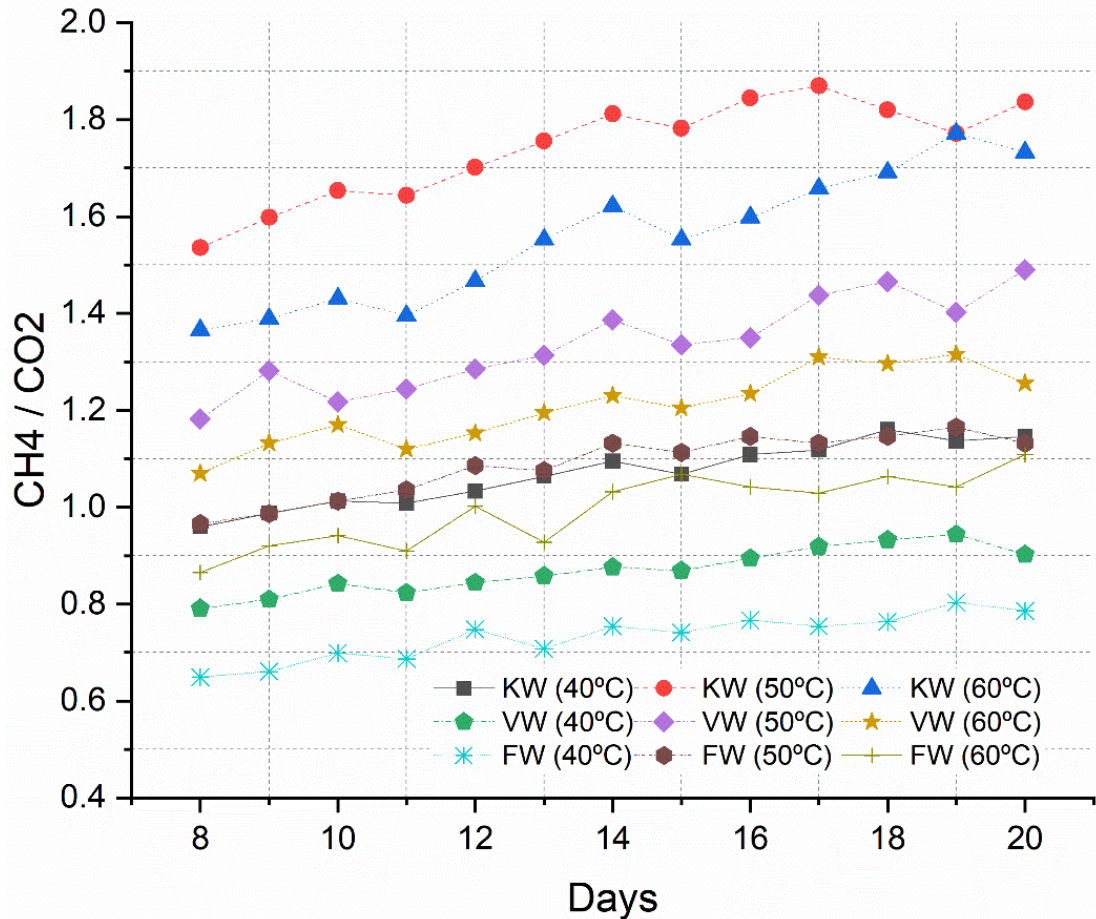


**Fig. 4. 6** CH<sub>4</sub>/CO<sub>2</sub> per day for varied feedstock and temperature

Since the processes involved in fermentation are athermic, it is known that temperature affects the rate of development of the microbial species involved in anaerobic digestion. At lower temperatures, the methane content of biogas is lower, because other gases, such as carbon dioxide and hydrogen sulfide, are produced in larger quantities. At higher temperatures, the methane content of biogas is higher, because the methane-producing bacteria are more active. The highest CH<sub>4</sub>/CO<sub>2</sub> is observed for the digester at 50°C, followed by the digester at 60°C and 40°C, regardless of the types of feedstocks, as given in Fig. 4.6. The three highest peak CH<sub>4</sub>/CO<sub>2</sub> is observed at 1.87 for Kitchen waste at 18<sup>th</sup> day at the digester temperature of 50C, followed by 1.77 for Kitchen waste at 19<sup>th</sup> day at the digester temperature of 60°C, and 1.46 for vegetable waste at 18<sup>th</sup> day at the digester temperature of 50°C. As for the average CH<sub>4</sub>/CO<sub>2</sub> for the recorded 13 days, an increase of 62% and 45% was observed for the kitchen waste with a digester temperature of 50°C and 60°C, in

comparison to kitchen waste with a digester at 40°C. A previous study with sewage sludge as its feedstock, observed CH<sub>4</sub> / CO<sub>2</sub> higher for anaerobic digestion at 55°C, compared to 42°C [125]. Similarly, another study for anaerobic digestion of Algal biomass *Laminaria digitata* observed the highest CH<sub>4</sub>/CO<sub>2</sub> at 55°C, compared to 35°C and 45°C [126]. A study that compared the effect of temperature(55 and 65°C) on anaerobic digestion of food waste, observed 14.87% higher CH<sub>4</sub> for 55°C in comparison to 65°C [127].

#### 4.1.3 Effect of Mixing Duration on Biogas Production Rate & CH<sub>4</sub>/CO<sub>2</sub>

Kitchen waste, vegetable waste, and fruit waste are considered to study the effect of feedstock on biogas production. The production was made at the condition of digester temperature being 40°C with mixing duration of 15 and 30 minutes, and no mixing condition.

**Table 4. 3** Experimental Matrix of the Biogas Production

Feedstock	Temperature	Mixing Duration
Kitchen Waste	40°C	Nil, 15 minutes, 30 minutes
Vegetable Waste		
Fruit Waste		

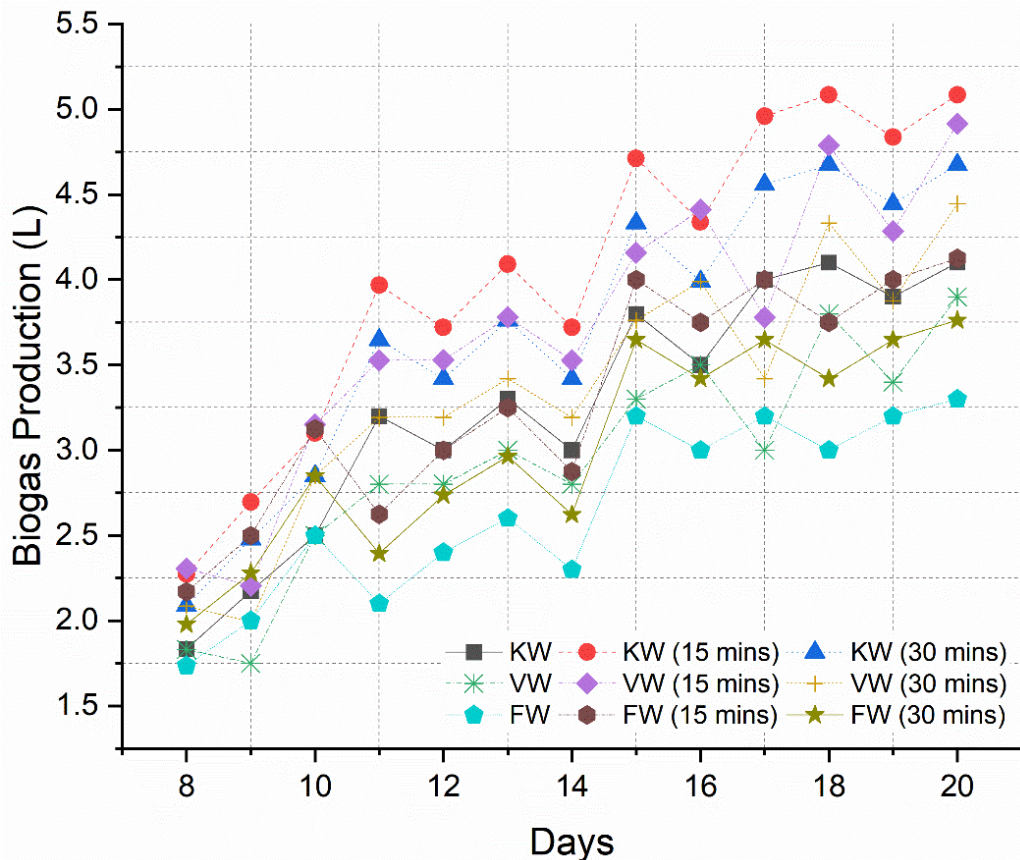


**Fig. 4. 7** Biogas Production per day for varied feedstock and mixing duration

As given in Fig. 4.7, for each feedstock, biogas production per day was observed highest for the digester at a mixing duration of 15 minutes, followed by 30 minutes and digester with no mixing. The three highest biogas production peaks were observed at 5 L for the digester with kitchen waste at a mixing duration of 15 minutes, followed by 4.9 L for the digester with vegetable waste at 15 minutes and 4.6 L for the digester with kitchen waste at 30 minutes mixing duration. The feed was distributed appropriately with a lower mixing duration of 10-20 minutes, which also allowed for the establishment of new spatial linkages and propionate turnover due to the dissolution of syntrophic relationships. Because hydrolysis and fermentation were slowed down by little mixing, syntrophs, and methanogens could consume the fermentation products without producing new molecules during this time. According to earlier studies, excessive mixing can speed up hydrolysis and fermentation. Still, the inhibitory effect of fermentation products makes it so syntrophic bacteria and methanogens can't convert them fast enough, lowering digestion performance [128].

Regardless of the types of feedstocks, the cumulative biogas production was observed highest for 15 15-minute mixing duration for feedstock, followed by 30 minutes and digester with no mixing, as given in Fig. 4.8. Research by Schink et al. (1990) found that kinetic efficacy is decreased when there is insufficient mixing. This is because, when cells expand, they are encircled by their progeniture, and sometimes, fresh cells need to be mixed in. Increasing mixing time can increase biogas production by evenly distributing substrate, removing solids, and keeping substrate aerobic. However, a decrease in CBP for higher mixing duration may be attributed to damaging the methane-producing bacteria [129]. Research by Stroot PG et al. (2001) lends credence to the idea that anaerobic digesters run more smoothly with less mixing, increasing specific gas production by facilitating excellent substrate-microbe interaction [130]. For Kitchen waste, an increase in CBP of 24% and 14% was observed for the digester at a mixing duration of 15 minutes and 30 minutes, in comparison to the digester with no mixing. Reducing mixing time from 45 minutes per hour to 15 minutes per hour increased biogas generation, according to studies by Lin and Pearce [131]. The effects of continuous mixing were explored in a previous study using lab-scale continuously stirred tank reactors with cow dung as the feedstock. This included mixing for 5 minutes at 15-minute intervals at 100 rpm. The reactors were operated at 35°C. Mixing boosted biogas output by 2.2% compared to non-mixing. Methane output increased by 3.21 % in the reactor with mixing compared to without mixing [132].

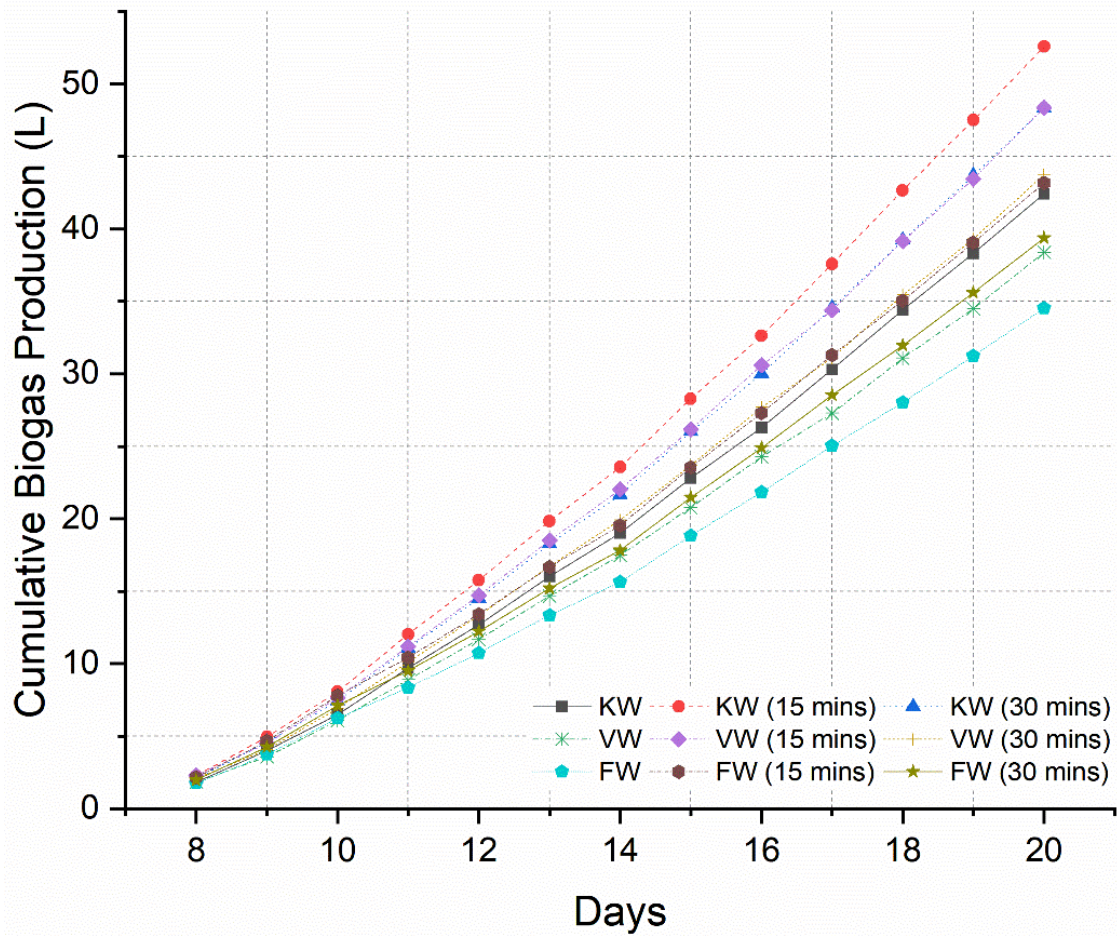


**Fig. 4. 8** Cumulative Biogas Production for varied feedstock and mixing duration

Regardless of the types of feedstocks, the highest  $\text{CH}_4 / \text{CO}_2$  is observed for the digester with mixing duration of 15 minutes, followed by the digester with 30 minutes and digester with no mixing respectively, as given in Fig. 4.6. The three highest peak  $\text{CH}_4/\text{CO}_2$  is observed at 1.55 for Kitchen waste at 18<sup>th</sup> day at the digester mixing duration of 15 minutes, followed by 1.37 for Kitchen waste at 18<sup>th</sup> day at the mixing duration of 30 minutes, and 1.22 for vegetable waste at 19<sup>th</sup> day at the digester mixing duration of 15 minutes. As for the average  $\text{CH}_4/\text{CO}_2$  for the recorded 13 days, an increase of 33.9% and 18.6% was observed for the kitchen waste with a digester with a mixing duration of 15 minutes and 30 minutes, in comparison to kitchen waste with a digester with no mixing. Mixing evenly distributes substrate to methanogenic bacteria. This ensures they have food to produce methane. Without mixing, some bacteria may not have enough food, leading to lower methane production. Therefore, mixing is vital for optimal methane production. In addition, mixing helps to prevent the formation of clumps, which can also lead to lower methane production.

A study by Lin and Pearce observed 2-3% higher CH<sub>4</sub> content for the mixed digester, in comparison to the unmixed digester [131].

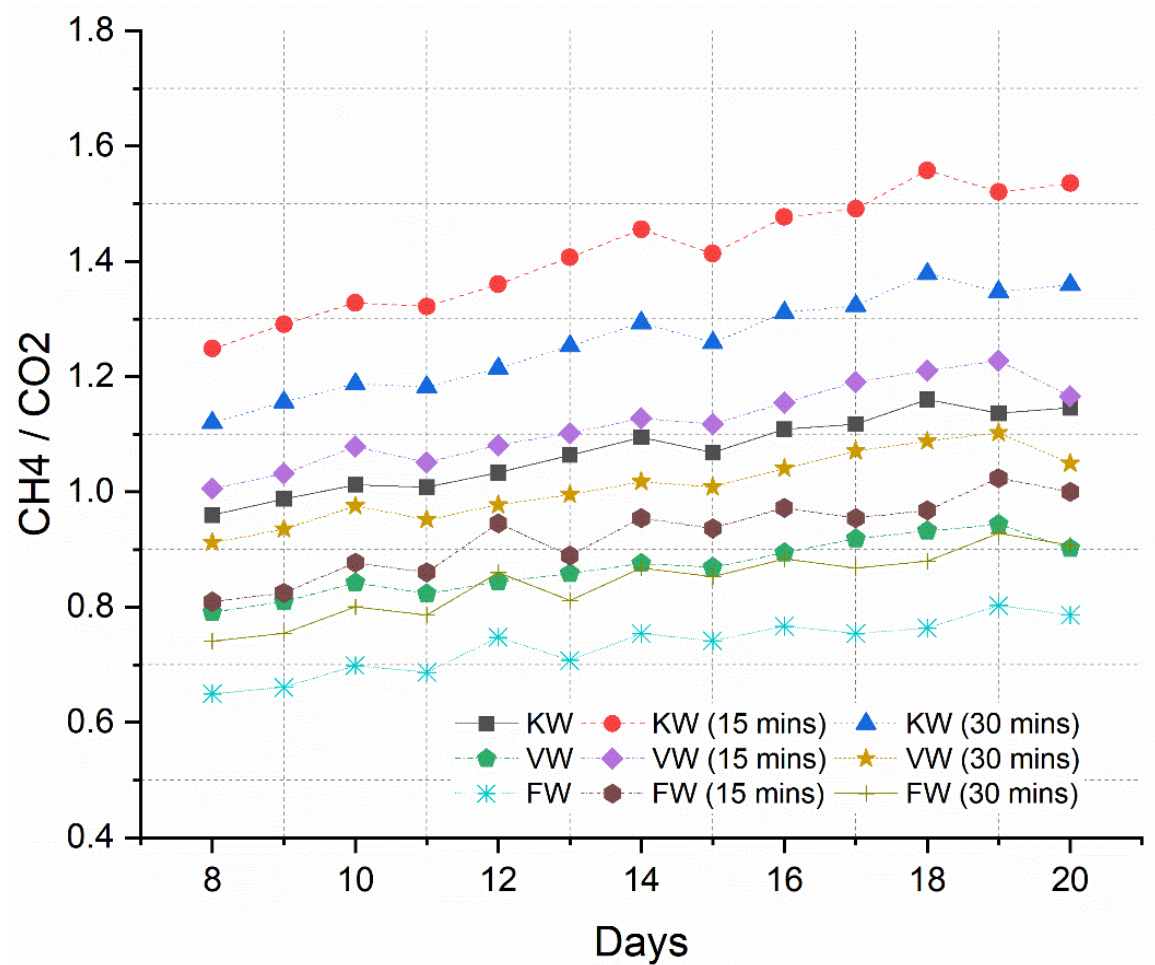


**Fig. 4. 9** CH<sub>4</sub>/CO<sub>2</sub> per day for varied feedstock and mixing duration

## 4.2 Biogas Production Optimization

Table 4.4 displays the experimental results obtained from DOE runs. The results were the same after three separate runs of each experiment. After data collection from each duplicate, a standard averaging procedure was used to get the mean value for each experimental condition.

**Table 4. 4** Design of Experiment for Biogas Production Optimization

	<b>Input 1</b>	<b>Input 2</b>	<b>Input 3</b>	<b>Response 1</b>	<b>Response 2</b>
<b>Run</b>	<b>Temp</b>	<b>Mixing Duration</b>	<b>Type of waste</b>	<b>CBP</b>	<b>CH<sub>4</sub>/ CO<sub>2</sub></b>
Unit	°C	min		L	
<b>1</b>	50	15	KW	61.48	2.11
<b>2</b>	60	0	KW	47.36	1.56
<b>3</b>	50	15	VW	52.00	1.42
<b>4</b>	60	30	KW	53.52	1.80
<b>5</b>	40	0	KW	42.41	1.07
<b>6</b>	60	30	FW	48.82	1.41
<b>7</b>	50	15	VW	52.24	1.45
<b>8</b>	50	15	VW	52.10	1.43
<b>9</b>	50	15	FW	56.74	1.78
<b>10</b>	50	30	VW	47.66	1.29
<b>11</b>	50	0	VW	41.50	1.09
<b>12</b>	60	15	VW	48.58	1.33
<b>13</b>	40	30	FW	44.14	1.03
<b>14</b>	60	0	FW	42.45	1.21
<b>15</b>	40	0	FW	38.38	0.87
<b>16</b>	50	15	VW	52.05	1.42
<b>17</b>	40	30	KW	48.12	1.26
<b>18</b>	40	15	VW	43.86	0.90
<b>19</b>	50	15	VW	52.30	1.46
<b>20</b>	50	15	VW	52.15	1.44

#### 4.2.1 RSM Model Analysis

Analysis of Variance (ANOVA) is evaluated by fitting Equation 1 into DOE data. The model formulated in the ANOVA Table 4.5 and 4.6 for the output parameter is considered significant since the P-value for all output parameters was less than 0.05 for both the model and existing inputs. High  $R^2$  and Adjusted (adj.)  $R^2$  values were observed for all the output responses, which implies that the model produces significantly similar data compared to the

experimental data. The adj.  $R^2$  and Predicted (Pred.)  $R^2$  values had a disparity of less than 2% for all the responses, indicating good prediction reliability. Tables 4.5 and 4.6 show that the lack of fit is insignificant since its  $P$  value is greater than 0.05. The second-order polynomial equation (Eqn. 3.1) derives the coded relationship for the RSM model formed between the input variables and engine responses.

**Table 4. 5** ANOVA table for CBP

Source	SS	df	Mean Square	F-value	p-value	Contribution (%)	Remarks
<b>Model</b>	605.9	9	67.32	5411.79	< 0.0001	99.98	significant
A-Temp	56.78	1	56.78	4564.73	< 0.0001	9.37	
B-MD	90.93	1	90.93	7309.68	< 0.0001	15.00	
C-Type of Waste	49.99	1	49.99	4018.15	< 0.0001	8.25	
AB	0.139	1	0.139	11.18	0.0074	0.02	
AC	0.321	1	0.321	25.81	0.0005	0.05	
BC	0.0081	1	0.0081	0.6518	0.4383	0.00	
A <sup>2</sup>	96.11	1	96.11	7726.03	< 0.0001	15.86	
B <sup>2</sup>	156.94	1	156.94	12616.16	< 0.0001	25.90	
C <sup>2</sup>	133.87	1	133.87	10761.25	< 0.0001	22.09	
<b>Residual</b>	0.1244	10	0.0124				
Lack of Fit	0.0592	5	0.0118	0.9067	0.5415		not significant
Pure Error	0.0652	5	0.013				
<b>Cor Total</b>	606.02	19	0.9998	R <sup>2</sup>			0.9998
Std. Dev.	0.1115			Adjusted R <sup>2</sup>			0.9996
Mean	48.89			Predicted R <sup>2</sup>			0.999
C.V. %	0.2281			Adeq Precision			292.0868

#### 4.2.2 Interaction effects for CBP

With the chosen input variables considered, the empirical model for analysing CBP is shown in equation 4.1. The presence of positive coefficients (i.e., Temperature, Mixing Duration) in all linear terms indicates that an increase in the fraction of this term results in a proportional rise in the CBP response. In contrast, negative coefficients (i.e., Type of waste) in all linear terms indicate that an increase in this term results in a proportional reduction in CBP response. Mixing Duration input has the largest coefficient for CBP response among the independent variables, followed by Temperature, and Type of waste respectively.

$$CBP = 52.1379 + 2.38295 * A + 3.01548 * B + -2.23573 * C + 0.131837 * AB + -0.200321 * AC + 0.0318357 * BC + -5.91179 * A^2 + -7.55448 * B^2 + 6.97706 * C^2 \quad (4.1)$$

Three-dimensional response surface graphs were used to explore the interaction effects of the selected response (CBP) by retaining two variables at the central level and differentiating others within the experimental range. As given in Fig. 4.10, The 3D surface plots of different combinations suggest that Temperature and Mixing duration have a synergistic interaction effect on CBP for up to about temperature of 50°C and 20 minutes of mixing duration while Temperature and Type of waste exhibit antagonistic interaction on CBP. Based on the slope of the graph, the combination of Temperature and Type of waste was demonstrated as the most sensitive or significant in impacting CBP.

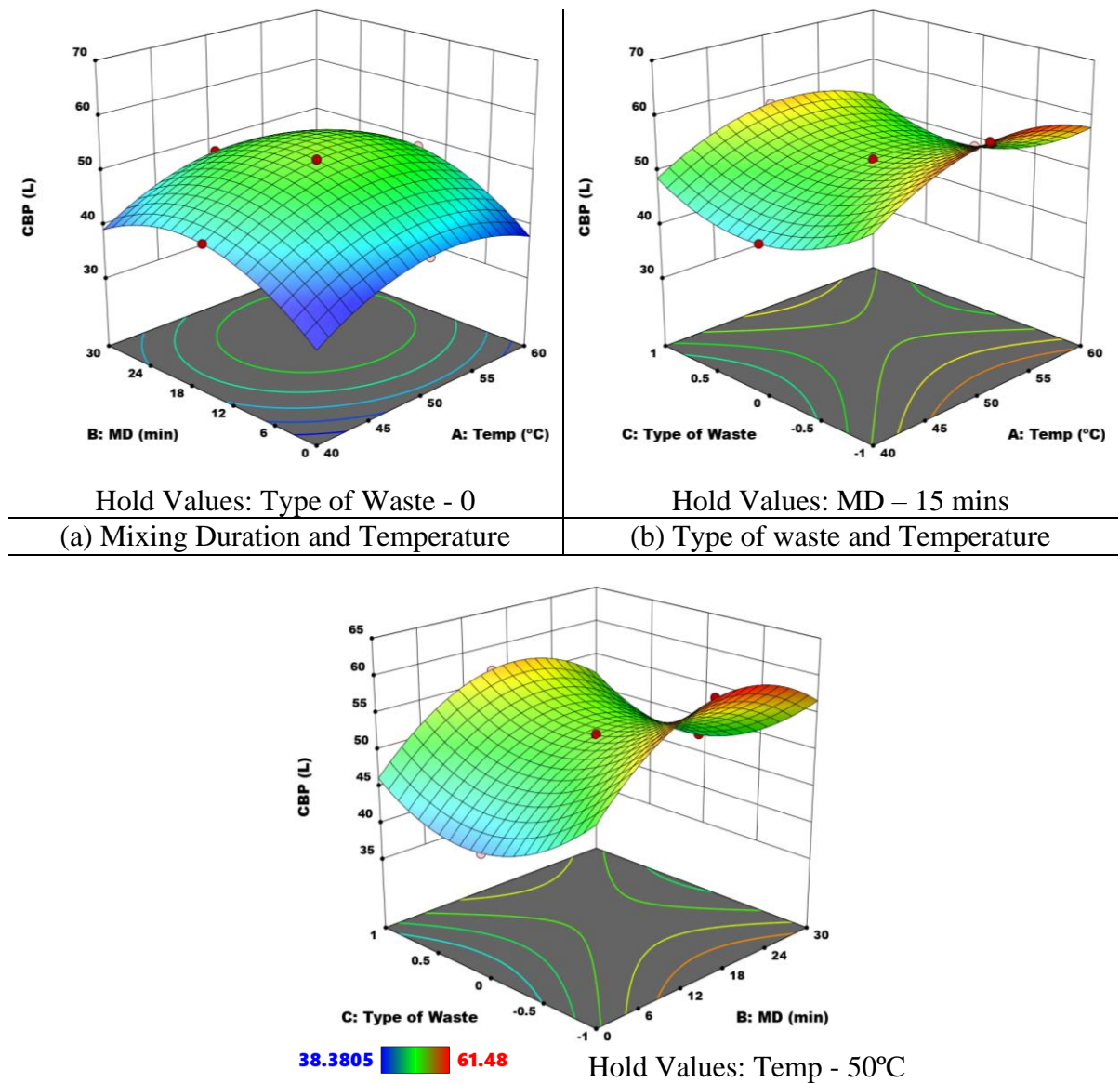


**Fig. 4. 10** Interaction effects of input parameters on CBP



Table 4. 6 ANOVA table for CH<sub>4</sub>/CO<sub>2</sub>

Source	SS	df	Mean Square	F-value	p-value	Contribution (%)	Remarks
<b>Model</b>	1.77	9	0.1962	302.47	< 0.0001	100.00	significant
A-Temp	0.4748	1	0.4748	731.87	< 0.0001	26.82	
B-MD	0.1016	1	0.1016	156.61	< 0.0001	5.74	
C-Type of Waste	0.227	1	0.227	349.97	< 0.0001	12.82	
AB	0.0014	1	0.0014	2.19	0.1698	0.08	
AC	0.0119	1	0.0119	18.41	0.0016	0.67	
BC	0.0008	1	0.0008	1.18	0.3033	0.05	
A <sup>2</sup>	0.3548	1	0.3548	546.86	< 0.0001	20.05	
B <sup>2</sup>	0.2183	1	0.2183	336.51	< 0.0001	12.33	
C <sup>2</sup>	0.6142	1	0.6142	946.69	< 0.0001	34.70	
<b>Residual</b>	0.0065	10	0.0006				
Lack of Fit	0.0052	5	0.001	4.23	0.0696		not significant
Pure Error	0.0012	5	0.0002				
<b>Cor Total</b>	1.77	19	0.9998	R <sup>2</sup>			0.9963
Std. Dev.	0.0255			Adjusted R <sup>2</sup>			0.993
Mean	1.37			Predicted R <sup>2</sup>			0.9853
C.V. %	1.87			Adeq Precision			66.6469

#### 4.2.3 Interaction effects for CH<sub>4</sub>/CO<sub>2</sub>

With the chosen input variables considered, the empirical model for analysing CH<sub>4</sub>/CO<sub>2</sub> is shown in equation 4.2. The presence of positive coefficients (i.e., Temperature, Mixing Duration) in all linear terms indicates that an increase in the fraction of this term results in a proportional rise in the CH<sub>4</sub>/CO<sub>2</sub> response. In contrast, negative coefficients (i.e., Type of waste) in all linear terms indicate that an increase in this term results in a proportional reduction in CH<sub>4</sub>/CO<sub>2</sub> response. Temperature input has the largest coefficient for CH<sub>4</sub>/CO<sub>2</sub> response among the independent variables, followed by Mixing Duration and Type of waste, respectively.

$$\text{CH}_4 / \text{CO}_2 = 1.44942 + 0.217899 * A + 0.100798 * B + -0.150679 * C + 0.013324 * AB + -0.0386438 * AC + -0.00977296 * BC + -0.35918 * A^2 + -0.281756 * B^2 + 0.472581 * C^2 \quad (4.1)$$

Three-dimensional response surface graphs were used to explore the interaction effects of the selected response (CH<sub>4</sub>/CO<sub>2</sub>) by retaining two variables at the central level and differentiating others within the experimental range. As given in Fig. 4.11, The 3D surface

plots of different combinations suggest that Temperature and Mixing duration have a synergistic interaction effect on CH<sub>4</sub>/CO<sub>2</sub> for up to about temperature of 55°C and 20 minutes mixing duration while Temperature and Type of waste exhibit antagonistic interaction on CH<sub>4</sub>/CO<sub>2</sub>. Based on the slope of the graph, the combination of Temperature and Type of waste was indicated as the most sensitive or significant in impacting CH<sub>4</sub>/CO<sub>2</sub>.

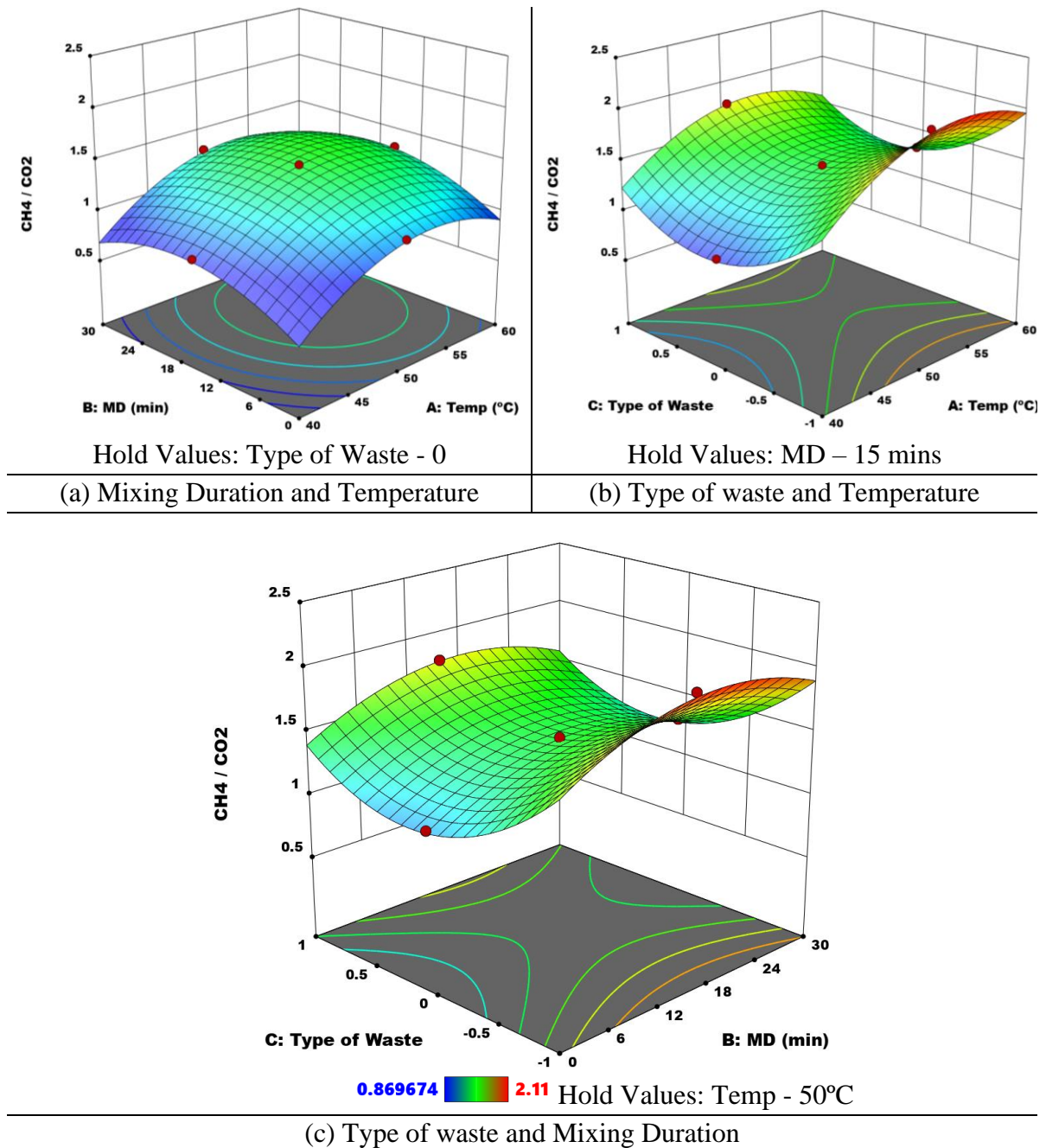
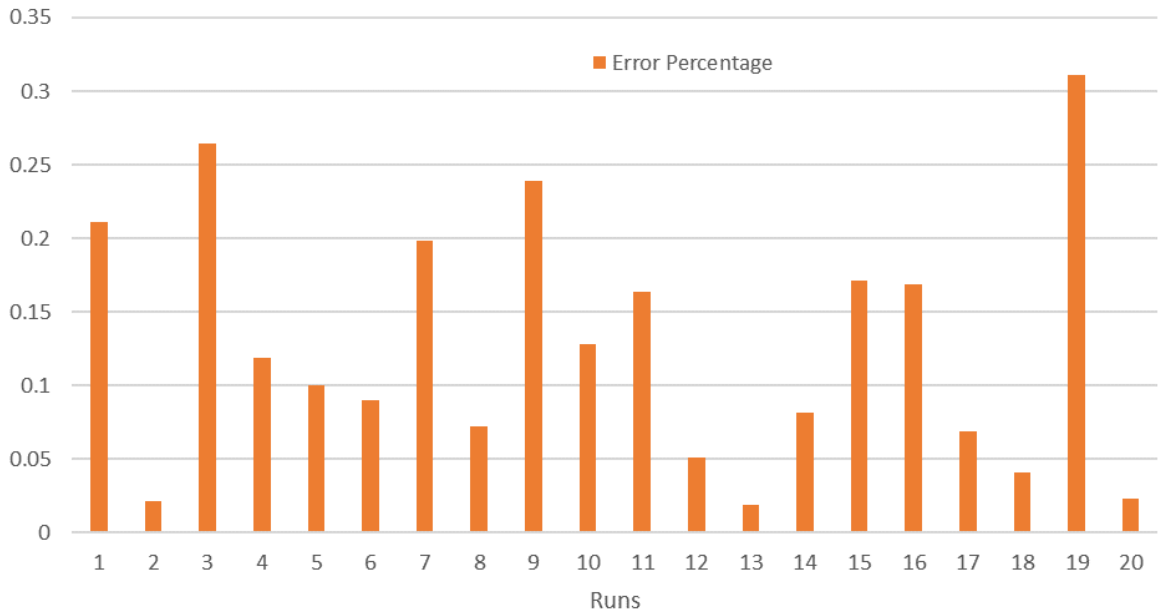


Fig. 4. 11 Interaction effects of input parameters on CH<sub>4</sub>/CO<sub>2</sub>

#### 4.2.4 Evaluated metrics

The proportion of error for the RSM projected output responses is determined for each run in the DOE using Equation 3.14, as shown in Fig. 4.12 and 4.13.



**Fig. 4. 12** Error percentage for DOE runs for CBP

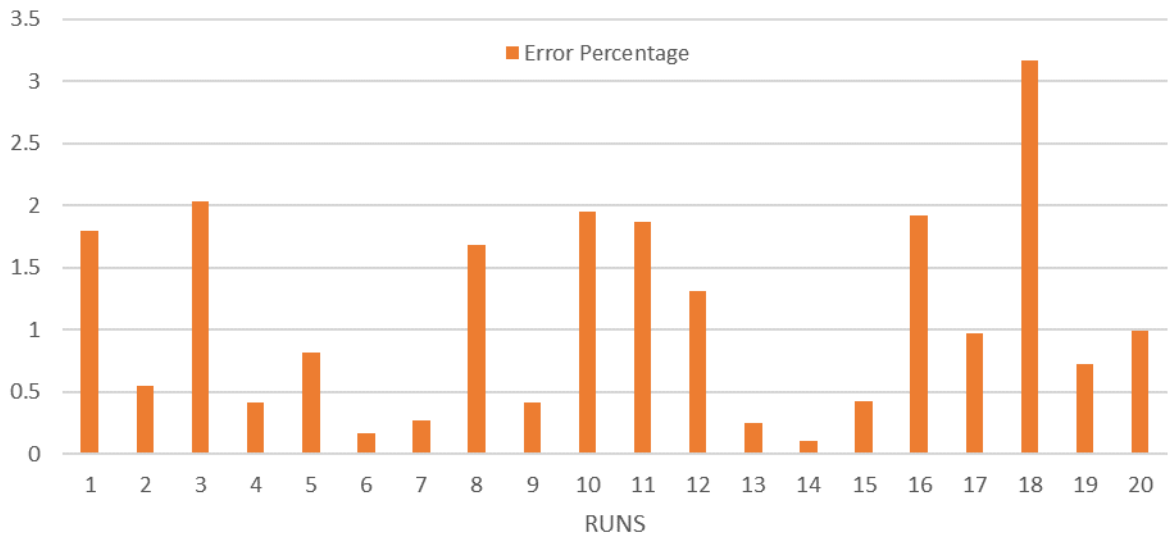


**Fig. 4. 13** Error percentage for DOE runs for CH<sub>4</sub>/CO<sub>2</sub>

Table 4.7 displays the evaluation metrics for the RSM model's prediction:  $R^2$ , RMSE, and MAD. For the most part, the RSM model's predictions had good  $R^2$ , minimal RMSE, and low MAD. The RSM model's accurate predictions and minimal error rates prove a trustworthy regression analysis for the input variables studied.

**Table 4. 7** Evaluation Metrics for RSM Model Predictions

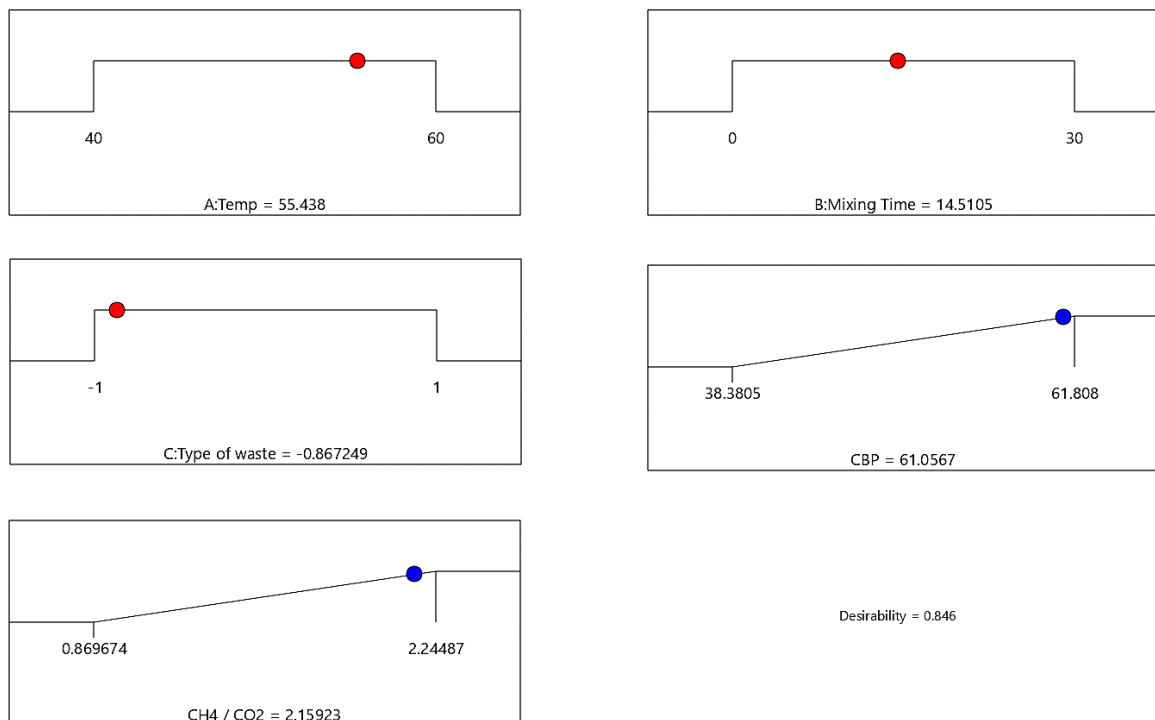
Outputs	R <sup>2</sup>	RMSE	MAD
CBP	0.9998	0.276	0.137
CH <sub>4</sub> /CO <sub>2</sub>	0.9963	0.928	0.411

#### 4.2.5 Optimization of input parameters and Validation

To optimize multiple responses, RSM took advantage of its desirability function optimization. Optimal values for the process parameters were obtained via the optimization process, and targets were established accordingly. It is configured to maximize both CBP and CH<sub>4</sub>/CO<sub>2</sub>. Table 4.8 provides a concise summary of the optimization method's criteria. An equal importance of 3 was set for each of the output parameters goals.

**Table 4. 8** Optimization Criteria for Biogas Production

Name	Goal	Lower Limit	Upper Limit	Importance
A: Temp	In range	40	60	3
B: MD	In range	0	30	3
C: Type of Waste	In range	-1	1	3
CBP	Maximize	38.38	61.48	3
CH <sub>4</sub> /CO <sub>2</sub>	Maximize	0.869	2.11	3

**Fig. 4. 14** Desirability Plot

The RSM model with the desirability of 0.846, as given in Fig. 4.14, observed an optimum value of CBP- 61.05 L, CH<sub>4</sub> / CO<sub>2</sub> - 2.16 as observed at optimal input parameters of Temperature 55.45°C, Mixing Duration of 14.51 minutes, and a mixture of 86% kitchen waste and 14% vegetable waste.

Table 4.9 displays the optimum predicted results, validation outcomes, and Errors. Results optimized by the model have a percentage error of less than 5%, deemed significant enough for acceptance.

**Table 4. 9** RSM optimized parameter's validation test results and error percentage

Output	Model Technique: ANN-GA		
	Experiment	Estimated	Errors (%)
CBP	58.3	61.05	4.5
CH <sub>4</sub> /CO <sub>2</sub>	2.05	2.16	4.9

### 4.3 Summary

This chapter presents the effect of parameters such as temperature, mixing duration, and feedstocks on biogas production rate and methane generation, as well as the optimization of CBP and CH<sub>4</sub>/CO<sub>2</sub>. The key findings summarizing the chapter are:

1. At 40°C digester temperature, the digesters containing kitchen waste, vegetable waste, and fruit waste produced biogas over 3L per day on the 11th, 13th, and 15th days, respectively. Also, the highest concentration of CH<sub>4</sub>/CO<sub>2</sub> was detected at 1.16 on the 18th day for Kitchen garbage, followed by 0.94 on the 19th day for Vegetable waste, and 0.81 on the 19th day for fruit waste.
2. Kitchen waste exhibit highest CBP and CH<sub>4</sub>/CO<sub>2</sub>, followed by vegetable and fruit waste. At 40°C digester temperature, kitchen waste anaerobic digestion yields 9.67% and 18.63% greater CBP than vegetable and fruit waste. For the recorded days, kitchen waste had the highest average CH<sub>4</sub>/CO<sub>2</sub> at 1.07, followed by vegetable waste at 0.87 and fruit waste at 0.73.

3. Digester CBP and CH<sub>4</sub>/CO<sub>2</sub> were maximum at 50°C, followed by 60°C and 40°C, regardless of feedstock source. At 50°C and 60°C, kitchen waste digesters showed a 19.47% and 11.68% increase in CBP compared to 40°C digesters. The average CH<sub>4</sub>/CO<sub>2</sub> increased by 62% and 45% for kitchen trash digested at 50°C and 60°C, respectively, compared to 40°C.
4. Regardless of the types of feedstocks, the highest CBP and CH<sub>4</sub>/CO<sub>2</sub> are observed for the digester with a mixing duration of 15 minutes, followed by the digester with 30 minutes and the digester with no mixing respectively. For Kitchen waste at a digestion temperature of 40°C, an increase in CBP of 24% and 14% was observed for the digester at a mixing duration of 15 minutes and 30 minutes, in comparison to the digester with no mixing. As for the average CH<sub>4</sub>/CO<sub>2</sub>, an increase of 33.9% and 18.6% was observed for the kitchen waste with digester mixing duration of 15 minutes and 30 minutes, in comparison to kitchen waste digester with no mixing.
5. The f-value of Biogas response output from the RSM model suggests that among the input variables, Temperature is the most substantial influence in deciding the value of CH<sub>4</sub>/CO<sub>2</sub>, while Mixing Duration is the most substantial influencing parameter in determining the value of CBP.
6. Most of the RSM model's predictions exhibited high R<sup>2</sup> values, minimum RMSE, and low MAD. The RSM model's low error rates demonstrate its reliability as a regression analysis for the examined input variables.
7. The RSM model observed an optimum value of CBP- 61.05 L, CH<sub>4</sub>/CO<sub>2</sub> -2.16 at Temperature of 54.44 °C, Mixing Duration of 14.51 min, and feedstock mixture of 86% kitchen and 14% vegetable waste. The optimization findings confirm the positive effect of tumbling for both biogas production rate and methane production.

## CHAPTER 5 : ENGINE PERFORMANCE AND EMISSION EVALUATION

### 5.1 Effect of Biodiesel, Biogas, and Nanoparticles on CI Engine

The following sections investigate the effects of adding biogas, biodiesel, and nanoparticle-biodiesel blends on the performance and emission characteristics of compression ignition (CI) engines.

#### 5.1.1 Effect of Biogas Flow Rate (BFR) on Engine Performance and Emission

Diesel is considered the pilot fuel, while biogas at varied BFR is the gaseous fuel considered for dual fueling. Table 5.1 provides the experimental matrix. From 20% (2.4kg) load to 100% (12 kg) load, with a 20% (2.4 kg) increment, the load variations were carried out. The diesel and dual fuel modes were compared at the constant settings of 18:1 compression ratio and 23° BTDC injection time.

**Table 5. 1** Experimental Matrix of the Diesel-Biogas Run Dual Fuel Diesel Engine

Mode	Fuel used	Loading Conditions (%)
Diesel	100% diesel	20,40,60,80,100
Dual	BFR – 0.5 kg/h, 0.75 kg/h, 1 kg/h	

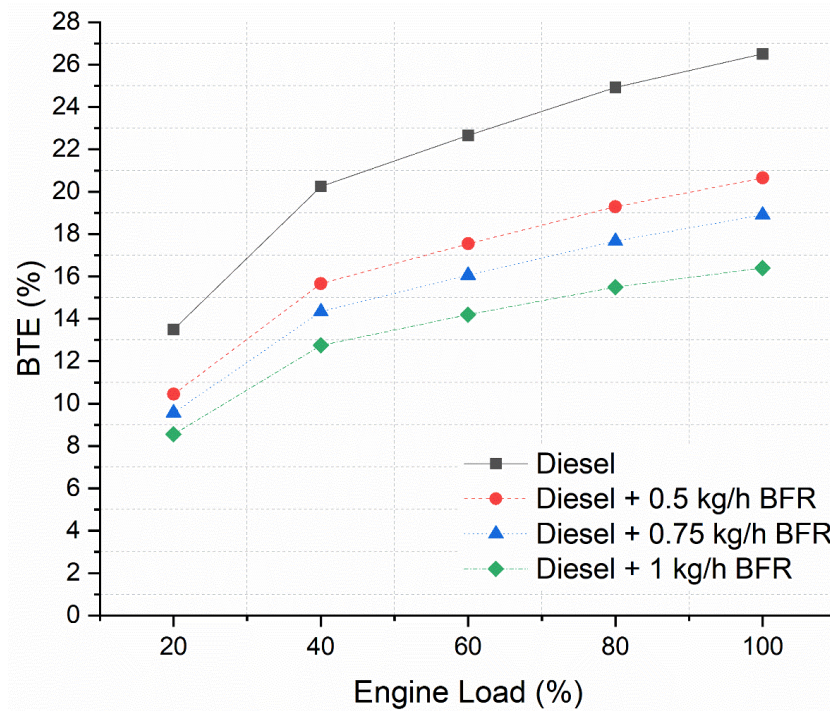


**Fig. 5. 1** Effect of BFR on BTE

BTE illustrates the conversion efficiency of fuel energy into mechanical work. Fig. 5.1 depicts the effect of load and BFR on BTE.

A rise in BTE was observed for increments in Load, with maximum BTE observed for the highest Load (100%) due to a surge in fuel supply and higher cylinder temperature [133]. BTE decreases with an increase in the BFR. Because of incomplete combustion induced by a lack of oxygen and the slower flame propagation speed of biogas, brake thermal efficiency has decreased [134]. At peak load conditions, compared to the engine run on neat diesel, BTE exhibits a decrease of 22%, 28.67%, and 38.11% for engine run on BFR of 0.5 kg/h, 0.75 kg/h, and 1 kg/h, respectively. Previous studies under a similar test setup with varying BFR reported a decline in BTE with an increment in BFR [96,135]. A study reported that compared to an engine run on neat diesel, at peak load conditions, the BTE exhibits a decrease of 16.5%, 20.46%, and 30.36% for an engine run on BFR of 0.6 kg/h, 0.9 kg/h, and 1.2 kg/h respectively [136].

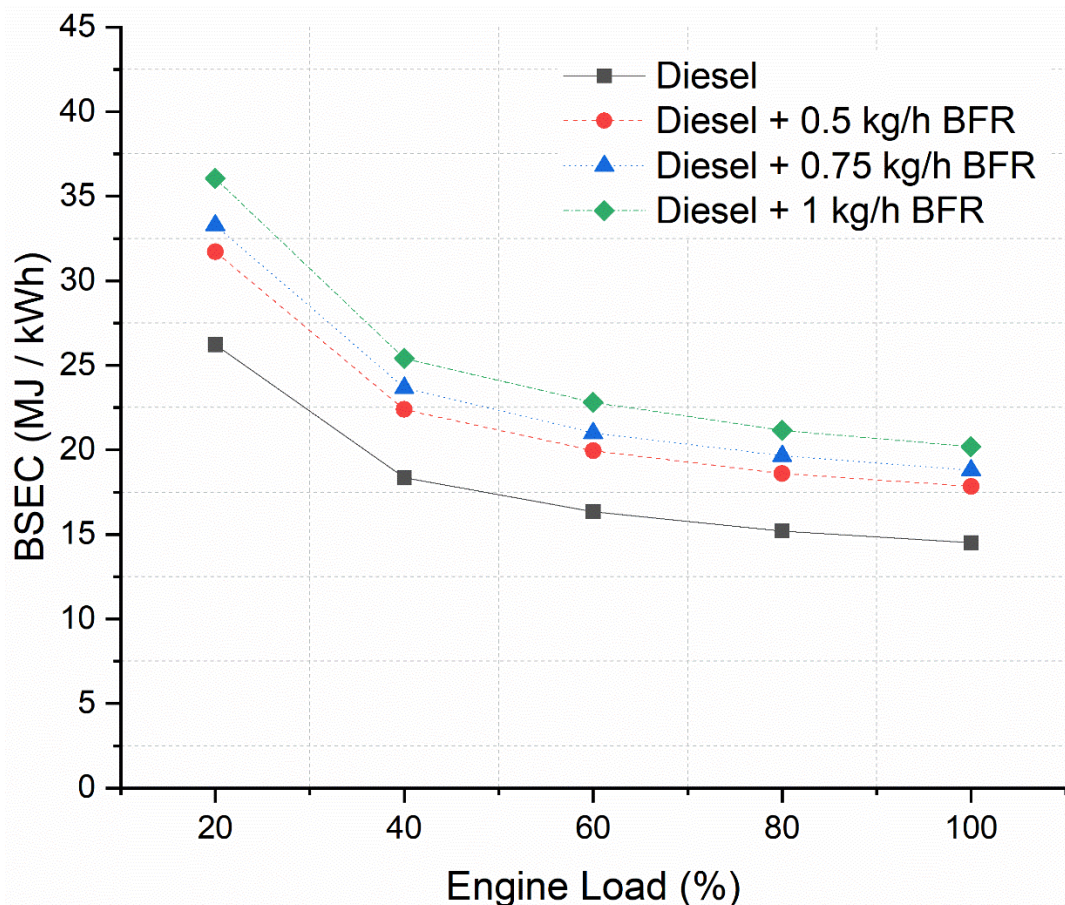


**Fig. 5. 2** Effect of BFR on BSEC

The amount of energy used from fuel energy to produce one kilowatt of power output is measured by BSEC [137]. Fig. 5.2 depicts the effect of Load and BFR for BSEC. BSEC for all BFR decreases with the rise in load. The drop in BSEC can be credited to better combustion quality brought by the rise in combustion temperature and pressure with an



increment in engine load. An increase in BSEC is observed with an increment in BFR. Since biogas has a lower calorific value than diesel, as biogas substitution increases, the fuel consumption increases resulting in increased BSEC [138]. As compared to the engine run on neat diesel, at peak load conditions, BSEC exhibits an increase of 23%, 29.65%, and 39.31% for engine run on BFR of 0.5 kg/h, 0.75 kg/h, and 1 kg/h, respectively. Previous studies done under a similar test setup with varying BFR reported an increase in BSEC with an increment in BFR [139,140]. A study reported that compared to an engine run on neat diesel, at peak load conditions, BSEC exhibits an increase of 15.92% and 35.6% for an engine run on BFR of 0.5 kg/h and 1 kg/h, respectively [96].

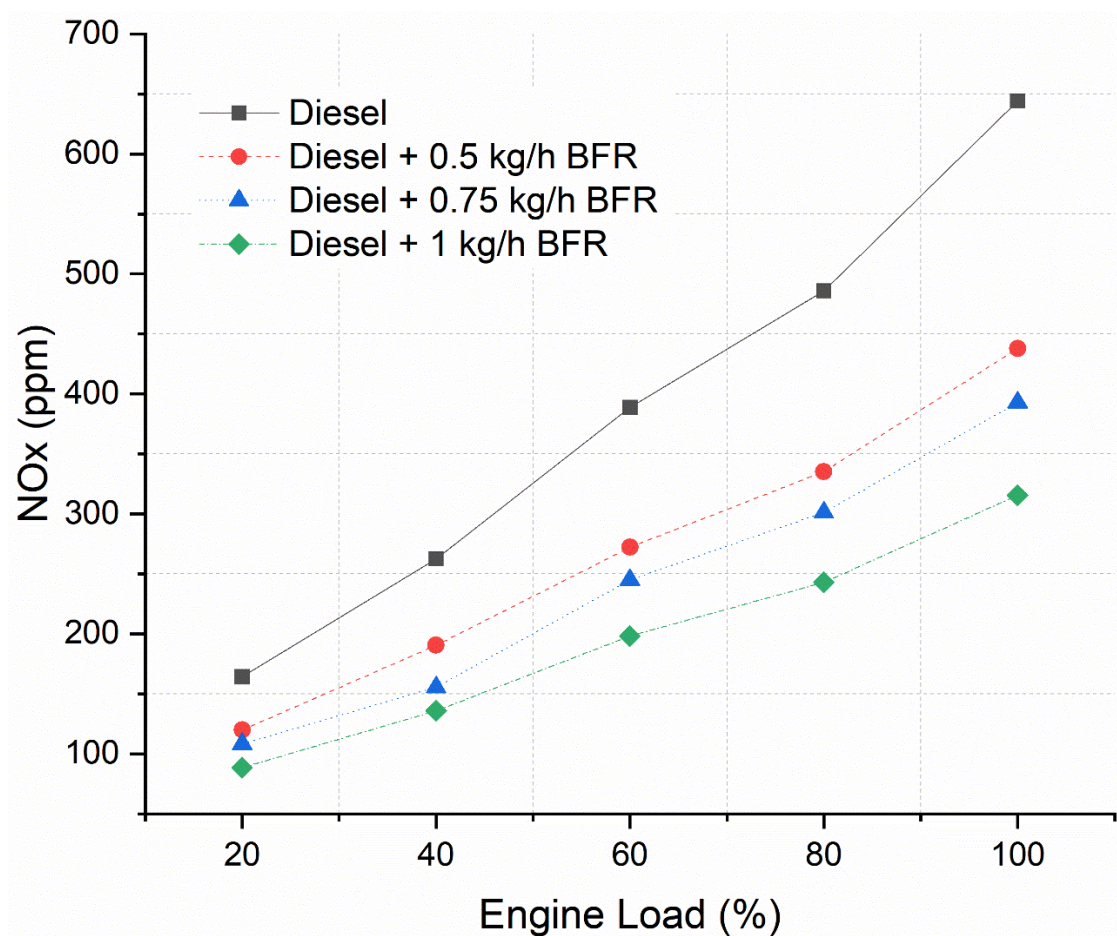


**Fig. 5.3** Effect of BFR on NO<sub>x</sub>

The high temperature of the combustion chamber and its prolonged duration are the factors that accelerate the oxidation of Nitrogen molecules, resulting in NO<sub>x</sub> formation [141]. Fig. 5.3 depicts the effect of BFR on NO<sub>x</sub>. As the load rises, NO<sub>x</sub> also increases, with maximum NO<sub>x</sub> to be found for the highest Load (100%) owing to the rise in fuel consumption and cylinder temperature [142]. A decline in NO<sub>x</sub> with an increment in the BFR for all loads

might be attributed to the increase in specific molar heat with an increment in BFR, which lowers the combustion chamber temperature [143]. As compared to the engine run on neat diesel, at peak load conditions,  $\text{NO}_x$  exhibits a decrease in 32%, 39%, and 51% for engine run on BFR of 0.5 kg/h, 0.75 kg/h, and 1 kg/h, respectively. Previous studies done under a similar test setup with varying BFR reported a decline in  $\text{NO}_x$  with an increment in BFR [96,135,139]. A study reported that compared to an engine run on neat diesel, at peak load conditions,  $\text{NO}_x$  exhibits a decrease of 41%, 49%, and 62% for an engine run on BFR of 0.6 kg/h, 0.9 kg/h, and 1.2 kg/h respectively [136].

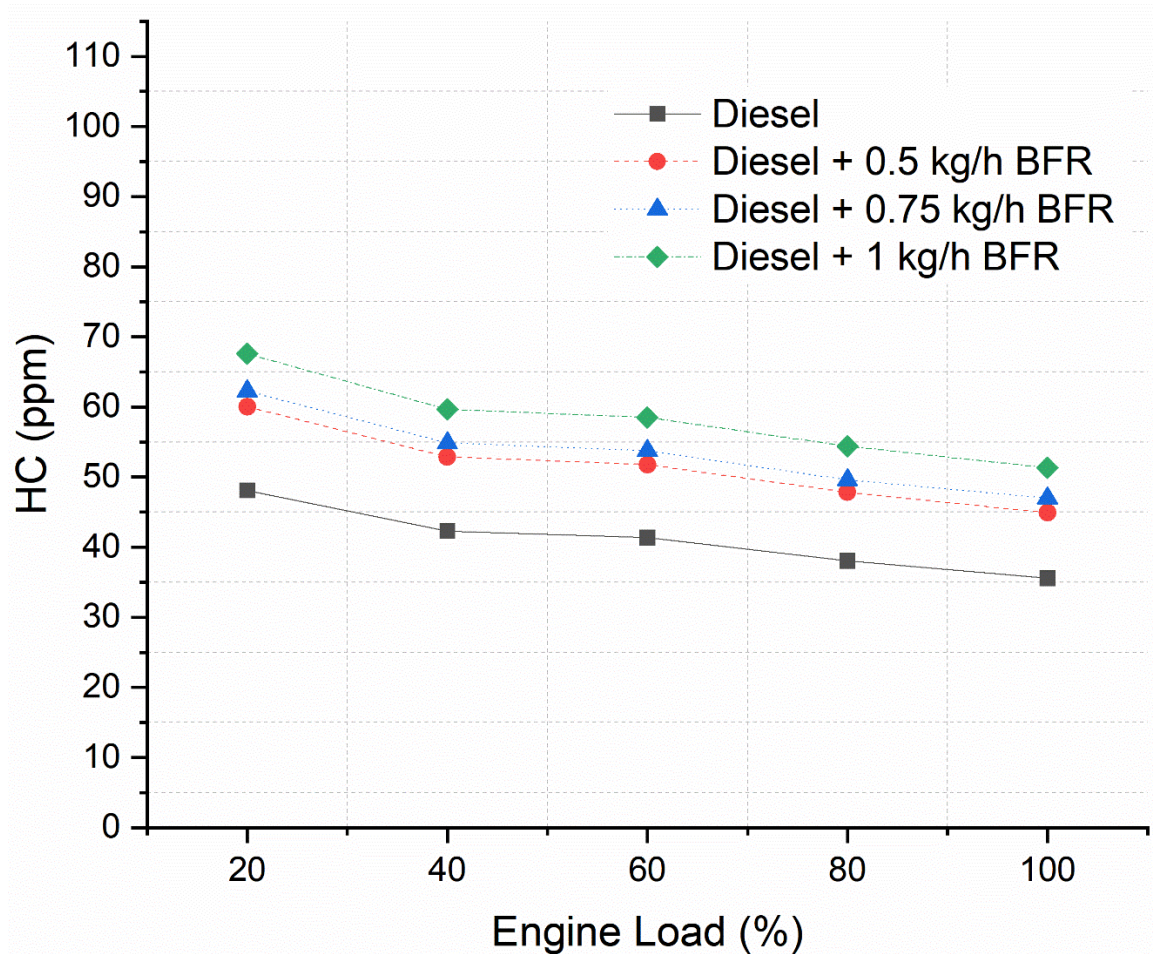


**Fig. 5. 4** Effect of BFR on HC

Unburned fuels that are present close to the cylinder walls due to insufficient in-cylinder temperature are known as hydrocarbon (HC) emissions [144]. Fig. 5.4 depicts the effect of BFR on HC. HC drops as the load increases. At low Load due to low engine cylinder temperature, improper combustion is attained, resulting in higher HC. At higher loads, homogeneous mixing of fuel with air reduces HC emissions [145]. HC increases with an increase in the BFR for all loads because there is insufficient fresh air input, which causes

the fuel to burn incompletely. The fuel mixture held in the crevice region and the clean fuel charge that escapes while the valve overlaps are additional factors that contribute to HC emission [146]. As compared to the engine run on neat diesel, at peak load conditions, HC exhibits an increase of 26.19%, 32.09%, and 44.23% for engine run on BFR of 0.5 kg/h, 0.75 kg/h, and 1 kg/h, respectively. Previous studies under a similar test setup with varying BFR reported an increase in HC with an increment in BFR. Previous studies reported that compared to an engine run on neat diesel, at peak load conditions, HC exhibits an increase of 41%, 35.17%, and 39.35% for an engine run on BFR of 1.2 kg/h [136], 1.2 kg/h [135], and 1 kg/h [96] respectively.

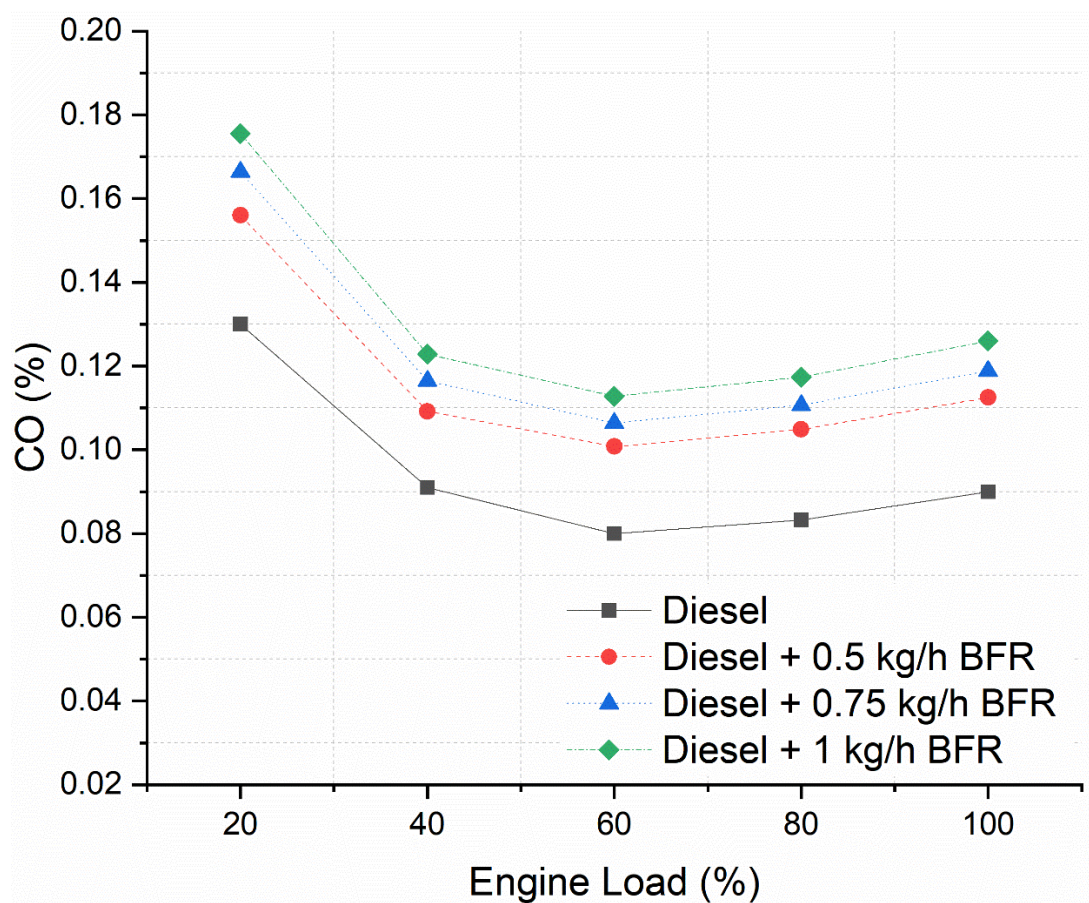


**Fig. 5. 5** Effect of BFR on CO

Carbon monoxide is produced due to poor fuel-to-oxidant mixing and incomplete combustion of fuel [147]. Fig. 5.5 depicts the effect of BFR on CO. From low to medium loading, the CO emission is reduced as the air-fuel mixture is closer to stoichiometric. At higher load conditions, the amount of CO emitted increases as more fuel is added to the combustion chamber, but the concentration of oxygen required for combustion is restricted. As a result, the fuel richness promotes CO emission [148]. Under all loads, CO is realized to

rise with an increment in BFR. Biogas's higher heat capacity and a lack of fresh air because of biogas substitution results in decreased in-cylinder temperature and incomplete combustion, two factors influencing the rise in CO emissions [149]. As compared to the engine run on neat diesel, at peak load conditions, CO exhibits an increase of 25%, 32%, and 40% for engine run on BFR of 0.5 kg/h, 0.75 kg/h, and 1 kg/h, respectively. Previous studies done under a similar test setup with varying BFR reported an increase in CO with an increment in BFR [96,135,139]. A study reported that compared to an engine run on neat diesel, at peak load conditions, CO exhibits an increase of 18.71%, 23.39%, and 38% for an engine run on BFR of 0.6 kg/h, 0.9 kg/h, and 1.2 kg/h respectively [136].

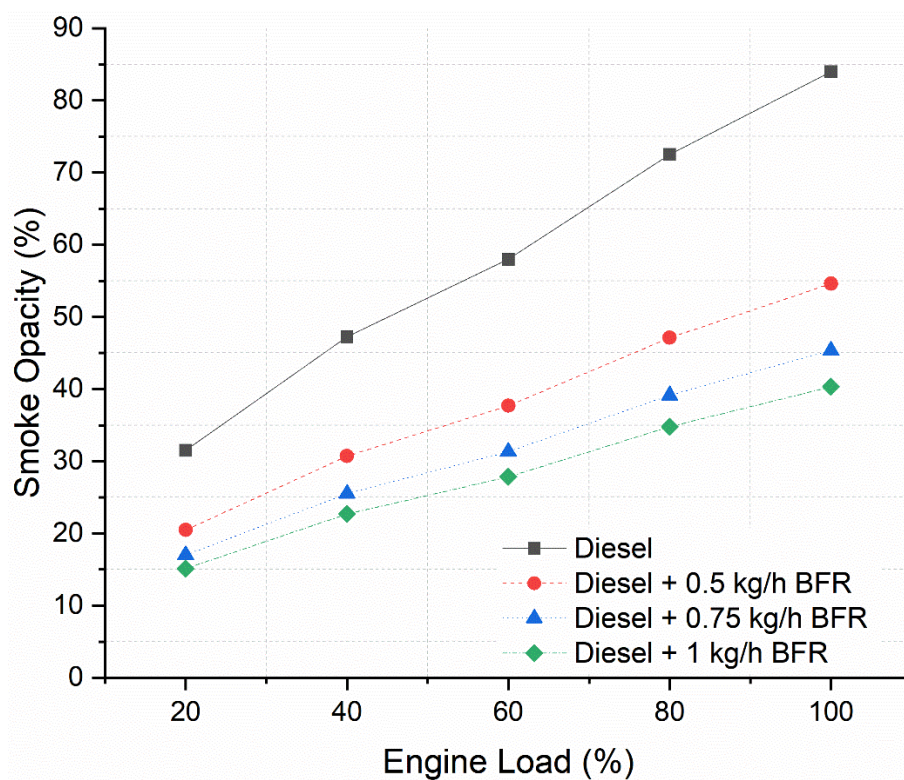


**Fig. 5. 6** Effect of BFR on Smoke Opacity

Diesel smoke opacity(SO) is a combination of partially combusted fuel and soot [150]. Fig. 5.6 depicts the effect of BFR on Smoke Opacity. A rise in smoke opacity with increment in Load, with maximum Smoke to be found for the highest Load (100%) owing to increased fuel consumption and cylinder temperature [142]. Smoke opacity realized a decline for increment in BFR for all loads because of the CO<sub>2</sub> content of biogas. The presence of CO<sub>2</sub> reduces the cylinder temperature, which inhibits smoke formation [151]. As compared to the engine run on neat diesel, at peak load conditions, SO exhibits a decrease in 35%, 46%, and 52% for engine run on BFR of 0.5 kg/h, 0.75 kg/h, and 1 kg/h, respectively. Previous studies

done under a similar test setup with varying BFR reported a decline in SO with an increment in BFR [96,135]. A study reported that compared to an engine run on neat diesel, at peak load conditions, SO exhibits a 41%, 49.5%, and 62.23% decrease for an engine run on BFR of 0.6 kg/h, 0.9 kg/h, and 1.2 kg/h respectively [136].

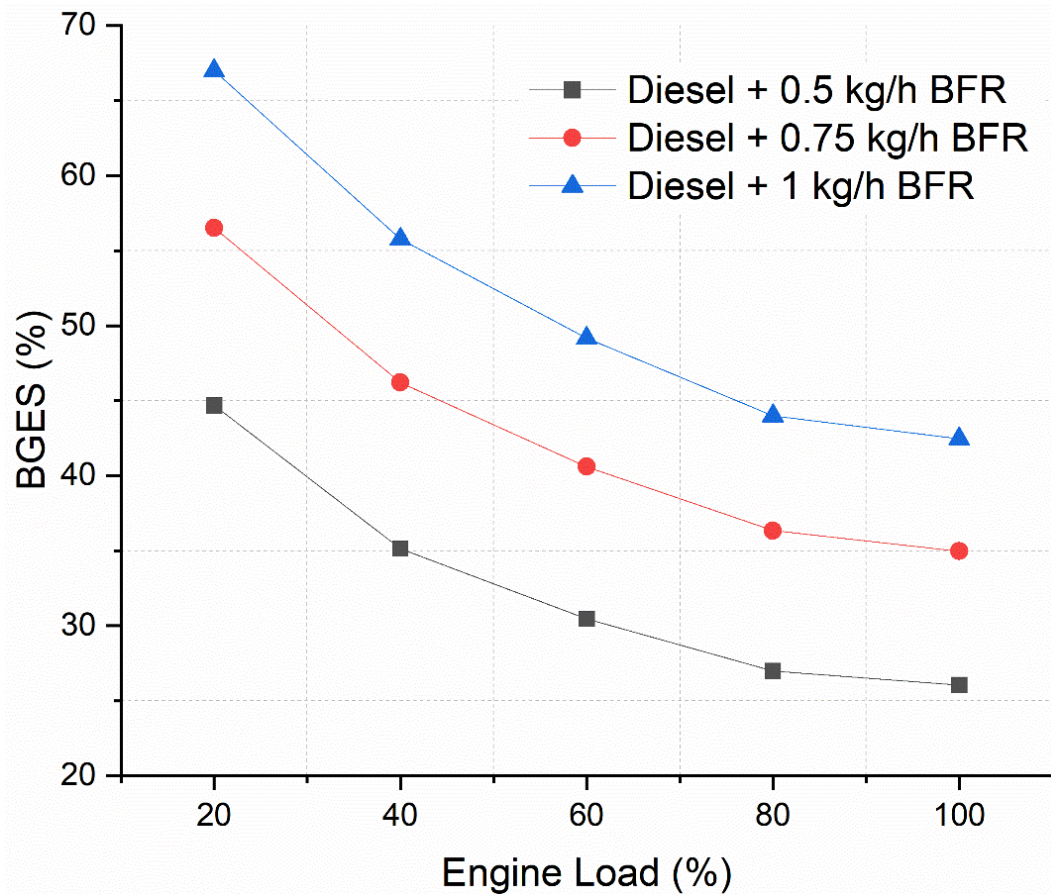


**Fig. 5. 7** Effect of BFR on BGES

The energy share in the dual fuel operation is defined as the ratio of energy supplied by the primary fuel (biogas) to the sum of the energy supplied by the primary fuel and the pilot fuel. As given in Fig. 5.7, BGES is observed to decrease with an increase in load for each BFR. The drop in BGES may be attributed to the engine experiencing a greater thermal load at full load conditions. This necessitates the use of additional diesel fuel to meet the increased thermal load, resulting in a decrease in BGES. At full load conditions, BGES for 0.5 kg/h, 0.75 kg, and 1 kg/h is observed at 26.06%, 34.96%, and 42.46%, respectively. Previous studies done under a similar test setup with varying BFR reported a decline in BGES with an increment in engine load. A study reported that for an engine run on BFR of 0.6 kg/h, 0.9 kg/h, and 1.2 kg/h, it was observed at 26.6%, 36.9%, and 43.9%, with diesel as the pilot fuel [136]. In comparison, another study reported that an engine run on BFR of 0.6 kg/h, 0.9 kg/h,

and 1.2 kg/h was observed at 21.7%, 30.1%, and 37.33%, with Karanja biodiesel as the pilot fuel [139].

### 5.1.2 Effect of Biodiesel Blend Rate (BBR) on Engine Performance and Emission

Three pilot fuels, i.e., diesel, BBR 10 (B10) blend, and BBR 20 (B20) blend, are considered and compared for their effect on engine performances and emissions. Tables 5.2 provide the experimental matrix. From 20% (2.4kg) load to 100% (12 kg) load, with a 20% (2.4 kg) increment, the load variations were carried out.

**Table 5. 2** Experimental Matrix of the Biodiesel Run Diesel Engine

Mode	Fuel used	Loading Conditions (%)
Diesel	100% diesel	20,40,60,80,100
Diesel	BBR – 10, 20 (B10, B20)	

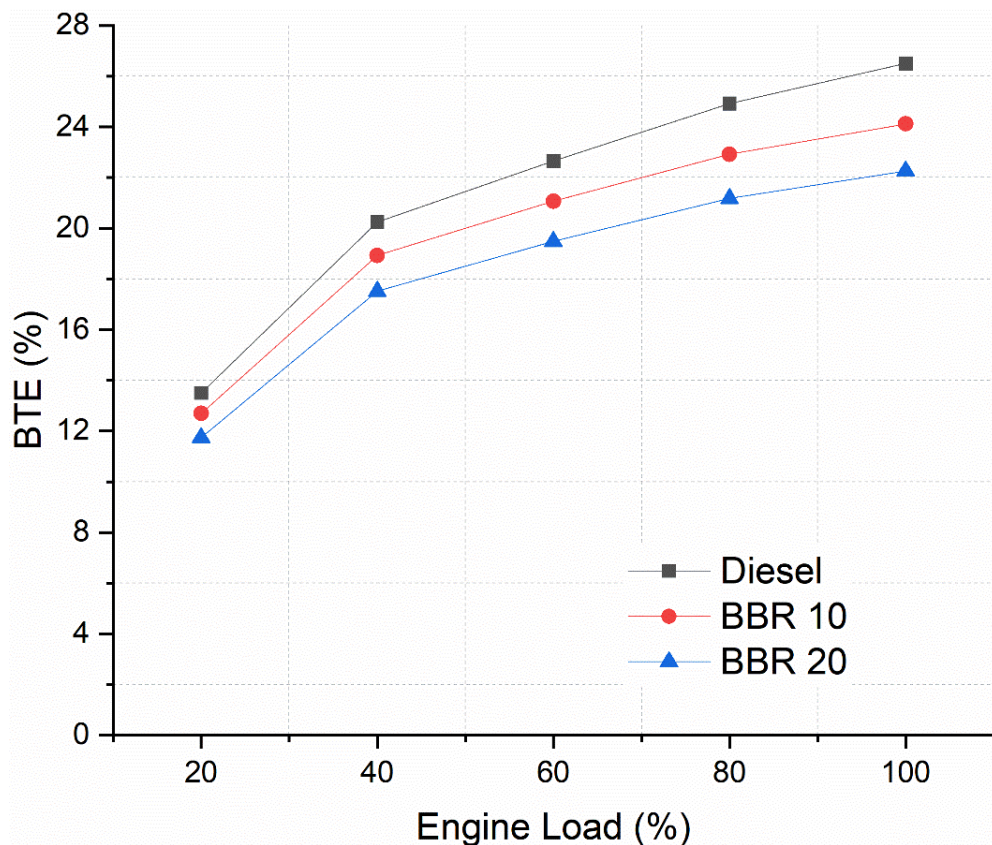


**Fig. 5. 8** Effect of BBR on BTE

Fig. 5.8 depicts the effect of BBR on BTE. BTE increases with engine load, reaching its maximum at the peak load (100%) owing to increased fuel supply and a rise in cylinder temperature [133]. Because of the higher viscosity and lower CV of linseed biodiesel, BTE declines with an increase in BBR [152]. Compared to the engine run on neat diesel, at peak

load conditions, BTE exhibits a 9% and 16% decrease for engine run on BBR 10 and BBR 20, respectively. Previous studies done under a similar test setup with varying BBR reported a decline in BTE with an increment in BBR. Researchers noted that compared to an engine run on neat diesel, at peak load conditions, BTE exhibits a decrease of 18.45% [142], 15.27% [153], and 18.128% [154] for an engine run on BBR 20.

Fig. 5.9 depicts the effect of BBR on BSEC. As the engine load increases, the combustion chamber's temperature increases, resulting in a decrease in BSEC. As the engine's load increases, BSEC tends to decrease due to the catalytic chemical oxidation of nanoparticle fuel blends, enhancing fuel combustion and greater fuel efficiency [155]. BSEC increases with increased BBR due to lower volatility and lower CV [156]. As compared to the engine run on neat diesel, at peak load conditions, BSEC exhibits an increase of 9.2% and 17% for engine run on BBR 10 and BBR 20, respectively. Previous studies done under a similar test setup with varying BBR reported an increase in BSEC with an increment in BBR. Researchers noted that compared to an engine run on neat diesel, at peak load conditions, BSEC exhibits an increase of 17% [107], 14.07% [148], and 12.72% [157] for an engine run on BBR 20.

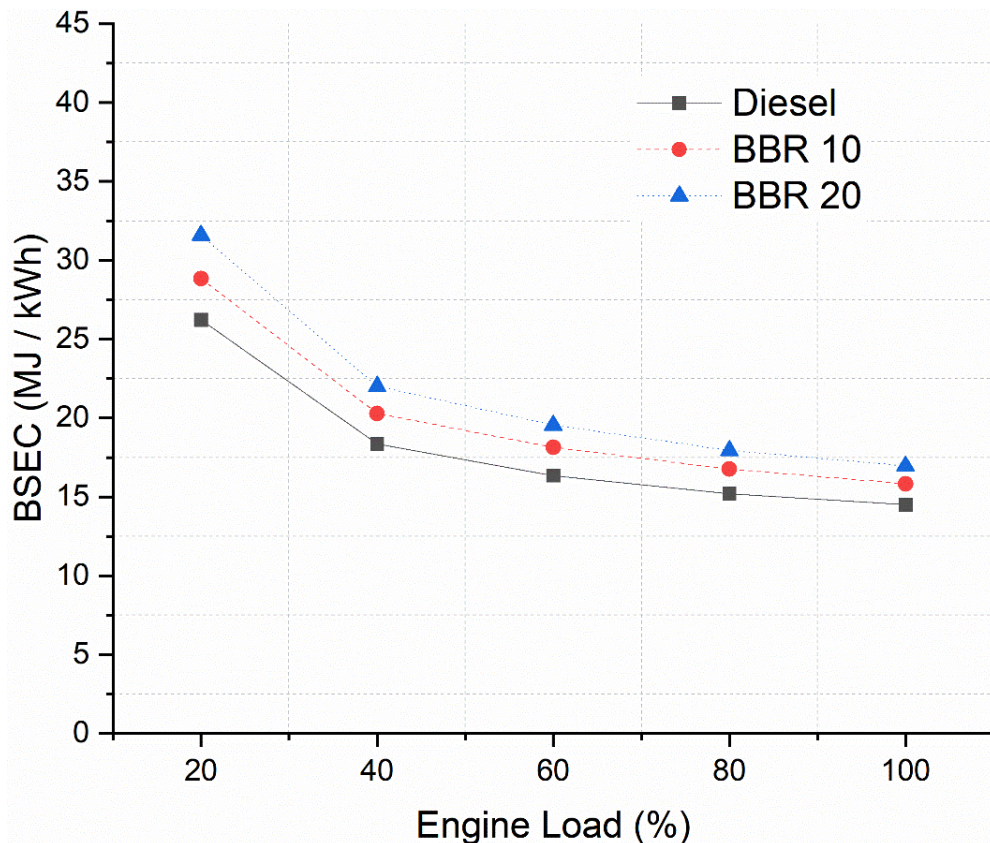
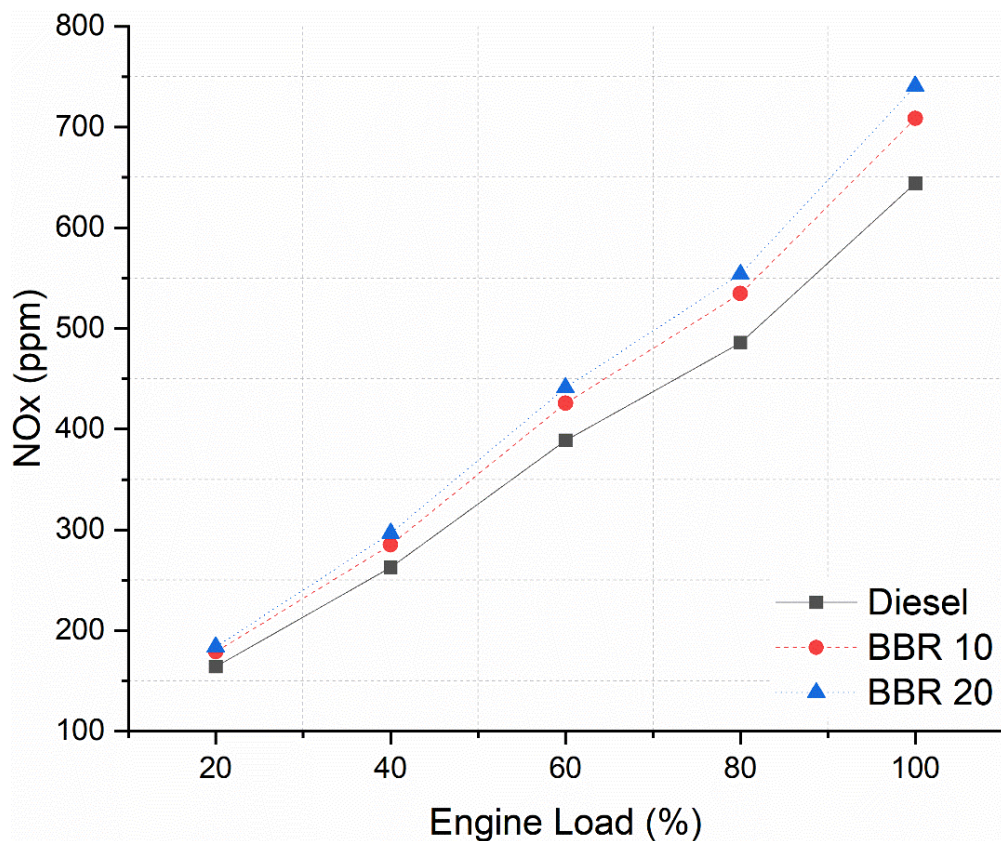


Fig. 5. 9 Effect of BBR on BSEC

Fig. 5.10 depicts the effect of BBR on NO<sub>x</sub>. As the load on the engine rises, there is a noticeable increase in NO<sub>x</sub>, highest at peak load(100%) owing to the rise in fuel consumption and cylinder temperature [142]. Using biodiesel in an engine increases the amount of oxygen available for combustion, leading to a higher peak combustion temperature, which causes an increase in NO<sub>x</sub> as BBR increases [158]. As compared to the engine run on neat diesel, at peak load conditions, NO<sub>x</sub> exhibits an increase of 10% and 15% for engine run on BBR 10 and BBR 20, respectively. Previous studies under a similar test setup with varying BBR reported an increase in NO<sub>x</sub> with an increment in BBR. Researchers noted that compared to an engine run on neat diesel, at peak load conditions, NO<sub>x</sub> exhibits an increase of 15.88% [159] and 14.28% [98] for an engine run on BBR 20.



**Fig. 5. 10** Effect of BBR on NO<sub>x</sub>

Fig. 5.11 depicts the effect of BBR on HC. At low Load due to low engine cylinder temperature, improper combustion is attained, resulting in higher HC. However, the homogenous mixing of fuel and air is more efficient at higher loads, resulting in lower HC emissions [145]. Increased oxygen availability in biodiesel leads to better combustion, resulting in lesser HC with increased BBR[160]. Compared to the engine run on neat diesel, at peak load conditions, HC exhibits a decrease of 8% and 11% for the engine run on BBR



10 and BBR 20, respectively. Previous studies done under a similar test setup with varying BBR reported a decline in HC with an increment in BBR. Researchers noted that compared to an engine run on neat diesel, at peak load conditions, HC exhibits a decrease of 9.52% [153] and 11.9% [148] for an engine run on BBR 20.

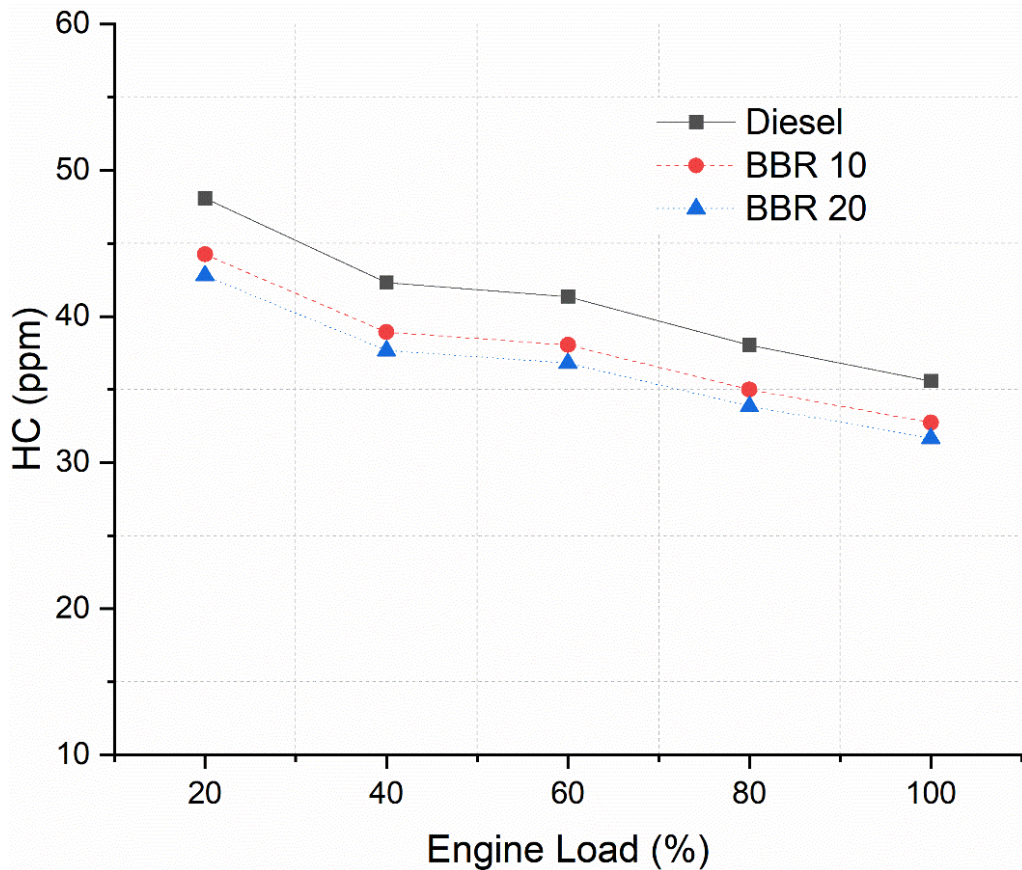


**Fig. 5. 11** Effect of BBR on HC

Fig. 5.12 depicts the effect of BBR on CO. When the engine operates at low to medium loads, the amount of carbon monoxide (CO) emitted is reduced because the air-fuel mixture is closer to the ideal stoichiometric ratio. However, as more fuel is added to the combustion process at higher loads, the amount of oxygen available for combustion is limited, resulting in a rich fuel mixture, thereby promoting an increase in CO emissions [161]. The stoichiometric air-fuel ratio of an engine running on biodiesel is lower than that of diesel, requiring less oxygen for combustion. Biodiesel contains more oxygen than diesel fuel, allowing carbon atoms to find enough oxygen to make CO<sub>2</sub>, decreasing CO emissions [158].

As compared to the engine run on neat diesel, at peak load conditions, CO exhibits a decrease of 5.5% and 11.1% for the engine run on BBR 10 and BBR 20, respectively. Previous studies done under a similar test setup with varying BBR reported a decline in CO with an increment in BBR. Researchers reported that compared to an engine run on neat diesel, at peak load conditions, CO exhibits a decrease of 10.52% [162], 11% [107], and 12.33% [163] for an engine run on BBR 20.

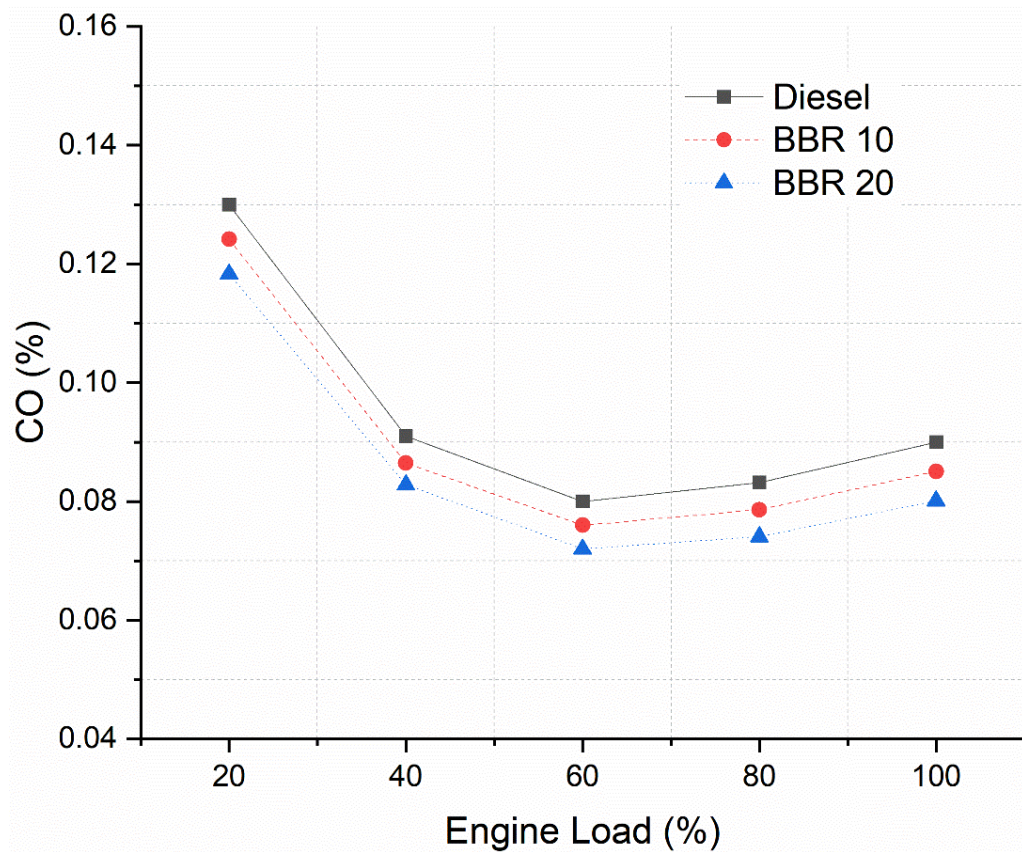


**Fig. 5. 12** Effect of BBR on CO

Fig. 5.13 depicts the effect of BBR on Smoke Opacity. A rise in smoke opacity with increment in engine load is observed, with maximum smoke opacity to be found for the peak engine load(100%) owing to the rise in fuel consumption and cylinder temperature [142]. Smoke opacity decreases with increased BBR because of a better combustion process due to increased oxygen availability in biodiesel [156]. Compared to the engine run on neat diesel, at peak load conditions, SO exhibits a decrease of 3% and 8% for the engine run on BBR 10 and BBR 20, respectively. Previous studies done under a similar test setup with varying BBR reported a decline in SO with an increment in BBR. Researchers noted that compared to an

engine run on neat diesel, at peak load conditions, SO exhibits a decrease of 10.12% [142], 6% [164], and 5.39% [107] for an engine run on BBR 20.

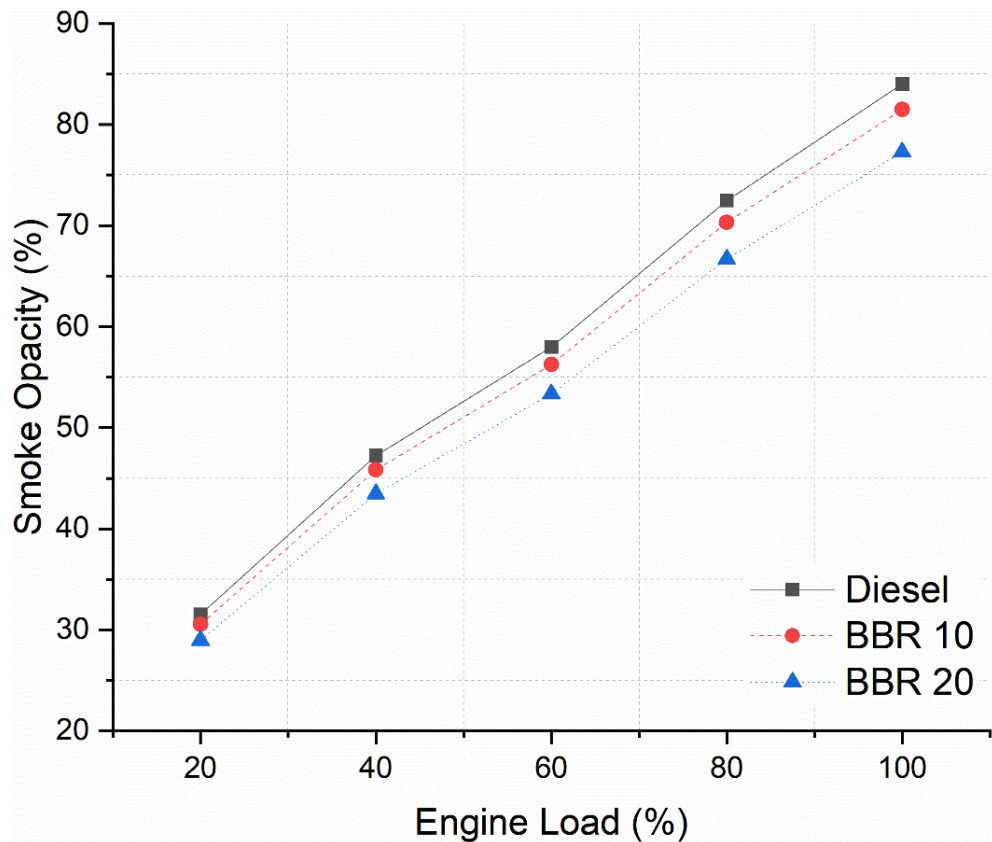


Fig. 5.13 Effect of BBR on Smoke Opacity

### 5.1.3 Effect of Nanoparticles Doped Rate (NDR) on Engine Performance and Emission

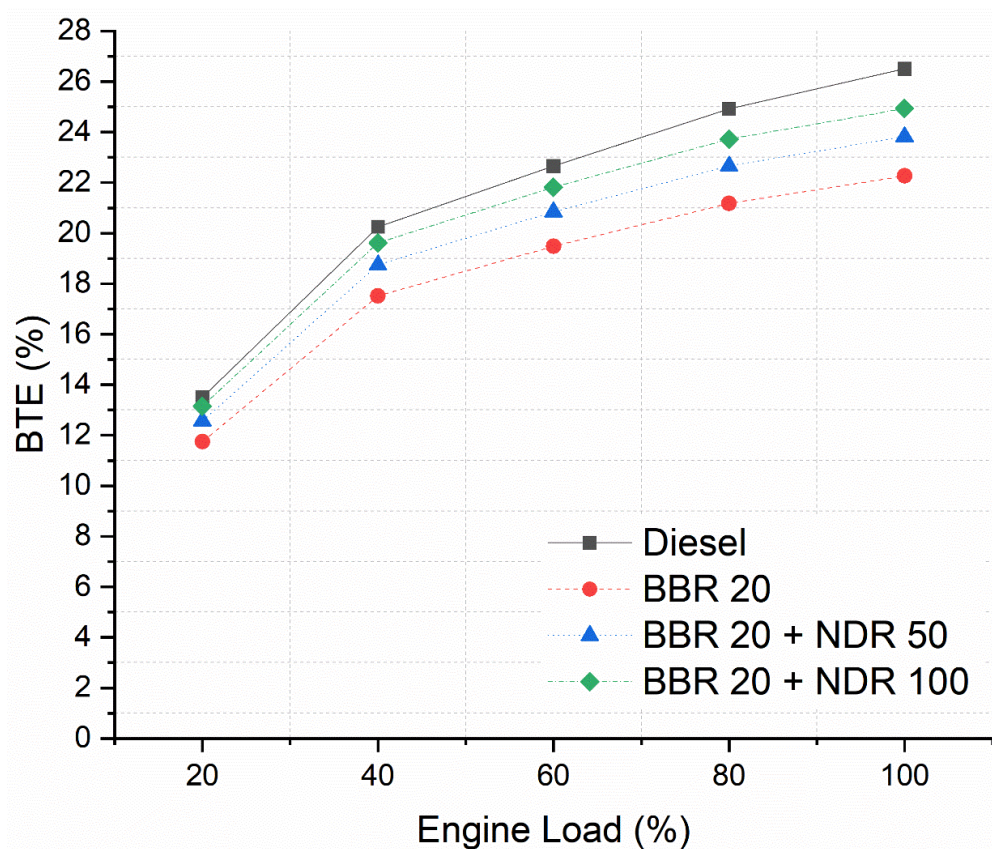
Diesel, BBR20 (B20) blend, and BBR20 blended with NDR of 50 and 100 ppm are considered and compared for their effects on the CI engine. Tables 5.3 provide the experimental matrix. From 20% (2.4kg) load to 100% (12 kg) load, with a 20% (2.4 kg) increment, the load variations were carried out.

Table 5.3 Experimental Matrix of the Biodiesel-Nanoparticles Blend Run Diesel Engine

Mode	Fuel used	Loading Conditions (%)
Diesel	100% diesel	20,40,60.80,100
Diesel	BBR 20 (B20)	
Diesel	BBR20 + NDR50, BBR20 + NDR100	

Fig. 5.14 depicts the effect of NDR on BTE. BTE increased with the increase in NDR because of  $\text{Co}_3\text{O}_4$ 's catalytic function as a combustion facilitator. At higher loads, enhanced fuel spray atomization and extensive fuel penetration into the in-cylinder lead to improved

air-fuel mixture mixing [165]. Compared to the engine run on the BBR 20 blend, at peak load conditions, BTE exhibits an increase of 7% and 12% for the engine run on BBR20+NDR50 and BBR20+NDR100 blends, respectively. Previous studies under a similar test setup with varying NDR reported an increase in BTE with an increment in NDR. Researchers noted that compared to an engine run on BBR 20 blend, at peak load conditions, BTE exhibits an increase of 13.09% [166], 11.3% [137], and 11.71% [167] for an engine run on BBR20+NDR100 blend.



**Fig. 5. 14** Effect of NDR on BTE

Fig. 5.15 depicts the effect of NDR on BSEC. As the engine's load increases, BSEC tends to decrease due to the catalytic chemical oxidation of nanoparticle fuel blends, enhancing fuel combustion and greater fuel efficiency [155]. Compared to the engine run on the BBR 20 blend, at peak load conditions, BSEC exhibits a 6% and 10% decrease for the engine run on BBR20+NDR50 and BBR20+NDR100 blends, respectively. Previous studies under a similar test setup with varying NDR reported a decrease in BSEC with an increment in NDR. Researchers reported that compared to an engine run on BBR 20 blend, at peak load conditions, BSEC exhibits a reduction of 8.92% [107] and 5.88% [137] for an engine run on BBR20+NDR100 blend.

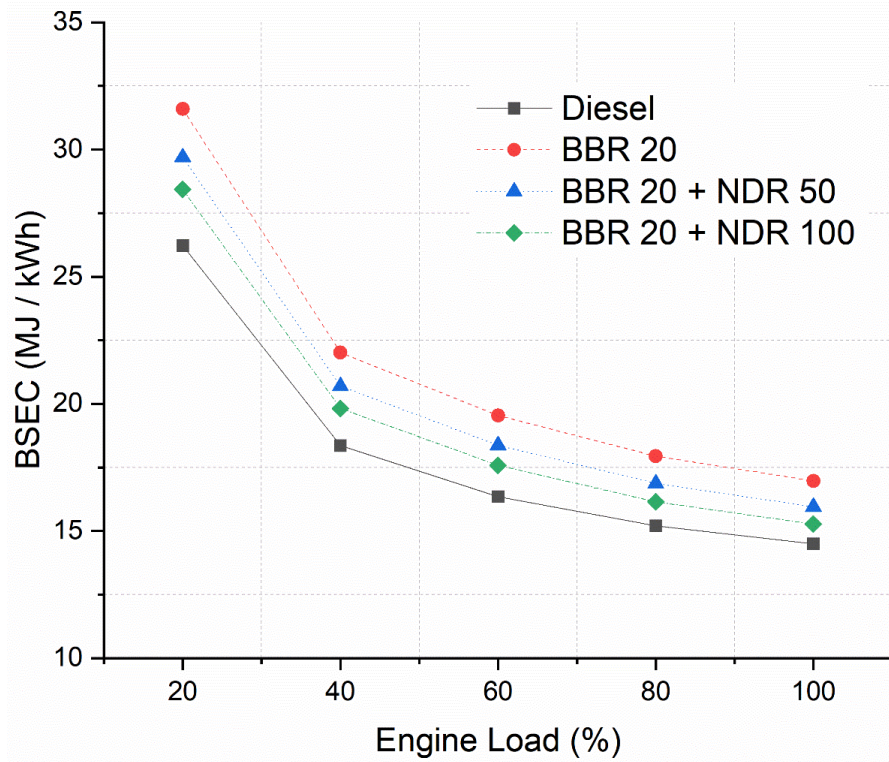


**Fig. 5.15** Effect of NDR on BSEC

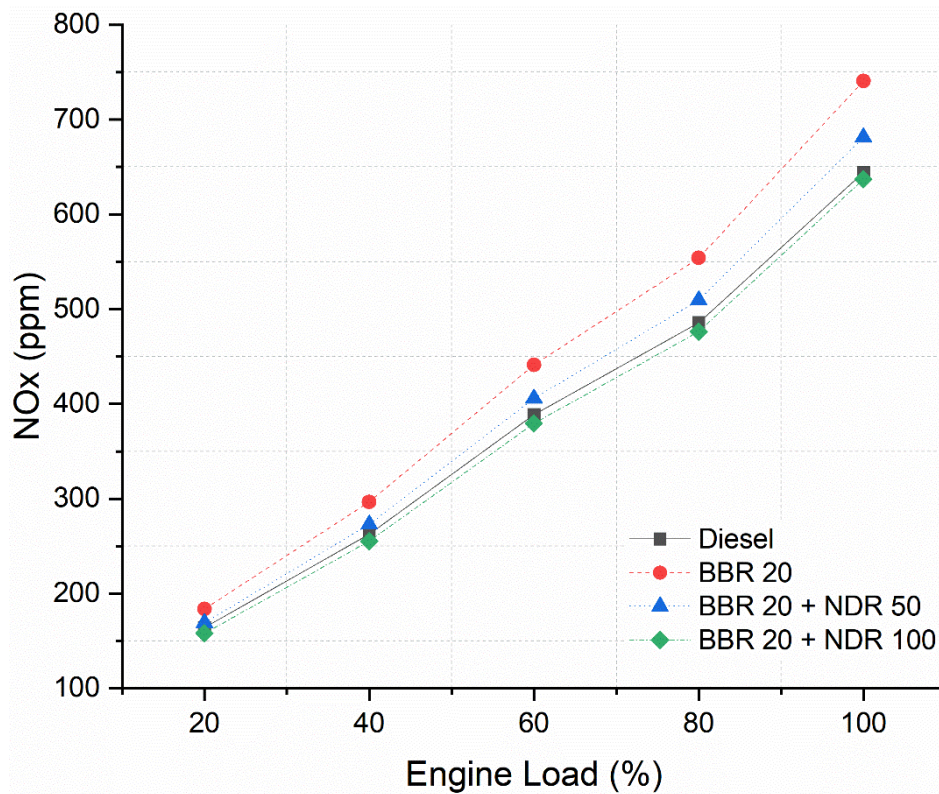


**Fig. 5.16** Effect of NDR on NO<sub>x</sub>

Fig. 5.16 depicts the effect of NDR on NO<sub>x</sub>. Including nanoparticles in the pilot fuel reduces the ignition delay and optimizes the combustion progression by serving as a reducing

element and converting  $\text{NO}_x$  to  $\text{N}_2$  and  $\text{O}_2$  [168]. As compared to the engine run on the BBR 20 blend, at peak load conditions,  $\text{NO}_x$  exhibits a decrease of 8% and 14% for the engine run on BBR20+NDR50 and BBR20+NDR100 blends, respectively. Previous studies done under a similar test setup with varying NDR reported a decrease in  $\text{NO}_x$  with an increment in NDR. Researchers noted that compared to an engine run on the BBR 20 blend, at peak load conditions,  $\text{NO}_x$  exhibits a reduction of 15.19% [107] and 20.84% [142] for an engine run on the BBR20+NDR100 blend.

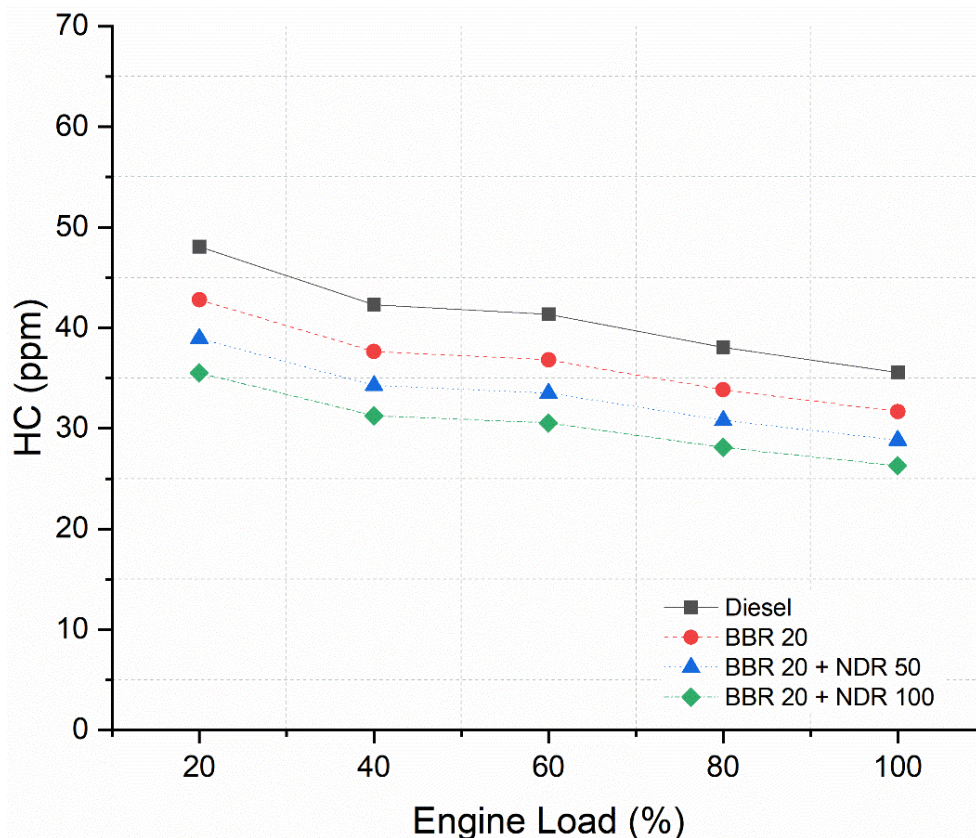
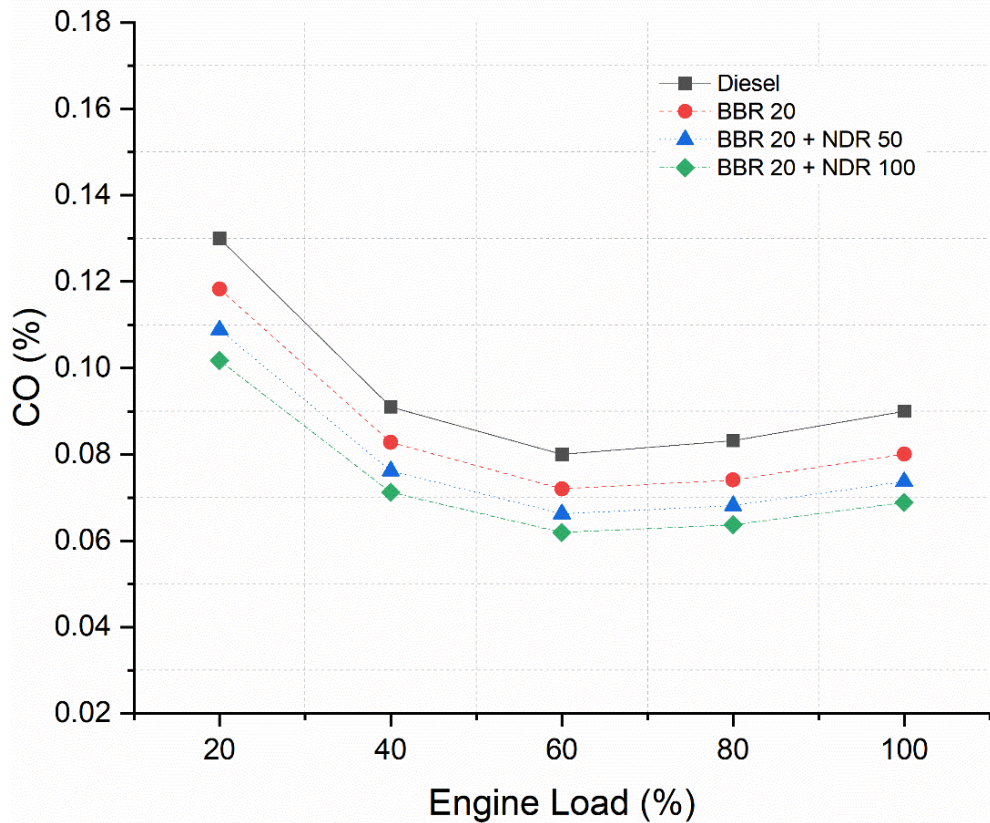


Fig. 5. 17 Effect of NDR on HC

Fig. 5.17 depicts the effect of NDR on HC. HC was found to decrease with the increase in NDR. The inclusion of  $\text{Co}_3\text{O}_4$  reduced the quantity of HC emission owing to secondary atomization and oxidation of HC. Additionally,  $\text{Co}_3\text{O}_4$  worked as an  $\text{O}_2$  reservoir, increasing the oxidation rate of HC [168]. Compared to the engine run on the BBR 20 blend, at peak load conditions, HC exhibits a 9% and 17% decrease for the engine run on BBR20+NDR50 and BBR20+NDR100 blends, respectively. Previous studies done under a similar test setup with varying NDR reported a decrease in HC with an increment in NDR. Researchers noted that compared to an engine run on BBR 20 blend, at peak load conditions, HC exhibits a reduction of 16.07% [137] and 19.61% [167] for an engine run on BBR20+NDR100 blend.



**Fig. 5. 18** Effect of NDR on CO

Fig. 5.18 depicts the effect of NDR on CO. CO was found to decrease with the increase in NDR. Improved fuel-oxidant mixing and uniform combustion were achieved owing to metal oxide nanoparticles functioning as oxidation catalysts, speeding up the combustion and shortening the ignition delay, resulting in CO emissions [147]. As compared to the engine run on the BBR 20 blend, at peak load conditions, CO exhibits a decrease of 8% and 14% for the engine run on BBR20+NDR50 and BBR20+NDR100 blends, respectively. Previous studies done under a similar test setup with varying NDR reported a decrease in CO with an increment in NDR. Researchers noted that compared to an engine run on BBR 20 blend, at peak load conditions, CO exhibits a reduction of 14.33% [169], 11% [170] and 18.18% [137] for an engine run on BBR20+NDR100 blend.

Fig. 5.19 depicts the effect of NDR on Smoke Opacity (SO). A rise in smoke opacity with increment in engine load is observed, with maximum smoke opacity to be found for the peak engine load (100%) owing to the rise in fuel consumption and cylinder temperature [142]. As compared to the engine run on the BBR 20 blend, at peak load conditions, SO exhibits a decrease of 5% and 13% for the engine run on BBR20+NDR50 and BBR20+NDR100 blends, respectively. Previous studies done under a similar test setup with varying NDR

reported a decrease in SO with an increment in NDR. Researchers noted that compared to an engine run on BBR 20 blend, at peak load conditions, SO exhibits a reduction of 14.87% [107], 8.22% [164] and 19.04% [137] for an engine run on BBR20+NDR100 blend.

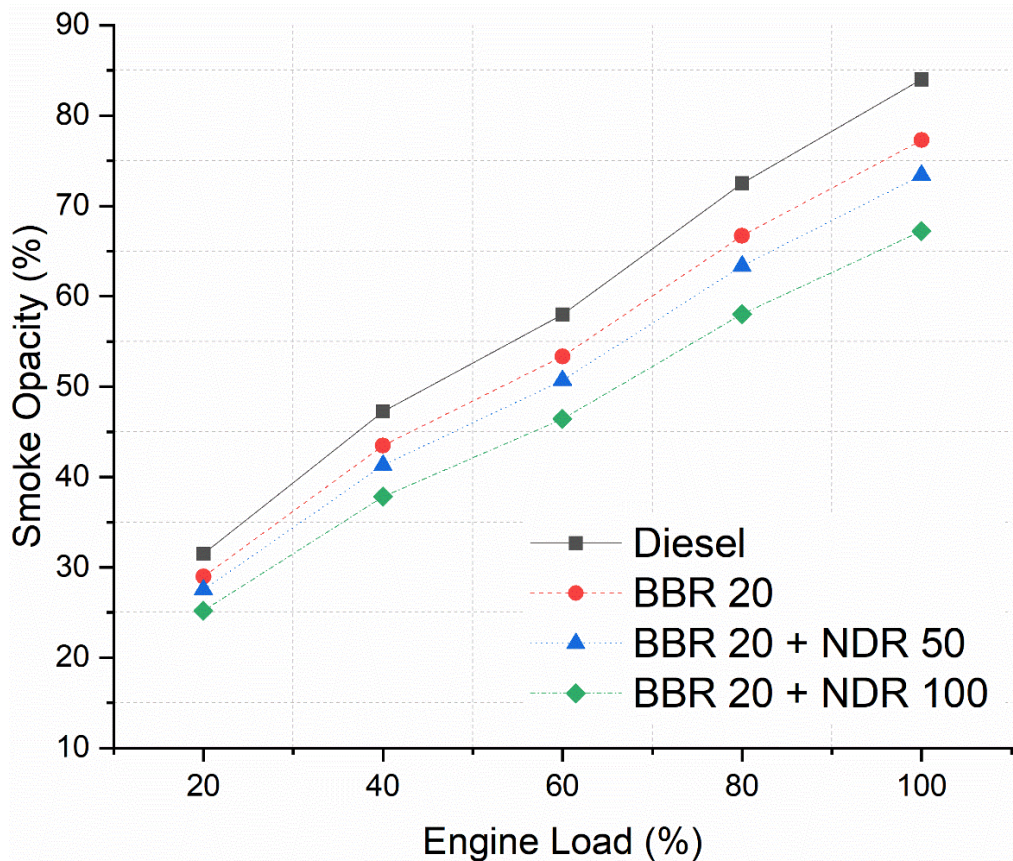


**Fig. 5. 19** Effect of NDR on Smoke Opacity

## 5.2 Engine Performance and Emission Optimization

Computational methods, using RSM and ANN, established a prediction model based on the Design of experiment (DOE) results. The interaction impact of input factors on output was studied using a 3D response surface plot. Desirability function and GA were used to optimize the RSM and ANN models, respectively, with respect to the output responses.

### 5.2.1 Design of Experiment Analysis

The experimental data observed from DOE runs are given in Table 5.4. Three repetitions of each experimental run were performed with consistent outcomes. After collecting data from each replicate, the mean value for each experimental condition was determined using a conventional averaging method.



Table 5. 4 DOE with experimental responses

Run	A: load %	B: NDR ppm	C: BBR %	D: BFR kg/h	BTE %	BSEC MJ/kWh	NO <sub>x</sub> ppm	HC ppm	CO %	SO %	BGES %
1	60	50	10	0.75	16.03	21.85	246	45	0.09	28.8	40.98
2	20	0	0	0.5	10.44	31.72	120	60	0.16	20.8	44.68
3	20	0	20	0.5	9.08	38.22	137	53	0.14	18.8	42.67
4	60	50	10	0.5	17.45	20.82	274	43	0.09	34.7	30.00
5	20	100	20	0.5	10.17	34.39	115	44	0.12	16.4	44.80
6	60	50	10	0.75	16.05	21.82	246	45	0.09	28.7	40.90
7	100	0	20	1	13.78	23.63	363	46	0.11	37.1	39.79
8	100	100	20	0.5	19.42	18.78	433	33	0.09	43.7	24.15
9	60	100	10	0.75	16.73	20.71	231	41	0.08	26.4	41.85
10	100	0	20	0.5	17.34	20.87	497	40	0.10	50.2	23.12
11	60	0	10	0.75	14.94	23.31	268	49	0.10	30.4	39.67
12	20	100	0	1	9.58	32.45	80	56	0.15	13.2	71.02
13	60	50	10	1	14.13	23.97	200	49	0.10	25.7	50.10
14	100	100	0	0.5	23.12	16.05	377	37	0.10	47.5	27.62
15	20	0	0	1	8.55	36.05	89	67	0.18	15.1	67.26
16	100	50	10	0.75	18.41	19.30	391	39	0.10	41.8	34.46
17	60	50	10	0.75	15.98	21.91	247	45	0.09	28.9	40.95

18	20	100	20	1	8.33	39.09	85	50	0.14	12.4	69.00
19	60	50	20	0.75	14.78	24.25	256	44	0.09	27.4	40.01
20	60	50	10	0.75	16.06	21.80	245	45	0.09	28.7	41.00
21	20	0	20	1	7.44	43.01	99	60	0.16	13.9	65.72
22	100	0	0	1	16.40	20.20	316	51	0.13	40.3	42.46
23	100	100	0	1	18.37	18.18	268	43	0.11	35.1	45.00
24	100	100	20	1	15.43	21.27	312	38	0.10	32	41.78
25	60	50	10	0.75	15.90	21.91	247	45	0.09	28.9	40.93
26	60	50	0	0.75	17.19	19.74	225	49	0.10	29.8	42.42
27	100	0	0	0.5	20.64	17.84	438	45	0.11	54.3	26.06
28	60	50	10	0.75	15.92	22.00	248	45	0.09	29	40.92
29	20	50	10	0.75	9.62	34.74	115	52	0.15	15.7	57.41
30	20	100	0	0.5	11.69	28.55	103	50	0.13	17.8	47.36

### 5.2.2 RSM Model Analysis

Analysis of Variance (ANOVA) is evaluated by fitting Equation 1 into DOE data. The model formulated in the ANOVA Table 5.5 to 5.11 for engine parameter outputs is considered significant since the P-value for all output parameters was less than 0.05 for both the model and existing inputs. High  $R^2$  and Adjusted (adj.)  $R^2$  values were observed for all the output responses, which implies that the model produces significantly similar data compared to the experimental data. The adj.  $R^2$  and Predicted (Pred.)  $R^2$  values had a disparity of less than 2% for all the responses, indicating good prediction reliability. Tables 5.5 to 5.11 show that the lack of fit is insignificant since its  $P$  value is greater than 0.05. The second-order polynomial equation (Eqn. 3.10) derives the coded relationship for the RSM model formed between the input variables and engine responses.

### 5.2.3 Interaction effects on BTE

With the chosen input variables considered, the empirical model for analysing BTE is shown in equation 5.1. The presence of positive coefficients (i.e., load, NDR) in all linear terms indicates that an increase in the fraction of this term results in a proportional rise in the BTE response. In contrast, negative coefficients (i.e., BFR, BBR) in all linear terms indicate that an increase in this term results in a proportional reduction in BTE response. Engine load input has the largest coefficient for BTE response among the independent variables, followed by BFR, BBR, and NDR, respectively.

$$\begin{aligned} \text{BTE} = & 15.9776 + 4.33371 * A + 0.79072 * B + -1.12249 * C + -1.5205 * D + 0.244867 * \\ & AB + -0.458222 * AC + -0.566295 * AD + -0.0629676 * BC + -0.0850689 * BD + 0.12252 \\ & * CD + -1.95413 * A^2 + -0.132335 * B^2 + 0.0170302 * C^2 + -0.173233 * D^2 \end{aligned} \quad (5.1)$$

Three-dimensional response surface graphs were used to explore the interaction effects of the selected response (BTE) by retaining two variables at the central level and differentiating others within the experimental range. As given in Fig. 5.20 to Fig. 5.22, The 3D surface plots of different combinations suggest that Load and NDR have a synergistic interaction effect on BTE, while Load with BFR or BBR exhibits antagonistic interaction on BTE. Based on the slope of the graph, the combination of load and BFR is indicated as the most sensitive or significant in impacting BTE.

At the same central load and BFR level, compared to the BBR20-NDR100 blend, BTE observed an increase of 10.34% over BBR20-NDR0. Meanwhile, compared to the BBR0-NDR100 blend, BTE observed a decrease of 13.01% for the BBR20-NDR100 blend. At the

same central level of load and BBR (i.e., 60% load and BBR 10), a reduction in BTE of 19.03% for BFR1-NDR100 compared to BFR0.5-NDR100 was observed. BTE increase of 12% for BFR1-NDR0 compared to BFR1-NDR100 was observed. At the same central level of load and NDR, a decrease in BTE of 19.04% for BFR1-BBR20 compared to BFR0.5-BBR20 was noted. Meanwhile, there was a 12% BTE reduction for BFR1-BBR0 compared to BFR1-BBR20.

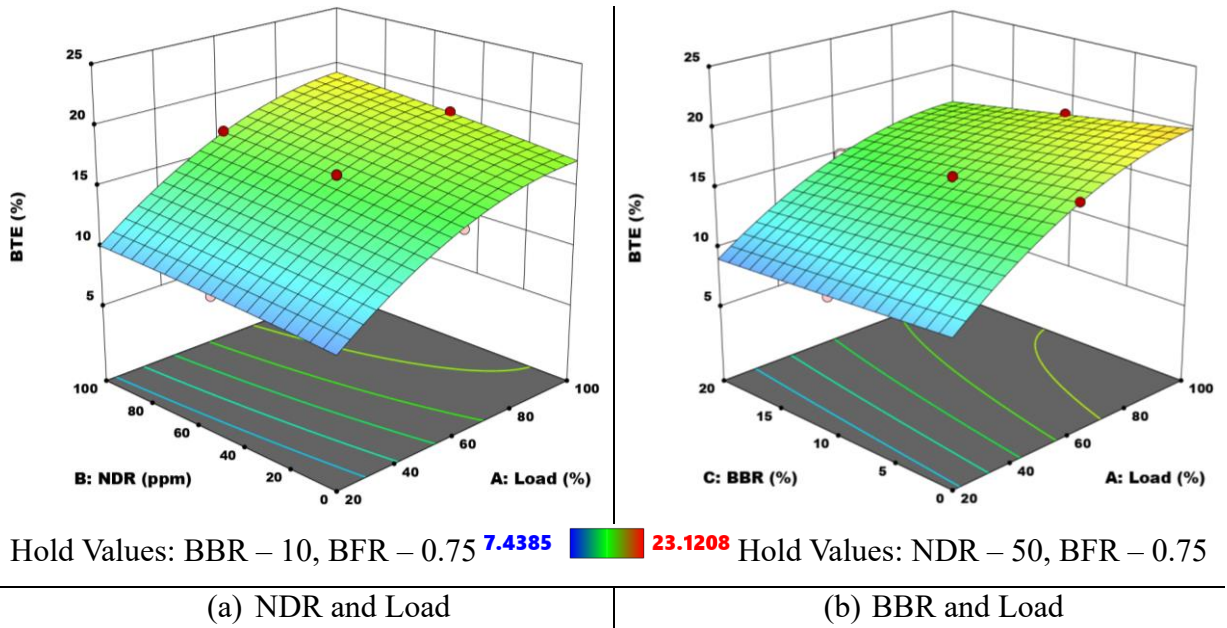


Fig. 5. 20 Interaction effects of (a) NDR and Load, (b) BBR and Load on BTE

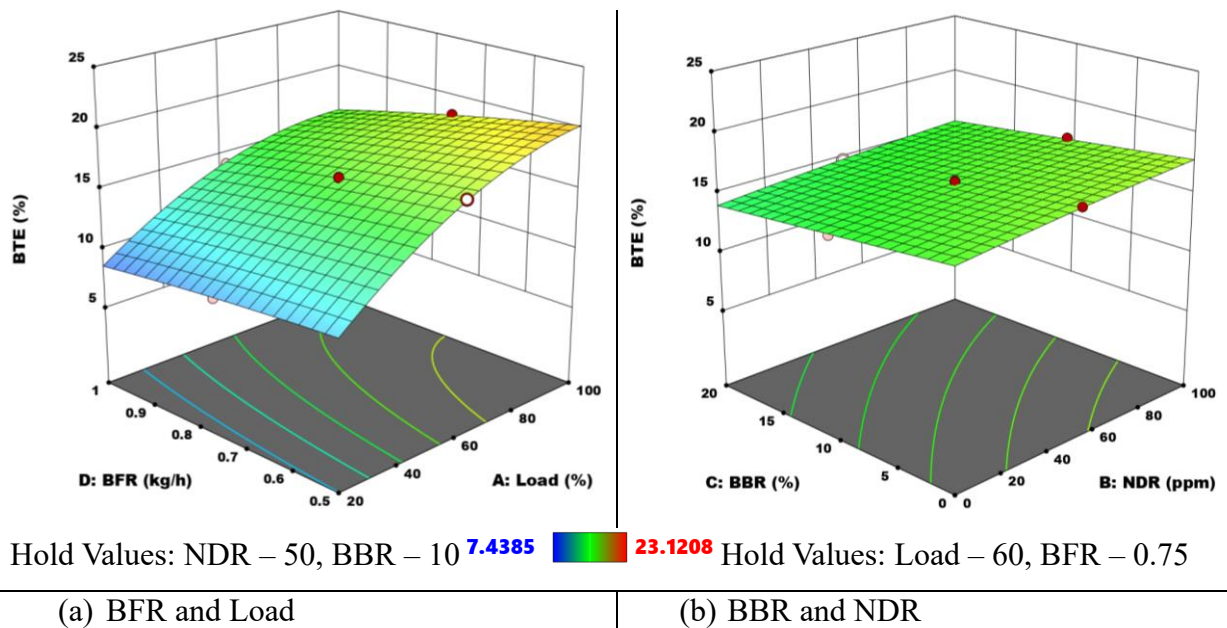
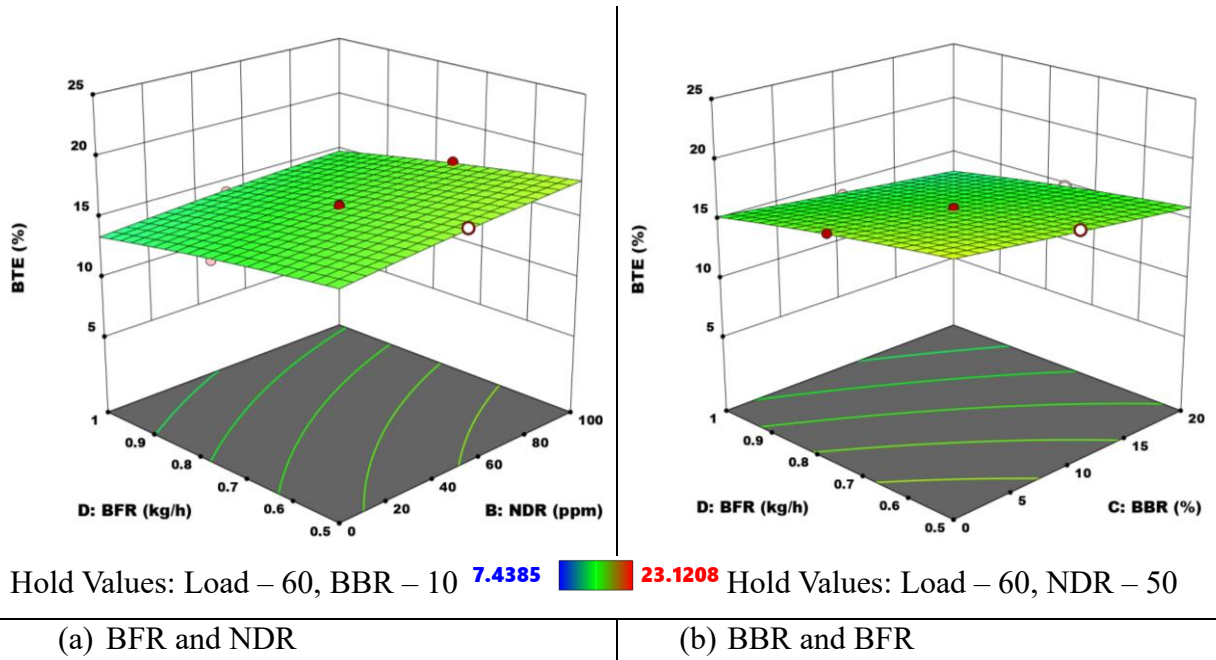


Fig. 5. 21 Interaction effects of (a) BBR and Load, (b) BBR and NDR on BTE



**Fig. 5.22** Interaction effects of (a) BFR and NDR, (b) BBR and BFR on BTE

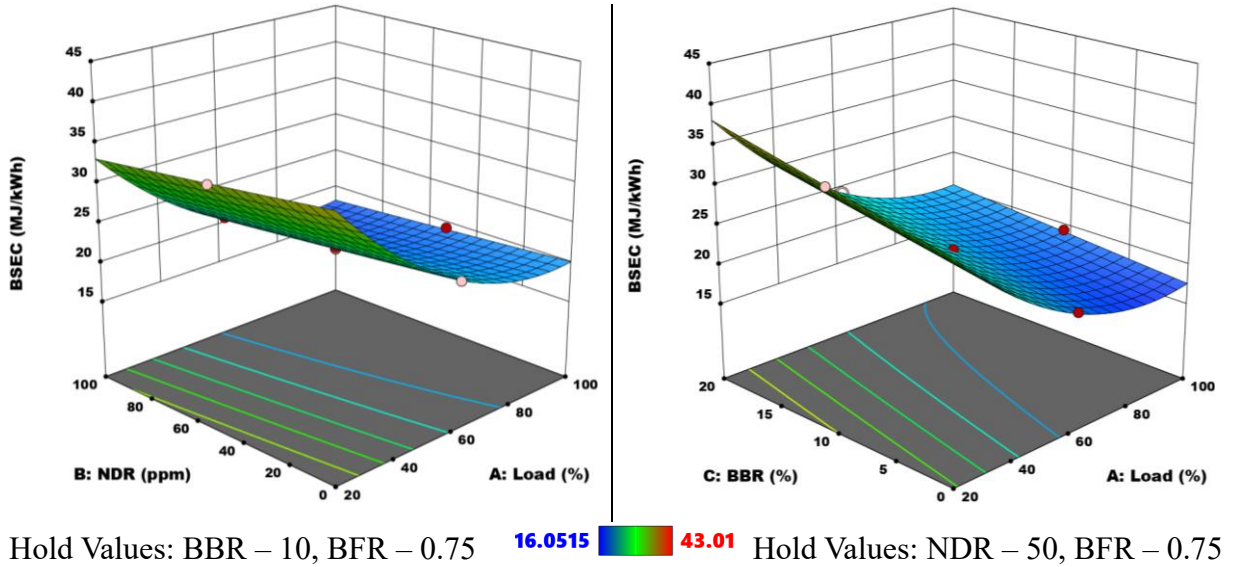
#### 5.2.4 Interaction Effects on BSEC

With the chosen input variables taken into consideration, the empirical model for analysing BSEC is shown in equation 5.2. The positive coefficients of BFR and BBR indicate a directly proportional relation to BSEC, while negative coefficients of Load and NDR in the equation suggest an inversely proportional relationship. Engine load input has the largest coefficient for BTE response among the independent variables, followed by BBR, BFR, and NDR respectively.

$$\begin{aligned} \text{BSEC} = & 21.9175 + -7.89433 * A + -1.40957 * B + 2.37464 * C + 1.70115 * D + 0.391571 \\ & * AB + -0.853927 * AC + -0.4978 * AD + -0.100708 * BC + -0.0652905 * BD + 0.126599 \\ & * CD + 5.06601 * A^2 + 0.0570941 * B^2 + 0.0420941 * C^2 + 0.440009 * D^2 \end{aligned} \quad (5.2)$$

As given in Fig. 5.23 to Fig. 5.25, The 3D surface plots of different combinations suggest that Load and NDR have a synergistic interaction effect on BSEC. At the same time, Load with BFR or BBR exhibits antagonistic interaction on BSEC. Based on the slope of the graph, the combination of load and BBR exhibited as the most sensitive or significant in impacting BSEC. At the same central load and BFR level, compared to the BBR20-NDR100 blend, BSEC observed a decrease of 10% over BBR20-NDR0.

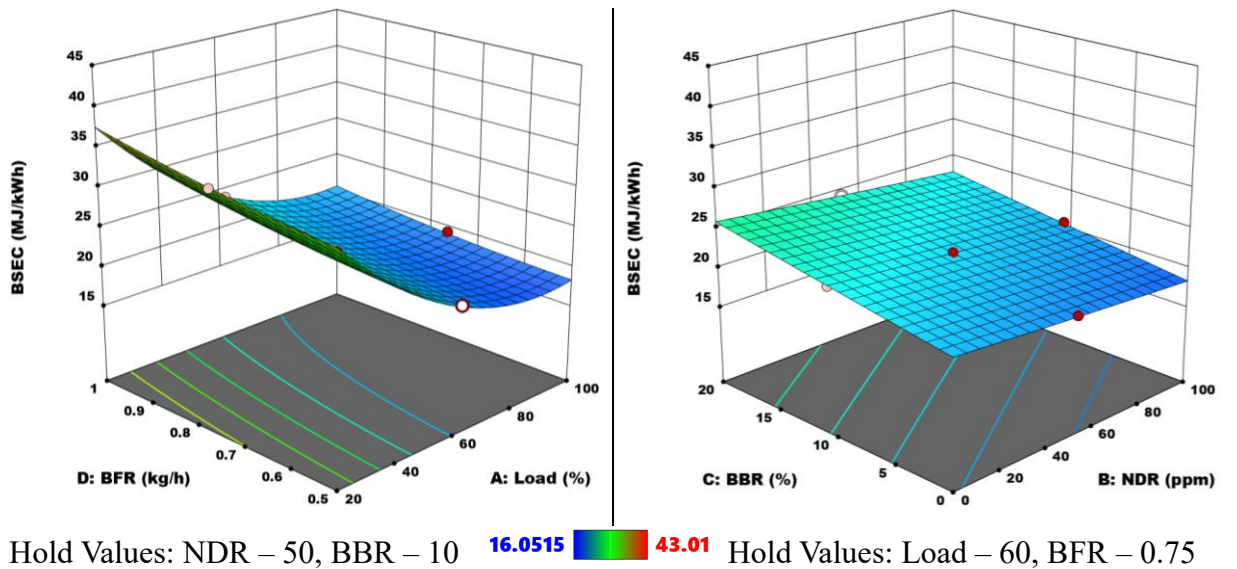
At the same central level of load and BBR, an increase in BSEC of 14.29% for BFR1-NDR100 compared to BFR0.5-NDR100 was observed. At the same central level of load and NDR, a rise of 19.51% for BFR1-BBR0 compared to BFR1-BBR20 was noted.



(a) NDR and Load

(b) BBR and Load

**Fig. 5. 23** Interaction effects of (a) NDR and Load, (b) BBR and Load on BSEC



(a) BFR and Load

(b) BBR and NDR

**Fig. 5. 24** Interaction effects of (a) BBR and Load, (b) BBR and NDR on BSEC

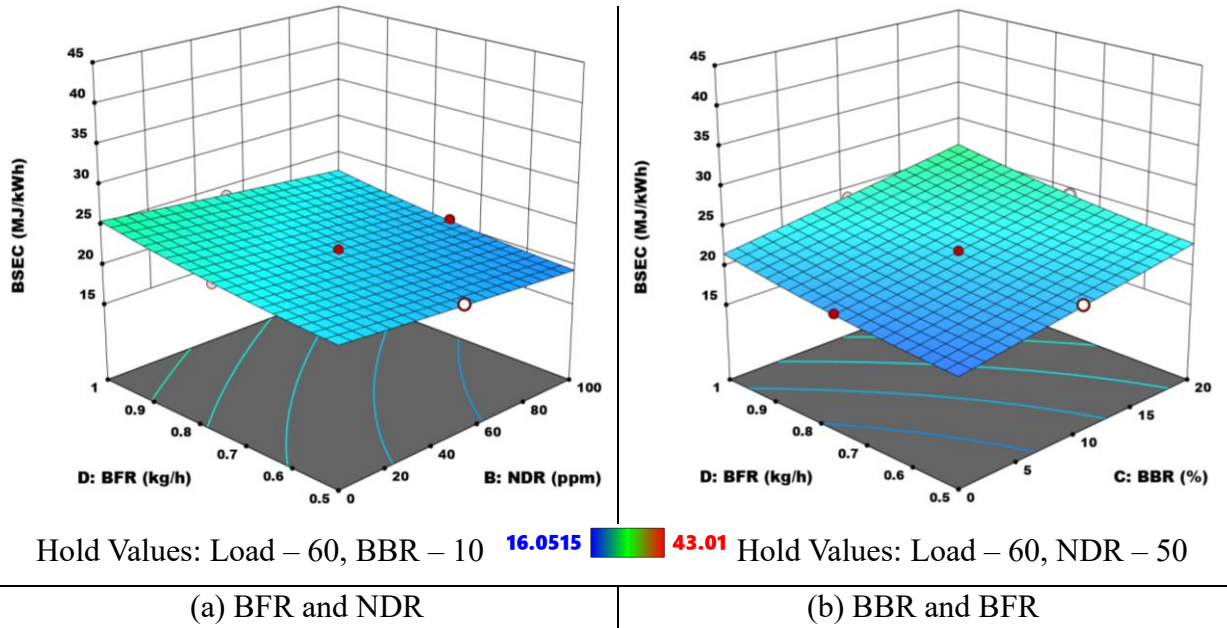


Fig. 5. 25 Interaction effects of (a) BFR and NDR, (b) BBR and BFR on BSEC

5.2.5 Interaction effects on NO<sub>x</sub>

With the chosen input variables considered, the empirical model for analyzing NO<sub>x</sub> is shown in equation 5.3.

$$\begin{aligned}
 \text{NO}_x = & 246.545 + 136.083 * A + -17.9106 * B + 15.7414 * C + -37.9381 * D + -10.0984 \\
 & * AB + 10.0213 * AC + -22.6869 * AD + -0.976769 * BC + 2.64935 * BD + -2.33765 * CD \\
 & + 6.23173 * A^2 + 2.68564 * B^2 + -6.19198 * C^2 + -9.78391 * D^2 \quad (5.3)
 \end{aligned}$$

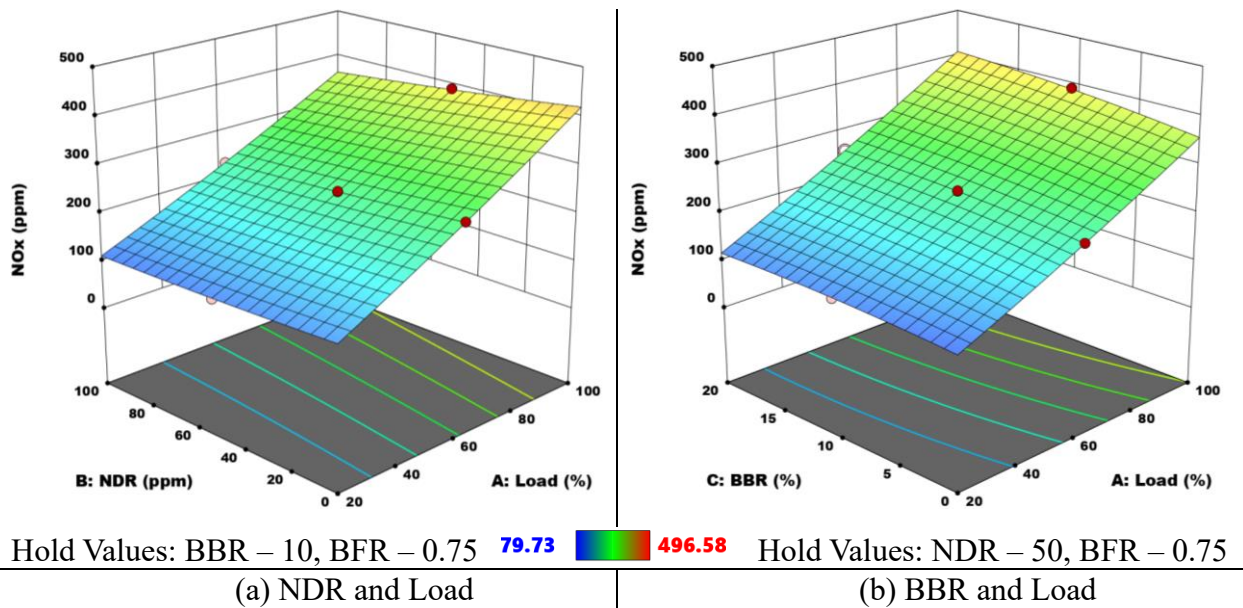


Fig. 5. 26 Interaction effects of (a) NDR and Load, (b) BBR and Load on NO<sub>x</sub>

The positive coefficients of Load and BBR indicate a directly proportional relation to NO<sub>x</sub>, while negative coefficients of BFR and NDR in the equation suggest an inversely

proportional relationship. With the highest F-value from the ANOVA Table, Engine load input is the most sensitive to NO<sub>x</sub> response among the independent variables, followed by BFR, NDR, and BBR, respectively. As given in Fig. 5.26 to Fig. 5.28, The 3D surface plots of different combinations suggest that Load with BBR and NDR with BBR and has a synergistic interaction effect on NO<sub>x</sub>. In contrast, the other combinations exhibit antagonistic interaction on NO<sub>x</sub>.

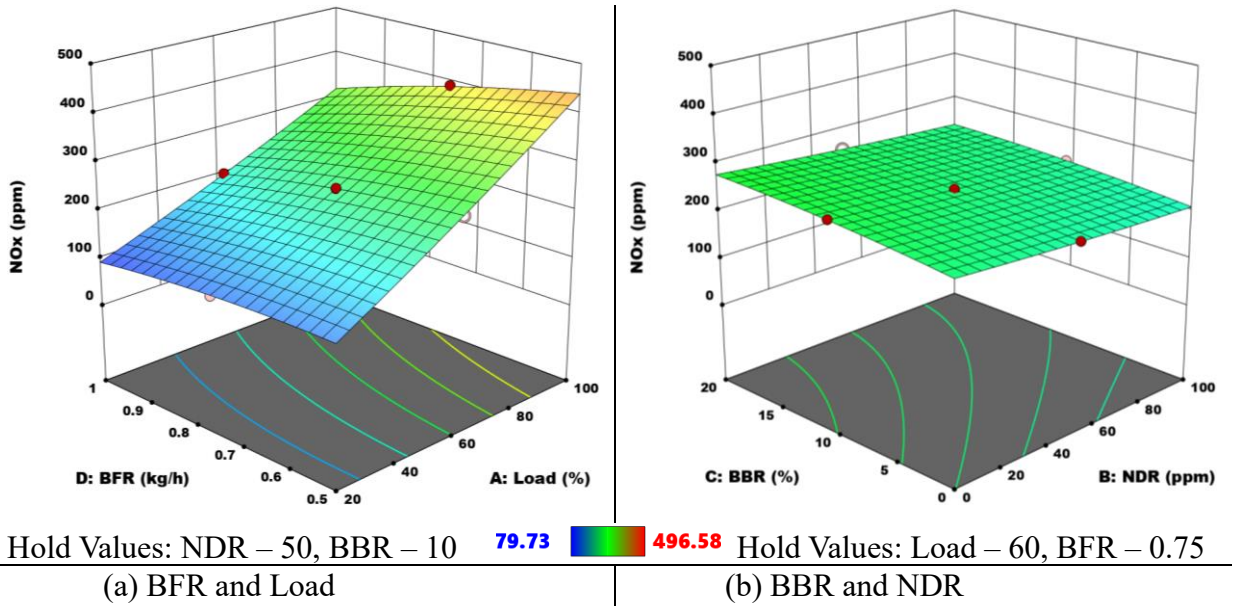


Fig. 5. 27 Interaction effects of (a) BBR and Load, (b) BBR and NDR on NO<sub>x</sub>

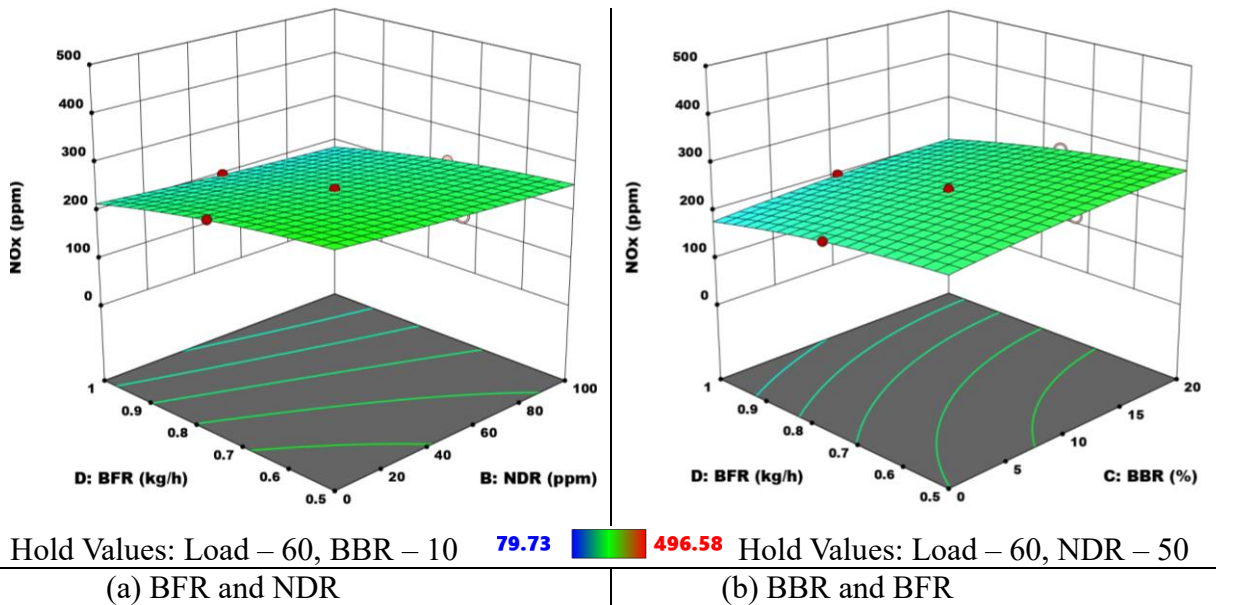


Fig. 5. 28 Interaction effects of (a) BBR and Load, (b) BBR and NDR on NO<sub>x</sub>

Based on the slope of the graph for each surface plot, the combination of load and BFR exhibited as the most sensitive or significant in impacting NO<sub>x</sub>. At the same central load and



BFR level, compared to the BBR20-NDR100 blend, NO<sub>x</sub> observed a decrease of 14% over BBR20-NDR0. At the same central level of load and BBR, there was a reduction in NO<sub>x</sub> of 27.15% for BFR1-NDR100 compared to BFR0.5-NDR100. At the same central level of load and NDR, an increase of 13.5% for BFR1-BBR0 compared to BFR1-BBR20 was noted.

### 5.2.6 Interaction effects on HC

With the chosen input variables taken into consideration, the empirical model for analysing HC is shown in equation 5.4.

$$\text{HC} = 44.9637 + -6.77761 * A + -4.45204 * B + -2.79144 * C + 2.98671 * D + 0.618654 * AB + 0.382929 * AC + -0.231771 * AD + 0.249148 * BC + -0.268035 * BD + -0.16326 * CD + 0.731055 * A^2 + 0.267014 * B^2 + 1.24267 * C^2 + 1.17926 * D^2 \quad (5.4)$$

The positive coefficients of BFR indicate a directly proportional relation to HC, while negative coefficients of Load, BBR, and NDR in the equation suggest an inversely proportional relationship. With the highest F-value from the ANOVA Table, Engine load input is the most sensitive to HC response among the independent variables, followed by NDR, BFR, and BBR, respectively.

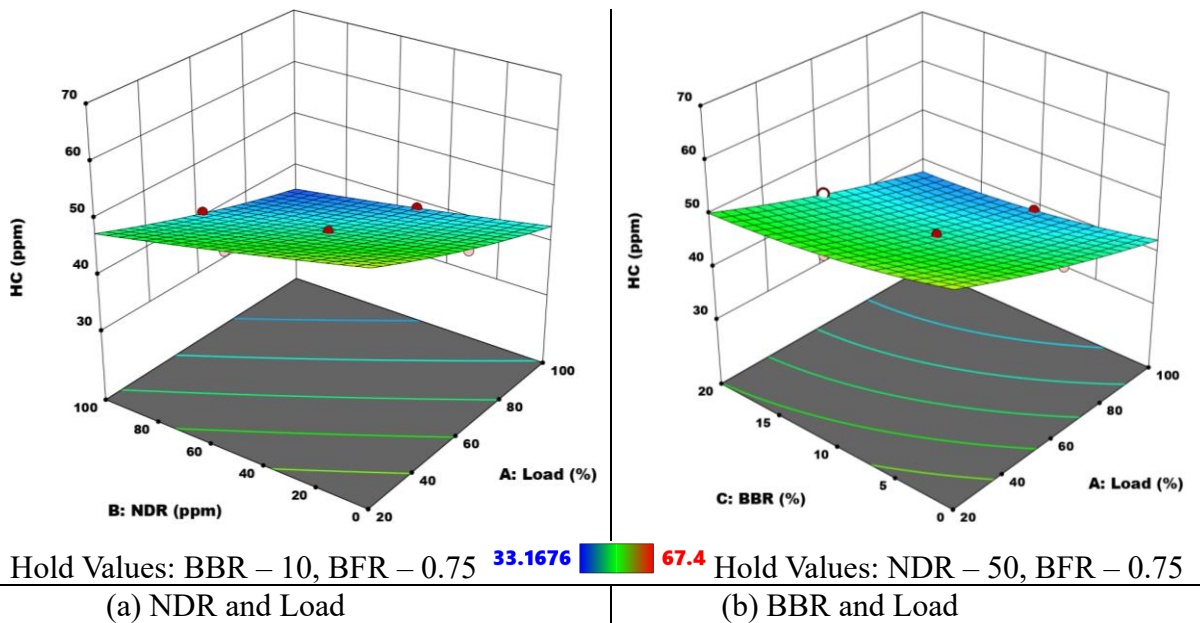
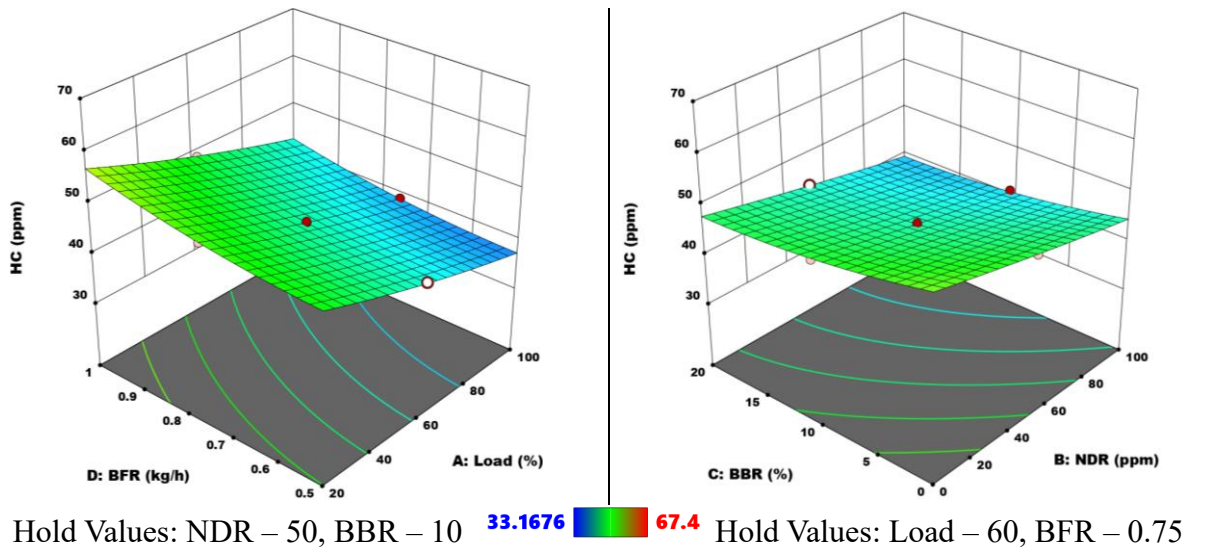


**Fig. 5.29** Interaction effects of (a) NDR and Load, (b) BBR and Load on HC

As given in Fig. 5.29 to Fig. 5.31, The 3D surface plots of different combinations suggest that Load with NDR, Load with BBR, and NDR with BBR and has a synergistic interaction effect on HC. In contrast, the other combinations exhibit antagonistic interaction on HC. Based on the slope of the graph for each surface plot, the combination of load and NDR was

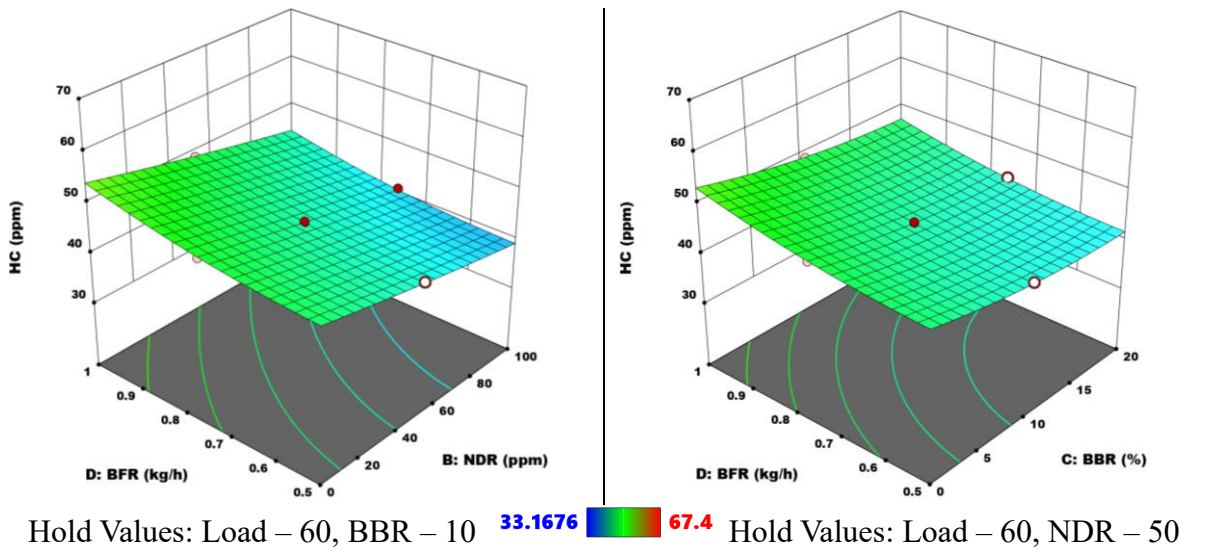
indicated as the most sensitive or significant in impacting HC. At the same central load and BFR level, compared to the BBR20-NDR100 blend, HC observed a decrease of 17% over BBR20-NDR0. At the same central level of load and BBR, an increase in HC of 13.02% for BFR1-NDR100 compared to BFR0.5-NDR100 was noted. At the same central level of load and NDR, a decrease of 11% for BFR1-BBR0 compared to BFR1-BBR20 was observed.



(a) BFR and Load

(b) BBR and NDR

**Fig. 5.30** Interaction effects of (a) BBR and Load, (b) BBR and NDR on HC



(a) BFR and NDR

(b) BBR and BFR

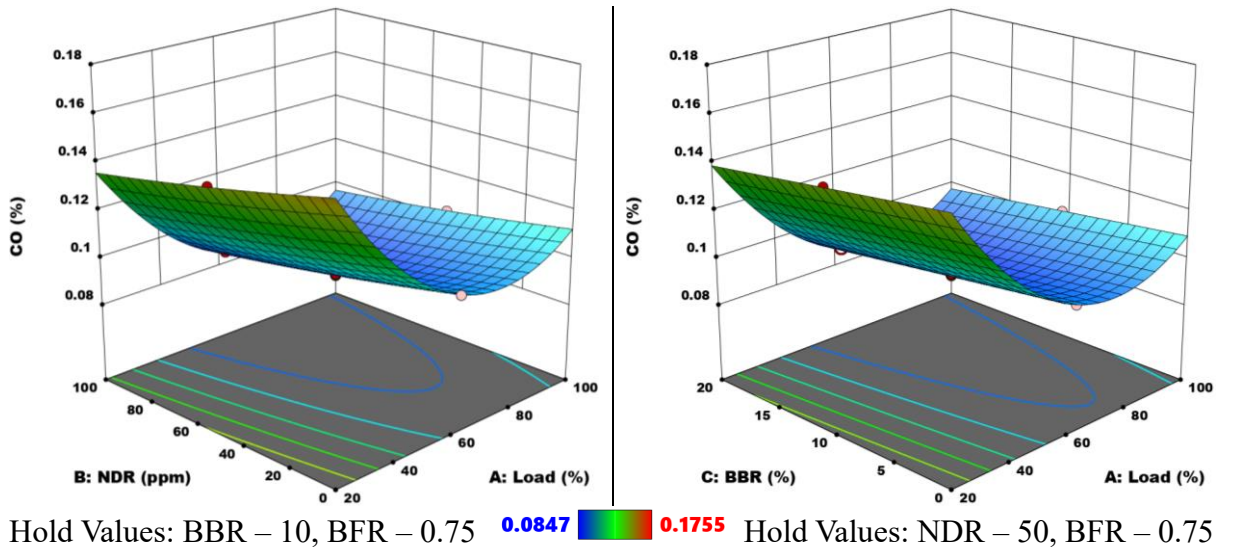
**Fig. 5.31** Interaction effects of (a) BFR and NDR, (b) BBR and BFR on HC

### 5.2.7 Interaction Effects on CO

With the chosen input variables taken into consideration, the empirical model for analyzing CO is shown in equation 5.5. Positive coefficients of BFR imply a directly proportionate link to CO, whereas negative coefficients of Load, BBR, and NDR suggest an inverse

association. Engine load input has the greatest F-value from ANOVA Table and is most sensitive to CO reaction, followed by NDR, BFR, and BBR.

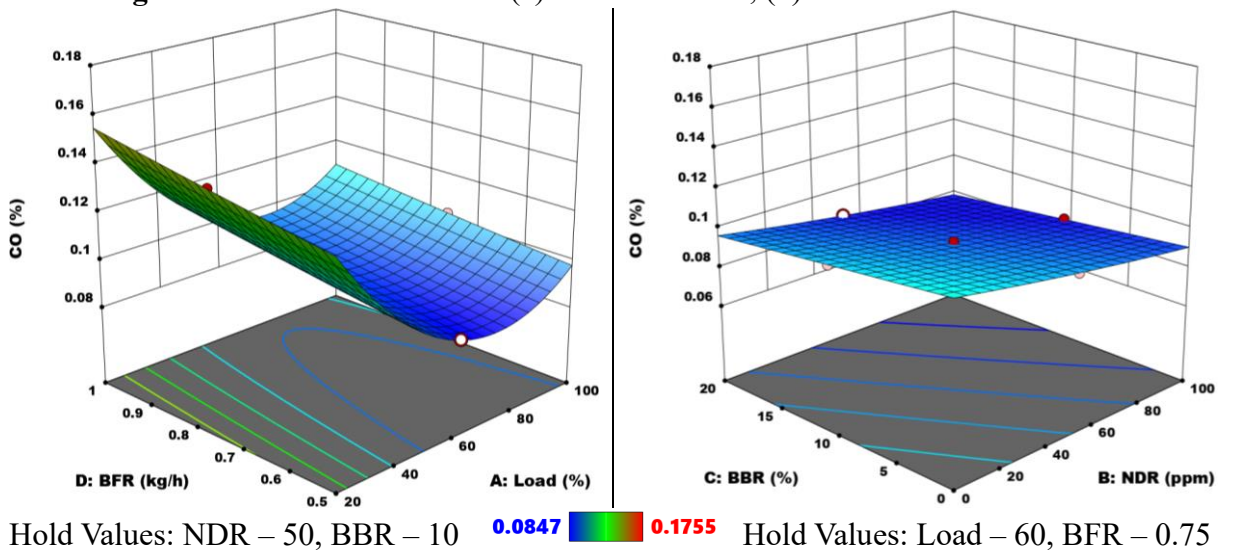
$$\begin{aligned}
 \text{CO} = & 0.0929081 + -0.0212321 * A + -0.00945834 * B + -0.00649946 * C + 0.00726853 \\
 & * D + 0.001596 * AB + 0.0004185 * AC + -0.00136361 * AD + 0.000490613 * BC + - \\
 & 0.00054915 * BD + -0.00037665 * CD + 0.0317948 * A^2 + 0.00100293 * B^2 + 2.9251e-06 \\
 & * C^2 + 0.000302925 * D^2
 \end{aligned}
 \tag{5.5}$$



(a) NDR and Load

(b) BBR and Load

**Fig. 5.32** Interaction effects of (a) NDR and Load, (b) BBR and Load on CO



(a) BFR and Load

(b) BBR and NDR

**Fig. 5.33** Interaction effects of (a) BBR and Load, (b) BBR and NDR on CO

As given in Fig. 5.32 to Fig. 5.34, According to 3D surface plots, Load with NDR, Load with BBR, and NDR with BBR interact synergistically with CO, whereas the other combinations interact antagonistically. The slope of each surface plot shows that load and NDR affect CO the most. At the same central load and BFR level, compared to the BBR20-

NDR100 blend, CO observed a decrease of 14% over BBR20-NDR0. At the same central level of load and BBR, there was an increase in CO of 11.9% for BFR1-NDR100 compared to BFR0.5-NDR100. At the same central level of load and NDR, there is a decrease in CO of 10% for BFR1-BBR0 compared to BFR1-BBR20.

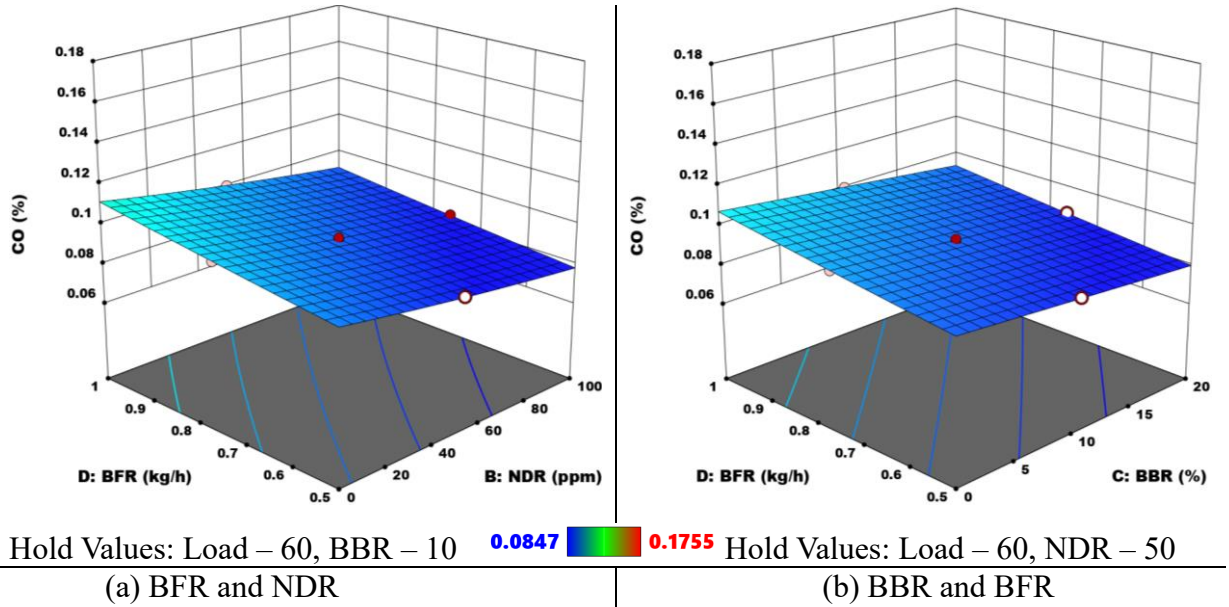


**Fig. 5.34** Interaction effects of a) BFR and NDR, (b) BBR and BFR on CO

### 5.2.8 Interaction effects on SO

With the chosen input variables taken into consideration, the empirical model for analysing SO is shown in equation 5.6. An inverse correlation is shown by the presence of negative coefficients of BFR, BBR, and NDR, but positive coefficients of engine load factor indicate that there is a direct proportional link to SO. The contribution calculation from ANOVA analysis suggests that the engine load input is the most sensitive to the CO response. This was followed by the BFR, NDR, and BBR.

$$\text{SO} = 28.8435 + 13.2206 * A + -2.02695 * B + -1.2147 * C + -4.41904 * D + -0.924537 * AB + -0.553756 * AC + -2.00184 * AD + 0.0855113 * BC + 0.306983 * BD + 0.184264 * CD + -0.127199 * A^2 + -0.458502 * B^2 + -0.300336 * C^2 + 1.33338 * D^2 \quad (5.6)$$

As given in Fig. 5.35 to Fig. 5.37, Based on the analysis of 3D surface plots, it can be seen that the combination of BBR with NDR, BFR with NDR, and BFR with BBR exhibits a synergistic interaction with SO. On the other hand, the other combinations display an antagonistic interaction. The gradient of each surface plot indicates that the combination of load and BFR has the most significant impact on SO.

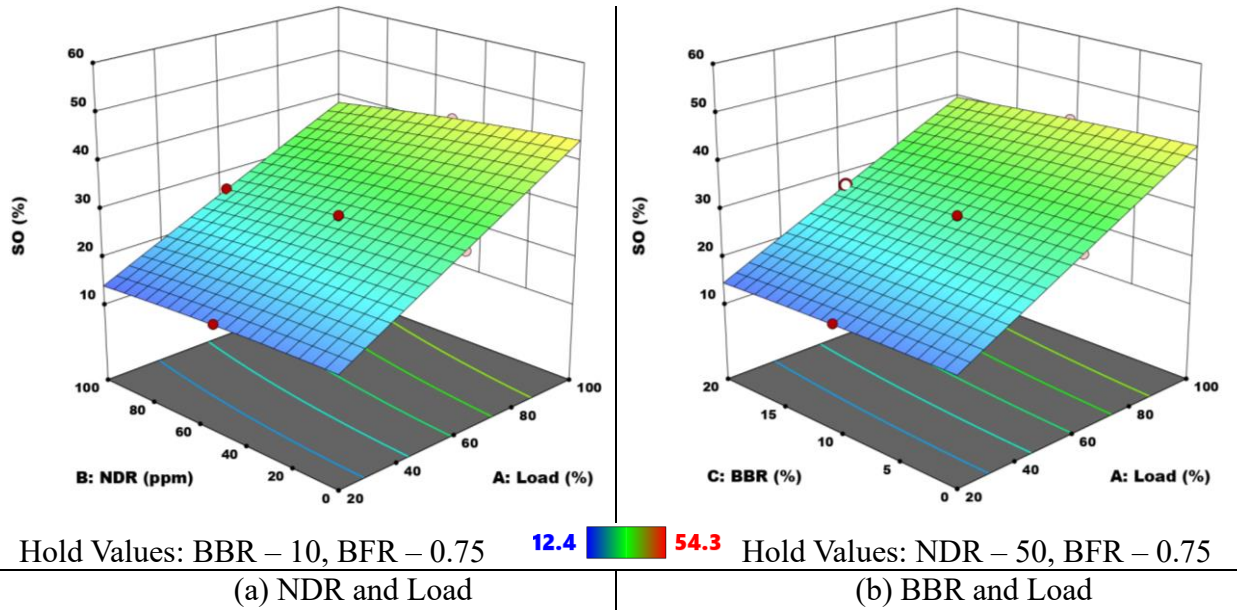


Fig. 5. 35 Interaction effects of (a) NDR and Load, (b) BBR and Load on SO

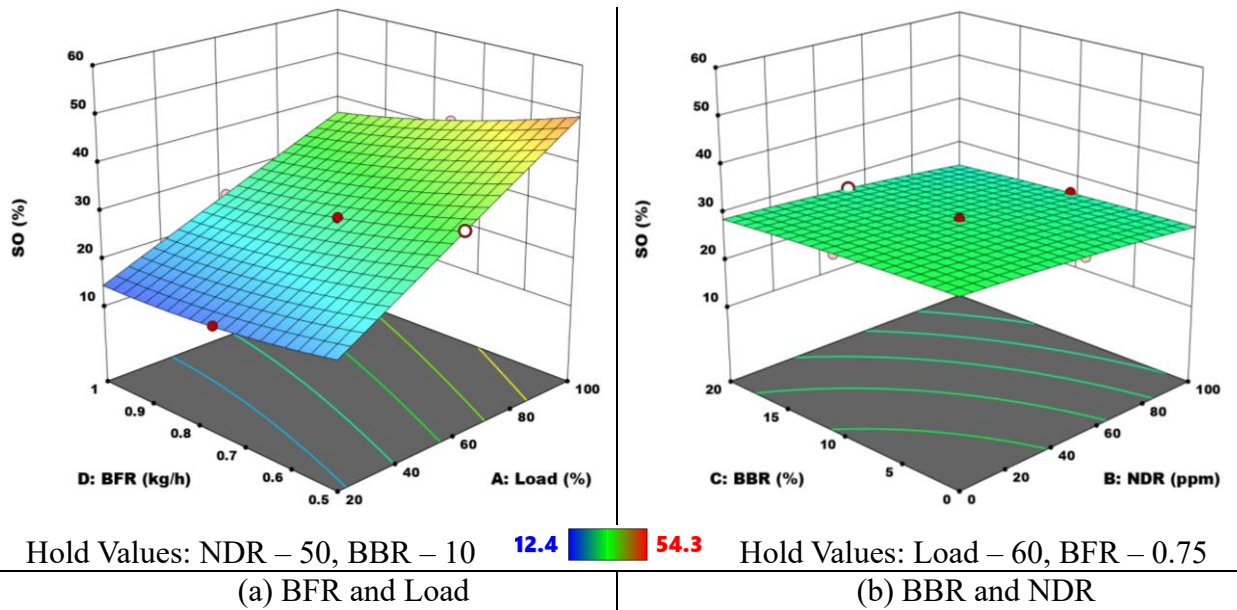
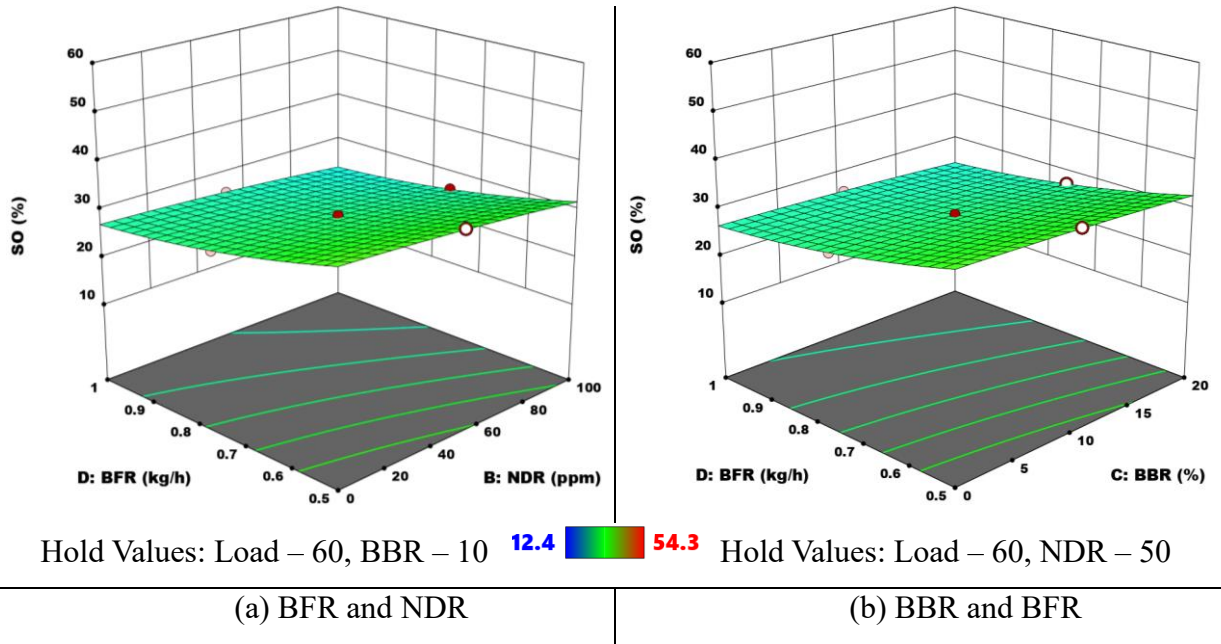


Fig. 5. 36 Interaction effects of (a) BBR and Load, (b) BBR and NDR on SO

At the same central load and BFR level, compared to the BBR20-NDR100 blend, SO observed a decrease of 13% over BBR20-NDR0. At the same central level of load and BBR, an increase in SO of 26.15% for BFR1-NDR100 compared to BFR0.5-NDR100 was observed. At the same central level of load and NDR, a decrease in SO of 8% for BFR1-BBR0 compared to BFR1-BBR20 was noted.



**Fig. 5. 37** Interaction effects of (a) BFR and NDR, (b) BBR and BFR on SO

### 5.2.9 Interaction Effects on BGES

With the chosen input variables considered, the empirical model for analysing BGES is shown in equation 5.7. Load and BBR have negative coefficients, which means they are negatively related to BGES. On the other hand, the NDR and BFR factor have a positive coefficient, which means it is directly proportional to BGES. Contribution calculations from ANOVA analysis show that the engine load input affects the CO reaction the most, closely followed by BFR.

$$\begin{aligned}
 \text{BGES} = & 40.9422 + -11.4161 * A + 1.17624 * B + -1.26952 * C + 10.0917 * D + -0.296028 \\
 & * AB + -0.260189 * AC + -1.58759 * AD + -0.132482 * BC + 0.261317 * BD + 0.0949908 \\
 & * CD + 4.99763 * A^2 + -0.173937 * B^2 + 0.277633 * C^2 + -0.887367 * D^2
 \end{aligned}
 \quad (5.7)$$

As given in Fig. 5.38 to Fig. 5.40, The examination of three-dimensional surface plots reveals that the amalgamation of BFR with NDR and BFR with BBR interact synergistically with BGES. Conversely, the remaining combinations exhibit a negative interaction. According to the gradient of each surface plot, the most substantial influence on BGES is exerted by the combination of load and BFR. At the same central load and BFR level, compared to the BBR20-NDR100 blend, BGES observed an increase of 5.5% over BBR20-NDR0. At the same central level of load and BBR, an increase in BGES of 65.3% for BFR1-NDR100 compared to BFR0.5-NDR100 was observed. At the same central level of load and NDR, a decrease in BGES of 3.01% for BFR1-BBR0 compared to BFR1-BBR20 was noted.

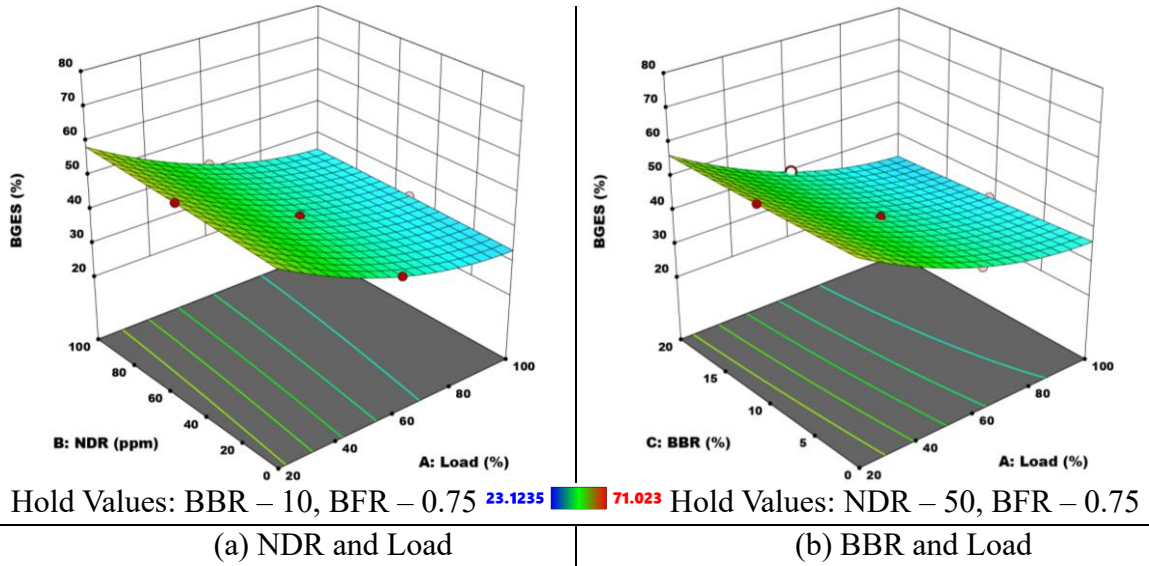


Fig. 5. 38 Interaction effects of (a) NDR and Load, (b) BBR and Load on BGES

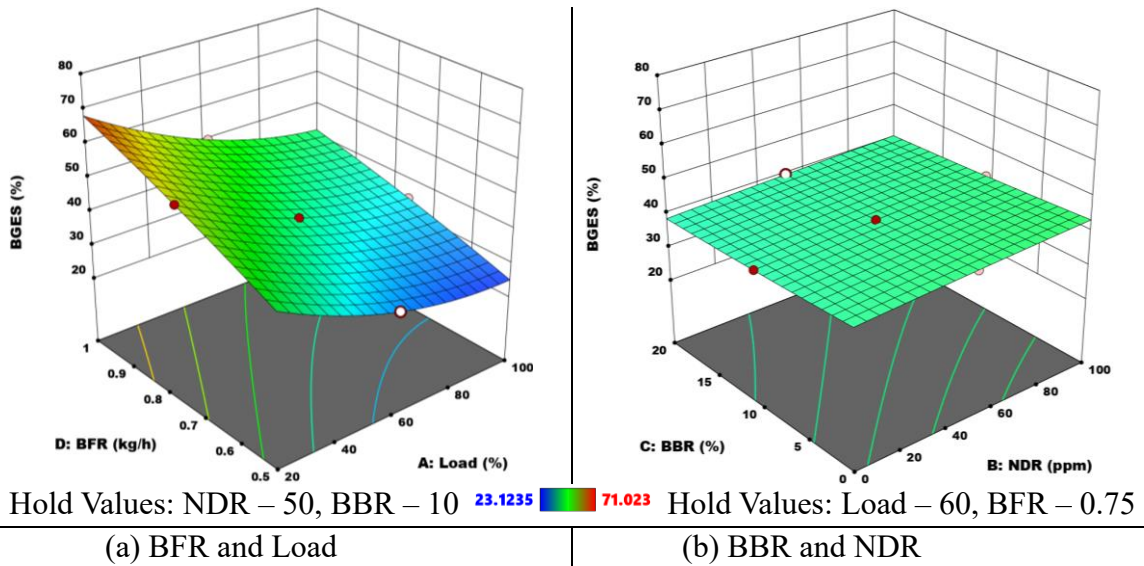


Fig. 5. 39 Interaction effects of (a) BFR and Load, (b) BBR and NDR on BGES

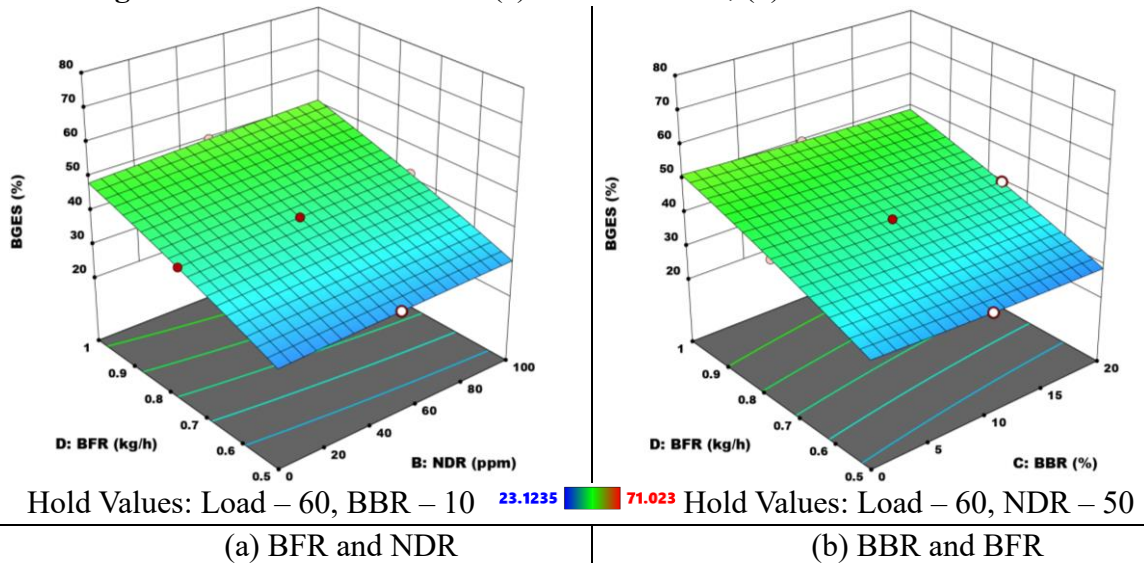


Fig. 5. 40 Interaction effects of (a) BFR and NDR, (b) BBR and BFR on BGES

Table 5. 5 ANOVA for table BTE

Source	SS	df	Mean Square	F-value	p-value	Contribution (%)	Remarks
Model	457.36	14	32.67	2464.5	< 0.0001	99.96	significant
A-Load	338.06	1	338.06	25502.84	< 0.0001	73.88	
B-NDR	11.25	1	11.25	849.02	< 0.0001	2.46	
C-BBR	22.68	1	22.68	1710.93	< 0.0001	4.96	
D-BFR	41.61	1	41.61	3139.37	< 0.0001	9.09	
AB	0.9594	1	0.9594	72.37	< 0.0001	0.21	
AC	3.36	1	3.36	253.44	< 0.0001	0.73	
AD	5.13	1	5.13	387.08	< 0.0001	1.12	
BC	0.0634	1	0.0634	4.79	0.0449	0.01	
BD	0.1158	1	0.1158	8.73	0.0098	0.03	
CD	0.2402	1	0.2402	18.12	0.0007	0.05	
A <sup>2</sup>	9.89	1	9.89	746.37	< 0.0001	2.16	
B <sup>2</sup>	0.0454	1	0.0454	3.42	0.0841	0.01	
C <sup>2</sup>	0.0008	1	0.0008	0.0567	0.815	0.00	
D <sup>2</sup>	0.0778	1	0.0778	5.87	0.0286	0.02	
Residual	0.1988	15	0.0133				
Lack of Fit	0.176	10	0.0176	3.85	0.075		not significant
Pure Error	0.0229	5	0.0046				
Cor Total	457.56	29		R <sup>2</sup>			0.9996
Std. Dev.	0.1151			Adjusted R <sup>2</sup>			0.9992
Mean	14.63			Predicted R <sup>2</sup>			0.9975
C.V. %	0.7869			Adeq Precision			190.8182



Table 5. 6 ANOVA table for BSEC

Source	SS	df	Mean Square	F-value	p-value	Contribution (%)	Remarks
Model	1544.8	14	110.34	6844.83	< 0.0001	99.96	significant
A-Load	1121.77	1	1121.77	69586.09	< 0.0001	73.88	
B-NDR	35.76	1	35.76	2218.54	< 0.0001	2.46	
C-BBR	101.5	1	101.5	6296.3	< 0.0001	4.96	
D-BFR	52.09	1	52.09	3231.31	< 0.0001	9.09	
AB	2.45	1	2.45	152.18	< 0.0001	0.21	
AC	11.67	1	11.67	723.74	< 0.0001	0.73	
AD	3.96	1	3.96	245.95	< 0.0001	1.12	
BC	0.1623	1	0.1623	10.07	0.0063	0.01	
BD	0.0682	1	0.0682	4.23	0.0575	0.03	
CD	0.2564	1	0.2564	15.91	0.0012	0.05	
A <sup>2</sup>	66.49	1	66.49	4124.8	< 0.0001	2.16	
B <sup>2</sup>	0.0084	1	0.0084	0.5239	0.4803	0.01	
C <sup>2</sup>	0.0046	1	0.0046	0.2848	0.6014	0.00	
D <sup>2</sup>	0.5016	1	0.5016	31.12	< 0.0001	0.02	
Residual	0.2418	15	0.0161				
Lack of Fit	0.2153	10	0.0215	4.06	0.0678		not significant
Pure Error	0.0265	5	0.0053				
Cor Total	1545.04			0.9998			0.9998
Std. Dev.	0.127			Adjusted R <sup>2</sup>			0.9997
Mean	25.28			Predicted R <sup>2</sup>			0.9993
C.V. %	0.5022			Adeq Precision			298.058

Table 5. 7 ANOVA table for NO<sub>x</sub>

Source	SS	df	Mean Square	F-value	p-value	Contribution (%)	Remarks
Model	3.82E+05	14	27270.31	14491.97	< 0.0001	100	significant
A-Load	3.33E+05	1	3.33E+05	1.77E+05	< 0.0001	87.3	
B-NDR	5774.2	1	5774.2	3068.52	< 0.0001	1.51	
C-BBR	4460.24	1	4460.24	2370.26	< 0.0001	1.17	
D-BFR	25907.41	1	25907.41	13767.7	< 0.0001	6.79	
AB	1631.65	1	1631.65	867.09	< 0.0001	0.43	
AC	1606.82	1	1606.82	853.9	< 0.0001	0.42	
AD	8235.16	1	8235.16	4376.32	< 0.0001	2.16	
BC	15.27	1	15.27	8.11	0.0122	0	
BD	112.31	1	112.31	59.68	< 0.0001	0.03	
CD	87.43	1	87.43	46.46	< 0.0001	0.02	
A <sup>2</sup>	100.62	1	100.62	53.47	< 0.0001	0.03	
B <sup>2</sup>	18.69	1	18.69	9.93	0.0066	0	
C <sup>2</sup>	99.34	1	99.34	52.79	< 0.0001	0.03	
D <sup>2</sup>	248.01	1	248.01	131.8	< 0.0001	0.06	
Residual	28.23	15	1.88				
Lack of Fit	24.86	10	2.49	3.7	0.081		not significant
Pure Error	3.36	5	0.6728				
Cor Total	3.82E+05	29		R <sup>2</sup>			0.9999
Std. Dev.	1.37			Adjusted R <sup>2</sup>			0.9999
Mean	242.31			Predicted R <sup>2</sup>			0.9995
C.V. %	0.5661			Adeq Precision			428.1972

Table 5. 8 ANOVA table for HC

Source	SS	df	Mean Square	F-value	p-value	Contribution (%)	Remarks
Model	1564.25	14	111.73	4697.42	< 0.0001	99.98	significant
A-Load	826.85	1	826.85	34762.25	< 0.0001	52.85	
B-NDR	356.77	1	356.77	14999.37	< 0.0001	22.8	
C-BBR	140.26	1	140.26	5896.73	< 0.0001	8.96	
D-BFR	160.57	1	160.57	6750.58	< 0.0001	10.26	
AB	6.12	1	6.12	257.45	< 0.0001	0.39	
AC	2.35	1	2.35	98.64	< 0.0001	0.15	
AD	0.8595	1	0.8595	36.13	< 0.0001	0.05	
BC	0.9932	1	0.9932	41.76	< 0.0001	0.06	
BD	1.15	1	1.15	48.33	< 0.0001	0.07	
CD	0.4265	1	0.4265	17.93	0.0007	0.03	
A <sup>2</sup>	1.38	1	1.38	58.21	< 0.0001	0.09	
B <sup>2</sup>	0.1847	1	0.1847	7.77	0.0138	0.01	
C <sup>2</sup>	4	1	4	168.21	< 0.0001	0.26	
D <sup>2</sup>	3.6	1	3.6	151.48	< 0.0001	0.23	
Residual	0.3568	15	0.0238				
Lack of Fit	0.2449	10	0.0245	1.09	0.4906		not significant
Pure Error	0.1119	5	0.0224				
Cor Total	1564.6	29		R <sup>2</sup>			0.9998
Std. Dev.	0.1542			Adjusted R <sup>2</sup>			0.9996
Mean	47.02			Predicted R <sup>2</sup>			0.9992
C.V. %	0.328			Adeq Precision			311.9136

Table 5. 9 ANOVA table for CO

Source	SS	df	Mean Square	F-value	p-value	Contribution (%)	Remarks
Model	0.0192	14	0.0014	19054.97	< 0.0001	100	significant
A-Load	0.0081	1	0.0081	1.13E+05	< 0.0001	42.19	
B-NDR	0.0016	1	0.0016	22323.99	< 0.0001	8.33	
C-BBR	0.0008	1	0.0008	10541.33	< 0.0001	4.17	
D-BFR	0.001	1	0.001	13183.63	< 0.0001	5.21	
AB	0	1	0	565.01	< 0.0001	0	
AC	2.80E-06	1	2.80E-06	38.85	< 0.0001	0.01	
AD	0	1	0	412.45	< 0.0001	0	
BC	3.85E-06	1	3.85E-06	53.39	< 0.0001	0.02	
BD	4.83E-06	1	4.83E-06	66.89	< 0.0001	0.03	
CD	2.27E-06	1	2.27E-06	31.47	< 0.0001	0.01	
A <sup>2</sup>	0.0026	1	0.0026	36310.6	< 0.0001	13.54	
B <sup>2</sup>	2.61E-06	1	2.61E-06	36.13	< 0.0001	0.01	
C <sup>2</sup>	2.22E-11	1	2.22E-11	0.0003	0.9862	0	
D <sup>2</sup>	2.38E-07	1	2.38E-07	3.3	0.0895	0	
Residual	1.08E-06	15	7.21E-08				
Lack of Fit	6.04E-07	10	6.04E-08	0.6319	0.7493		not significant
Pure Error	4.78E-07	5	9.56E-08				
Cor Total	1564.6	29		R <sup>2</sup>			0.9999
Std. Dev.	0.0003			Adjusted R <sup>2</sup>			0.9999
Mean	0.1128			Predicted R <sup>2</sup>			0.9998
C.V. %	0.2382			Adeq Precision			478.1814

Table 5. 10 ANOVA table for SO

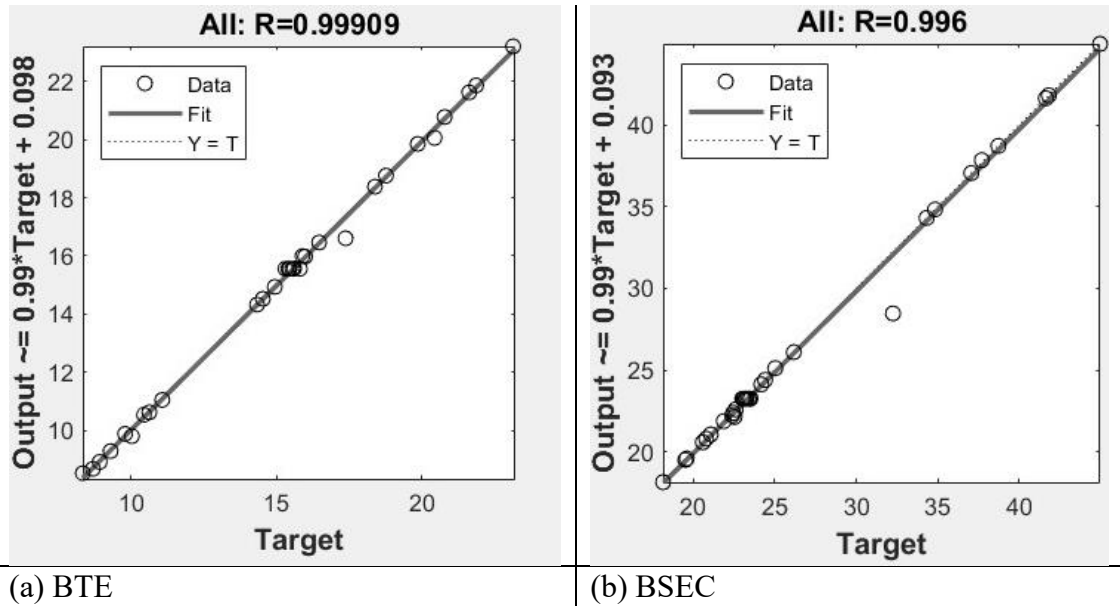
Source	SS	df	Mean Square	F-value	p-value	Contribution (%)	Remarks
Model	3688.21	14	263.44	16152.16	< 0.0001	99.99	significant
A-Load	3146.09	1	3146.09	1.93E+05	< 0.0001	85.3	
B-NDR	73.95	1	73.95	4534.23	< 0.0001	2	
C-BBR	26.56	1	26.56	1628.36	< 0.0001	0.72	
D-BFR	351.5	1	351.5	21551.19	< 0.0001	9.53	
AB	13.68	1	13.68	838.52	< 0.0001	0.37	
AC	4.91	1	4.91	300.82	< 0.0001	0.13	
AD	64.12	1	64.12	3931.16	< 0.0001	1.74	
BC	0.117	1	0.117	7.17	0.0172	0	
BD	1.51	1	1.51	92.45	< 0.0001	0.04	
CD	0.5433	1	0.5433	33.31	< 0.0001	0.01	
A <sup>2</sup>	0.0419	1	0.0419	2.57	0.1297	0	
B <sup>2</sup>	0.5447	1	0.5447	33.39	< 0.0001	0.01	
C <sup>2</sup>	0.2337	1	0.2337	14.33	0.0018	0.01	
D <sup>2</sup>	4.61	1	4.61	282.42	< 0.0001	0.12	
Residual	0.2447	15	0.0163				
Lack of Fit	0.1986	10	0.0199	2.16	0.205		not significant
Pure Error	0.046	5	0.0092				
Cor Total	3688.45	29		R <sup>2</sup>			0.9999
Std. Dev.	0.1277			Adjusted R <sup>2</sup>			0.9999
Mean	29.11			Predicted R <sup>2</sup>			0.9996
C.V. %	0.4387			Adeq Precision			462.4588

Table 5. 11 ANOVA table for BGES

Source	SS	df	Mean Square	F-value	p-value	Contribution (%)	Remarks
Model	4421.41	14	315.81	71309.05	< 0.0001	100.00	significant
A-Load	2345.91	1	2345.91	5.30E+05	< 0.0001	53.06	
B-NDR	24.9	1	24.9	5623.11	< 0.0001	0.56	
C-BBR	29.01	1	29.01	6550.32	< 0.0001	0.66	
D-BFR	1833.17	1	1833.17	4.14E+05	< 0.0001	41.46	
AB	1.4	1	1.4	316.59	< 0.0001	0.03	
AC	1.08	1	1.08	244.57	< 0.0001	0.02	
AD	40.33	1	40.33	9105.62	< 0.0001	0.91	
BC	0.2808	1	0.2808	63.41	< 0.0001	0.01	
BD	1.09	1	1.09	246.7	< 0.0001	0.02	
CD	0.1444	1	0.1444	32.6	< 0.0001	0.00	
A <sup>2</sup>	64.71	1	64.71	14611.44	< 0.0001	1.46	
B <sup>2</sup>	0.0784	1	0.0784	17.7	0.0008	0.00	
C <sup>2</sup>	0.1997	1	0.1997	45.09	< 0.0001	0.00	
D <sup>2</sup>	2.04	1	2.04	460.65	< 0.0001	0.05	
Residual	0.0664	15	0.0044			100.00	
Lack of Fit	0.0592	10	0.0059	4.09	0.0669		not significant
Pure Error	0.0072	5	0.0014				
Cor Total	4421.47	29		R <sup>2</sup>			0.9999
Std. Dev.	0.0665			Adjusted R <sup>2</sup>			0.9999
Mean	43.47			Predicted R <sup>2</sup>			0.999
C.V. %	0.1531			Adeq Precision			1018.058

### 5.2.10 ANN Model Analysis

The coefficient of correlation (R) for each stage (i.e., training, testing, and validation) is obtained for the network created corresponding to output parameters. The overall coefficient of correlation (R) for every dependent response is given in Fig.5.41 to Fig. 5.44. High R values for each network suggest good data training from DOE, and a further conclusion of the reliable regression model was reached.



**Fig. 5. 41** R for the trained network in response to outputs (a) BTE, (b) BSEC

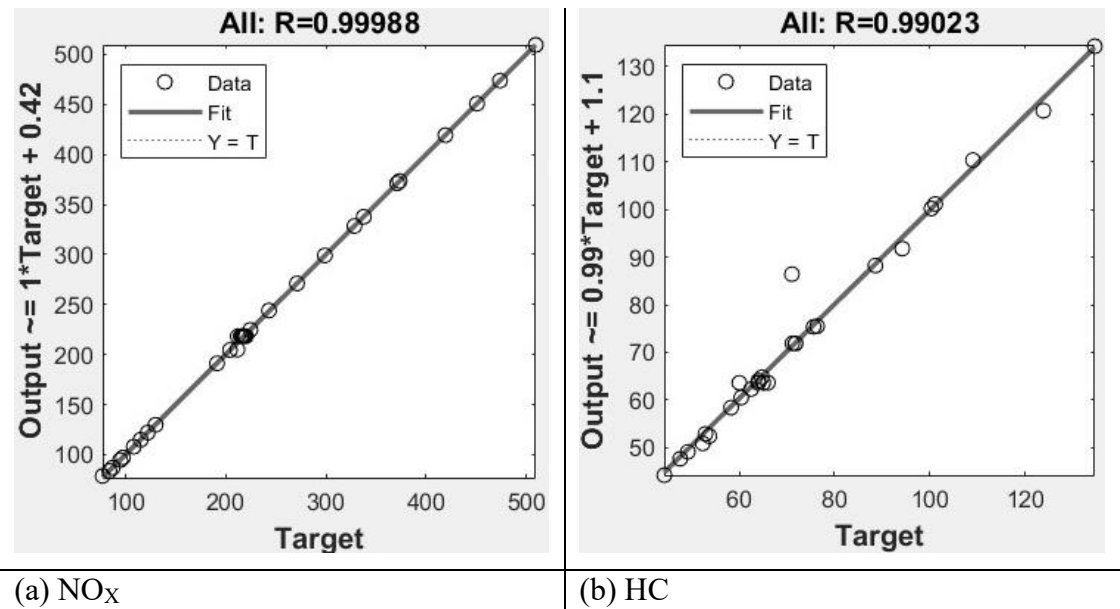
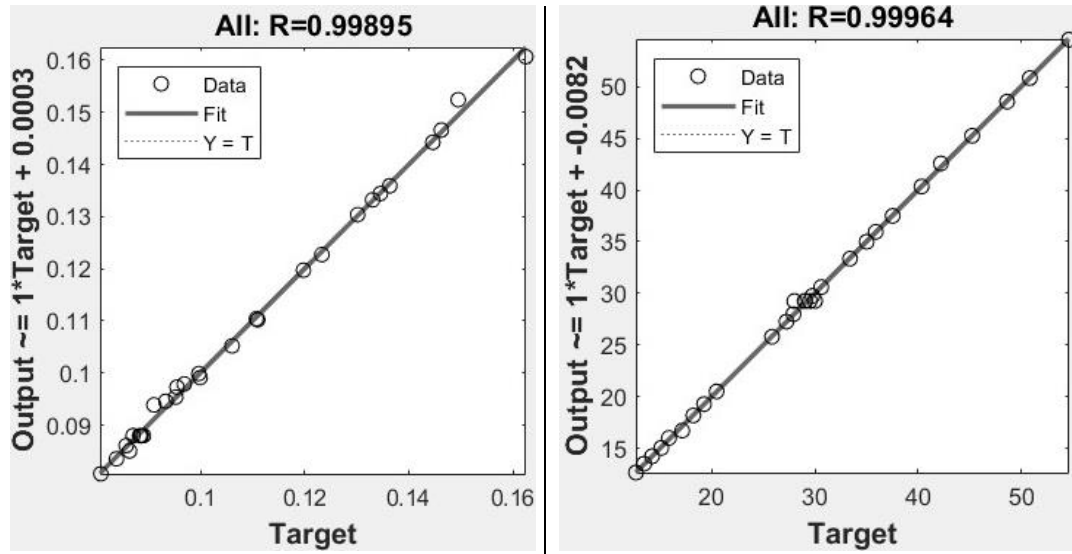


**Fig. 5. 42** R for the trained network in response to outputs (a) NO<sub>x</sub>, (b) HC



(a) CO

(b) Smoke opacity

Fig. 5. 43 R for the trained network in response to outputs (a)CO and (b) SO

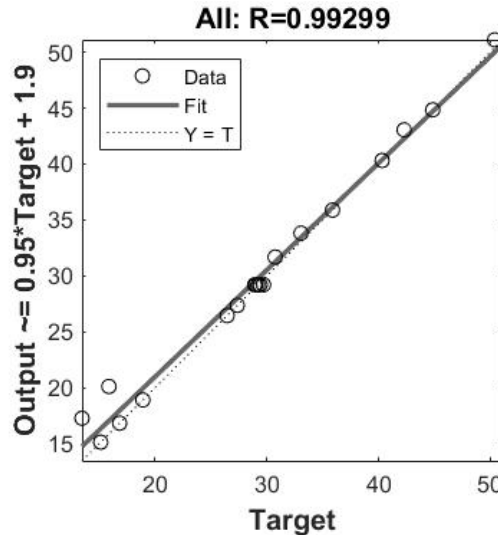


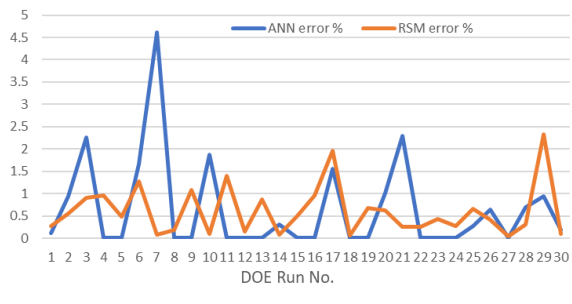
Fig. 5. 44 R for the trained network in response to outputs BGES

**5.2.11 Comparison of the ANN Model and RSM Model**

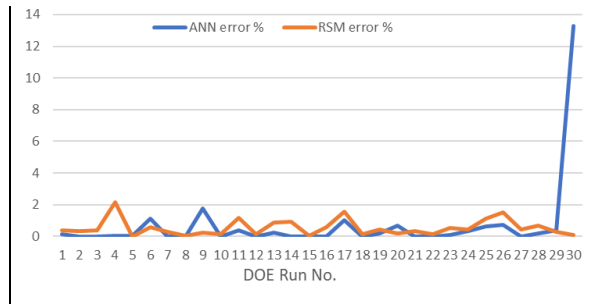
For each run in the DOE Table (Table 5.4), the percentage error using Equation 3.14 is calculated for the ANN and RSM predicted responses and presented in Fig. 5.45.

In contrast, Table 5.12 shows the  $R^2$ , RMSE, and MAD evaluation metrics for prediction by the ANN and RSM models. Higher  $R^2$  values, while lower RMSE and MAD values were analyzed mainly for the RSM prediction model compared to the ANN prediction model. Although the ANN model exhibits good prediction, lower error percentages were observed in the RSM model, indicating a better regression analysis for the input variables.

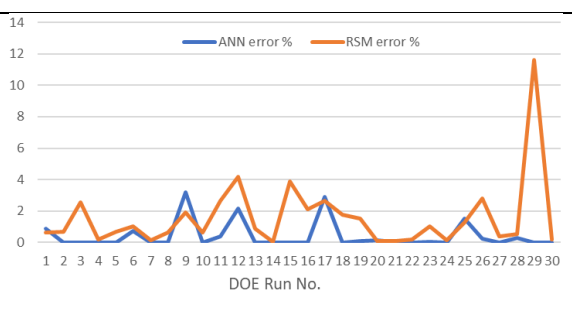




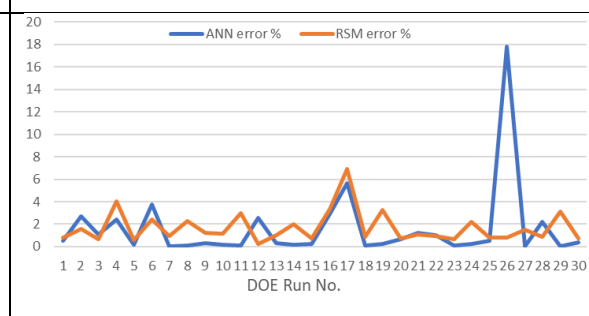
(a) %Error for predicted BTE responses



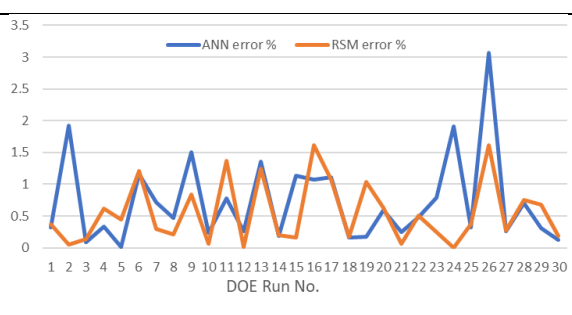
(b) %Error for predicted BSEC responses



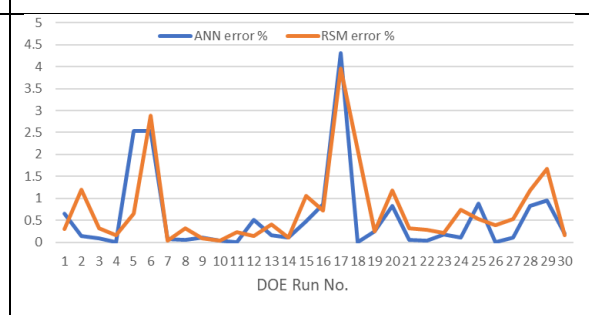
(c) %Error for predicted NO<sub>x</sub> responses



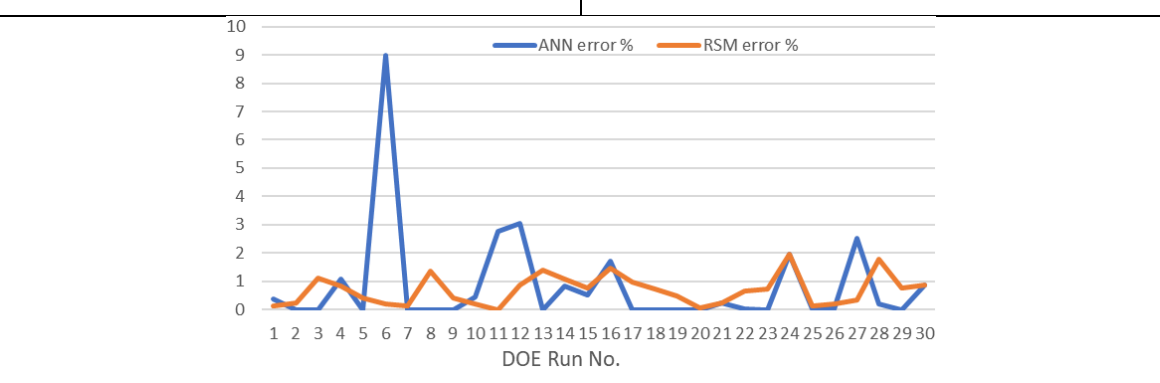
(d) %Error for predicted HC responses



(e) %Error for predicted CO responses



(f) %Error for predicted SO responses



(g) %Error for predicted BGES responses

**Fig. 5. 45** Percentage in error for predicted engine performance and emission responses

**Table 5. 12**  $R^2$ , RMSE, and MAD evaluation metrics for RSM and ANN Model

Responses	$R^2$		RMSE		MAD	
	ANN	RSM	ANN	RSM	ANN	RSM
BTE	0.9982	0.9992	0.184	0.116	0.092	0.087
BSEC	0.9920	0.9995	0.701	0.172	0.189	0.131
NO <sub>x</sub>	0.9998	0.9991	1.875	3.601	0.815	2.657
HC	0.9805	0.9957	3.061	1.438	1.231	1.132
CO	0.9979	0.9991	0.001	0.001	0.001	0.001
SO	0.9992	0.9992	0.302	0.310	0.152	0.194
BGES	0.9929	0.9999	0.216	0.503	0.108	0.015

### 5.2.12 Optimization of Engine Performance and Emission Parameters

To optimize multiple responses, RSM took advantage of its desirability function optimization. Optimal values for the process parameters were obtained via the optimization process, and targets were established accordingly. It was configured to minimize smoke opacity, NO<sub>x</sub>, HC, and CO, and maximize BTE and BGES. Table 5.13 provides a concise summary of the optimization method's criteria. An equal importance of 3 was set for each of the output parameters goals.

**Table 5. 13** Optimization Criteria for Engine Performance and Emission

Factors	Goal	Lower Limit	Upper Limit	Importance
A: Load	In range	20	100	3
B: NDR	In range	0	100	3
C: BBR	In range	0	20	3
D: BFR	In range	0.5	1	3
BTE	maximize	7.44	23.12	3
BSEC	minimize	16.05	43.01	3
NO <sub>x</sub>	minimize	79	496	3
HC	minimize	33	67	3
CO	minimize	0.08	0.17	3
SO	minimize	12.4	54.3	3
BGES	maximize	23.12	71.02	3

For the RSM model with the highest desirability of 0.71(Fig.5.46), the optimal solution selected predicted an optimal value of BTE, BSEC, NO<sub>x</sub>, HC, CO, SO, and BGES at 16.58 %, 20.28 MJ/kWh, 239.704 ppm, 41.06 ppm, 0.085 %, 27.2 %, and 43.66% respectively at 67.45% engine load, 96.06 ppm NDR, 10.7 % BBR and 0.85 kg/h BFR.

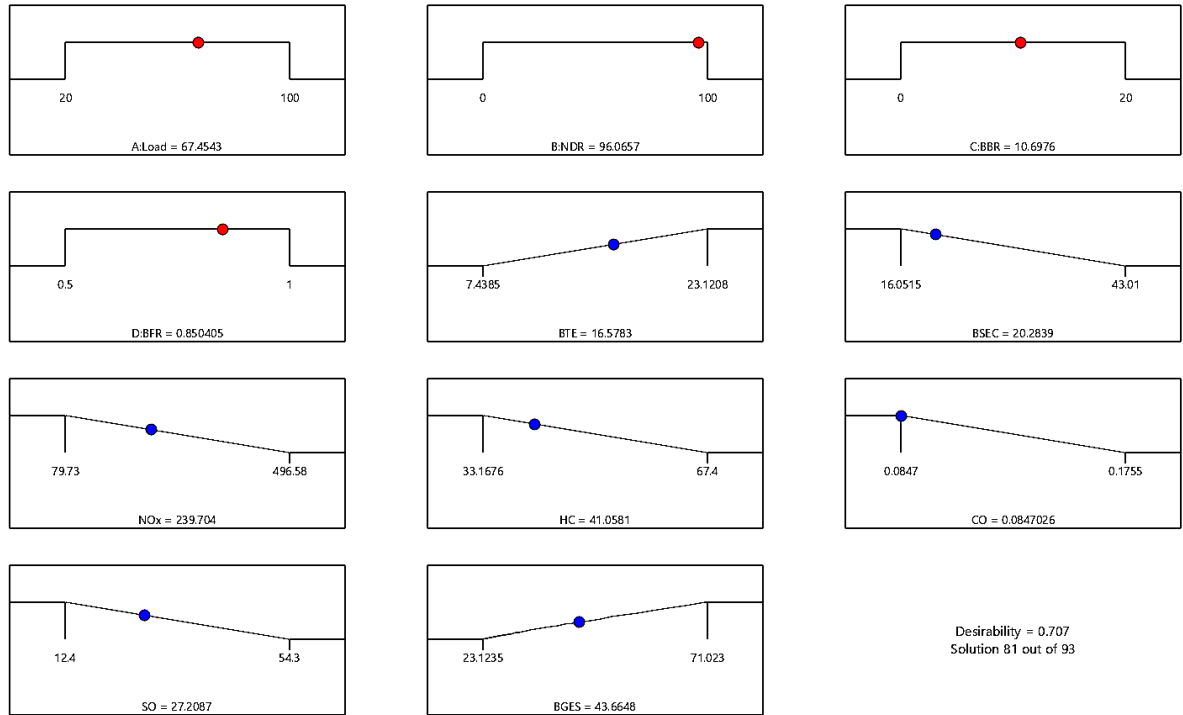


Fig. 5. 46 Desirability Plot

ANN-GA optimization process terminated at 102 generations, predicting an optimal value of BTE, BSEC, NO<sub>x</sub>, HC, CO, SO, and BGES at 16.87 %, 19.76 MJ/kWh, 234.85 ppm, 41.47 ppm, 0.0857 %, 27.26 %, and 43.99% respectively at 67.01% engine load, 98.39 ppm NDR, 8.41% BBR and 0.846 kg/h BFR.

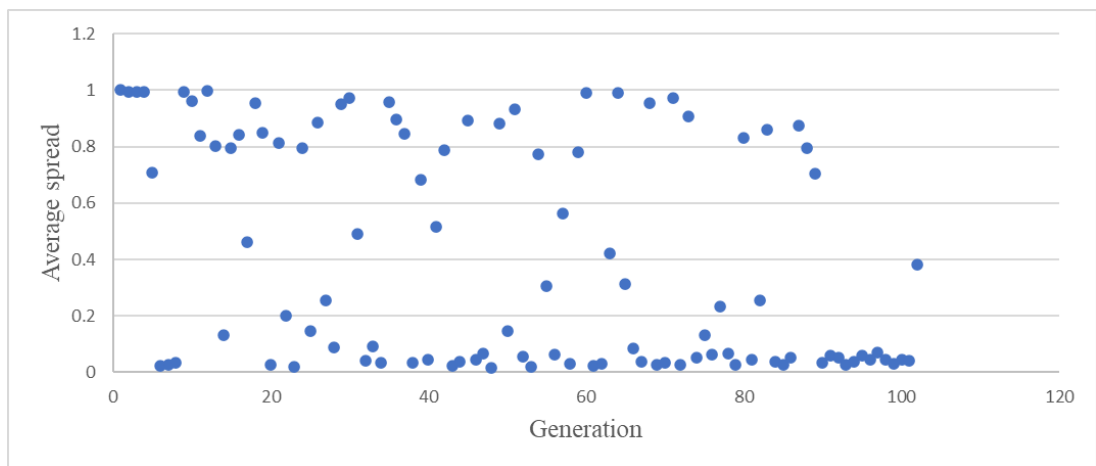


Fig. 5. 47 Average spread vs Generation

### 5.2.13 Validation of optimized results from ANN and RSM Model

Three experiments were conducted at the optimum input conditions that RSM and ANN models identified. Data was collected from each repetition, and the average value for each experimental condition was calculated using a standard averaging technique. Table 5.14 displays the optimized predicted results from RSM and ANN, experimental test validation results, and the percentage error. The percentage error was less than 5% for both model-optimized results, which are considered significant for acceptance. The RSM-optimized result exhibits a lower error percentage than the ANN-GA results, thus confirming that RSM optimization is more accurate and reliable.

**Table 5. 14** Validation test result and Percentage of error for the ANN & RSM optimized parameter

Responses	Model Technique: RSM			Model Technique: ANN		
	Experimental	Predicted	Error	Experimental	Predicted	Error
<b>BTE</b>	16.57	16.58	1.774	17.27	16.87	2.36
<b>BSEC</b>	20.72	20.28	2.166	20.32	19.76	2.84
<b>NO<sub>x</sub></b>	247	239.7	2.955	239	234.85	1.76
<b>HC</b>	42	41.05	1.833	43	41.47	3.69
<b>CO</b>	0.088	0.085	3.9	0.089	0.0857	3.85
<b>SO</b>	27.97	27.208	2.8	27.93	27.26	2.46
<b>BGES</b>	45.64	43.67	4.5	41.88	43.99	4.8

### 5.3 Effect of Enriched Biogas on CI engine performance and emission

Diesel is considered the pilot fuel, while raw biogas and enriched biogas at BFR of 1 kg/h are the gaseous fuel for dual fueling. Enriched Biogas of 90.1% CH<sub>4</sub> (Fig.3.11) is used for this study. Table 5.15 provides the experimental matrix. From 20% (2.4kg) load to 100% (12 kg) load, with a 20% (2.4 kg) increment, the load variations were carried out. The diesel and dual fuel modes were compared at the constant settings of 18:1 compression ratio and 23° BTDC injection time.

**Table 5. 15** Experimental Matrix of the Diesel-Biogas Run Dual Fuel Diesel Engine

Mode	Fuel used	Loading Conditions (%)
Diesel	100% diesel	20,40,60.80,100
Dual	BFR – 1 kg/h (raw)	
Dual	BFR – 1 kg/h (enriched)	

Fig. 5.48 depicts the effect of enriched biogas on BTE. A rise in BTE was observed for increments in Load, with maximum BTE observed for the highest Load (100%) due to better combustion at higher temperatures, leading to a rise in BTE.

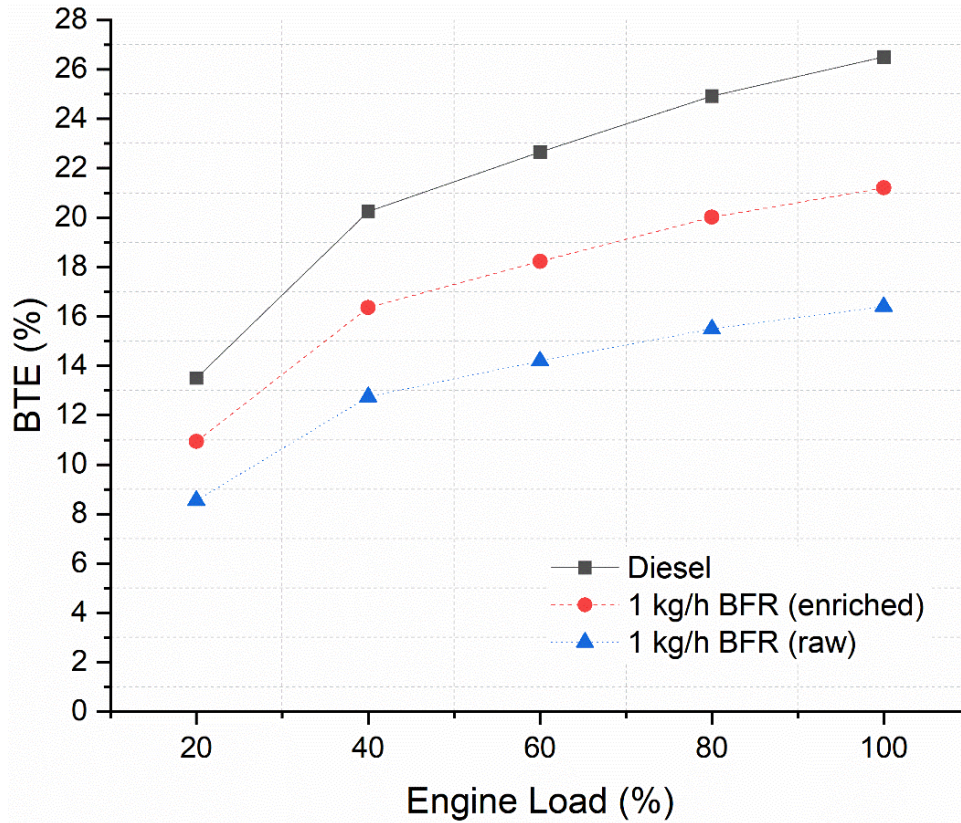


**Fig. 5. 48** Effect of enriched biogas on BTE

A 38.11% and 20% BTE decrease was observed for raw biogas and enriched biogas, respectively. Compared to the engine operated on raw biogas at peak load conditions, BTE observed an increase of 29.26%. A higher percentage of  $\text{CH}_4$  improves combustion by increasing the fuel's calorific value and flame speed. Previous studies under a similar test setup with enriched biogas reported an increase in BTE compared to an engine run on raw biogas [171,172]. A study reported that compared to an engine run on diesel, BTE exhibits a decrease of 34% for an engine run on enriched biogas with a BFR of 1 kg/h [140].

Fig. 5.49 depicts the effect of enriched biogas on BSEC. A decrease in BSEC was observed for increments in Load as a result of an increase in the temperature of the combustion chamber, with minimum BSEC observed for the highest Load (100%). At peak load, an increase in BSEC of 39.31% and 20.07% was observed for raw biogas and enriched biogas, respectively. Whereas in comparison to engine operated on raw biogas, BSEC observed a decrease of 13.81%.

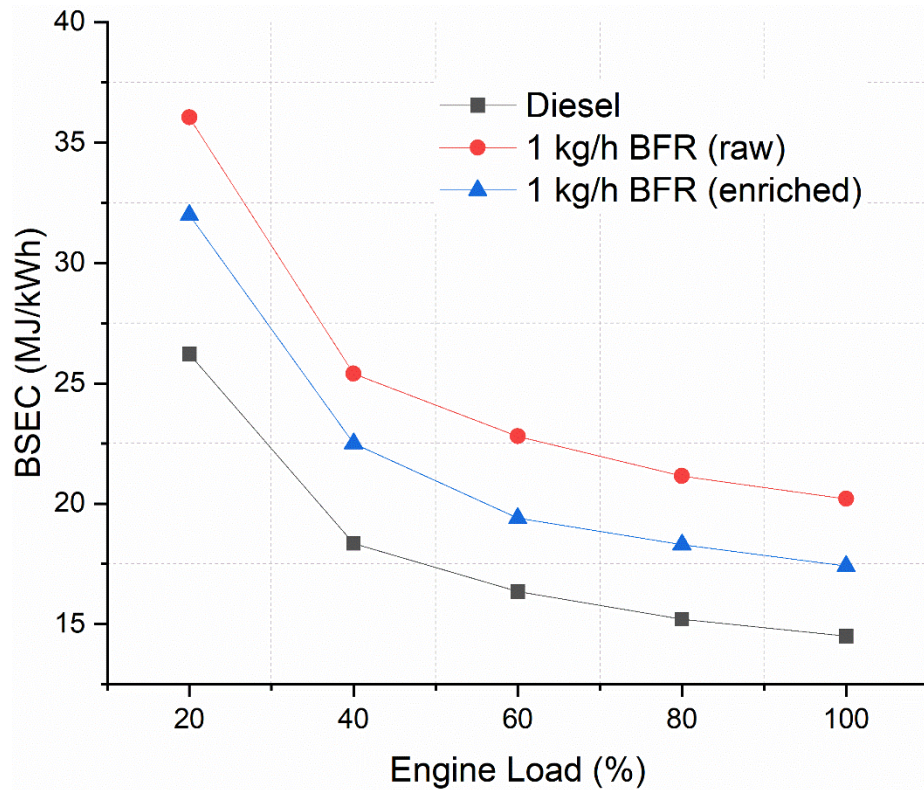


**Fig. 5. 49** Effect of enriched biogas on BSEC

Since enriched biogas has a higher calorific value than raw biogas, the engine consumes less fuel at a lessened rate to produce the same amount of BP, therefore decreasing BSEC as biogas methane percentage increases. Prior research conducted using a comparable experimental configuration with enhanced biogas indicated a decrease in BSEC in comparison to an engine operated on untreated biogas [172,173]. Previous research found that the BSEC of an engine running on enriched biogas at a flow rate of 1 kg/h is 30% lower compared to an engine running on diesel fuel [140].

Fig. 5.50 depicts the effect of enriched biogas on  $\text{NO}_x$ . An increase in  $\text{NO}_x$  was observed for increments in Load due to an increase in the temperature of the combustion chamber, with maximum  $\text{NO}_x$  observed for the highest Load (100%). A decrease in  $\text{NO}_x$  of 51% and 37.88% was observed for raw biogas and enriched biogas, respectively. In comparison to engine operated on raw biogas,  $\text{NO}_x$  observed an increase of 26.78%. Higher  $\text{NO}_x$  for enriched biogas results from the increase in the adiabatic flame temperature due to the lessened presence of  $\text{CO}_2$  in enriched biogas, which has a high specific heat. Prior research conducted using a comparable experimental configuration and enriched biogas revealed a higher  $\text{NO}_x$  in comparison to an engine running on raw biogas [172,173]. Previous research

found that the  $\text{NO}_x$  of an engine running on enriched biogas with a flow rate of 1 kg/h is 48% lower than that of an engine running on diesel fuel [140].

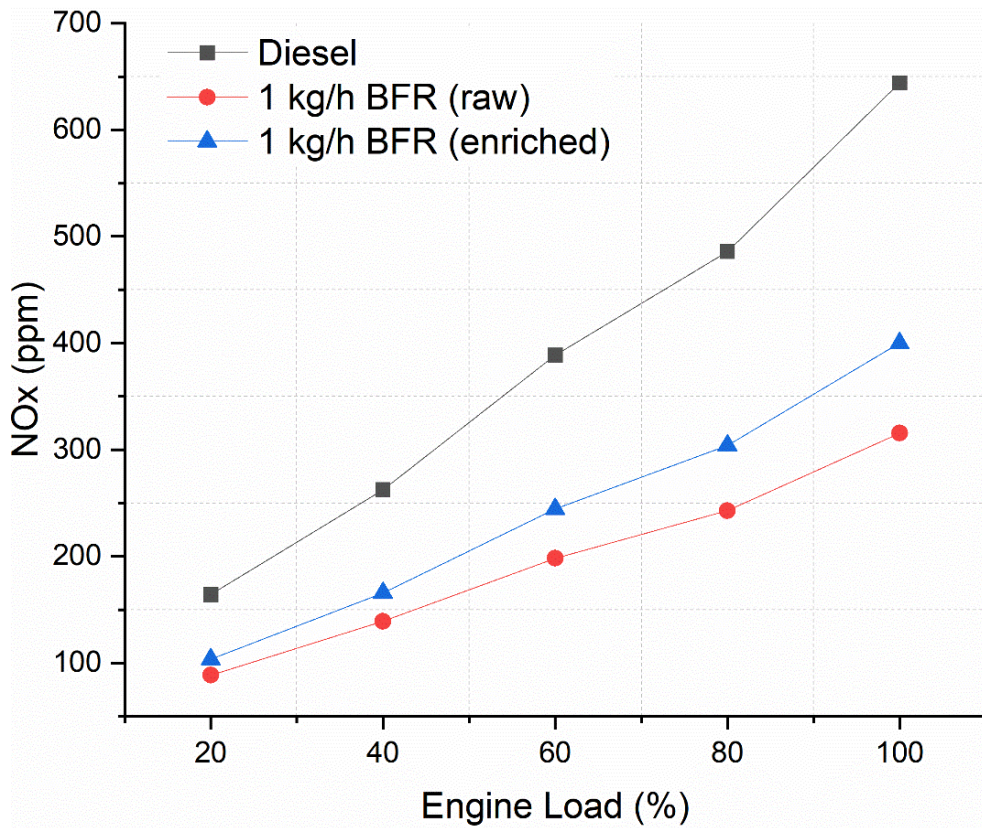


**Fig. 5. 50** Effect of enriched biogas on  $\text{NO}_x$

Fig. 5.51 depicts the effect of enriched biogas on HC. A decrease in HC was observed for increment in Load, with minimum HC observed for the highest Load (100%). Low engine cylinder temperature causes improper combustion at low load, increasing HC. At greater loads, homogeneous fuel-air mixing reduces HC emissions. At peak load conditions, an increase in HC of 44.24% and 35.07% was observed for raw biogas and enriched biogas, respectively. Compared to engine operated on raw biogas, HC observed a decrease of 6.35%. Incomplete combustion occurs when fuel is not burned completely, resulting in the release of HC emissions. Methane is less likely to undergo incomplete combustion than other biogas components due to its high reactivity and low ignition temperature. Prior research conducted using a comparable experimental configuration with enhanced biogas indicated a decrease in HC in comparison to an engine running on untreated biogas [172,173]. Previous research found that at peak load conditions, HC of an engine running on enriched biogas with a fuel flow rate (BFR) of 1 kg/h is 50% higher compared to an engine running on diesel fuel [140].

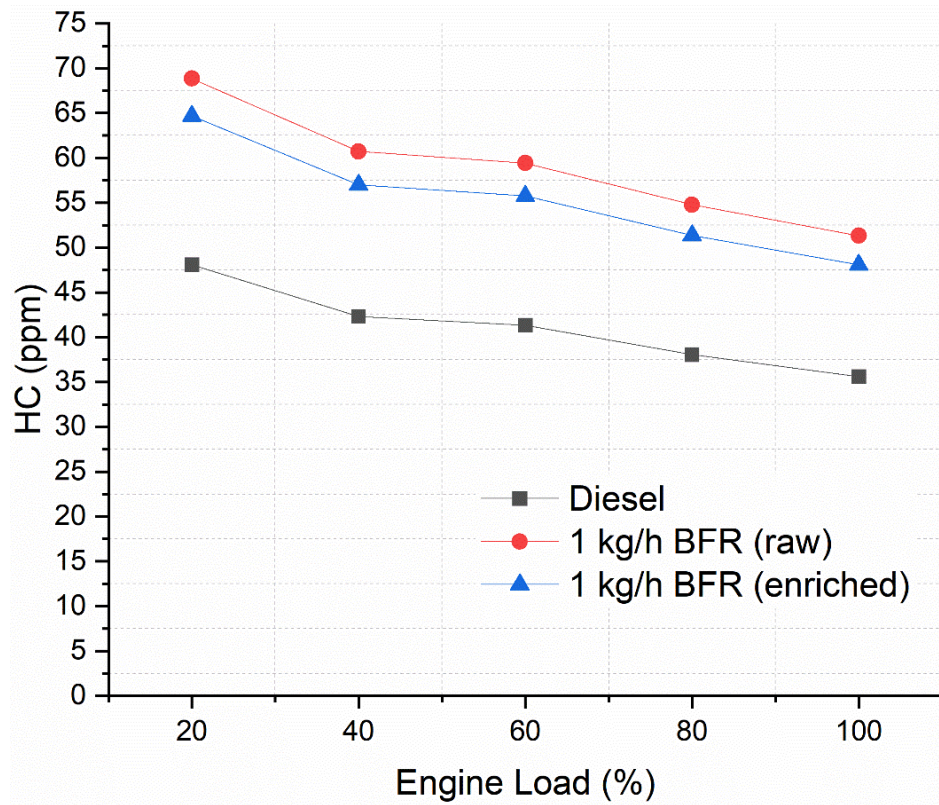


Fig. 5. 51 Effect of enriched biogas on HC

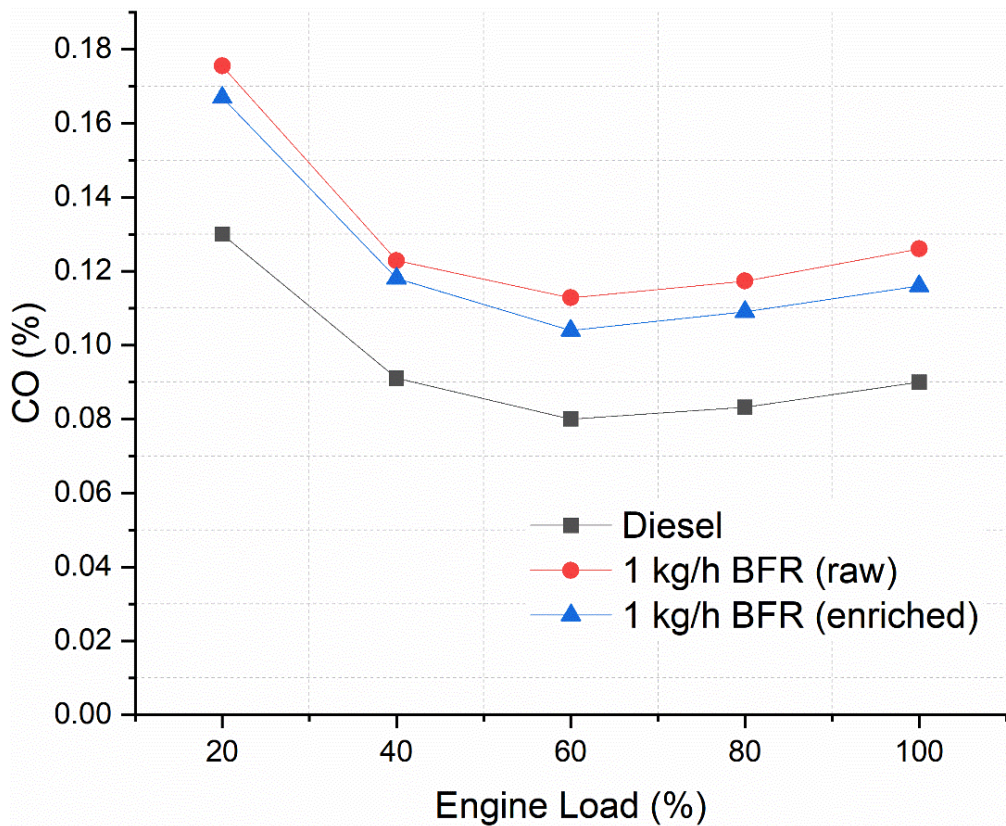
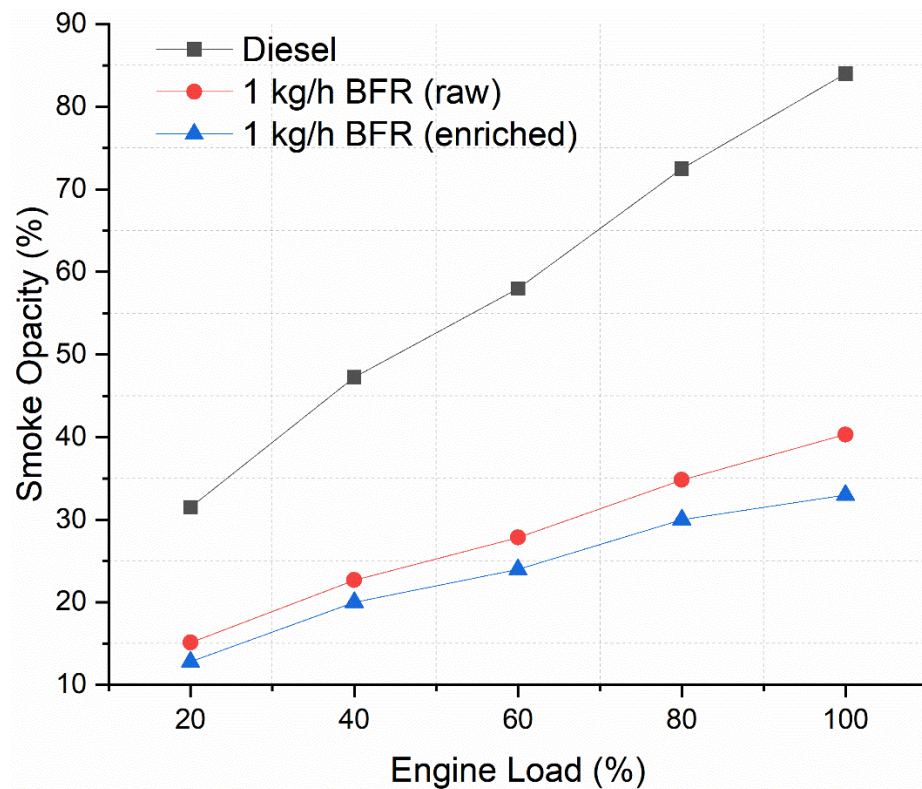


Fig. 5. 52 Effect of enriched biogas on CO



Fig. 5.52 depicts the effect of enriched biogas on CO. A decrease in CO was observed for up to 60% load and thereafter increases. The air-fuel combination becomes more stoichiometric at low to medium loading, reducing CO emissions. With additional fuel in the combustion chamber, CO emissions rise. An increase in CO of 40% and 28.89% was observed for raw biogas and enriched biogas, respectively. Whereas in comparison to engine operated on raw biogas, CO observed a decrease of 7.94%. Incomplete combustion occurs when fuel is not burned completely, resulting in the release of CO emissions. The diluting effect of CO<sub>2</sub> in raw biogas with greater CO<sub>2</sub> concentration leads to incomplete combustion and increased CO emissions. CO formation and oxidation depend on the mixture temperature. Lower cycle temperatures in raw biogas fuel operation increase CO emissions. Prior research conducted using a comparable experimental configuration with enhanced biogas indicated a decrease in CO in comparison to an engine running on untreated biogas [172,173]. Previous research found that the CO of an engine running on enriched biogas with a fuel flow rate (BFR) of 1 kg/h is 40% higher compared to an engine running on diesel fuel [140].



**Fig. 5.53** Effect of enriched biogas on Smoke Opacity

Fig. 5.53 depicts the effect of enriched biogas on Smoke Opacity. A rise in Smoke Opacity was observed for increments in Load, with maximum Smoke Opacity observed for the highest Load (100%) owing to the increase in fuel consumption and cylinder temperature. A decrease in Smoke Opacity of 52% and 60.71% was observed for raw biogas and enriched

biogas respectively. Whereas in comparison to engine operated on raw biogas, Smoke Opacity observed a decrease of 18.16% for enriched gas operation. CI engines with enriched biogas due to better air-fuel mixing and combustion lead to enhanced soot particle oxidation results. Prior research conducted using a comparable experimental configuration and enriched biogas revealed a lower SO in comparison to an engine running on raw biogas [172,173]. Previous research found that the SO of an engine running on enriched biogas with a flow rate of 1 kg/h is 54% lower than that of an engine running on diesel fuel [140].

Fig. 5.54 depicts the effect of enriched biogas on BGES. A decrease in BGES was observed for increment in Load, with minimum BGES observed for the highest Load (100%) due to the engine's increased heat load under full load circumstances. BGES of 42.25% and 58% were observed for raw biogas and enriched biogas respectively. Compared to the engine operated on raw biogas, BGES observed an increase of 36.6%. A greater methane concentration in biogas may substantially enhance its energy contribution by offering a higher energy density and increased combustion efficiency. Prior research conducted using a comparable experimental configuration and enriched biogas revealed a higher BGES in comparison to an engine running on raw biogas. Previous research found that the BGES of an engine running on enriched biogas is 45% [140] and 72.3% [173] compared to an engine running on diesel.

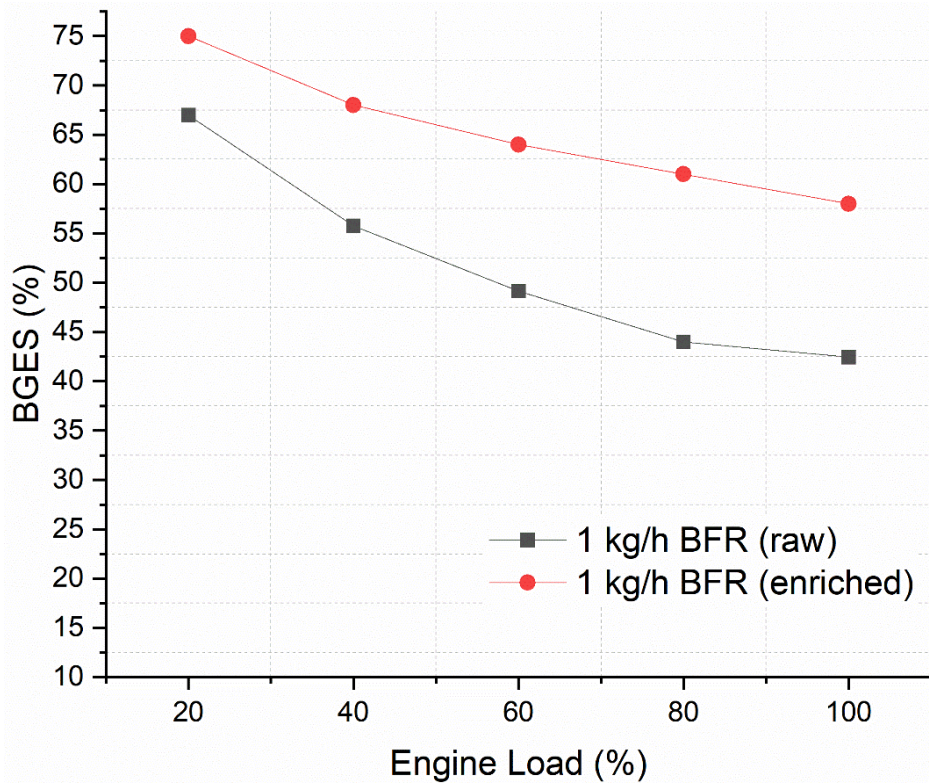


**Fig. 5. 54** Effect of enriched biogas on BGES

## 5.4 Summary

This chapter presents the effect of BFR, NDR, and BBR on engine performances. The optimization of engine performance and emission is also included. Further, the effect of enriched gas on the CI engine is also investigated. The key findings summarizing the chapter are:

1. When compared to neat diesel, the engine run on BFR of 0.5 kg/h, 0.75 kg/h, and 1 kg/h, respectively, exhibits a decrease in BTE by 22%, 28.67%, and 38.11%, NO<sub>x</sub> by 32%, 39%, and 51%, and SO by 35%, 46%, and 52%. At full load conditions, BGES for 0.5 kg/h, 0.75 kg, and 1 kg/h were observed at 26.06%, 34.96%, and 42.46%, respectively.
2. Compared to neat diesel, the engine run on BBR 10 and BBR 20, respectively, shows a decrease in BTE by 9% and 16%, HC by 8% and 11%, CO by 5.5% and 11.1%, and SO by 3% and 8%. Meanwhile, compared to neat diesel, the engine run on BBR 10 and BBR 20 exhibits an increase in NO<sub>x</sub> by 9.2% and 17% and BSEC by 10% and 15%, respectively.
3. BBR20, with the addition of nanoparticles, outperforms the BBR 20 blend on multiple fronts. BTE increases by 7% and 12% for NDR50 and NDR100 blends, respectively. BSEC, NO<sub>x</sub>, HC, and CO emissions all decrease compared to BBR 20: BSEC by 6% and 10%, NO<sub>x</sub> by 8% and 14%, HC by 9% and 17%, and CO by 8% and 14%. Even SO shows a modest reduction, dropping by 5% and 13% with NDR50 and NDR100 blends. These findings suggest significant performance improvements with the addition of Nanoparticles to the BBR 20 blend.
4. The F-value of engine outputs from the RSM model suggests that among the input variables, Engine load is the most substantial influence in deciding the value of output responses, followed by BFR, NDR, and BBR, respectively.
5. The evaluation metrics suggest low prediction error and high model performance for both regression analysis RSM and ANN. Higher R<sup>2</sup>, lower RMSE, and lower MAD were observed mainly for RSM model prediction, indicating RSM to be more accurate and reliable.

6. RSM optimization predicted an optimal value of engine output responses at 67.45% engine load, 96.06 ppm NDR, 10.7 % BBR and 0.85 kg/h BFR. The optimization on the ANN-GA model indicated an optimum engine output response at 67.01% engine load, 98.39 ppm NDR, 8.41% BBR, and 0.846 kg/h BFR. Considering the optimized results from both the RSM and ANN models, a conclusion can be drawn that combining nanoparticles
7. In comparison to engine operated on raw biogas, BTE, and BGES observed an increase of 29.26% and 36.6% respectively for enriched biogas. However, in contrast to engine operated on raw biogas, HC, CO, and Smoke Opacity observed a decrease of 6.35%, 7.94%, and 18.16% respectively for enriched gas operation.

## CHAPTER 6 : CONCLUSIONS AND FUTURE SCOPE

---

### 6.1 Conclusions

The following outcomes emerged as significant insights from the conducted research:

#### **For Biogas Production:**

- Highest Cumulative Biogas Production (CBP) and  $\text{CH}_4/\text{CO}_2$  were observed for Kitchen waste as feedstock for biogas production, followed by Vegetable waste and Fruit waste. At 40°C digester temperature, anaerobic digestion of Kitchen waste exhibits 9.67% and 18.63% higher CBP compared to Vegetable and Fruit waste, respectively. As for the average  $\text{CH}_4/\text{CO}_2$  for the recorded 13 days, the highest was observed for Kitchen waste with 1.07, followed by 0.87 for Vegetable waste and 0.73 for Fruit waste.
- Regardless of the types of feedstocks, the CBP and  $\text{CH}_4/\text{CO}_2$  observed highest for digester at 50°C, followed by 60°C and 40°C. For Kitchen waste, an increase in CBP of 19.47% and 11.68% was observed for the digester at 50°C and 60°C, compared to the digester at 40°C. As for the average  $\text{CH}_4/\text{CO}_2$ , a 62% and 45% increase was observed for the kitchen waste with a digester at 50°C and 60°C, compared to kitchen waste with a digester at 40°C.
- Regardless of the types of feedstocks, the highest CBP and  $\text{CH}_4/\text{CO}_2$  are observed for the digester with a mixing duration of 15 minutes, followed by the digester with 30 minutes and the digester with no mixing, respectively. For Kitchen waste at a digestion temperature of 40°C, an increase in CBP of 24% and 14% was observed for the digester at a mixing duration of 15 minutes and 30 minutes, compared to the digester with no mixing. As for the average  $\text{CH}_4/\text{CO}_2$ , an increase of 33.9% and 18.6% was observed for the kitchen waste with digester mixing duration of 15 minutes and 30 minutes, respectively, in comparison to kitchen waste digester with no mixing.

#### **For RSM Modelling and Optimization of CBP and $\text{CH}_4/\text{CO}_2$**

- The F-value of Biogas response output from the RSM model suggests that among the input variables, Temperature is the most substantial influence in deciding the value of  $\text{CH}_4/\text{CO}_2$ , while Mixing Duration is the most substantial influencing parameter in determining the value of CBP.

- The majority of the RSM model's CBP and CH<sub>4</sub>/CO<sub>2</sub> predictions exhibited high R<sup>2</sup> values, low RMSE values, and low MAD values. The RSM model's low error rates demonstrate its reliability as a regression analysis for the examined input variables on Biogas Production.
- The RSM model observed an optimum value of CBP- 61.05 L, CH<sub>4</sub>/CO<sub>2</sub> -2.16 at the temperature of 54.44 °C, mixing duration of 14.51 min, and feedstock mixture of 86% kitchen and 14% vegetable waste.
- The optimization findings confirm the positive effect of tumbling for both biogas production rate and methane production.

**For effects of BFR, BBR, and NDR on Engine Performance and Emission:**

- As compared to the engine run on neat diesel, NO<sub>x</sub> and Smoke exhibit a decrease of 51% and 52%, respectively, for the engine run on BFR 1 kg/h.
- At full load conditions, Biogas Energy share (BGES) for 0.5 kg/h, 0.75 kg, and 1 kg/h is observed at 26.06%, 34.96%, and 42.46%, respectively.
- As compared to the engine run on neat diesel, HC, CO, and Smoke Opacity exhibit a decrease of 11%, 11.1%, and 8%, respectively, for the engine run on BBR 20 blend.
- As compared to the engine run on the BBR 20 blend, BTE exhibits an increase of 12% for the engine run on the BBR20-NDR100 blend. Whereas, compared to the engine run on the BBR 20 blend, HC, CO, and Smoke Opacity decreased 17%, 14%, and 13%, respectively, for the engine run on the BBR20+NDR100 blend.

**For RSM and ANN Modelling, and Optimization of Engine Performance and Emissions**

- The F-value of engine outputs from the RSM model suggests that among the input variables, Engine load is the most substantial influence in deciding the value of output responses, followed by BFR, NDR, and BBR, respectively.
- The evaluation metrics suggest low prediction error and high model performance for both regression analysis RSM and ANN. Higher R<sup>2</sup>, lower RMSE, and lower MAD were observed mainly for RSM model prediction, indicating RSM to be more accurate and reliable.
- RSM optimization predicted an optimal value of engine output responses at 67.45% engine load, 96.06 ppm NDR, 10.7 % BBR and 0.85 kg/h BFR.

- The optimization on the ANN-GA model indicated an optimum engine output response at 67.01% engine load, 98.39 ppm NDR, 8.41% BBR, and 0.846 kg/h BFR.
- Considering the optimized results from the RSM and ANN model, a conclusion can be drawn that combining nanoparticles, biodiesel, and biogas benefits CI engine performance and emissions.

#### **For Enriched Biogas:**

- The use of Enriched Biogas with a CH<sub>4</sub> content of 90.1 % in a CI engine leads to improved engine performance and reduced emissions, except for NO<sub>x</sub>.
- In comparison to engine operated on raw biogas, BTE, and BGES observed an increase of 29.26% and 36.6% respectively for enriched biogas.
- In comparison to engine operated on raw biogas, HC, CO, and Smoke Opacity observed a decrease of 6.35%, 7.94%, and 18.16% respectively for enriched gas operation.

#### **6.2 Key points for Future scope**

- The vast amount of floral and leaf waste generated globally presents a significant environmental challenge and a missed opportunity for renewable energy production. Researching the potential of these wastes for biogas production holds much promise.
- Blending biogas with other gaseous fuels (Producer gas, Syngas, Hydrogen, CNG, LPG) presents a promising avenue for optimizing engine performance, reducing emissions, and expanding the use of renewable energy sources
- Potential avenues for further investigation involve refining engine parameters, including but not limited to compression ratio, fuel injection timing, and EGR.
- Study of different alcohols and optimize the addition in CI engines.
- Investigation of the use of compressed biogas in SI engines using various alcohols (methanol, ethanol, butanol, methyl acetate) and mixes, including nanoparticles.
- Investigation into the combustion properties of fuel blends used in this study may result in novel combustion models and enhanced comprehension of the combustion mechanisms in compression ignition engines.

## REFERENCES

- 
- [1] A. Taqizadeh, O. Jahanian, S.I.P. Kani, Effects of equivalence and fuel ratios on combustion characteristics of an RCCI engine fueled with methane/n-heptane blend, *J Therm Anal Calorim* 139 (2020) 2541–2551. <https://doi.org/10.1007/s10973-019-08669-9>.
- [2] M. M. Rahman, M. K. Mohamme, R. A. Bakar, Air Fuel Ratio on Engine Performance and Instantaneous Behavior of Crank Angle for Four Cylinder Direct Injection Hydrogen Fueled Engine, *Journal of Applied Sciences* 9 (2009) 2877–2886. <https://doi.org/10.3923/jas.2009.2877.2886>.
- [3] BP, Statistical Review of World Energy, 71st edition (2022). <https://www.bp.com/content/dam/bp/business-sites/en/global/corporate/pdfs/energy-economics/statistical-review/bp-stats-review-2022-full-report.pdf> (accessed June 6, 2023).
- [4] R.M. Andrew, A comparison of estimates of global carbon dioxide emissions from fossil carbon sources, *Earth Syst Sci Data* 12 (2020) 1437–1465. <https://doi.org/10.5194/essd-12-1437-2020>.
- [5] IARI, Crop residues management with conservation agriculture: Potential, constraints and policy needs., Indian Agricultural Research Institute, New Delhi (2012). [https://www.iari.res.in/files/Publication/important-publications/Important\\_Publications-2012-13.pdf](https://www.iari.res.in/files/Publication/important-publications/Important_Publications-2012-13.pdf) (accessed January 18, 2023).
- [6] Department of Animal Husbandry and Dairying, 20th Livestock Census - 2019, Ministry of Fisheries, Animal Husbandry and Dairying, New Delhi (2019). <https://ruralindiaonline.org/en/library/resource/20th-livestock-census-2019-all-india-report/> (accessed May 6, 2023).
- [7] O.P. Chawla, Advances in Biogas Technology, Publications and Information Division, Indian Council of Agricultural Research, 1986. <https://books.google.co.in/books?id=gSIBAAAAYAAJ> (accessed August 21, 2022).
- [8] CPCB, Annual Report (2017–18) on Status of implementation of MSW rules. Central Pollution Control Board, India., (2018). [https://www.cpcb.nic.in/uploads/MSW/MSW\\_AnnualReport\\_2017-18.pdf](https://www.cpcb.nic.in/uploads/MSW/MSW_AnnualReport_2017-18.pdf) (accessed June 6, 2023).
- [9] Ministry of Urban Development, Municipal Solid Waste Management Manual, New Delhi, 2016. <http://swachhbharaturban.gov.in/writereaddata/Manual.pdf> (accessed November 21, 2023).
- [10] S. Cointreau, Occupational and Environmental Health Issues of Solid Waste Management Special Emphasis on Middle and Lower-Income Countries, Washington, D.C. : World Bank Group. 1 (2006). <http://documents.worldbank.org/curated/en/679351468143072645/Occupational-and-environmental-health-issues-of-solid-waste-management-special-emphasis-on-middle-and-lower-income-countries> (accessed January 22, 2023).
- [11] N. Konnoth, Your Clean City at Whose Cost: A Study on the Working Conditions and Occupation Hazards at the Dumping Sites of Bombay, *The Forum for Environmental Concern* (1996) 1–56.



<https://documents1.worldbank.org/curated/zh/679351468143072645/pdf/337790REVISED0up1201PUBLIC1.pdf> (accessed September 8, 2023).

- [12] S. Lee, J. Kim, W.O. Chong, The Causes of the Municipal Solid Waste and the Greenhouse Gas Emissions from the Waste Sector in the United States, *Procedia Eng* 145 (2016) 1074–1079. <https://doi.org/10.1016/j.proeng.2016.04.139>.
- [13] IPCC (Inter Governmental Panel on Climate Change), Guidelines for National Greenhouse Gas Inventories, National Greenhouse Gas Inventories Programme, Japan, 2006. <https://www.ipcc-nggip.iges.or.jp/public/2006gl/index.html> (accessed November 21, 2023).
- [14] IPCC (Inter Governmental Panel on Climate Change), Climate Change 2007: The Physical Science Basis. Contribution of Working Group I to the Fourth Assessment Report of the Intergovernmental Panel on Climate Change, Cambridge University Press, Cambridge, United Kingdom, 2007. [https://www.ipcc.ch/site/assets/uploads/2018/05/ar4\\_wg1\\_full\\_report-1.pdf](https://www.ipcc.ch/site/assets/uploads/2018/05/ar4_wg1_full_report-1.pdf) (accessed November 21, 2023).
- [15] B. Amon, Th. Amon, J. Boxberger, Ch. Alt, Emissions of NH<sub>3</sub>, N<sub>2</sub>O and CH<sub>4</sub> from dairy cows housed in a farmyard manure tying stall (housing, manure storage, manure spreading), *Nutr Cycl Agroecosyst* 60 (2001) 103–113. <https://doi.org/10.1023/A:1012649028772>.
- [16] A. Barragán-Escandón, J.M. Olmedo Ruiz, J.D. Curillo Tigre, E.F. Zalamea-León, Assessment of Power Generation Using Biogas from Landfills in an Equatorial Tropical Context, *Sustainability* 12 (2020) 2669. <https://doi.org/10.3390/su12072669>.
- [17] J.A. Usmani, G.N. Tiwari, A. Chandra, Performance characteristic of a greenhouse integrated biogas system, *Energy Convers Manag* 37 (1996) 1423–1433. [https://doi.org/10.1016/0196-8904\(95\)00228-6](https://doi.org/10.1016/0196-8904(95)00228-6).
- [18] W. Parawira, Biogas technology in sub-Saharan Africa: status, prospects and constraints, *Rev Environ Sci Biotechnol* 8 (2009) 187–200. <https://doi.org/10.1007/s11157-009-9148-0>.
- [19] Ørtenblad H., Anaerobic digestion : making energy and solving modern waste problems, Herning : Herning municipal authorities, 2000. <http://lib.ugent.be/catalog/rug01:000719108> (accessed November 28, 2022).
- [20] J.M. Balsam, D. Ryan, Anaerobic Digestion of Animal Wastes: Factors to Consider, in: A Publication of ATTRA-National Sustainable Agriculture Information Service, 2006. <https://api.semanticscholar.org/CorpusID:131358220> (accessed December 25, 2022).
- [21] J. Zheng, J. Ma, Z.J. Feng, C.Y. Zhu, J. Wang, Y. Wang, Effects of biogas slurry irrigation on tomato (*solanum lycopersicum* l.) Physiological and ecological indexes, yield and quality as well as soil environment, *Appl Ecol Environ Res* 18 (2020) 1013–1029. <https://api.semanticscholar.org/CorpusID:226556512> (accessed November 30, 2022).
- [22] V. Ganesan, Internal Combustion Engines, Mc-Graw-Hill (1996). [https://doi.org/https://books.google.co.in/books/about/Internal\\_Combustion\\_Engines.html?id=gVI3twEACAAJ&redir\\_esc=y](https://doi.org/https://books.google.co.in/books/about/Internal_Combustion_Engines.html?id=gVI3twEACAAJ&redir_esc=y).
- [23] K. von Mitzlaff, Engines for biogas : theory, modification, economic operation, John Wiley & Sons, 1988. <https://api.semanticscholar.org/CorpusID:108093712> (accessed January 11, 2022).

- [24] B.B. Sahoo, Clean Development Mechanism Potential of Compression Ignition Diesel Engines Using Gaseous Fuels in Dual Fuel Mode, PhD Thesis, IIT Guwahati, 2011. <http://hdl.handle.net/10603/484773> (accessed January 17, 2022).
- [25] W. Parawira, M. Murto, J.S. Read, B. Mattiasson, Profile of hydrolases and biogas production during two-stage mesophilic anaerobic digestion of solid potato waste, *Process Biochemistry* 40 (2005) 2945–2952. <https://doi.org/10.1016/j.procbio.2005.01.010>.
- [26] K. Boe, Online monitoring and control of the biogas process, in: Kgs. Lyngby: DTU Environment, 2006. [https://web.archive.org/web/20181104002601/http://orbit.dtu.dk/ws/files/127333186/MR2006\\_055.pdf](https://web.archive.org/web/20181104002601/http://orbit.dtu.dk/ws/files/127333186/MR2006_055.pdf) (accessed September 18, 2023).
- [27] J.A. Eastman, J.F. Ferguson, Solubilization of Particulate Organic Carbon during the Acid Phase of Anaerobic Digestion, *J Water Pollut Control Fed* 53 (1981) 352–366. <http://www.jstor.org/stable/25041085> (accessed June 25, 2022).
- [28] N. Sawyerr, C. Trois, T. Seyoum Workneh, V. Okudoh, An Overview of Biogas Production: Fundamentals, Applications and Future Research, *International Journal of Energy Economics and Policy* 9 (2019) 105–115. <https://doi.org/10.32479/ijee.7375>.
- [29] S. Kalyuzhnyi, A. Veecken, B. Hamelers, Two-particle model of anaerobic solid state fermentation, *Water Science and Technology* 41 (2000) 43–50. <https://doi.org/10.2166/wst.2000.0054>.
- [30] I. Angelidaki, L. Ellegaard, B.K. Ahring, Applications of the Anaerobic Digestion Process, in: *Biomethanation II. Advances in Biochemical Engineering, Biotechnology*, 2003: p. 33. [https://doi.org/10.1007/3-540-45838-7\\_1](https://doi.org/10.1007/3-540-45838-7_1).
- [31] S. Dauber, B. Böhnke, W. Bischofsberger, C.F. Seyfried, *Anaerobtechnik: Handbuch der anaeroben Behandlung von Abwasser und Schlamm*, Springer-Verlag, 2013. <https://books.google.com.na/books?id=jDHQBgAAQBAJ&printsec=copyright#v=onepage&q&f=false> (accessed November 18, 2023).
- [32] B. Schink, Energetics of syntrophic cooperation in methanogenic degradation, *Microbiology and Molecular Biology Reviews* 61 (1997) 262–280. <https://doi.org/10.1128/mmbr.61.2.262-280.1997>.
- [33] C. Wolf, Simulation, optimization and instrumentation of agricultural biogas plants, PhD Thesis, National University of Ireland , 2013. <https://mural.maynoothuniversity.ie/4604/> (accessed November 21, 2023).
- [34] R.K. Dhaked, P. Singh, L. Singh, Biomethanation under psychrophilic conditions, *Waste Management* 30 (2010) 2490–2496. <https://doi.org/10.1016/j.wasman.2010.07.015>.
- [35] Å. Davidsson, Increase of Biogas Production at Wastewater Treatment Plants Addition of urban organic waste and pre-treatment of sludge, Lund University, 2007. <https://portal.research.lu.se/en/publications/increase-of-biogas-production-at-wastewater-treatment-plants-addi> (accessed February 17, 2023).
- [36] S. Banerjee, N. Prasad, S. Selvaraju, Reactor Design for Biogas Production-A Short Review, *Journal of Energy and Power Technology* 04 (2022) 004. <https://doi.org/10.21926/jept.2201004>.

- [37] U. Misra, S. Singh, A. Singh, G.N. Pandey, A new temperature controlled digester for anaerobic digestion for biogas production, *Energy Convers Manag* 33 (1992) 983–986. [https://doi.org/10.1016/0196-8904\(92\)90132-G](https://doi.org/10.1016/0196-8904(92)90132-G).
- [38] T. Schmidt, A.M. Ziganshin, M. Nikolausz, F. Scholwin, M. Nelles, S. Kleinsteuber, J. Pröter, Effects of the reduction of the hydraulic retention time to 1.5 days at constant organic loading in CSTR, ASBR, and fixed-bed reactors – Performance and methanogenic community composition, *Biomass Bioenergy* 69 (2014) 241–248. <https://doi.org/10.1016/j.biombioe.2014.07.021>.
- [39] H. El-Mashad, R. Zhang, Biogas Energy from Organic Wastes, in: *The Introduction to Biosystems Engineering Textbook*; ASABE: St. Joseph, MI, USA, 2020. <https://doi.org/10.21061/IntroBiosystemsEngineering/Biogas>.
- [40] C. Liu, X. Yuan, G. Zeng, W. Li, J. Li, Prediction of methane yield at optimum pH for anaerobic digestion of organic fraction of municipal solid waste, *Bioresour Technol* 99 (2008) 882–888. <https://doi.org/10.1016/j.biortech.2007.01.013>.
- [41] C. Cavinato, M. Gottardo, F. Micolucci, D. Bolzonella, P. Pavan, Ammonia concentration and pH control in pilot scale two-phase anaerobic digestion of food waste for hydrogen production: focus on start-up, *Chem Eng Trans* 49 (2016) 151–156. <https://doi.org/http://dx.doi.org/10.3303/CET1649026>.
- [42] K. Stamatelatos, G. Lyberatos, C. Tsiligianis, S. Pavlou, P. Pullammanappallil, S.A. Svoronos, Optimal and suboptimal control of anaerobic digesters, *Environmental Modeling & Assessment* 2 (1997) 355–363. <https://doi.org/10.1023/A:1019034032664>.
- [43] M. Tabatabaei, H. Ghanavati, *Biogas: fundamentals, process, and operation*, Springer, 2018. <https://lib.ugent.be/catalog/ebk01:4100000003359523> (accessed January 17, 2023).
- [44] L. Dong, G. Cao, Y. Tian, J. Wu, C. Zhou, B. Liu, L. Zhao, J. Fan, N. Ren, Improvement of biogas production in plug flow reactor using biogas slurry pretreated cornstalk, *Bioresour Technol Rep* 9 (2020) 100378. <https://doi.org/10.1016/j.biteb.2019.100378>.
- [45] D.J. Batstone, J. Keller, I. Angelidaki, S.V. Kalyuzhnyi, S.G. Pavlostathis, A. Rozzi, W.T.M. Sanders, H. Siegrist, V.A. Vavilin, The IWA Anaerobic Digestion Model No 1 (ADM1), *Water Science and Technology* 45 (2002) 65–73. <https://doi.org/10.2166/wst.2002.0292>.
- [46] M. Lebuhn, F. Liu, H. Heuwinkel, A. Gronauer, Biogas production from mono-digestion of maize silage—long-term process stability and requirements, *Water Science and Technology* 58 (2008) 1645–1651. <https://doi.org/10.2166/wst.2008.495>.
- [47] P. Weiland, Biogas production: current state and perspectives, *Appl Microbiol Biotechnol* 85 (2010) 849–860. <https://doi.org/doi:10.1007/s00253-009-2246-7>.
- [48] N.F. Gray, *Biology of wastewater treatment*, in: *Series on Environmental Science and Management*, World Scientific, 2004. [https://www.worldscientific.com/doi/pdf/10.1142/9781860945243\\_fmatter](https://www.worldscientific.com/doi/pdf/10.1142/9781860945243_fmatter) (accessed December 7, 2022).
- [49] D. Mara, N.J. Horan, *Handbook of water and wastewater microbiology*, Academic Press, London, 2003. <https://doi.org/https://doi.org/10.1016/B978-0-12-470100-7.50047-9>.

- [50] L. Björnsson, M. Murto, T.G. Jantsch, B. Mattiasson, Evaluation of new methods for the monitoring of alkalinity, dissolved hydrogen and the microbial community in anaerobic digestion, *Water Res* 35 (2001) 2833–2840. [https://doi.org/10.1016/S0043-1354\(00\)00585-6](https://doi.org/10.1016/S0043-1354(00)00585-6).
- [51] L. Megido, L. Negral, Y. Fernández-Nava, B. Suárez-Peña, P. Ormaechea, P. Díaz-Caneja, L. Castrillón, E. Marañón, Impact of organic loading rate and reactor design on thermophilic anaerobic digestion of mixed supermarket waste, *Waste Management* 123 (2021) 52–59. <https://doi.org/10.1016/j.wasman.2021.01.012>.
- [52] F. Almomani, Prediction of biogas production from chemically treated co-digested agricultural waste using artificial neural network, *Fuel* 280 (2020) 118573. <https://doi.org/10.1016/j.fuel.2020.118573>.
- [53] Z. Zahan, M.Z. Othman, W. Rajendram, Anaerobic Codigestion of Municipal Wastewater Treatment Plant Sludge with Food Waste: A Case Study, *Biomed Res Int* 2016 (2016) 8462928. <https://doi.org/10.1155/2016/8462928>.
- [54] Peris Serrano R, Biogas Process Simulation using Aspen Plus, Syddansk Universitet, 2010. <https://upcommons.upc.edu/handle/2099.1/14429> (accessed December 16, 2022).
- [55] S. Mihic, Biogas fuel for internal combustion engines, *Annals of Faculty Engineering Hunedoara* 2 (2004) 179–190. <https://annals.fih.upt.ro/pdf-full/2004/ANNALS-2004-3-24.pdf> (accessed June 16, 2023).
- [56] D. Huang, H. Zhou, L. Lin, Biodiesel: an Alternative to Conventional Fuel, *Energy Procedia* 16 (2012) 1874–1885. <https://doi.org/10.1016/j.egypro.2012.01.287>.
- [57] D.C. Rakopoulos, C.D. Rakopoulos, E.G. Giakoumis, R.G. Papagiannakis, D.C. Kyritsis, Influence of properties of various common bio-fuels on the combustion and emission characteristics of high-speed DI (direct injection) diesel engine: Vegetable oil, bio-diesel, ethanol, n-butanol, diethyl ether, *Energy* 73 (2014) 354–366. <https://doi.org/10.1016/j.energy.2014.06.032>.
- [58] J. Pullen, K. Saeed, Factors affecting biodiesel engine performance and exhaust emissions – Part I: Review, *Energy* 72 (2014) 1–16. <https://doi.org/10.1016/j.energy.2014.04.015>.
- [59] N. Elahi, M. Kamali, M.H. Baghersad, Recent biomedical applications of gold nanoparticles: A review, *Talanta* 184 (2018) 537–556. <https://doi.org/10.1016/j.talanta.2018.02.088>.
- [60] M.E.M. Soudagar, N.-N. Nik-Ghazali, Md. Abul Kalam, I.A. Badruddin, N.R. Banapurmath, N. Akram, The effect of nano-additives in diesel-biodiesel fuel blends: A comprehensive review on stability, engine performance and emission characteristics, *Energy Convers Manag* 178 (2018) 146–177. <https://doi.org/10.1016/j.enconman.2018.10.019>.
- [61] A. Amrollahi, A.A. Hamidi, A.M. Rashidi, The effects of temperature, volume fraction and vibration time on the thermo-physical properties of a carbon nanotube suspension (carbon nanofluid), *Nanotechnology* 19 (2008) 315701. <https://doi.org/10.1088/0957-4484/19/31/315701>.
- [62] B. Ruan, A.M. Jacobi, Ultrasonication effects on thermal and rheological properties of carbon nanotube suspensions, *Nanoscale Res Lett* 7 (2012) 127. <https://doi.org/10.1186/1556-276X-7-127>.

- [63] M. Hatami, M. Hasanpour, D. Jing, Recent developments of nanoparticles additives to the consumables liquids in internal combustion engines: Part I: Nano-fuels, *J Mol Liq* 318 (2020) 114250. <https://doi.org/10.1016/j.molliq.2020.114250>.
- [64] S.S. Hoseini, G. Najafi, B. Ghobadian, M.T. Ebadi, R. Mamat, T. Yusaf, Performance and emission characteristics of a CI engine using graphene oxide (GO) nano-particles additives in biodiesel-diesel blends, *Renew Energy* 145 (2020) 458–465. <https://doi.org/10.1016/j.renene.2019.06.006>.
- [65] S. Lalhriatpuia, A. Pal, Computational optimization of engine emissions and performance of a CI engine powered with biogas and NiO nanoparticles doped diesel, *Environ Prog Sustain Energy* (2023). <https://doi.org/10.1002/ep.14207>.
- [66] S. Lalhriatpuia, A. Pal, Computational optimization of engine performance and emission responses for dual fuel CI engine powered with biogas and Co<sub>3</sub>O<sub>4</sub> nanoparticles doped biodiesel, *Fuel* 344 (2023) 127892. <https://doi.org/10.1016/j.fuel.2023.127892>.
- [67] S. Achinas, Y. Li, V. Achinas, G.J. Willem Euverink, Influence of sheep manure addition on biogas potential and methanogenic communities during cow dung digestion under mesophilic conditions, *Sustainable Environment Research* 28 (2018) 240–246. <https://doi.org/10.1016/j.serj.2018.03.003>.
- [68] C. J. Banks and A. M. Salter, EU Cropgen: biogas from energy crops and agrowastes, in: *Bioenergy 2007: 3rd International Bioenergy Conference and Exhibition*, Jyväskylä, 2007. <https://eprints.soton.ac.uk/75916/> (accessed June 18, 2023).
- [69] R. Li, S. Chen, X. Li, J. Saifullah Lar, Y. He, B. Zhu, Anaerobic Codigestion of Kitchen Waste with Cattle Manure for Biogas Production, *Energy & Fuels* 23 (2009) 2225–2228. <https://doi.org/10.1021/ef8008772>.
- [70] J. Zhou, R. Zhang, F. Liu, X. Yong, X. Wu, T. Zheng, M. Jiang, H. Jia, Biogas production and microbial community shift through neutral pH control during the anaerobic digestion of pig manure, *Bioresour Technol* 217 (2016) 44–49. <https://doi.org/10.1016/j.biortech.2016.02.077>.
- [71] V.A. Vavilin, I. Angelidaki, Anaerobic degradation of solid material: Importance of initiation centers for methanogenesis, mixing intensity, and 2D distributed model, *Biotechnol Bioeng* 89 (2005) 113–122. <https://doi.org/10.1002/bit.20323>.
- [72] P. Kaparaju, I. Buendia, L. Ellegaard, I. Angelidakia, Effects of mixing on methane production during thermophilic anaerobic digestion of manure: Lab-scale and pilot-scale studies, *Bioresour Technol* 99 (2008) 4919–4928. <https://doi.org/10.1016/j.biortech.2007.09.015>.
- [73] I.S. Ogiehor, U.J. Ovueni, Effect of temperature, pH, and solids concentration on biogas production from poultry waste, *Int J Sci Eng Res* 5 (2014) 62–69. <https://www.ijser.org/researchpaper/effect-of-temperature-ph-and-solids-concentration.pdf> (accessed June 12, 2023).
- [74] P. K. Pandey, M. L. Soupir, Impacts of Temperatures on Biogas Production in Dairy Manure Anaerobic Digestion, *International Journal of Engineering and Technology* 4 (2012) 629–631. <https://doi.org/10.7763/IJET.2012.V4.448>.

- [75] K. Karim, K. Thomasklasson, R. Hoffmann, S. Drescher, D. Depaoli, M. Aldahhan, Anaerobic digestion of animal waste: Effect of mixing, *Bioresour Technol* 96 (2005) 1607–1612. <https://doi.org/10.1016/j.biortech.2004.12.021>.
- [76] M. Wu, K. Sun, Y. Zhang, Influence of temperature fluctuation on thermophilic anaerobic digestion of municipal organic solid waste, *J Zhejiang Univ Sci B* 7 (2006) 180–185. <https://doi.org/10.1631/jzus.2006.B0180>.
- [77] S. Elagroudy, A.G. Radwan, N. Banadda, N.G. Mostafa, P.A. Owusu, I. Janajreh, Mathematical models comparison of biogas production from anaerobic digestion of microwave pretreated mixed sludge, *Renew Energy* 155 (2020) 1009–1020. <https://doi.org/10.1016/j.renene.2020.03.166>.
- [78] E.B. Gueguim Kana, J.K. Oloke, A. Lateef, M.O. Adesiyan, Modeling and optimization of biogas production on saw dust and other co-substrates using Artificial Neural network and Genetic Algorithm, *Renew Energy* 46 (2012) 276–281. <https://doi.org/10.1016/j.renene.2012.03.027>.
- [79] S. Jacob, R. Banerjee, Modeling and optimization of anaerobic codigestion of potato waste and aquatic weed by response surface methodology and artificial neural network coupled genetic algorithm, *Bioresour Technol* 214 (2016) 386–395. <https://doi.org/10.1016/j.biortech.2016.04.068>.
- [80] H. Akbaş, B. Bilgen, A.M. Turhan, An integrated prediction and optimization model of biogas production system at a wastewater treatment facility, *Bioresour Technol* 196 (2015) 566–576. <https://doi.org/10.1016/j.biortech.2015.08.017>.
- [81] B.K. Zaied, M. Rashid, M. Nasrullah, B.S. Bari, A.W. Zularisam, L. Singh, D. Kumar, S. Krishnan, Prediction and optimization of biogas production from POME co-digestion in solar bioreactor using artificial neural network coupled with particle swarm optimization (ANN-PSO), *Biomass Convers Biorefin* 13 (2023) 73–88. <https://doi.org/10.1007/s13399-020-01057-6>.
- [82] L.C. Gopal, M. Govindarajan, M.R. Kavipriya, S. Mahboob, K.A. Al-Ghanim, P. Virik, Z. Ahmed, N. Al-Mulhm, V. Senthilkumaran, V. Shankar, Optimization strategies for improved biogas production by recycling of waste through response surface methodology and artificial neural network: Sustainable energy perspective research, *J King Saud Univ Sci* 33 (2021) 101241. <https://doi.org/10.1016/j.jksus.2020.101241>.
- [83] E.O. Otieno, R. Kiplimo, U. Mutwiwa, Optimization of anaerobic digestion parameters for biogas production from pineapple wastes co-digested with livestock wastes, *Heliyon* 9 (2023) e14041. <https://doi.org/10.1016/j.heliyon.2023.e14041>.
- [84] B. Sajeenabeevi, P. Jose, G. Madhu, Optimization of Process Parameters Affecting Biogas Production from Organic Fraction of Municipal Solid Waste via Anaerobic Digestion, *World Academy of Science, Engineering and Technology, International Journal of Environmental, Chemical, Ecological, Geological and Geophysical Engineering* 8 (2014) 43–48. <https://zenodo.org/record/1336939/files/9997252.pdf?download=1> (accessed August 17, 2023).
- [85] H. Ingabire, M.M. M'arimi, K.H. Kiriamiti, B. Ntambara, Optimization of biogas production from anaerobic co-digestion of fish waste and water hyacinth, *Biotechnology for Biofuels and Bioproducts* 16 (2023) 110. <https://doi.org/10.1186/s13068-023-02360-w>.

- [86] S. S, V. S, Optimization of Different Parameters Affecting Biogas production from Rice Straw: An Analytical Approach, *International Journal of Simulation Systems Science & Technology* (2020). <https://doi.org/10.5013/IJSSST.a.15.02.11>.
- [87] S. Lalhriatpuia, A. Pal, Performance and Emissions Analysis of a Dual Fuel Diesel Engine with Biogas as Primary Fuel, in: *Recent Advances in Mechanical Engineering*, Springer Nature Singapore, Singapore, 2021: pp. 327–339. [https://doi.org/https://doi.org/10.1007/978-981-15-9678-0\\_29](https://doi.org/https://doi.org/10.1007/978-981-15-9678-0_29).
- [88] S.K. Mahla, V. Singla, S.S. Sandhu, A. Dhir, Studies on biogas-fuelled compression ignition engine under dual fuel mode, *Environmental Science and Pollution Research* 25 (2018) 9722–9729. <https://doi.org/10.1007/s11356-018-1247-4>.
- [89] H. Ambarita, Performance and emission characteristics of a small diesel engine run in dual-fuel (diesel-biogas) mode, *Case Studies in Thermal Engineering* 10 (2017) 179–191. <https://doi.org/10.1016/j.csite.2017.06.003>.
- [90] F.Z. Aklouche, K. Loubar, A. Bentebbiche, S. Awad, M. Tazerout, Experimental investigation of the equivalence ratio influence on combustion, performance and exhaust emissions of a dual fuel diesel engine operating on synthetic biogas fuel, *Energy Convers Manag* 152 (2017) 291–299. <https://doi.org/10.1016/j.enconman.2017.09.050>.
- [91] D. Barik, S. Murugan, Investigation on combustion performance and emission characteristics of a DI (direct injection) diesel engine fueled with biogas–diesel in dual fuel mode, *Energy* 72 (2014) 760–771. <https://doi.org/10.1016/j.energy.2014.05.106>.
- [92] K. Senthilkumar, S. Vivekanandan, Investigating the Biogas as Secondary Fuel for CI Engine, *International Journal of Applied Environmental Sciences* 11 (2016) 155–163. [https://www.ripublication.com/ijaes16/ijaesv11n1\\_12.pdf](https://www.ripublication.com/ijaes16/ijaesv11n1_12.pdf) (accessed January 21, 2023).
- [93] Salve, A. Kolekar, K. Jadhav, Experimental Evaluation of Dual Fuel CI Engine Using Synthesized Biogas, *International Engineering Research Journal* 2 (2016) 1223–1229. <https://www.ierjournal.org/pupload/mit/EE1-1.pdf> (accessed September 17, 2023).
- [94] D. Barik, S. Murugan, Experimental investigation on the behavior of a DI diesel engine fueled with raw biogas–diesel dual fuel at different injection timing, *Journal of the Energy Institute* 89 (2016) 373–388. <https://doi.org/10.1016/j.joei.2015.03.002>.
- [95] D. Barik, S. Murugan, N.M. Sivaram, E. Baburaj, P. Shanmuga Sundaram, Experimental investigation on the behavior of a direct injection diesel engine fueled with Karanja methyl ester-biogas dual fuel at different injection timings, *Energy* 118 (2017) 127–138. <https://doi.org/10.1016/j.energy.2016.12.025>.
- [96] G. Venkadesan, N.M. Mohandoss, Combustion, performance and emission analysis of dual fuel engine using tsrb biogas, *Energy Sources, Part A: Recovery, Utilization, and Environmental Effects* 41 (2019) 2171–2183. <https://doi.org/10.1080/15567036.2018.1550538>.
- [97] A. Murugesan, C. Umarani, R. Subramanian, N. Nedunchezian, Bio-diesel as an alternative fuel for diesel engines—A review, *Renewable and Sustainable Energy Reviews* 13 (2009) 653–662. <https://doi.org/10.1016/j.rser.2007.10.007>.
- [98] R.K. Rai, R.R. Sahoo, Engine performance, emission, and sustainability analysis with diesel fuel-based *Shorea robusta* methyl ester biodiesel blends, *Fuel* 292 (2021) 120234. <https://doi.org/10.1016/j.fuel.2021.120234>.

- [99] H.H. Masjuki, M.A. Kalam, M.A. Maleque, A. Kubo, T. Nonaka, Performance, emissions and wear characteristics of an indirect injection diesel engine using coconut oil blended fuel, *Proceedings of the Institution of Mechanical Engineers, Part D: Journal of Automobile Engineering* 215 (2001) 393–404. <https://doi.org/10.1243/0954407011525728>.
- [100] T.K. Gogoi, D.C. Baruah, Performance and energy analyses of a diesel engine fuelled with Koroch seed oil methyl ester and its diesel fuel blends, *International Journal of Energy Technology and Policy* 7 (2011) 433. <https://doi.org/10.1504/IJETP.2011.045235>.
- [101] S.K. Angappamudaliar Palanisamy, S. Rajangam, J. Saminathan, Experimental investigation to identify the effect of nanoparticles based diesel fuel in VCR engine, *Energy Sources, Part A: Recovery, Utilization, and Environmental Effects* (2020) 1–15. <https://doi.org/10.1080/15567036.2020.1778142>.
- [102] P. Sathiamurthi, K.S. Karthi Vinith, A. Sivakumar, Performance and emission test in CI engine using magnetic fuel conditioning with nano additives, *International Journal of Recent Technology and Engineering* 8 (2019) 7823–7826. <https://doi.org/10.35940/ijrte.C6213.098319>.
- [103] J. Sadhik Basha, An Experimental Analysis of a Diesel Engine Using Alumina Nanoparticles Blended Diesel Fuel, in: *SAE Technical Paper*, 2014: pp. 1–12. <https://doi.org/10.4271/2014-01-1391>.
- [104] R.R. Sahoo, A. Jain, Experimental analysis of nanofuel additives with magnetic fuel conditioning for diesel engine performance and emissions, *Fuel* 236 (2019) 365–372. <https://doi.org/10.1016/j.fuel.2018.09.027>.
- [105] A. Yaşar, A. Keskin, Ş. Yıldızhan, E. Uludamar, Emission and vibration analysis of diesel engine fuelled diesel fuel containing metallic based nanoparticles, *Fuel* 239 (2019) 1224–1230. <https://doi.org/10.1016/j.fuel.2018.11.113>.
- [106] K. Fangsuwannarak, K. Triratanasirichai, Effect of metalloids compound and bio-solution additives on biodiesel engine performance and exhaust emissions, *Am J Appl Sci* 10 (2013) 1201–1213. <https://doi.org/10.3844/ajassp.2013.1201.1213>.
- [107] A. Suhel, N. Abdul Rahim, M.R. Abdul Rahman, K.A. Bin Ahmad, Y.H. Teoh, N. Zainal Abidin, An Experimental Investigation on the Effect of Ferrous Ferric Oxide Nano-Additive and Chicken Fat Methyl Ester on Performance and Emission Characteristics of Compression Ignition Engine, *Symmetry (Basel)* 13 (2021) 265. <https://doi.org/10.3390/sym13020265>.
- [108] S.T. Kumaravel, A. Murugesan, C. Vijayakumar, M. Thenmozhi, Enhancing the fuel properties of tyre oil diesel blends by doping nano additives for green environments, *J Clean Prod* 240 (2019) 118128. <https://doi.org/10.1016/j.jclepro.2019.118128>.
- [109] S.K. Mahla, S.M. Safieddin Ardebili, M. Mostafaei, A. Dhir, G. Goga, B.S. Chauhan, Multi-objective optimization of performance and emissions characteristics of a variable compression ratio diesel engine running with biogas-diesel fuel using response surface techniques, *Energy Sources, Part A: Recovery, Utilization, and Environmental Effects* (2020) 1–18. <https://doi.org/10.1080/15567036.2020.1813847>.
- [110] M. Ghanbari, L. Mozafari-Vanani, M. Dehghani-Soufi, A. Jahanbakhshi, Effect of alumina nanoparticles as additive with diesel–biodiesel blends on performance and emission characteristic of a six-cylinder diesel engine using response surface methodology (RSM),



- [111] S. Chandra Sekhar, K. Karuppasamy, N. Vedaraman, A.E. Kabeel, R. Sathyamurthy, M. Elkelawy, H. Alm EIDin Bastawissi, Biodiesel production process optimization from *Pithecellobium dulce* seed oil: Performance, combustion, and emission analysis on compression ignition engine fuelled with diesel/biodiesel blends, *Energy Convers Manag* 161 (2018) 141–154. <https://doi.org/10.1016/j.enconman.2018.01.074>.
- [112] S.H. Hosseini, A. Taghizadeh-Alisaraei, B. Ghobadian, A. Abbaszadeh-Mayvan, Artificial neural network modeling of performance, emission, and vibration of a CI engine using alumina nano-catalyst added to diesel-biodiesel blends, *Renew Energy* 149 (2020) 951–961. <https://doi.org/10.1016/j.renene.2019.10.080>.
- [113] M. Elkelawy, H.A.-E. Bastawissi, K.K. Esmaeil, A.M. Radwan, H. Panchal, K.K. Sadasivuni, M. Suresh, M. Israr, Maximization of biodiesel production from sunflower and soybean oils and prediction of diesel engine performance and emission characteristics through response surface methodology, *Fuel* 266 (2020) 117072. <https://doi.org/10.1016/j.fuel.2020.117072>.
- [114] A. Singh, S. Sinha, A.K. Choudhary, H. Panchal, M. Elkelawy, K.K. Sadasivuni, Optimization of performance and emission characteristics of CI engine fueled with *Jatropha* biodiesel produced using a heterogeneous catalyst (CaO), *Fuel* 280 (2020) 118611. <https://doi.org/10.1016/j.fuel.2020.118611>.
- [115] S.M. Safieddin Ardebili, A. Taghipoor, H. Solmaz, M. Mostafaei, The effect of nano-biochar on the performance and emissions of a diesel engine fueled with fusel oil-diesel fuel, *Fuel* 268 (2020) 117356. <https://doi.org/10.1016/j.fuel.2020.117356>.
- [116] J. Stewart, A. Clarke, R. Chen, An experimental study of the dual-fuel performance of a small compression ignition diesel engine operating with three gaseous fuels, *Proceedings of the Institution of Mechanical Engineers, Part D: Journal of Automobile Engineering* 221 (2007) 943–956. <https://doi.org/10.1243/09544070JAUTO458>.
- [117] K.P. Latha, C. Prema, S.M. Sundar, Synthesis and Characterization of Cobalt Oxide Nanoparticles, *Journal of Nanoscience and Technology* 4 (2018) 475–477. <https://doi.org/10.30799/jnst.144.18040504>.
- [118] J. van Gerpen, B. Shanks, R. Pruszko, D. Clements, G. Knothe, *Biodiesel Analytical Methods: August 2002--January 2004*, Golden, CO (United States), 2004. <https://doi.org/10.2172/15008800>.
- [119] M. Tayyab, S. Ahmad, M.J. Akhtar, P.M. Sathikh, Ranganath.M. Singari, Prediction of mechanical properties for acrylonitrile-butadiene-styrene parts manufactured by fused deposition modelling using artificial neural network and genetic algorithm, *Int J Comput Integr Manuf* (2022) 1–18. <https://doi.org/10.1080/0951192X.2022.2104462>.
- [120] S.J. Ojolo, R.R. Dinrifo, K.B. Adesuyi, Comparative Study of Biogas Production from Five Substrates, *Adv Mat Res* 18–19 (2007) 519–525. <https://doi.org/10.4028/www.scientific.net/AMR.18-19.519>.
- [121] A. Mekonnen Tura, T. Seifu Lemma, Production and Evaluation of Biogas from Mixed Fruits and Vegetable Wastes Collected from Arba Minch Market, *American Journal of Applied Chemistry* 7 (2019) 185. <https://doi.org/10.11648/j.ajac.20190706.16>.

- [122] S. Sandhu, R. Kaushal, Anaerobic Digestion of Vegetable, Fruit and Cafeteria Wastes with Cow Dung by Chemical Pretreatment for Biogas Production in Batch Digester, *J Phys Conf Ser* 1240 (2019) 012132. <https://doi.org/10.1088/1742-6596/1240/1/012132>.
- [123] B. Deepanraj, V. Sivasubramanian, S. Jayaraj, Kinetic study on the effect of temperature on biogas production using a lab scale batch reactor, *Ecotoxicol Environ Saf* 121 (2015) 100–104. <https://doi.org/10.1016/j.ecoenv.2015.04.051>.
- [124] G. Paramaguru, M. Kannan, N. Senthilkumar, P. Lawrence, Effect of temperature on biogas production from food waste through anaerobic digestion, *Desalination Water Treat* 85 (2017) 68–72. <https://doi.org/10.5004/dwt.2017.21189>.
- [125] G.A.W. Sudiarta, T. Imai, C. Mamimin, A. Reungsang, Effects of Temperature Shifts on Microbial Communities and Biogas Production: An In-Depth Comparison, *Fermentation* 9 (2023) 642. <https://doi.org/10.3390/fermentation9070642>.
- [126] E. Membere, P. Sallis, Effect of temperature on kinetics of biogas production from macroalgae, *Bioresour Technol* 263 (2018) 410–417. <https://doi.org/10.1016/j.biortech.2018.05.023>.
- [127] J.C. Gaby, M. Zamanzadeh, S.J. Horn, The effect of temperature and retention time on methane production and microbial community composition in staged anaerobic digesters fed with food waste, *Biotechnol Biofuels* 10 (2017) 302. <https://doi.org/10.1186/s13068-017-0989-4>.
- [128] B. Singh, Z. Szamosi, Z. Siménfalvi, State of the art on mixing in an anaerobic digester: A review, *Renew Energy* 141 (2019) 922–936. <https://doi.org/10.1016/j.renene.2019.04.072>.
- [129] B. Schink, Anaerobic degradation of aromatic compounds., *Microbial Degradation of Natural Products* (1990) 219–242. <https://cir.nii.ac.jp/crid/1571980074480102656> (accessed February 22, 2023).
- [130] P. Stroot, Anaerobic codigestion of municipal solid waste and biosolids under various mixing conditions—I. digester performance, *Water Res* 35 (2001) 1804–1816. [https://doi.org/10.1016/S0043-1354\(00\)00439-5](https://doi.org/10.1016/S0043-1354(00)00439-5).
- [131] K.C. Lin, M.E.J. Pearce, Effects of mixing on anaerobic treatment of potato-processing wastewater, *Canadian Journal of Civil Engineering* 18 (1991) 504–514. <https://doi.org/10.1139/191-061>.
- [132] R. Nandi, C.K. Saha, M.S. Huda, M.M. Alam, Effect of mixing on biogas production from cow dung, *Eco Friendly Agric. J* 10 (2017) 7–13. [https://www.researchgate.net/profile/Chayan-Saha-2/publication/313973914\\_Effect\\_of\\_Mixing\\_on\\_Biogas\\_Production\\_from\\_Cowdung/links/58b06e7ba6fdcc6f03f601bd/Effect-of-Mixing-on-Biogas-Production-from-Cowdung.pdf](https://www.researchgate.net/profile/Chayan-Saha-2/publication/313973914_Effect_of_Mixing_on_Biogas_Production_from_Cowdung/links/58b06e7ba6fdcc6f03f601bd/Effect-of-Mixing-on-Biogas-Production-from-Cowdung.pdf) (accessed January 19, 2022).
- [133] J. Ramachander, S.K. Gugulothu, G.R.K. Sastry, J. Kumar Panda, M.S. Surya, Performance and emission predictions of a CRDI engine powered with diesel fuel: A combined study of injection parameters variation and Box-Behnken response surface methodology based optimization, *Fuel* 290 (2021) 120069. <https://doi.org/10.1016/j.fuel.2020.120069>.
- [134] S.H. Yoon, C.S. Lee, Experimental investigation on the combustion and exhaust emission characteristics of biogas–biodiesel dual-fuel combustion in a CI engine, *Fuel Processing Technology* 92 (2011) 992–1000. <https://doi.org/10.1016/j.fuproc.2010.12.021>.

- [135] G. Goga, B.S. Chauhan, S.K. Mahla, A. Dhir, H.M. Cho, Effect of varying biogas mass flow rate on performance and emission characteristics of a diesel engine fuelled with blends of n-butanol and diesel, *J Therm Anal Calorim* 140 (2020) 2817–2830. <https://doi.org/10.1007/s10973-019-09055-1>.
- [136] D. Barik, S. Murugan, Investigation on combustion performance and emission characteristics of a DI (direct injection) diesel engine fueled with biogas–diesel in dual fuel mode, *Energy* 72 (2014) 760–771. <https://doi.org/10.1016/j.energy.2014.05.106>.
- [137] AR.M. Kumar, M. Kannan, G. Nataraj, A study on performance, emission and combustion characteristics of diesel engine powered by nano-emulsion of waste orange peel oil biodiesel, *Renew Energy* 146 (2020) 1781–1795. <https://doi.org/10.1016/j.renene.2019.06.168>.
- [138] D. Barik, S. Murugan, Experimental investigation on the behavior of a DI diesel engine fueled with raw biogas–diesel dual fuel at different injection timing, *Journal of the Energy Institute* 89 (2016) 373–388. <https://doi.org/10.1016/j.joei.2015.03.002>.
- [139] D. Barik, M. Sivalingam, Investigation on Performance and Exhaust Emissions Characteristics of a DI Diesel Engine Fueled with Karanja Methyl Ester and Biogas in Dual Fuel Mode, in: *SAE Technical Paper*, 2014. <https://doi.org/10.4271/2014-01-1311>.
- [140] S.P. Jena, S.K. Acharya, Investigation on influence of thermal barrier coating on diesel engine performance and emissions in dual-fuel mode using upgraded biogas, *Sustainable Environment Research* 29 (2019) 24. <https://doi.org/10.1186/s42834-019-0025-4>.
- [141] A.K. Agarwal, J.G. Gupta, A. Dhar, Potential and challenges for large-scale application of biodiesel in automotive sector, *Prog Energy Combust Sci* 61 (2017) 113–149. <https://doi.org/10.1016/j.pecs.2017.03.002>.
- [142] S. Abdel Razek, M.S. Gad, M. Abd El Hakeem, Experimental Investigation using CNTS as an Additive to Palm Biodiesel Blend on a DI Diesel Engine Performance, Emission and Combustion Characteristics, *Int J Res Appl Sci Eng Technol* 887 (2017). <https://www.ijraset.com/files/serve.php?FID=9012> (accessed January 17, 2022).
- [143] S. Saravanan, G. Nagarajan, S. Anand, S. Sampath, Correlation for thermal NO<sub>x</sub> formation in compression ignition (CI) engine fuelled with diesel and biodiesel, *Energy* 42 (2012) 401–410. <https://doi.org/10.1016/j.energy.2012.03.028>.
- [144] S.P. Venkatesan, P.N. Kadiresh, N. Beemkumar, J. Jeevahan, Combustion, performances, and emissions characteristics of diesel engine fuelled with diesel-aqueous zinc oxide nanofluid blends, *Energy Sources, Part A: Recovery, Utilization, and Environmental Effects* (2019) 1–15. <https://doi.org/10.1080/15567036.2019.1666933>.
- [145] V. Praveena, M.L.J. Martin, V.E. Geo, Experimental characterization of CI engine performance, combustion and emission parameters using various metal oxide nanoemulsion of grapeseed oil methyl ester, *J Therm Anal Calorim* 139 (2020) 3441–3456. <https://doi.org/10.1007/s10973-019-08722-7>.
- [146] I.D. Bedoya, A.A. Arrieta, F.J. Cadavid, Effects of mixing system and pilot fuel quality on diesel–biogas dual fuel engine performance, *Bioresour Technol* 100 (2009) 6624–6629. <https://doi.org/10.1016/j.biortech.2009.07.052>.
- [147] M. Mehregan, M. Moghiman, Effects of nano-additives on pollutants emission and engine performance in a urea-SCR equipped diesel engine fueled with blended-biodiesel, *Fuel* 222 (2018) 402–406. <https://doi.org/10.1016/j.fuel.2018.02.172>.

- [148] D. Balasubramanian, I. Papla Venugopal, K. Viswanathan, Characteristics Investigation on di Diesel Engine with Nano-Particles as an Additive in Lemon Grass Oil, in: SAE Technical Papers, SAE International, 2019. <https://doi.org/10.4271/2019-28-0081>.
- [149] M.M. Abdelaal, B.A. Rabee, A.H. Hegab, Effect of adding oxygen to the intake air on a dual-fuel engine performance, emissions, and knock tendency, *Energy* 61 (2013) 612–620. <https://doi.org/10.1016/j.energy.2013.09.022>.
- [150] D. Rangabashiam, H. Suresh Babu Rao, G. Subbiah, M. Vinayagam, Study of Annona squamosa as alternative green power fuel in diesel engine, *Biomass Convers Biorefin* (2021). <https://doi.org/10.1007/s13399-021-01347-7>.
- [151] R. Karthikeyan, N. Mahalakshmi, Performance and emission characteristics of a turpentine–diesel dual fuel engine, *Energy* 32 (2007) 1202–1209. <https://doi.org/10.1016/j.energy.2006.07.021>.
- [152] K. Surendrababu, K.G. Muthurajan, M. Prabhakar, S. Prakash, M. Saravana Kumar, M. Jayakumar, Performance, Emission, and Study of DI Diesel Engine Running on Pumpkin Seed Oil Methyl Ester with the Effect of Copper Oxide Nanoparticles as an Additive, *J Nanomater* 2022 (2022) 1–9. <https://doi.org/10.1155/2022/3800528>.
- [153] A.K. Patil, S.G. Ganur, Comparative study on the effect of nano additives with biodiesel blend on the performance and emission characteristics of a laboratory ci engine, *International Journal of Mechanical and Production Engineering Research and Development (Ijimperd)* ISSN (p) (n.d.) 2249–6890. <https://www.academia.edu/download/57545216/114IJMPERDAUG2018114.pdf> (accessed September 19, 2022).
- [154] M.E.M. Soudagar, N.R. Banapurmath, A. Afzal, N. Hossain, M.M. Abbas, M.A.C.M. Haniffa, B. Naik, W. Ahmed, S. Nizamuddin, N.M. Mubarak, Study of diesel engine characteristics by adding nanosized zinc oxide and diethyl ether additives in Mahua biodiesel–diesel fuel blend, *Sci Rep* 10 (2020) 15326. <https://doi.org/10.1038/s41598-020-72150-z>.
- [155] D. Ganesh, G. Gowrishankar, Effect of nano-fuel additive on emission reduction in a biodiesel fuelled CI engine, in: 2011 International Conference on Electrical and Control Engineering, IEEE, 2011: pp. 3453–3459. <https://doi.org/10.1109/ICECENG.2011.6058240>.
- [156] K. Ramalingam, A. Kandasamy, D. Balasubramanian, M. Palani, T. Subramanian, E.G. Varuvel, K. Viswanathan, Forecasting of an ANN model for predicting behaviour of diesel engine energised by a combination of two low viscous biofuels, *Environmental Science and Pollution Research* 27 (2020) 24702–24722. <https://doi.org/10.1007/s11356-019-06222-7>.
- [157] H. Venu, P. Appavu, Combustion and emission characteristics of tamarind seed biodiesel–diesel blends in a compression ignition engine, *International Journal of Ambient Energy* 42 (2021) 1441–1446. <https://doi.org/10.1080/01430750.2019.1611652>.
- [158] S. Şahin, H. Ögüt, Investigation of the Effects of Linseed Oil Biodiesel and Diesel Fuel Blends on Engine Performance and Exhaust Emissions, *International Journal of Automotive Engineering and Technologies* 7 (2018) 149–157. <https://doi.org/10.18245/ijaet.476775>.
- [159] C.R. Seela, R.S. B., Emulsified nano Al<sub>2</sub>O<sub>3</sub> – Jatropa methyl ester blends: application in variable compression ratio engine, *World Journal of Engineering* 17 (2020) 733–737. <https://doi.org/10.1108/WJE-04-2020-0135>.

- [160] A.K. Namdeo, R. Gupta, Potential Of Linseed Oil Biodiesel As Fuel For CI-Engines in india, international journal of scientific & technology research 9 (2020) 2. <https://www.ijstr.org/final-print/feb2020/Potential-Of-Linseed-Oil-Biodiesel-As-Fuel-For-Ci-engines-In-India.pdf> (accessed September 17, 2022).
- [161] V. Hemadri, M. Swamy, Impact of Cobalt Oxide Nanoparticles Dispersed in Water in Diesel Emulsion in Reduction of Diesel Engine Exhaust Pollutants, Pollution 2022 (2022) 579–593. <https://doi.org/10.22059/POLL.2021.331156.1198>.
- [162] K. Sandeep, C.R. Rajashekhar, S.R. Karthik, Experimental Studies on Effect of Nano particle blended Biodiesel Combustion on Performance and Emission of CI Engine, IOP Conf Ser Mater Sci Eng 376 (2018) 012019. <https://doi.org/10.1088/1757-899X/376/1/012019>.
- [163] P.J. Prakash, K. Raja, A.T.P. Kumar, Performance of DI diesel engine with pongamia biodiesel and Al<sub>2</sub>O<sub>3</sub> nano additive, IJCRT 6 (2018). <https://ijcrt.org/papers/IJCRT1893001.pdf> (accessed August 17, 2023).
- [164] D. Balasubramanian, K.R. Lawrence, Influence on the effect of titanium dioxide nanoparticles as an additive with Mimuspops elengi methyl ester in a CI engine, Environmental Science and Pollution Research 26 (2019) 16493–16502. <https://doi.org/10.1007/s11356-019-04826-7>.
- [165] C. Srinidhi, A. Madhusudhan, S. v. Channapattana, Parametric studies of CI engine at various injection strategies using biodiesel blended nanoparticles as fuel, International Journal of Ambient Energy 43 (2022) 117–127. <https://doi.org/10.1080/01430750.2019.1630303>.
- [166] K. Kalaimurugan, S. Karthikeyan, M. Periyasamy, G. Mahendran, T. Dharmaprabhakaran, Performance Analysis of CuO<sub>2</sub> Nanoparticles Addition with Neochloris Oleoabundans Algae Biodiesel on CI Engine, J Sci Ind Res (India) 78 (2019) 802–805. <https://nopr.niscpr.res.in/bitstream/123456789/51185/1/JSIR%2078%2811%29%20802-805.pdf> (accessed August 22, 2023).
- [167] P. Purushothaman, S. Masimalai, V. Subramani, Effective utilization of mahua oil blended with optimum amount of Al<sub>2</sub>O<sub>3</sub> and TiO<sub>2</sub> nanoparticles for better performance in CI engine, Environmental Science and Pollution Research 28 (2021) 11893–11903. <https://doi.org/10.1007/s11356-020-07926-x>.
- [168] N.S. Senthur, C. Anand, M. Ramesh Kumar, P.V. Elumalai, M.I. Shajahan, A.C. Benim, E.A. Nasr, H.M.A. Hussein, M. Parthasarathy, Influence of cobalt chromium nanoparticles in homogeneous charge compression ignition engine operated with citronella oil, Energy Sci Eng 10 (2022) 1251–1263. <https://doi.org/10.1002/ese3.1088>.
- [169] R. Thirugnanasambantham, T. Elango, Emission Analysis of Chlorella sp. Microalgae Biodiesel with Oxide Nano Additives in Diesel Engine, J Sci Ind Res (India) 79 (2020) 1031–1034. <https://nopr.niscpr.res.in/bitstream/123456789/55619/1/JSIR%2079%2811%29%201031-1034.pdf> (accessed May 11, 2023).
- [170] K. Sathasivam, A. Elango, A. Prathima, Performance and Emission Study on Zinc Oxide Nano Particles Addition with Pomolion Stearin Wax Biodiesel of CI Engine, J Sci Ind Res (India) 73 (2014) 187–190. <https://nopr.niscpr.res.in/bitstream/123456789/27382/1/JSIR%2073%283%29%20187-190.pdf> (accessed February 27, 2023).

- [171] H.S. Salave, A.D. Desai, Numerical analysis of a single cylinder stationary diesel engine using enriched biogas, *Mater Today Proc* 72 (2023) 1673–1677. <https://doi.org/10.1016/j.matpr.2022.09.455>.
- [172] P.S. Gaddigoudar, Y.H. Basavarajappa, N.R. Banapurmath, P.A. Harari, Effect of biogas flow rate on the combustion, emission and performance characteristics of dual fuel engine fuelled with ceiba pentandra biodiesel, *Mater Today Proc* (2023). <https://doi.org/10.1016/j.matpr.2023.06.259>.
- [173] S. Verma, L.M. Das, S.C. Kaushik, Effects of varying composition of biogas on performance and emission characteristics of compression ignition engine using exergy analysis, *Energy Convers Manag* 138 (2017) 346–359. <https://doi.org/10.1016/j.enconman.2017.01.066>.

## LIST OF PUBLICATIONS

---

### JOURNAL PAPER SCI/SCIE PUBLISHED

1. S Lalhriatpuia, & Amit Pal. (2023). “Computational optimization of engine performance and emission responses for dual fuel CI engine powered with biogas and Co<sub>3</sub>O<sub>4</sub> nanoparticles doped biodiesel.” *Fuel*, 344, 127892. <https://doi.org/10.1016/j.fuel.2023.127892>
2. S Lalhriatpuia, & Amit Pal. (2023). “Computational optimization of engine emissions and performance of a CI engine powered with Biogas and NiO nanoparticles doped diesel.” *Environmental Progress & Sustainable Energy*. <https://doi.org/10.1002/ep.14207>

### INTERNATIONAL CONFERENCE PAPERS

1. S Lalhriatpuia, & Amit Pal. (2020), Performance and Emissions Analysis of a Dual Fuel Diesel Engine with Biogas as Primary Fuel, 2nd International Conference on Recent Advances in Mechanical Engineering, RAME-2020, September 18-19, DTU Delhi, India.
2. S Lalhriatpuia, & Amit Pal. (2021), Comparative Performance and Emission Analysis of CI engine run on Biodiesel Octanol blend, International Conference on Energy and Environment, ICEE-2021, April 09-10, JECC Thrissur, India.
3. S Lalhriatpuia, & Amit Pal. (2022), Energy and Exergy Analysis of CI engine dual fuelled with Linseed Biodiesel and Biogas, 3<sup>rd</sup> International Conference on Recent Advances in Materials, Manufacturing and Thermal Engineering (RAMMTE-2022), July 8-9, DTU Delhi, India.

## CURRICULUM VITAE

---

### S. LALHRIATPUIA

- Born and raised in Aizawl, Mizoram, India, S.Lalhriatpuia completed his HSLC in 2008 at St. Paul's Higher Secondary School and his HSSLC in 2010 at Mizoram Institute of Comprehensive Education.
- Currently pursuing a Ph.D. in Mechanical Engineering at Delhi Technological University (DTU), the individual's educational journey reflects a consistent commitment to academic excellence and a clear aspiration to thrive in demanding research environments at leading engineering institutions.
- The individual completed his B.Tech in Mechanical Engineering from North Eastern Regional Institute of Science and Technology (NERIST), Itanagar, India, followed by an M.Tech in Thermal Engineering from DTU, Delhi, India.
- Publications in respected academic journals evidence the individual's scientific achievements. Their dedication to the field extends beyond research, as demonstrated by winning the best paper award at a technical session, volunteering in a faculty development program on alternative energy sources, and serving as a reviewer for the 2nd International Conference on "Recent advances in mechanical engineering" (RAME-2020).